Design and Characterization of Central Functionalized Asymmetric tri-Block Copolymer Modified Surfaces

Jianli Wang

Dissertation Submitted to the Faculty of the
Virginia Polytechnic Institute and State University
in partial fulfillment of the requirements for the degree of

Doctor of Philosophy

in

Chemistry

APPROVED:

Thomas C. Ward, Chair
Harry C. Dorn
William A. Ducker
James E. McGrath
Allan R. Shultz

October 30, 2001
Blacksburg, Virginia

Keywords: Polymer Brush, Surface Energy, Interface, Block Copolymer, Thin Film

Abstract

Well-defined central functionalized asymmetric *tri*-block copolymers (CFABC) were designed as a new type of polymer brush surface modifier, with a short central functionalized block that can form chemical bonds with a suitable substrate surface. A combination of sequential living anionic polymerization and polymer modification reactions were used for the synthesis of two CFABCs: PS-*b*-poly(4-hydroxystyrene)-*b*-PMMA and PS-*b*-poly(4-urethanopropyl triethoxysilylstyrene)-*b*-PMMA. GPC and NMR characterization indicated that the block copolymers possessed controlled molecular weights and narrow molecular weight distributions.

CFABC polymer brushes were successfully prepared by chemically grafting PS-*b*-poly(4-urethanopropyl triethoxysilylstyrene)-*b*-PMMA onto silicon wafer surfaces. AFM, XPS and ellipsometry were used to confirm the CFABC polymer brush structures and thickness.

The surface properties of CFABC polymer brush modified silicon wafer substrates subjected to different environmental parameters were studied. Reversibly switchable surface energies were observed when the polymer brush modified surfaces were exposed to solvents with different polarities. The phenomenon was attributed to the chain configuration auto-adjustment in the polymer brush systems. The same mechanism was also used to explain the enhanced adhesion capability between the modified surfaces and different polymer materials (PS and PMMA).

Phase behaviors of polymer thin films on unmodified and CFABC polymer brush modified silicon wafer surfaces were also studied. For thin films of polymer blends, PS *blend* PS-*co*-PMMA, the effects of film thickness, chemical composition and temperature on the phase separation mechanism were investigated. The phase behavior in thin films of triblock copolymers with or without central functionalities were compared to reveal the role of the central functionalized groups in controlling film structures. Finally, the presence of CFABC polymer brush at the interface between PS-*b*-PMMA diblock copolymer thin film and silicon wafer substrate was found to decrease the characteristic lamellar thickness in the thin film. A mechanism of tilted chain configurations in the thin film due to the interactions with the CFABC polymer brushes was proposed.

Acknowledgements

There is no doubt that the best decision I have ever made in my research life was to join Dr. T. C. Ward's research group in the fall of 1996, when I came to this small town but big university from the other side of the earth to pursue my dream of being one of the best scientists in the world. With that dream still hanging in the air, I am lucky enough to have spent my last five years in one of the best research groups in the world. Dr. Ward's unparalleled enthusiasm in teaching, enormous trust in his students, and keen insight in science have made him the best advisor a graduate student can dream of. Thank you, Dr. Ward, for all of the guidance, trust, and understanding. I also owe special thanks to my other committee members, Dr. H. C. Dorn, Dr. W. A. Ducker, Dr. J. E. McGrath, and Dr. A. R. Shultz for their instructions during my research. It has been a great opportunity for me to learn directly from world class scientists in such different disciplines. I want to sincerely thank Dr. T. E. Long for his suggestions and discussions on my research. His expertise in polymer chemistry and patience in teaching me doing synthesis were critical for my research success. I also express appreciation to Dr. J. G. Dillard and Dr. D. A. Dillard, the former and current directors of the Center for Adhesive and Sealant Science (CASS). I have enjoyed attending all CASS activities and am proud to have been a student fellowship awardee during the last three and a half years.

I want to express sincere appreciation to one of my best friends, Dr. Qing Ji, for his great help to both my research and my family during the last five years. Many other fellows (postdocs and graduate students) were also very helpful in my research, and only a few of them are named here, Dr. Sheng Wang, Dr. Charles Tchatchoua, Dr. Taigyoo Park, Dr. Jim Yang, Mr. Shu Guo, Ms. Sebnem Kara, Mr. Dave Williams, Dr. M. Sankar, Dr. Yongning Liu.

I acknowledge Mr. Steve McCartney, Mr. Frank Cromer, and Mr. Tom Glass for their technical assistance for my research. Special thanks go to secretaries (Esther, Tammy, Linda, Millie, and Laurie).

I have been giving the fellows of the PolyPkem group a very hard time in understanding what I am exactly saying, so here I want to deliver my appreciation to Emmett O'Brien, Amy Eichstadt, Sandra Henderson, Jennifer Brooks, Catherine Keel,

and Rebecca Fall in a clear, precise way: Thank you for the help, Mei Guo Gui Zi (Emmett knows it). The group, which just like a family in helping me on research and offering me invaluable friendship, will always be in my good memory. The former PolyPkem crew, Drs. Ojin Kwon, Kermit Kwan, Dave Porter, Rob Jensen, and Mark Muggli also deserve my sincere thanks for teaching me research skills and helping me become a classic PolyPkem member in the shortest possible time. I still remember the good time when Ojin and I were intensely arguing over some scientific problems until 1:00 am, and then Kermit came to the lab to start his working day. Of course, the "Big Mouth 5.19" is the best volleyball team forever.

My greatest thanks go to my family. I want to thank my sister, Lei Wang, for her understanding and support, and taking over my part of duty in taking care of our retired parents in China. I cannot image my success today without the love from my dear wife, Huaiying Kang, during the last five years. We started our new life together in a new country right after our marriage, and it was she who gave me enough encouragement to overcome numerous difficulties and be successful. As to my parents, Mr. Wenheng Wang and Mrs. Xiuying Wang, and parents-in-law, Prof. Shixiu Kang and Mrs. Manxiang Zhou, who always stand behind their children, there are no appropriate words to describe my thanks to them.

CHAPTER 1. INTRODUCTION 1

CHAPTER 2. BACKGROUND AND LITERATURE REVIEW 4

2.1. Surface/Interface Modifications and Characterizations 4
2.1.1. Surface/Interface Modification Methods 4
2.1.1.1. Chemical Etching Surface Modifications 5
2.1.1.2. Plasma Surface Modifications 5
2.1.1.3. SAM (self-assembled monolayers) 6
2.1.1.4. Copolymers at interfaces 7
2.1.1.5. Polymer brushes 8
2.1.2. Characterization Techniques 8
2.1.2.1. Microscopic techniques (AFM, TEM, FE-SEM) 8
2.1.2.2. X-ray Photoelectron Spectroscopy (XPS) 9
2.1.2.3. Contact Angle 9
2.1.2.4. Dynamic Secondary Ion Mass Spectrometry (DSIMS) 10
2.1.2.5. Forward Recoil Spectroscopy (FRES) 11
2.1.2.6. Neutron and X-ray Reflectivity 11
2.1.2.7. ATR-FTIR 12

2.2. Characteristics of Polymer Brushes 13
2.2.1. General Background of Polymer Brushes 13
2.2.2. Types of Polymer Brush Systems 14
2.2.3. Preparation of Polymer Brushes 17
2.2.3.1. Preparation of polymer brushes by physisorption 18
2.2.3.2. Preparation of polymer brushes by "grafting to" 19
2.2.3.3. Preparation of polymer brushes by "grafting from" 21

2.3. Theory and Modeling of Polymer Brushes 22
2.3.1. Alexander-de Gennes model — chain configuration in homopolymer brushes 22
2.3.2. Theoretical studies of copolymer brushes 30
2.3.3. Theoretical studies on other types of polymer brushes 31

2.4. Roles of Polymer Brushes in Interfacial Adhesion Energy 33
2.4.1. Experimental studies of polymer brushes – elastomer interactions 33
2.4.2. Effects of grafting density on interfacial adhesion energy – de Gennes model 34
2.4.3. Mechanical Tests for Adhesion Strength in an Interface 36
2.4.3.1. Experimental Design of ADCB Test 36
2.4.3.2. Some Application Examples of ADCB Technique 38

2.5. Polymer Thin Film Phase Behaviors 39
2.5.1. Phase Behaviors in Bulk (3-D) Systems 40
2.5.1.1. Kinetics of phase separation of polymer blends in bulk (3-D) systems. 40
2.5.1.2. Phase behaviors of block copolymers in bulk (3-D) systems 41
2.5.2. Block Copolymer Thin Films 42
2.5.2.1. Block copolymer thin films between two solid walls 42

2.5.2.2. Block thin films between a solid wall (substrate) and air 44
2.5.3. Polymer Blend Thin Films 45
2.5.4. Influence of polymer brushes on polymer thin film phase behaviors..... 50

CHAPTER 3. SYNTHESIS 51

3.1. Introduction 51

3.2. Experimental 53
3.2.1. Monomer, initiator, and solvent purification 53
3.2.2. Synthesis of p-[(tert-butyldimethylsilyl)oxy]styrene (1) 53
3.2.3. Synthesis of PS-b-poly(p-[(tert-butyldimethylsilyl)oxy]styrene)-b-PMMA (**2**) 55
3.2.4. Synthesis of PS and PS-b-PMMA 57
3.2.5. Desilylation of PS-b-poly(p-[(tert-butyldimethylsilyl)oxy]styrene)-b-PMMA 58
3.2.6. PS-b-poly(4-urethanopropyl triethoxysilylstyrene)-b-PMMA (4) 59
3.2.7. Characterization 59

3.3. Results and Discussion 59
3.3.1. Characterization of p-[(tert-butyldimethylsilyl)oxy]styrene (1) 59
3.3.2. Characterization of the Polymers 65

3.4. Conclusions 78

CHAPTER 4. CFABC POLYMER BRUSH PREPARATION AND CHARACTERIZATION 80

4.1. Introduction 80

4.2. Experiments 81
4.2.1. Materials 81
4.2.2. CFABC polymer brush preparation 82
4.2.3. Characterization 83

4.3. Results and Discussions 83
4.3.1. Topology of CFABC polymer brush 83
4.3.2. Surface Chemical Composition and Brush Thickness 86

4.4. Conclusions 90

CHAPTER 5. SURFACE PROPERTIES ON CFABC MODIFIED SUBSTRATES 94

5.1. Introduction 94

5.2. Experiments 94
5.2.1. Sample preparation 94
5.2.2. Characterizations 95

5.3. Results and Discussions 96
5.3.1. Nanopatterns influenced by washing solvents 96

5.3.2. Switchable surface energies 100
5.3.2.1. Contact angles on CFABC polymer brush modified silicon surfaces .. 100
5.3.2.2. Surface energies 102
5.3.3. Interfacial adhesion energy control 104
5.3.3.1. Wettability study of different polymer thin films on CFABC modified silicon surfaces 104

5.4. Conclusions 108

CHAPTER 6. POLYMER ULTRA-THIN FILM PHASE BEHAVIORS 109

6.1. Introduction 109

6.2. Ultra-thin Film of Polymer Blends 110
6.2.1. Background on polymer blend thin film studies 110
6.2.2. Preparation of polymer blend thin films 111
6.2.2.1. Materials 111
6.2.2.2. Polymer blend thin film preparation 111
6.2.2.3. Characterization 113
6.2.3. Compositional influence on polymer blend thin film phase behaviors 113
6.2.4. Thickness influence on polymer blend thin film phase behaviors 125
6.2.5. Temperature influence on polymer blend thin film phase behaviors 130
6.2.6. Conclusions of polymer blend thin film studies 132

6.3. Influence of CFABC Polymer Brush On Block Copolymer Ultra-thin Film Phase Behaviors 133
6.3.1. Background on block copolymer thin film studies 133
6.3.2. Self-assembled lamellar structures in thin films of triblock copolymer with protected central functionality 135
6.3.3. CFABC tri-block copolymer (tri-block copolymer with central functionality) film on Si wafer surface 142
6.3.4. Diblock copolymer thin film on CFABC polymer brush modified surfaces 145

6.4. Conclusions 147

CHAPTER 7. CONCLUSIONS 149

VITA 152

Figure 2.1. A general model for a polymer brush system..... 13

Figure 2.2 Examples of polymer systems comprising polymer brushes. 15

Figure 2.3 Polymer brushes with different chemical compositions, (a1-a4) homopolymer brushes; (b) binary polymer brush; (c) random copolymer brush; (d) block copolymer brush. 16

Figure 2.4. Different polymer brush fabrication methods. 17

Figure 2.5. a) Schematic representation of a polymer brush. L is the layer thickness and D the average spacing between two grafting points. b) The monomer density profile **f** vs distance from the grafting plane z according to the Alexander-de Gennes model. 23

Figure 2.6. Plot of $Ld^{2/3}$ *vs* M for grafted PDMS in a good solvent (dichloromethane).[135] 29

Figure 2.7. Normalized enhanced adhesive strength (G-W)/W as a function of the surface density, **s** , for two PDMS elastomers in contact with silicon wafers covered with irreversibly adsorbed chains. From ref. [167]. 34

Figure 2.8 Schematic picture of the pull-out process that takes place as the crack grows along the interface. As the crack advances, each connector is progressively stretched until it reaching its maximal length. At that point the connectors collapses onto the surface. 35

Figure 2.9. A sketch of the "razor" specimen.[175]..... 37

Figure 2.10. A sketch that shows the mode of failure of a symmetrically 38

Figure 2.11. Phase diagram for linear AB diblock copolymers in 3-D, comparing theory (plots, top) and experiment (cartoons, bottom).[188]..... 41

Figure 2.12. Morphologies for linear ABC triblock copolymers in bulk (3D).[188]..... 41

Figure 2.13. Possible lamellar structures of block copolymers in a thin film of thickness D in between two equivalent walls. See the text for details. From Binder[194]..... 43

Figure 2.14. Lamellar structures of block copolymers in a thin film of thickness D in between two equivalent walls. From Binder[194]..... 44

Figure 2.15. Structures of a diblock copolymer thin film between a wall (substrate) and air. From Ausserre *et al.*..... 45

Figure 2.16. Phase diagram of a symmetrical binary (AB) polymer blend in a thin film. See the text for details. From Flebbe *et al.*[198]..... 46

Figure 2.17. Schematic description of phase structures of phase separated binary polymer blend (AB) thin films. From Donley *et al.*[200]..... 48

Figure 2.18. Dewetting in a thin film containing two components A and B on a substrate. From Keblinski, *et al.*[201]..... 49

Figure 3.1. ^{1}H NMR spectrum of TDBMS-Cl..... 60

Figure 3.2. ^{1}H NMR spectrum of *p*-hydroxystyrene (recrystallized from hexane) 61

Figure 3.3. ^{1}H NMR spectrum of *p*-[(*tert*-butyldimethylsilyl)oxy]styrene (1) before distillation..... 63

Figure 3.4. ^{1}H NMR spectrum of *p*-[(*tert*-butyldimethylsilyl)oxy]styrene (1) after distillation (10^{-5} torr, 45 °C). (a) the whole spectrum; (b) & (c), partly enlarged spectra of (a). 65

Figure 3.5. GPC traces of the synthesized polymers. *a*) PS homopolymer; *b*1 & *b*2) PS-*b*-PMMA *di*-block copolymers; *c*) *tri*-block copolymer 2. 66

Figure 3.6. ^{1}H NMR spectrum (400 MHz, chloroform-*d*) of living anionic polymerized polystyrene (PS) homopolymer. 67

Figure 3.7. ^{1}H NMR spectrum (400 MHz, chloroform-*d*) of living anionic polymerized PS-*b*-PMMA di-block copolymer. Peak *b* was from the methoxy group in the PMMA block. The signal corresponding to the initiator (sec-butyl) was still observed at around 0.7 ppm. 68

Figure 3.8. ^{1}H NMR spectrum (400 MHz, chloroform-*d*) of living anionic polymerized PS-*b*-poly(*p*-[(*tert*-butyldimethylsilyl)oxy]styrene)-*b*-PMMA(2). Peaks *a* and *b* were from the dimethyl and t-butyl groups of TBDMS, respectively. The signal corresponding to the initiator (sec-butyl) was still observed at around 0.7 ppm. 69

Figure 3.9 GPC traces of the synthesized *tri*-block copolymers. a) *tri*-block copolymer 2; b) *tri*-block copolymer 3; c) *tri*-block copolymer 4. 71

Figure 3.10 NMR spectra of PS - *b* – poly(*p*-[(*tert*-butyldimethylsilyl) oxy]styrene) - *b* – PMMA (top), PS - *b* - PSOH - *b* – PMMA (center), and PS - *b* - PSSi - *b* - PMMA (bottom) 73

Figure 3.11. NMR spectra of isocynato propyl triethoxysilane (top) and PS - *b* - PSSi - *b* - PMMA (bottom) 74

Figure 3.12. ^{29}Si NMR spectra of of PS-*b*-poly(*p*-[(*tert*-butyldimethylsilyl)oxy] styrene)-*b*-PMMA 2, a) without adding inside standard TMS, b) with TMS. The peak for the silyl protection group in the polymer appeared at 19.98ppm in a) and b). 75

Figure 3.13. ^{13}C NMR of *tri*-block copolymer **3**. 75

Figure 3.14. DSC curves (2nd heat) of PS-*b*-PMMA and *tri*-block copolymer 2. 78

Figure 4.1. AFM (deflection mode) images of blank silicon wafer surface (a), and CFABC (PS-b-PSSi-b-PMMA) grafted silicon wafer surface (b). The same washing process was used for each sample: 10 hours Soxhlet extraction (toluene). 84

Figure 4.2 AFM (tapping mode) phase images of PS-b-PMMA spin coated Si wafer surface(a), and CFABC (PS-b-PSSi-b-PMMA) grafted silicon wafer surface (b). The same washing process was used for each sample: 10 hours Soxhlet extraction (toluene). 85

Figure 4.3. AFM (tapping mode) height images of CFABC (PS-b-PSSi-b-PMMA) grafted silicon wafer surface at different washing stages. a), unwashed; b), partially washed (~10 minutes); c), partially washed (~ 1 hours); d), completely washed (~ 10 hours). 85

Figure 4.4. XPS of a clean (unmodified) silicon wafer surface with a collect angle of 90° 87

Figure 4.5. XPS Si2p multiplex result of a clean (unmodified) silicon wafer surface with a collect angle of 45° 88

Figure 4.6. XPS Si2p multiplex result of a clean (unmodified) silicon wafer surface with a collect angle of 15° 88

Figure 4.7. XPS of CFABC brush grafted silicon wafer surface with a collect angle of 90° 91

Figure 4.8. XPS of CFABC brush grafted silicon wafer surface with a collect angle of 45° 92

Figure 4.9. XPS of CFABC brush grafted silicon wafer surface with a collect angle of 15° 93

Figure 5.1. Nanopatterns of CFABC polymer brush after being washed by toluene. AFM (Tapping Mode®), 1 μm scan. Top: 3D height image; Bottom: 3D phase image 97

Figure 5.2. Nanopatterns of CFABC polymer brush after being washed by toluene. AFM (Tapping Mode®), 1 μm scan. Phase image. 98

Figure 5.3. Nanopatterns of CFABC polymer brush after being washed by chloroform. AFM (Tapping Mode®), 1 μm scan. Phase image. 99

Figure 5.4. Water contact angles on CFABC modified surfaces with different processing solvents and proposed mechanism of chain conformation auto-adjustments 100

Figure 5.5. Switchable surface properties of CFABC modified surfaces 102

Figure 5.6 Polar part of the surface energy of CFABC modified surface with different processing solvents 104

Figure 5.7 AFM (height image) of PS (10 kg/mol) on blank silicon wafer surface 106

Figure 5.8. Contact angles of dewetted PS micro-droplets on blank silicon wafer measured by AFM 107

Figure 5.9. AFM images of PMMA thin film spin-coated on blank silicon wafer surface. 1μm scan. Height image. 107

Figure 5.10 AFM (height image) of PS (10 kg/mol) and PMMA (120 kg/mol) on CFABC modified surfaces 108

Figure 6.1. AFM images of PS-*co*-PMMA thin film on silicon wafer 111

Figure 6.2. AFM of PS and PS-*co*-PMMA blend thin film (PS-10 in Table 6.1) on silicon wafer 114

Figure 6.3. AFM phase images of PS and PS-*co*-PMMA blend thin films (PS-10, PS-20, PS-30, PS-40 and PS-70) on silicon wafers 115

Figure 6.4. AFM 3-D height images of PS and PS-*co*-PMMA blend thin films (PS-10, PS-30, PS-40 and PS-70) on silicon wafers 116

Figure 6.5. AFM contact angle measurement based the cross section analysis of the surface of PS and PS-*co*-PMMA blend thin film (PS-10) on silicon wafer..... 118

Figure 6.6. AFM contact angle measurement based the cross section analysis of the surface of PS and PS-*co*-PMMA blend thin film (PS-20) on silicon wafer..... 119

Figure 6.7. AFM contact angle measurement based the cross section analysis of the surface of PS and PS-*co*-PMMA blend thin film (PS-30) on silicon wafer..... 120

Figure 6.8. AFM contact angle measurement based the cross section analysis of the surface of PS and PS-*co*-PMMA blend thin film (PS-40) on silicon wafer..... 121

Figure 6.9. AFM contact angle measurement based the cross section analysis of the surface of PS and PS-*co*-PMMA blend thin film (PS-70) on silicon wafer..... 122

Figure 6.10. Contact angle values from the AFM cross section analysis on the surfaces of PS and PS-*co*-PMMA blend thin films on silicon wafers..... 123

Figure 6.11. Cross section analysis of the surface of PS and PS-*co*-PMMA blend thin film (PS-70) on silicon wafer..... 124

Figure 6.12. Cross section analysis of the surface of PS and PS-*co*-PMMA blend thin film (PS-40) on silicon wafer..... 125

Figure 6.13. Influence of film thickness on polymer blend thin film topologies. AFM 3D height images..... 127

Figure 6.14. Influence of film thickness on polymer blend thin film topologies. Spin coating speeds: top, 1k rpm; middle, 2k rpm; bottom, 3k rpm. AFM height and phase images..... 128

Figure 6.15. Effect of polymer blend thin film thickness on the characteristics of the particles (PS rich domain). Samples: PS-50a and PS-50b..... 129

Figure 6.16. Effect of polymer blend thin film thickness on the characteristics of the particles (PS rich domain). Samples: PS-50a and PS-50b..... 130

Figure 6.17. Thermal reversible phase behavior in polymer blend thin film (PS-50c). AFM height images..... 132

Figure 6.18. Thermal reversible phase behavior in polymer blend thin film (PS-50c).. 133

Figure 6.19. Optical image of the edge of a triblock copolymer thin film (4k rpm) on a silicon wafer from a high resolution CCD camera. The image size is about 40 40 μm. 136

Figure 6.20. AFM height image and cross section analysis of the edge of a triblock copolymer thin film (4k rpm) on a silicon wafer..... 137

Figure 6.21. AFM height image and cross section analysis of the edge of a triblock copolymer thin film (4k rpm) on a silicon wafer..... 138

Figure 6.22. Influence of film thickness on the topologies of non-functionalized tri-block copolymer thin films. 140

Figure 6.23. FE-SEM images of the topology of the non-functionalized tri-block copolymer thin film on silicon wafer (3k rpm)..... 141

Figure 6.24. AFM height images of a CFABC thin film at different washing stages. a), unwashed; b), partially washed (~10 minutes); c), partially washed (~ 1 hours); d), completely washed (~ 10 hours). 143

Figure 6.25. 3D AFM height images of CFABC thin film at different washing stages. 144

Figure 6.26 AFM images of thin film structures of tri-Si (a) and tri-TBDMS (b). 145

Figure 6.27 AFM cross section analysis. 146

Table 2.1 The relationship between the dimensions of polymer chains and *N* 26

Table 3.1. Molecular weights and compositions of some of the synthesized polymers .. 70

Table 3.2. Molecular weights and compositions of the synthesized *tri*-block 77

Table 4.1. Summary of XPS data for different collect angles on CFABC brush grafted silicon wafer surface 93

Table 5.1. Preferred values of surface tension and its components for water and methylene iodide used for the calculation of surface tension from contact angles by the harmonic-mean method.[3] 103

Table 6.1. Sample information of polymer blend thin films 112

Table 6.2. Effect of polymer blend thin film thickness on the characteristics of the particles (PS rich domain). Samples: PS-50a and PS-50b 129

Table 6.3. Effect of polymer blend thin film thickness on the characteristics of the particles (PS rich domain). Samples: PS-50a and PS-50b 130

Scheme 1.1. A stable, heterogeneous (chain scale) polymer brush structure 2

Scheme 3.1. Strategy for the synthesis of CFABC polymers 52

Scheme 3.2 Synthesis of *p*-[(tert-butyldimethylsilyl)oxy]styrene monomer 1. 55

Scheme 3.3 Sequential living polymerization of PS-*b*-poly(*p*-[(*tert* butyldimethylsilyl)oxy]styrene)-*b*-PMMA 57

Scheme 3.4 Desilyation of PS-*b*-poly(*p*-[(*tert*-butyldimethylsilyl)oxy]styrene-*b*-PMMA and polymer modification 58

Scheme 4.1 The concept of CFABC polymer brushes 81

Scheme 4.2. Chemical structure of a CFABC polymer 82

Scheme 4.3. CFABC polymer brush grafting process 83

Scheme 6.1. Illustration of contact angle calculation from AFM cross section analysis……. 117

Scheme 6.2. Block copolymer thin film lamellar structure 134

Scheme 6.3. Thickness gradient at the edge of a spin-coated thin film. 136

Scheme 6.4. Illustration of lamellar structure in the thin film of the triblock copolymer with protected functional groups in the center block. **l** is a characteristic parameter for a block copolymer, which is related to the radius of gyration of a polymer chain. 142

Scheme 6.5. Possible mechanism of the influence of CFABC polymer brush on diblock copolymer thin film lamellar structures. 147

CHAPTER 1. INTRODUCTION

Earlier research efforts demonstrated that polymer brushes efficiently modify diverse substrate surfaces.[1,2,3,4,5] Recent focus has been directed towards the control of intermolecular interactions between polymer brush modified surfaces and external agents such as solvents and polymers.[6,7,8] Hawker *et al* have reported an interesting tunable polymer brush system composed of poly(*tert*-butyl acrylate) and poly(acrylic acid).[9] Patterned polymer brushes containing discrete micrometer-scale hydrophilic and hydrophobic square areas were successfully prepared by combining photolithographic techniques with surface-initiated polymerization.

On the other hand, understanding phase behaviors and controlling nano-structures in ultra-thin polymer films (10 – 100 nm) stands as a great challenge to the scientific community and will yield tremendous application potentials in areas such as microelectronics.[10,11] Because of the quasi-2D character in an ultra-thin polymer thin film, the interaction between the film and its substrate is very important. Polymer brushes have proven to be efficient surface modifiers for tailoring polymer thin film structures. For example, Russell and coworkers[12] presented the preparation of a "neutral" surface by using end-grafted polystyrene-*co*-PMMA random copolymer brushes, and perpendicular lamella structures were observed in block copolymer (PS-*b*-PMMA) thin films which were spin-coated on the modified surface.

[1] de Gennes, P. G. *J. Phys*. (Paris) **1976**, 37, 1443.
[2] Alexander, S. *J. Phys*. (Paris) **1977**, 38, 983.
[3] Milner, S. T. *Science* **1991**, 251, 905.
[4] Jones, R. A. L.; Richards, R. W. Polymers at Surfaces and Interfaces; Cambridge University Press: Cambridge, UK, 1999; pp 244-292.
[5] Mansky, P.; Liu, Y.; Huang, E.; Russell, T. P.; Hawker, C. J. *Science* **1997**, 275, 1458.
[6] Zhao, B.; Brittain, W. J. *J. Am. Chem. Soc*. **1999**, 121, 3557.
[7] Huang, E.; Pruzinsky, S.; Russell, T. P.; Mays, J.; Hawker, C. J. *Macromolecules* **1999**, 32, 5299.
[8] Bernard, B.; Brown, H. R.; Hawker, C. J.; Kellock, A. J.; Russell, T. P. *Macromolecules* **1999**, 32 6254.
[9] Husemann, M.; Morrison, M.; Benoit, D.; Frommer, J.; Mate, C. M.; Hinsberg, W. D.; Hedrick, J. L.; Hawker, C. J. *J. Am. Chem. Soc*. **2000**, 122, 1844.
[10] Yethiraj, A., *Phys. Rev. Lett*. **1995**, 74, 2018
[11] Binder, K., Advaces in Polymer Science, Vol. 138, Springer-Verlag Berlin Heidleberg**, 1999**
[12] Jones, R. L.; Kumar, S. K.; Ho, D. L.; Russell, T. P.; et al. *Nature* **1999**, 400 (6740), 146

Polymer brush modifiers are traditionally tethered to the substrate via either **a)** physisorption or **b)** chain-end chemical grafting.[13] Obviously, the latter method provides a more stable polymer brush system due to the strength of the chemical bond between the polymer chain end and the substrate. A typical feature for chemically grafted polymer brush systems is that only a single chain is bound to each grafting site via the chain terminus. Although there have been extensive studies on such polymer brush systems, and interesting results have been obtained in both theoretical and experimental arenas, a brush system with multiple, asymmetric chains, which are *chemically* connected to each grafting site has only been addressed in a theoretical fashion.[14] Our research was motivated by the creation of such a new polymer brush model system as a "switchable" surface modifying agent. This novel polymer brush modifier has been achieved by designing an asymmetric *tri*-block copolymer (ABC) with a short central functionalized block (B) that can form chemical bonds with a suitable substrate surface.

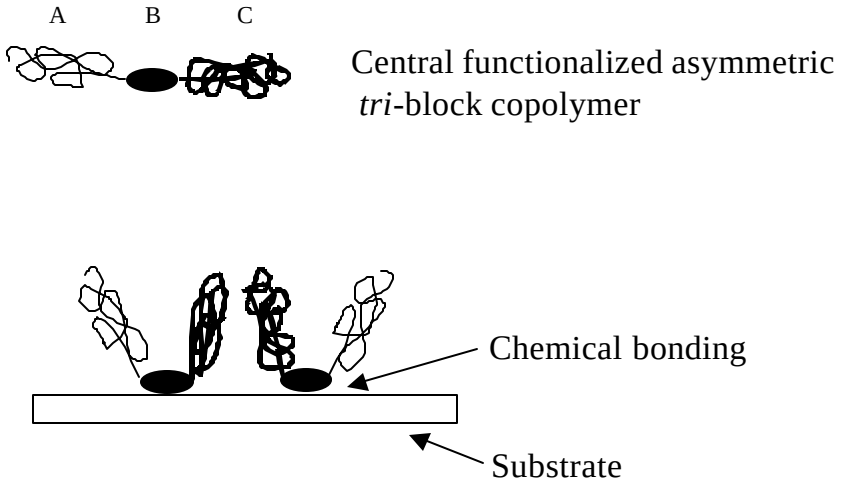

Scheme 1.1. A stable, heterogeneous (chain scale) polymer brush structure

In Chapter 3, the synthesis of two well-defined central functionalized asymmetric *tri*-block copolymers (ABC), PS-*b*-PSOH-*b*-PMMA (PSOH: poly(4-hydroxystyrene)) and PS-*b*-PSSi-*b*-PMMA (PSSi: poly(4-urethanopropyl triethoxysilylstyrene)) is described through a combination of sequential living anionic polymerization and polymer

[13] Milner, S. T. *Science* **1991**, 251, 905
[14] Zhulina, E.; Balazs, A. C. *Macromolecules* **1996**, 29, 2667

modification. Stable, well-defined, heterogeneous (chain scale) polymer brush attachments were obtained when a silicon wafer surface was modified using the copolymers. The detailed discussion of the polymer brush preparation and characterization is provided in Chapter 4. Scheme 1.1 depicts the ideal covalent attachment of a CFABC *tri*-block copolymer in the absence of any external agent such as solvent, or another polymer surface.

A new concept based on "smart adhesion" behavior between the modified surfaces and other polymers is developed and described in Chapter 5. "Smart adhesion" is defined as the ability for a surface to modify adhesion characteristics based on the introduction of an external agent. In Chapter 6, the influence of the polymer brush on phase behaviors and nano-structures of block copolymer ultra-thin films is discussed. Some results on the synthesis of other well-defined functionalized block copolymers, as well as the characterization of the synthesized polymers used in the research in bulk state, are presented in Chapter 7. Finally, the results are summarized in Chapter 8.

CHAPTER 2. BACKGROUND AND LITERATURE REVIEW

In a multi-component polymer system, an interface (interphase) acts not just as a boundary between different phases, but more importantly, is a key component which can be utilized to tune/control the overall physical, chemical, and mechanical properties of the whole system. The importance of the interface is more obvious in the era of nano-technology, during which materials are usually encountered in restricted geometries (i.e., ultra-thin films, nano-pores, etc.) with a scale of 1 – 100 nm. This literature review was focused on understanding the role of surface/interface structures in controlling interfacial adhesion energy and phase behaviors. First, some general background on surface/interface modifications and characterization techniques is introduced. After that, various aspects of polymer brushes, including experiments, theories, and applications in interfacial adhesion energy control, are extensively covered because of their essential role in this dissertation. Finally, recent advancements in polymer thin film structures are discussed to provide necessary background information for my own research efforts (using polymer brush to control film structure) in this important field.

In this dissertation the terms "interface" and "interphase" are not always distinguished, although they have subtle differences according to the literature.[1] Also, with no surprise, the terms "surface" and "interface" are closely related. Except in a vacuum, the surface of a solid (or liquid) is actually an interface between a solid (or liquid) and a gas. Additionally, a "surface" becomes an "interface" (at least part of "interface") when another solid (or liquid) material is put onto the "surface" of a solid (liquid) substrate. New "surfaces" are created when a material is broken along an "interface".

2.1. Surface/Interface Modifications and Characterizations

2.1.1. Surface/Interface Modification Methods

In order to understand the mechanisms of wettability and to improve bonding performance, solid (inorganic or polymer) surfaces are often modified by various

[1] Binder, K., Advances in Polymer Science, Vol. 138, Springer-Verlag Berlin Heidleberg**, 1999**

methods, such as chemical etching, plasma, SAM (self-assembled mono-layers) and grafting (polymer brushes) treatments. Interfaces between polymers or polymer-inorganic solids can be modified by adding copolymers (block or random) or polymer brushes between the two phases. These modifications generally cause physical or chemical changes in a thin surface/interface layer of 10 nm – 1 μm thick.

2.1.1.1. Chemical Etching Surface Modifications

Sodium etching was successfully used to treat fluoropolymers such as polytetrafluoroethylene (PTFE) and fluorinated ethylene-propylene (FEP), which have low wettability and bondability. Chromic acid is used commercially to etch polypropylene and ABS prior to metal plating, as well as polyethylene, polyether and polystyrene.[2,3] A recent review paper by Perdigao *et al*.[4] summarized the progress of phosphoric acid etching technique in the design of all-in-one dental adhesives.

Numerous other chemicals have been used to treat polymer surfaces, primarily for polyolefins and vulcanized rubbers. Typically, the improved wettability and bondability will be lost if the treated surfaces are heated to near the softening point of the polymers. This phenomena were explained by noting that the bulk material, which has lower surface energy than the treated surface, tends to migrate to the surface upon heating.[5]

2.1.1.2. Plasma Surface Modifications

Plasmas are ionized gases that contain ions, electrons, radicals, excited molecules, and atoms.[6] These ionized gases are luminous, electrically neutral, and are generated by electrical discharges, high-frequency electromagnetic oscillations, shock waves, high-energy radiations, etc. There are three types of plasmas: thermal plasma, cold plasma, and hybrid plasma.[7] The modifications cause chain scission, ablation, cross-linking, and oxidation to a depth of typically 5 – 50 nm. The preferred mechanism of the bondability improvement by plasma is the combination of increased wettability (by the introduction of polymer groups) and an increased molecular mobility (by interfacial diffusion/lowered

[2] Snogren, R. C., Handbook of Surface Preparation, Palmerton, New York, **1974**
[3] Blais, P.; Carlsson, D. J.; Csullog, G. W.; Wiles, D. M., *J. Colloid Interface Sci*., 47, 636, **1974**
[4] Perdigao, J.; Frankenberger, R.; Rosa, B. T.; Breschi, L., *American J. of Dentistry*, 13, 25, **2000**
[5] Baszkin, A.; Nishino, M.; Minassian-Sarage, L., *J. of Colloid Interface Sci*., 54, 317, **1976**
[6] McTaggart, F. K., Plasma Chemistry in Electrical Discharges, Elsevier, Amsterdam, **1967**

surface viscosity). With plasma treatments, the bonding temperature required to produce a strong adhesive bond is greatly lowered.

Plasma surface modification methods are widely used to improve the wettability and bondability of polyolefins, polyesters, and many other polymers.[8] The effect on water diffusion in bisphenol-A polycarbonate sample by Ar- and He-plasma treatments was also investigated.[9] Pulsed plasma polymerization of maleic anhydride was used to depose well-defined anhydride functionalized films on solid surfaces, with potential applications in adhesion and biocompatibility.[10]

2.1.1.3. SAM (self-assembled monolayers)

A self-assembled monolayer (SAM) is created by the spontaneous organization of molecules into stable, structurally well-defined aggregates one molecular thick.[11] SAMs were preceded historically by Langmuir-Blodgett (LB) monolayers.[12] LB films, however, are neither convenient to prepare nor sufficiently robust for most applications. SAMs, in contrast, are stable, simple to generate and can be formed from a wide variety of ligands and supports. The most widely-studied SAMs are alkanethiolates on gold[13] and alkylsiloxanes on silicon dioxide[14]

Several major applications for SAMs on surface modifications are, a) the use of SAMs for passivation of surfaces (protection from corrosion or contamination);[15,16] b) the use of patterned SAMs against wet and dry chemical etches[17,18,19], and c) the use of patterned SAMs as materials to control the surface free energy of materials.[20,21,22,23]

---

[7] Bradley, A.; Fales, J. D., *Chem. Tech*., 232, April **1971**
[8] Wu, S., Polymer Interface and Adhesion, Dekker, New York 1982, p298
[9] Schafer, M. M.; Seidel, C.; Fuchs, H.; Voetz, M., *Applied Surface Science*, 173, 1, **2001**
[10] Evenson, S. A.; Fail, C. A; Badyal, J. P. S., *Chemistry of Materials* 12, 3038, **2000**
[11] Whitesides, G. M.; Mathias, J. P.; Seto, C. T., *Science* 254, 1312, **1991**
[12] Ulman, A., An Introduction to Ultrathin Organic Films, San Diego: Academic Press, 1991
[13] Bain, C. D.; Whitesides, G. M., *J. Am. Chem. Soc*. 111, 7164, **1989**
[14] Wasserman, S. R.; Tao, Y. T.; Whitesides, G. M., *Langmuir* 5, 1074, **1989**
[15] Laibinis, P. E.; Whitesides, G. M., *J. Am. Chem. Soc*. 114, 9022, **1992**
[16] Sheen, C. W., *et al*., *J. Am. Chem. Soc*. 114, 1514, **1992**
[17] Kumar, A., *et al*., *J. Am. Chem. Soc*. 114, 9188, **1992**
[18] Kumar, A.; Whitesides, G. M., *Science*, 263, 60, **1994**
[19] Huck, W. T. S.; Yan, L.; Strook, A.; Haag, R.; Whitesides G. M., *Langmuir*, 15, 6862, **1999**
[20] Tidswell, I. M., *Phys. Rev. B* 44, 10869, **1991**
[21] Chidsey, C. E. D.; Loiacono, D. N., *Langmuir* 1990, 682, **1990**
[22] Ferguson, G. S., *et al*., *Science* 253, 776, **1991**
[23] Chaudhury, M. K.; Whitesides, G. M., *Science* 258, 1230, **1992**

Further information about structures, mechanisms, properties, and applications can be found in the two recent reviews.[24,25]

2.1.1.4. Copolymers at interfaces

In order to improve the wettability of polymers on solid surfaces or the compatibility between two immiscible polymers, random or block copolymers have been widely used to serve as "bridges" between two phases. The unique advantage from copolymers is that two or more distinct chemical components are connected by chemical bonds, so copolymers have "multi-functionality" which are important in designing multi-component systems. Copolymers anchored onto surfaces belong to the category of polymer brushes and will be discussed later. Some examples of copolymers located at the interface between two different polymers are provided below.

The reduction of interfacial tension between polyethylene oxide (PEO) and polypropylene oxide (PPO) was studied using either a triblock copolymer EO-PO-EO or a diblock copolymer of styrene-EO.[26] Kang *et al.*[27] reported the effects of polycarbonate (PC)-b-PMMA block copolymer on the compatibility and interfacial properties of PC / SAN (styrene-*co*-acrylonitrile copolymer) blends. With the use of an A-B-A type block copolymer synthesized from a commercial polybutadiene rubber (PBD) and an unsaturated polyester (UP) prepolymer, a better interface adhesion and an increase of localized shear yielding in the UP matrix around the rubber particles were achieved.[28] A series of well-defined phosphine oxide containing poly(ether sulfone)s were used to tune the strength of interfacial energies between two phases in toughened epoxy composites, and improved mechanical properties (i.e., fracture toughness) were contributed by the enhanced interfacial adhesion energy.[29,30]

[24] Schreiber, F., *Prog. In Surface Science* 65, 151, **2000**
[25] Wilbur, J. L., Whitesides, G. M., in Nanotechnology, Timp, G. Ed., Springer-Verlag, New York, **1999**
[26] Welge, I.; Wolf, B. A., *Polymer* 42, 3467, **2001**
[27] Kang, E. A., Kim, J. H.; Kim, C. K.; Oh, S. Y.; Rhee, H. W., *Polymer Engineering and Science* 40, 2374, **2000**
[28] Ragosta, G.; Bombace, M; Martuscelli, E.; Musto, P.; Russo, P.; Scarinzi, G., *J. of Materials Science* 34, 1037, **1999**
[29] Wang, J.; Wang, S.; Kwon, O.; Ji, Q.; McGrath, J. E.; Ward, T. C., *PMSE*, 184, 78, **1998**
[30] Wang, S.; Wang, J.; Ji, Q.; Ward, T. C.; McGrath, J. E., *J. Polym. Sci. Part B: Polym. Physics* 38, 2409, **2000**

2.1.1.5. Polymer brushes

Polymer brushes refer to an assembly of polymer chains which are tethered by one end to a surface or an interface.[31] Either homopolymers or copolymers can be used to construct polymer brushes. By carefully designing the chemical structures of polymer brushes, the modified surfaces can be tuned to have dramatically different properties, i. e., smart adhesion behaviors.[32] The detailed review will be discussed in sections 2.2, 2.3, and 2.4.

2.1.2. Characterization Techniques

2.1.2.1. Microscopic techniques (AFM, TEM, FE-SEM)

Some advantages of atomic force microscopy (AFM) for studying surface topologies and polymer thin films include its high resolution (~1 nm in lateral directions and ~ 0.1 nm in vertical direction) and easy sample preparation. Using a Digital Instrument AFM with Tapping Mode®, a height image and a phase image can be collected at the same time. While a height image gives the information about topology, a phase image can provide the information about elasticity changes at different positions. The combination of topology and phase information has proven to be extremely valuable in studies of phase behaviors of polymer thin films.[33,34]

Because of its spatial resolution of ~ 1 nm, transmission electron microscopy (TEM) has often been used to investigate the surface ordering of block copolymers.[35,36] Working on a principle of element dependent electron density, TEM can be used as a complementary tool to AFM for studying polymer thin film micro-structure. One of the disadvantages of TEM is that, usually, the specimen requires microtoming and staining to enhance the contrast. It is also very difficult to peel off a thin film from a substrate in order to perform a TEM experiment.

[31] Milner, S. T., *Science* 251, 905, **1991**
[32] Wang, J.; Kara, S.; Long, T. E.; Ward, T. C., *J. of Polym. Sci. Part A: Polym. Chemistry* 38, 3743, **2000**
[33] Strausser, Y. E.; Heaton, M. G., *An introduction to scanning probe microscopy*, in *American Laboratory*, May **1994**
[34] Karim, A; Douglas, J. F.; Satija, S. K.; Han, C. C.; Goyette, R. J., *Macromolecules* **1999**, 32, 1119
[35] Ishizu, K.; Fukuyama, T., *Macromolecules*, **1989**, 22, 244
[36] Goldacker, T.; Abetz, V.; Stadler, R.; Erukhimovich, I.; Leibler, L., *Nature* **1999**, 398, 137

Field-Emission Scanning Electron Microscopy (FE-SEM) is a relatively new technique for the study of polymer surfaces.[37] FE-SEM has much higher resolution (~1 nm) than traditional SEM (~100 nm). Furthermore, FE-SEM works with a very low electron voltage, which prevents polymer thin films from high energy damage during the experiment. Another benefit, which is good for thin film topology studies, is that there is little or no sputtering process is needed for sample preparation.

2.1.2.2. X-ray Photoelectron Spectroscopy (XPS)

Since the first use of XPS to probe polymer surfaces by Clark and co-workers[38], it has become a standard, quantitative tool for their characterization. The energy-analyzed electrons, photoemitted during irradiation of a solid sample by monochromatic X-rays, exhibit sharp peaks which correspond to the binding energies of core-level electrons in the sample. The peaks of these binding energies can be used to identify the chemical constituents in the specimen.

The mean free path of electrons in solids is very short ($\lambda \sim 2.3$ nm).[39] The effective sampling depth, Z, of XPS can be calculated by $Z = 3\lambda \cos\theta$, where θ is the angle between the surface normal and the emitted electron path to the analyzer. So the maximum depth that can be probed is about 7 nm at $\theta = 0$. For typical atomic components of polymers, C, N, and O, optimized XPS can detect compositions of 0.2 atom percent.[42] XPS is also very sensitive to F and Si. Such quantitative information is very useful in understanding polymer surface behaviors.

2.1.2.3. Contact Angle

Contact angle measurements provide a simple but very useful surface characterization technique. First, a droplet of fluid (deionized water and CH_2I_2 are used in this thesis) is placed on the surface of a specimen. The angle formed between the surface plane and tangent to the surface of the drop is measured. The contact angle depends upon the difference between the solid-vapor and liquid-solid interfacial tension divided by the liquid-vapor interfacial tension. Thus, the contact angle reveals surface

[37] Russell, T. P.; Karim, a.; Mansour, A.; Felcher, G. P., *Macromolecules* **1988**, 21, 1890
[38] Clark, D. T.; Thomas, H. R., *J. Polym. Sci. Polym. Chem. Ed.* **1977**, 15, 2843
[39] Bhatia, W. S.; Pan, D. H.; Koberstein, J. T., *Macromolecules* **1988**, 21, 2166

energetics. Simply by knowing whether or not a fluid wets a surface can give important information on the surface features of a multi-component polymer system. Detailed procedures of contact angle measurements will be discussed in the experimental section of Chapter 5.

2.1.2.4. Dynamic Secondary Ion Mass Spectrometry (DSIMS)

In 1989, Russell and co-workers[40] successfully implemented DSIMS to study homopolymer interdiffusion. Since that time, DSIMS has been a valuable tool for many research groups, notably, those of Kramer[41] and Wool[42] for the characterization of the surface and interfacial behavior of polymers.

Experimentally, a primary ion beam sputters neutral and ionized atomic and polyatomic particles from the surface over an area of ~ 500 μm ×500 μm. As material is sputtered from the surface, a crater is formed whose base gradually penetrates into the specimen. The center of the crater is sputtered with a uniform current density so that depth profiling proceeds parallel to the surface of the film. The secondary ions sputtered from a selected area at the center of the crater, typically ~ 80 μm in diameter, are extracted, energy analyzed, and mass separated with the use of a mass spectrometer. DSIMS can measure elemental variations as a function of depth with a resolution at ~ 5 – 10 nm.

While DSIMS is straightforward to interpret, it does have several drawbacks. For example, it is not easy to calibrate the sputtering time with the depth, especially for those multi-component systems whose composition varies with depth. Also, the ^{1}H signal can be obscured sometimes by the background ^{1}H signal arising from the residual water within the spectrometer. So very careful experimental design, e.g., good depth calibration, is often needed.

[40] Russell, T. P.; Coulon, G.; Deline, V. R.; Miller, D. C., *Macromolecules* **1989**, 22, 4600
[41] Yokoyama, H.; Kramer, E.; Hajduk, D. A.; Bates, F. S., *Macromolecules*, **1999**, 32, 3353
[42] Agrawal, G.; Wool, R. P.; Dozier, W. d.; Felcher, G. P.; Zhou, J.; Pispas, S.; Mays, J. W.; Russell, T. P., *J. Poly. Sci. B. Poly. Phys*. **1996**, 34, 2919

2.1.2.5. Forward Recoil Spectroscopy (FRES)

Kramer and co-workers[43,44] pioneered the use of FRES for the investigation of polymeric materials in studies on polymer interdiffusion.

A monoenergetic beam of He ions with an energy in the MeV range impinges on a specimen with an incidence angle α. The incident ions undergo kinetic collisions with nuclei within the specimen, which result in the recoiling of some of the nuclei. An energy-sensitive detector is placed at an angle θ with respect to the incident ion beam, which records the number of recoiling nuclei as a function of energy. The energies of the detected recoiling nuclei are dependent upon the mass of the target nuclei and the distance of the target nuclei from the surface.

The depth resolution of FRES is ~ 80 nm. Sokolov *et al.*[45] have shown that the resolution can be improved to ~ 30 nm by removing the stopper foil and using a time of flight geometry to effectively discriminate between the forward scattered He ions and the recoiling nuclei.

2.1.2.6. Neutron and X-ray Reflectivity

Neutron reflectivity and X-ray reflectivity have been applied to the study of polymers for the past 10 years.[46] Recently, there have been some applications relating to polymer thin films.[47,48]

The neutron or X-ray refractive index of a specimen is given by

$$n = 1-\delta + i\beta$$

where the imaginary component of the refractive index results from absorption.

Experimentally, the measurement of the reflectivity is straightforward. Radiation impinges on a surface at an angle θ and the number of neutron or X-rays reflected at an angle θ are measured. Variation of the scattering length density within the specimen will

[43] Green, P. F.; Mills, P. J.; Kramer, E. J., *Polymer* **1986**, 27, 1063
[44] Smith, J. W.; Kramer, E. J.; Mills, P. J., J. *of Poly.Sci. B Poly. Phys*. **1994**, 32, 1731
[45] Sokolov, J.; Rafailovich, M. H.; Jones, R. A. L.; Kramer, E. J., *Appl. Phys. Lett*. **1989**, 54, 5990
[46] Yokoyama, H.; Kramer, E.; Hajduk, D. a.; Bates, F. S., *Macromolecules*, **1999**, 32, 3353
[47] Agrawal, G.; Wool, R. P.; Dozier, W. d.; Felcher, G. P.; Zhou, J.; Pispas, S.; Mays, J. W.; Russell, T. P., *J. Poly. Sci. B. Poly. Phys*. **1996**, 34, 2919
[48] Karim, A; Douglas, J. F.; Satija, S. K.; Han, C. C.; Goyette, R. J., *Macromolecules* **1999**, 32, 1119

modify the reflectivity profile, which can be analyzed by modeling the density profile and fitting to the observed data.

Neutron reflectivity and X-ray reflectivity can have a high depth resolution of 1 nm. However, it is important to remember that reflectivity yields the transform of the concentration gradient within the specimen. This, by nature of the inverse problem, can lead to some uncertainty in the interpretation of the results in that more than one model concentration profile could describe the observed reflectivity. Thus in most cases, it is mandatory to have independent information to quantitatively interpret reflectivity data.

2.1.2.7. ATR-FTIR

Another example of a well-developed routine surface characterization technique is infrared attenuated total reflection (ATR)-FTIR, which has been demonstrated to be very useful in polymer brush studies.[49]

Fourier-transform infrared spectroscopy in combination with attenuated total reflection (ATR) enables one to characterize very thin surface films.[50] The ATR technique is based on the presence of an evanescent wave (i.e., an exponentially decaying standing wave) that is produced upon total reflection. Only the region over which the evanescent wave extends (~ 1 nm) is sampled.[51] Recently, Chen and Gardella[52] used ATR-FTIR to study the surface structure of polymer thin films coated on an ATR prism. Beek and his coworkers[53] studied polymer adsorption and desorption on / from an oxidized silicon surface by using ATR-FTIR. Zhao *et al*.[54] used ATR-FTIR to monitor the grafting density of polymer brushes on a Si prism.

[49] Zhao, B.; Brittain, W. J., *J. A. C. S*. **1999**, 121, 3557
[50] Iwamoto, R.; Ohta, K., *Appl. Spectrosc*. **1984**, 3, 359
[51] Peyser, P.; Stromberg, R. R.; *J. Phys. Chem.* **1967**, 71, 2066
[52] Chen, J. X.; Gardella, J. A., *Macromolecules*, **1998**, 31, 9328
[53] van der Beek, G. P.; Cohen, M. A.; Fleer, G. J., *Macromolecules*, **1991**, 24, 3553
[54] Zhao, B.; Brittain, W. J., *J. A. C. S*. **1999**, 121, 3557

2.2. Characteristics of Polymer Brushes

2.2.1. General Background of Polymer Brushes

The term "polymer brushes" refers to an assembly of polymer chains which are tethered by one end to a surface or an interface.[55,56,57] Figure 2.1 shows a general model for a polymer brush system.

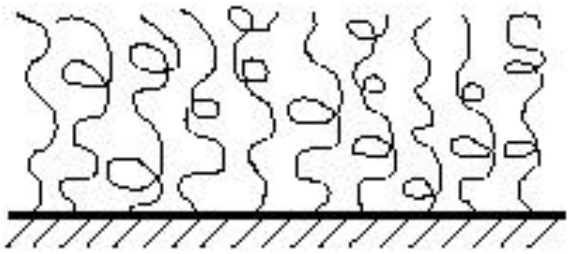

Figure 2.1. A general model for a polymer brush system

The study of polymer brushes extends into many fields, including physics, chemistry, biology, material science and engineering. Polymer brushes (or tethered polymers) first attracted attention in the 1950s when it was found that grafting polymer molecules to colloidal particles was a very effective way to prevent flocculation.[58,59,60] Subsequently it was found that polymer brushes can be useful in other applications such as new adhesive materials[61,62], protein-resistant biosurfaces[63], chromatographic devices[64], lubricants[65], polymer surfactants and polymer compatibilizers.[66] Tethered polymers which possess a lower critical solution temperature (LCST) exhibit different wetting properties above and below their LCST.[67] A very promising field that has been

[55] Milner, S. T., *Science* 251, 905, **1991**
[56] Halperin A, Tirrell M, Lodge TP. *Adv. Polym. Sci.* **1992**, 100, 31.
[57] Szleofer I, Carignano MA. *Adv. Chem. Phys.* **1996**, 94, 165.
[58] Van der Waarden M. *J. Colloid Sci.* **1950**, 5, 317.
[59] Mackor E. L. *J. Colloid Sci.* **1951**, 6, 492.
[60] Clayfield E. J., Lumb EC. *J. Colloid Interface Sci.* **1966**, 22, 269.
[61] Raphael, E.; de Gennes, P. G., *J. Phys. Chem.* 96, 4002, **1992**
[62] Ji. H.; de Gennes, P. G., *Macromolecules* 26, 520, **1993**
[63] Amiji M, Park K J. *Biomater. Sci. Polym. Ed.* **1993**, 4, 217.
[64] Van Zanten J. H. *Macromolecules* **1994**, 27, 6796.
[65] Joanny J-F. *Langmuir* **1992**, 8, 989.
[66] Milner, S. T., *Science* 251, 905, **1991**
[67] Takei Y. G., Aoki T, Sanui K, Ogata N, Sakurai Y, Okano T. *Macromolecules* **1994**, 27, 6163.

extensively investigated is one using polymer brushes as chemical gates. Ito et al.[68,69,70] have reported pH sensitive, photosensitive, oxidoreduction sensitive polymer brushes covalently tethered on porous membranes, which are used to regulate the liquid flow rate through porous membranes. Suter and coworkers[71] have prepared polystyrene brushes on high surface area mica for the fabrication of organic–inorganic hybrids. Cation-bearing peroxide free-radical initiators were attached to mica surfaces via ion exchange and used to polymerize styrene. This process is important in the field of nanocomposites. Patterned thin organic films could be useful in microelectronics[72], cell growth control[73,74], biomimetic material fabrication[75], micro-reaction vessel and drug delivery.[76]

2.2.2. Types of Polymer Brush Systems

Generally, polymer brushes can be grouped based on three different standards: the type of substrate, the chemical compositions of tethered polymer chains, and the tethering method. Recently, more and more novel polymer brushes have been designed by taking advantage of the combination of the characteristics of different classic polymer brush systems, and the boundary among those classes is no longer as clear as before.

[68] Ito Y., Ochiai Y., Park Y. S., Imanishi Y. *J Am. Chem. Soc.* **1997**, 119, 1619.
[69] Ito Y., Park Y. S., Imanishi Y. *J. Am. Chem. Soc.* **1997**, 119, 2739.
[70] Ito Y., Nishi S. W., Park Y. S., Imanishi Y. *Macromolecules* **1997**, 30, 5856.
[71] Velten, U., Shelden, R. A., Caseri, W. R., Suter, U. W., Li, Y. Z. *Macromolecules* **1999**, 32, 3590.
[72] Niu Q. J., Fre´chet J. M. J. *Angew Chem, Int Ed Engl* **1998**, 37, 667.
[73] Singhvi R., Kumar A., Lopez G. P., Stephanopoulos G. N., Wang D. I. C., Whitesides G. M., Ingber D. E. *Science* **1996**, 273, 892.
[74] Chen C. S., Mrksich M., Huang S., Whitesides G. M., Ingber D. E. *Science* **1997**, 276, 1425.
[75] Aksay A., Trau M., Manne S., Honma I., Yao N., Zhou L., Fenter P., Eisenberger P. M., Gruner S. M. *Science* **1996**, 273, 892.
[76] Balazs A. C., Singh C., Zhulina E., Gersappe D., Pickett G. *MRS Bull* **1997**, 16, 1.

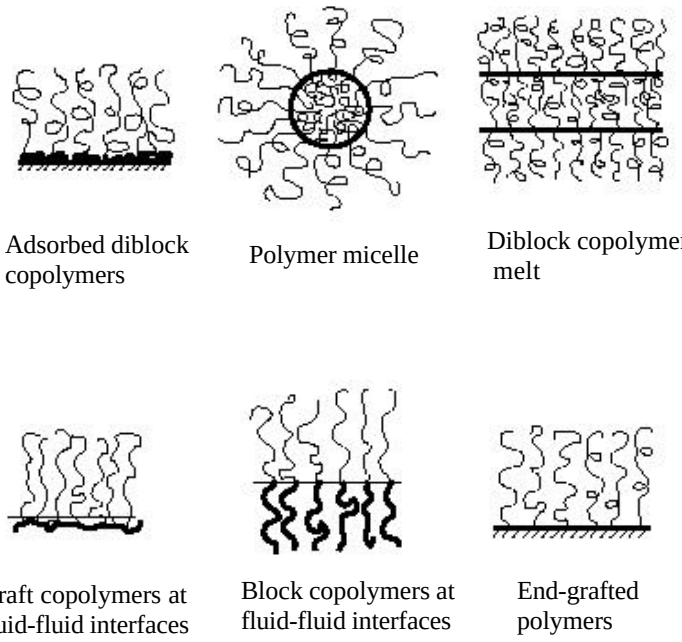

Figure 2.2 Examples of polymer systems comprising polymer brushes.[77]

The polymer brush is a central model for many practical polymer systems such as polymer micelles, block copolymers at fluid–fluid interfaces (e.g. microemulsions and vesicles), grafted polymers on a solid surface, adsorbed diblock copolymers and graft copolymers at fluid–fluid interfaces. All of these systems, illustrated in Fig. 2.2, have a common feature: the polymer chains exhibit deformed chain configurations (shapes) when contrasted to an untethered chain. Solvent can be either present or absent in polymer brushes. In the presence of a good solvent, the polymer chains try to avoid contact with each other to maximize contact with solvent molecules. With solvent absent (melt conditions) polymer chains must stretch away from the interface to avoid overfilling incompressible space.

The interface to which polymer chains are tethered in the polymer brushes may be a solid substrate surface or an interface between two liquids, between a liquid and air, or between melts or solutions of homopolymers. The remainder of this review will be restricted to polymer brushes on *solid substrate surfaces*.

[77] Zhao, B.; Brittain, W. J., *Progress in Polymer Science* **2000**, 25, 677

In terms of polymer chemical compositions, polymer brushes tethered on a solid substrate surface can be divided into homopolymer brushes, mixed homopolymer brushes, random copolymer brushes and block copolymer brushes. These different polymer brushes are illustrated in Fig. 2.3. The homopolymer brushes are an assembly of tethered polymer chains consisting of one type of repeat unit. Binary homopolymer brushes are composed of two types of homopolymer chains.[78] Random copolymer brushes refer to an assembly of tethered polymer chains consisting of two different repeat units, which are randomly distributed along the polymer chain.[79] Block copolymer brushes refer to an assembly of tethered polymer chains consisting of two or more homopolymer chains covalently connected to each other at one end.[80] Homopolymer brushes can be further divided into neutral polymer brushes and charged polymer brushes. They may also be classified in terms of rigidity of the polymer chain and would include flexible polymer brushes, semiflexible polymer brushes and liquid crystalline polymer brushes, as illustrated.

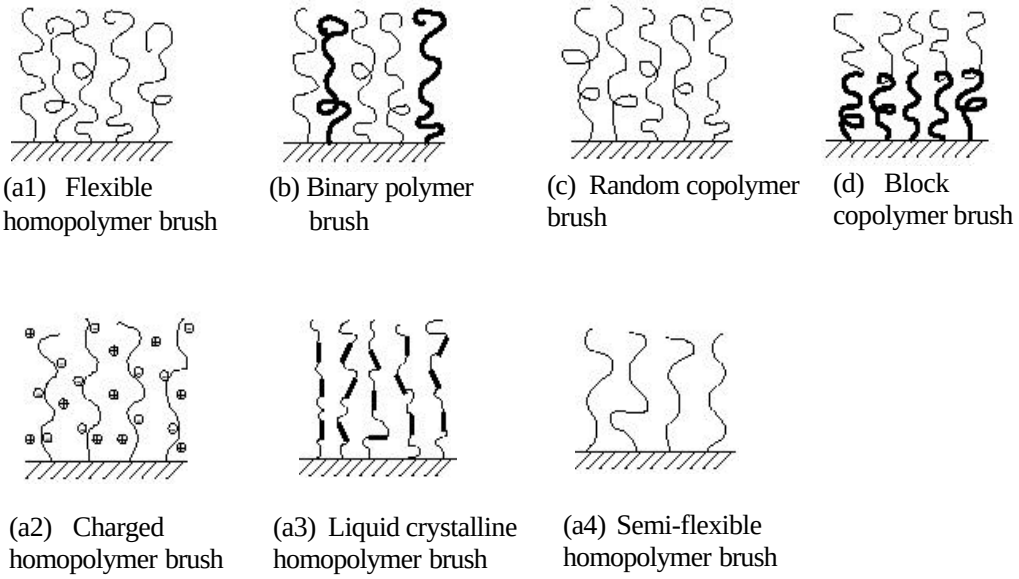

Figure 2.3 Polymer brushes with different chemical compositions, (a1-a4) homopolymer brushes; (b) binary polymer brush; (c) random copolymer brush; (d) block copolymer brush.

[78] Soga K., Zuckermann M. J., Guo H. *Macromolecules* **1996**, 29, 1998.
[79] Mansky P., Liu Y., Huang E., Russell T. P., Hawker C. J. *Science* **1997**, 275, 1458.
[80] Zhao B., Brittain W. J. *J. Am. Chem. Soc.* **1999**, 121, 3557.

2.2.3. Preparation of Polymer Brushes

Generally, there are two ways to fabricate polymer brush chains onto a solid surface: physisorption and covalent attachment (see Fig. 2.4).

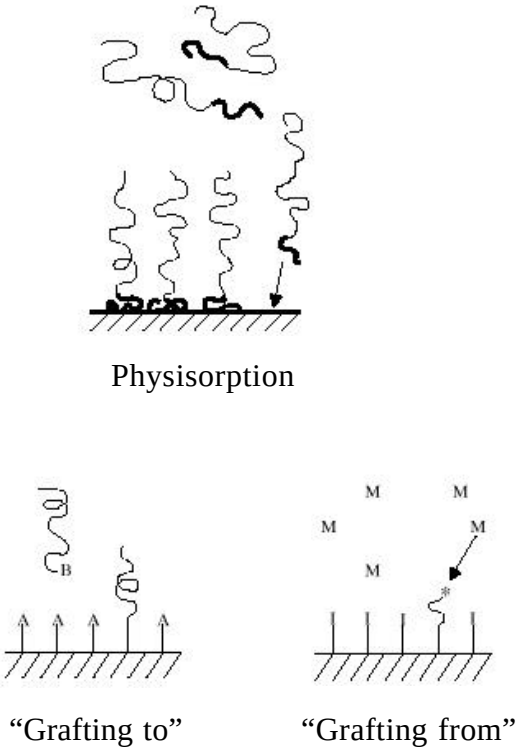

Figure 2.4. Different polymer brush fabrication methods.

In the case of polymer physisorption, block copolymers adsorb onto a suitable substrate with one block interacting strongly with the surface and the other block interacting weakly with the substrate. Covalent attachment can be accomplished by either "grafting to" or "grafting from" approaches. In a "grafting to" approach, preformed end-functionalized polymer molecules react with an appropriate substrate to form polymer brushes. A polymer brush prepared by "grafting to" can have well-defined polymer chain structures, since those polymer chains were pre-synthesized before the tethering. However, these usually do not have high graft density because of diffusion problems.[81] On the other hand, in the "grafting from" approach, in which polymerization

[81] Zhao, B.; Brittain, W. J., *Progress in Polymer Science* **2000**, 25, 677

happens on a surface with immobilized initiators, it is possible to get high grafting density. However, while this method suffers from the difficult control and characterization of polymer molecular weight and distribution. Recent progress in polymer synthesis techniques has shown that it is possible to produce polymer chains with controllable lengths from the "grafting from" mode, which makes the approach a very attractive one. Nevertheless, the "grafting to" approach is still an important method, because it is possible to incorporate multi-functionality into the polymers via sophisticated synthesis techniques, as evidenced by the recent work of Wang *et al.*[82]

Some literature results on different polymer brush preparation methods are reviewed below.

2.2.3.1. Preparation of polymer brushes by physisorption

Physisorption is a reversible process and is achieved by the self-assembly of polymeric surfactants or end-functionalized polymers on a solid surface.[83] The surface grafting density and all other characteristic dimensions of the structure are controlled by thermodynamic equilibrium, albeit with possible kinetic effects.[84]

Physisorption of block copolymer or graft copolymer usually occurs in the presence of selective solvents or selective surfaces, giving rise to selective solvation and selective adsorption, respectively. The detailed polymer brush structure depends on the selectivities of these media and the nature of the copolymers, the architecture of copolymers, the length of each block and the interactions between blocks and surface. In the case of selective solvents[85], an ideal solvent is a precipitant for one block which forms an "anchor" layer on the surface and a good solvent for the other block which forms polymer brushes in the solution. In the case of a selective surface[86], one block is preferentially adsorbed on the surface and the other one forms the polymer brush.

[82] Wang, J.; Kara, S.; Long, T. E.; Ward, T. C., *J. of Polym. Sci. Part A: Polym. Chemistry* 38, 3743, **2000**
[83] Bug A. L. R., Cates M. E., Safran S. A., Witten T. A. *J Chem Phys* **1987**, 87, 1824.
[84] Halperin A., Tirrell M., Lodge T. P. *Adv Polym Sci* **1992**, 100, 31
[85] Parsonage E., Tirrell M., Watanabe H., Nuzzo R. *Macromolecules* **1987**, 24, 1987
[86] Guzonas D., Boils D., Hair M. L. *Macromolecules* **1991**, 24, 3383

Using PS-b-PEO to form polymer brushes on silicon wafers by adsorption from toluene, Motschmann *et al*.[87] studied the adsorption kinetics and adsorption isotherm. Their experimental results revealed that the adsorption kinetics show two processes on a clearly separated time scale. In the beginning, the adsorption process was diffusion controlled, leading to a surface coverage with small interaction between chains. A denser brush was formed by the penetration of chains through the existing monolayer combined with the conformation rearrangement.

Preparation of polymer brushes by adsorption of a block copolymer from a selective solvent (or on a selective surface) is not difficult. However, the polymer brushes exhibit thermal and solvolytic instability due to the weak interactions between the substrate and the block copolymers.[88] The interactions in most cases are van der Waals forces or hydrogen bonding. Desorption could occur upon exposure to other good solvents. Or, the adsorbed polymers are displaced by other polymers or other low molecular weight compounds. If these polymer ultra-thin films are heated to a high temperature (e.g. above glass transition temperature or melting temperature), dewetting occurs and the polymer films are no longer homogeneous due to formation of polymer droplets.[89,90] Some of these drawbacks could be overcome by covalently tethering polymer chains to substrates.

2.2.3.2. Preparation of polymer brushes by "grafting to"

The "grafting to" approach refers to preformed, end-functionalized polymers which react with a suitable substrate surface under appropriate conditions to form a tethered polymer brush. The covalent bond formed between surface and polymer chain makes the polymer brushes robust and resistant to common chemical environmental conditions. This method has been used often in the preparation of polymer brushes. End-functionalized polymers with a narrow molecular weight distribution can be synthesized by living anionic, cationic, radical, group transfer and ring opening metathesis

[87] Motschmann H., Stamm M., Toprakcioglu C. *Macromolecules* **1991**, 24, 3681
[88] Fleer G. J., Cohen-Stuart M. A., Scheutjens J. M. H., Cosgrove T., Vincent B. Polymers at interfaces. London: Chapman and Hall, 1993
[89] Zerushalmi-Royen R., Klein J., Fetters L. *Science* **1994**;263:793.
[90] Reiter G. *Europhys Lett* **1996**;33:29.

polymerizations. The substrate surface also can be modified to introduce suitable functional groups by coupling agents or SAMs.

Koutsos *et al.* [91] synthesized a series of thiol-terminated polystyrenes with a low polydispersity (~1.2) by anionic polymerization. Chemically end-grafted polystyrene chains on a gold surface were prepared by exposing the gold substrate to a toluene solution of these polymers. Microphase separation of polymer monolayer into globular clusters was observed at higher surface coverage. It was found that the sizes of these clusters were consistent with the scaling laws, which were predicted for pinned micelles.

Mansky *et al.*[92] synthesized a series of hydroxy-terminated random copolymers of styrene and methyl methacrylate with different ratios by a "living" radical polymerization. These end-functionalized polymers were reacted with silanol groups on the silicon wafer surface under vacuum at 140°C to form tethered random copolymer brushes. They found that a random copolymer brush with a specific composition provided a surface with no preferential affinity for either a PS component or a PMMA component. This surface has been successfully used to control the domain orientation of PS-*b*-PMMA films spin coated on this copolymer brush surface.

Using a similar strategy, Bergbreiter *et al.*[93] tethered terminally functionalized poly(*ter*t-butyl acrylate) onto oxidized polyethylene films. Yang *et al.*[94] prepared vinyl-terminated SAMs on silicon surfaces and used hydrosilation reaction to covalently tether poly(methylhydrosiloxane) and its derivatives onto the solid surface. Ebata *et al.*[95] synthesized end-grafted polysilane on quartz surfaces by the "grafting to" approach and characterized the tethered polysilane by UV spectroscopy. Poly(amido-amine) dendrimers were also successfully tethered to a mercaptoundecanoic acid SAM.[96] Tran *et al.*[97] studied the structure of polyelectrolyte brushes that were prepared by the attachment of trichlorosilyl-functionalized PS to a substrate followed by sulfonation of the tethered PS.

[91] Koutsos V, Van der Vegte E. M., Hadziioannou G. *Macromolecules* **1999**;32:1233
[92] Mansky P., Liu Y., Huang E., Russell T. P., Hawker C. J. *Science* **1997**;275:1458
[93] Bergbreiter DE, Franchina JG, Kabza K. *Macromolecules* **1999**;32:4993
[94] Yang X, Shi J, Johnson S, Swanson B. *Langmuir* **1998**;14:1505.
[95] Ebata K, Furukawa K, Matsumoto N. *J Am Chem Soc* **1998**;120:7367.
[96] Wells M, Crooks RM. *J Am Chem Soc* **1996**;118:3988

Prucker *et al.*[98] prepared surface-immobilized polymer films by a photochemical process. A silicate surface was modified with 4-(30 chlorodimethylsilyl)propyl-oxybenzophenone followed by deposition of a polystyrene or poly(ethyloxazoline) film. Illumination with UV light produced a covalently bound film via a photochemical attachment. Typically, several nanometers of polymeric overcoat could be attached.

Ward and coworkers[99] recently reported the first fabrication of covalently bonded central functionalized asymmetric tri-block copolymer brush systems. A novel well-defined tri-block copolymer of PS-PSSi-PMMA (defined in Chapter 3) was synthesized by sequential living anionic polymerization and polymer modification, and the polymer brush modified surfaces demonstrated switchable properties because of the multi-functionalities incorporated in the copolymers.

2.2.3.3. Preparation of polymer brushes by "grafting from"

The "grafting from" approach has attracted considerable attention in recent years in the preparation of tethered polymers on a solid substrate surface. The initiators are immobilized onto the surface followed by *in situ* surface initiated polymerization to generate tethered polymers.

Using plasma and glow-discharge treatment to introduce initiators onto substrate surfaces, Ito *et al.*[100] prepared tethered poly(γ-benzyl l-glutamide) and poly(glutamic acid) on porous PTFE membranes as pH-sensitive chemical gates.

Radical polymerization was intensively used to prepare polymer brushes. Some interesting examples follow. Biesalski *et al.*[101] prepared and characterized a tethered cationic polyelectrolyte monolayer [poly(4-vinyl-N-n-butylpyridinium) bromide] on a flat silicate substrate. Peng *et al.*[102] reported the synthesis of polymer brushes with liquid crystalline (LC) chains. The immobilization of radical initiators usually involved a series of steps[103], which makes it very difficult to characterize the exact composition of the

[97] Tran Y, Auroy P, Lee LT. *Macromolecules* **1999**;32:8952
[98] Prucker O, Naumann CA, Ruhe J, Knoll W, Frank CW. *J Am Chem Soc* **1999**;121:8766.
[99] Wang, J.; Kara, S.; Long, T. E.; Ward, T. C., *J. of Polym. Sci. Part A: Polym. Chemistry* 38, 3743, **2000**
[100] Ito Y, Ochiai Y, Park YS, Imanishi Y. *J Am Chem Soc* **1997**;119:1619
[101] Biesalski M, Ruhe J. *Macromolecules* **1999**;32:2309
[102] Peng B, Johannsmann D, Ruhe J. *Macromolecules* **1999**;32:6759
[103] Boven G, Oosterling MCLM, Challa G, Schouten AJ. *Polymer* **1991**;31:2377

initial layer. To circumvent this problem, Ruhe and coworkers[104] reported a strategy in which the complete initiator was attached to the substrate's surface in one step by SAM techniques.

In order to achieve better control of molecular weight and molecular weight distribution and synthesize novel polymer brushes like block copolymer brushes, controlled radical polymerizations including ATRP, reverse ATRP, and TEMPO-mediated radical polymerizations have been used to synthesize tethered polymer brushes on solid substrate surfaces.[105,106] Some other polymerization methods were also reported, such as carbocationic polymerization[107,108], living anionic polymerization[109], ring-opening metathesis polymerization (ROMP)[110], and group transfer polymerization (GTP)[111], etc.

2.3. Theory and Modeling of Polymer Brushes

2.3.1. Alexander-de Gennes model — chain configuration in homopolymer brushes

As shown by Alexander and de Gennes in their pioneering work on polymer brushes[112,113], the behavior of such end-grafted chains is qualitatively different from that of free chains. For a polymer brush in a good solvent, for instance, the average layer thickness, L, is expected to vary *linearly* with the index of polymerization of the chains, N, while the average radius, R, of a free chain in a dilute solution varies as $R \propto N^{3/5}$. The Alexander-de Gennes model was first established using scaling theory, and this has been followed more recently by self-consistent field (SCF) calculations[114,115] and by computer simulations.[116,117] Several review articles on the subject are now available.[118,119]

---

[104] Biesalski M, Ruhe J. *Macromolecules* **1999**;32:2309
[105] Benoit D, Chaplinski V, Hawker CJ. *J Am Chem Soc* **1999**;121:3904
[106] Weimer MW, Chen H, Giannelis EP, Sogah DY. *J Am Chem Soc* **1999**;121:1615
[107] Jordan R, Ulman A. *J Am Chem Soc* **1998**;120:243
[108] Zhao B, Brittain WJ. *Macromolecules* **2000**;33:342
[109] Ingall MDK, Honeyman CH, Mercure JV, Bianconi PA, Kunz RR. *J Am Chem Soc* **1999**;121:3607
[110] Buchmeiser MR, Sinner F, Mupa M, Wurst K. *Macromolecules* **2000**;33:32
[111] Huber DL, Gonsalves KE, Carlson G, Seery TAP. In: Lohse DJ, Russell TP, Sperling LH, editors. Interfacial aspects of multicomponent polymer materials, New York: Plenum Press, 1997
[112] Alexander, S., *J. Phys. (Paris)* **1977**, 38, 977
[113] de Gennes, P. G., *Macromolecules*, **1980**, 13, 1069
[114] Cosgrov, T.; Heath, T.; van Lent, B.; Leermakers, f.; Scheutiens, J., *Macromolecules* **1987**, 20, 1692
[115] Zhulina, E. B.; Borisov, O. V.; Pryamitsyn, V. A., *J. Colloid Interface Sc*i. **1990**, 137, 495
[116] Murat, M.; Grest, G. S., *Macromolecules*, **1989**, 22, 4054

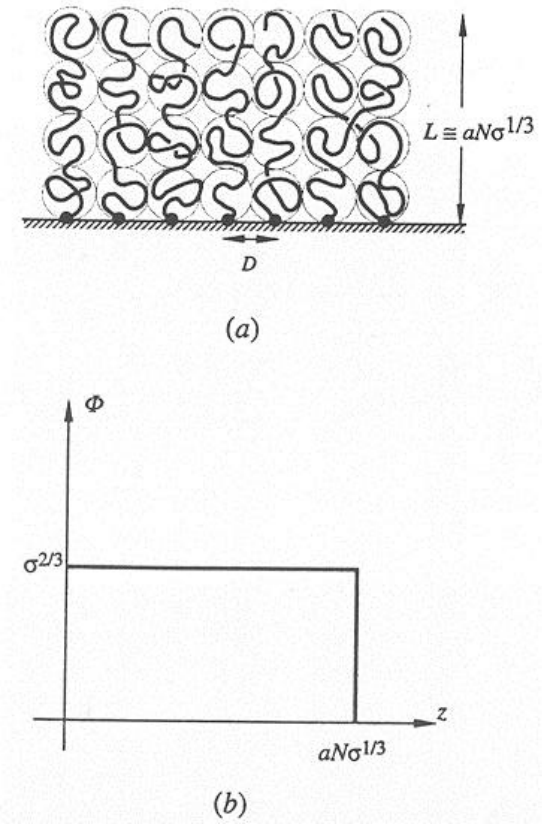

Figure 2.5. a) Schematic representation of a polymer brush. L is the layer thickness and D the average spacing between two grafting points. b) The monomer density profile ϕ vs distance from the grafting plane z according to the Alexander-de Gennes model.[120]

Alexander[121] was one of the first scientists who noted the distinctive properties of polymer brushes through his theoretical analysis concerning the end-adsorption of terminally functionalized polymers on a flat surface. Further elaboration by de Gennes[122] and by Cantor[123] stressed the utility of tethered chains to for describing self-assembled block copolymers. A brief description of their model is now given, and reference to figure 2.5 will be helpful.

[117] Lai, P. Y.; Binder, K., *J. Chem. Phys*. **1991**, 95, 9299
[118] Grest, G. S.; Murat, M., in Monte Carlo and Molecular Simulations in Polymer Science Oxford University Press, New York, **1995**, p476
[119] Milner, S. T., *Science* **1991**, 251, 905
[120] Aubouy, M.; Guiselin, O.; Raphael, E., *Macromolecules* **1996**, 29, 7261
[121] Alexander SJ. *J Phys (Paris)* **1977**;38:977
[122] de Gennes PG. *Macromolecules* **1980**;13:1069.
[123] Cantor R. *Macromolecules* **1981**;14:1186.

The configurational space of the polymer chains is limited by the presence of an interface in the case of polymer brushes. The deformation of densely tethered polymer chains reflects a balance between interaction and elastic free energies. Dense tethering of polymer chains on an interface enforces a strong overlap among the undeformed coils, increases the monomer–monomer unit contacts and the corresponding interaction energy. The polymer chains are forced to stretch away along the direction normal to the grafting sites, thereby lowering the monomer concentration in the layer and increasing the layer thickness, L. Stretching lowers the interaction energy per chain, F_{int}, at the price of a high elastic free energy, F_{el}. The interplay of these two terms determines the equilibrium thickness of the layer.

It is easy to use the Alexander-de Gennes model to clarify this argument.[124] The Alexander-de Gennes model considers a flat, non-adsorbing surface to which monodisperse polymer chains are tethered. The polymer chains consist of N statistical segments of diameter a. The average distance between the tethering points is d, which is much smaller than the radius of gyration of a free, undeformed chain. The free energy per chain includes two terms:

$$F = F_{int} + F_{el} \qquad (2.1)$$

F_{int} refers to the interaction energy between two statistical segments and F_{el} refers to the elastic free energy. Two assumptions are made to enable simple expressions for these two terms. The first one is that the depth profile of statistical segments is step-like (see Fig. 2.5). The concentration of statistical segments is a constant within brushes, $phi = Na^3 / d^2$ L. The second assumption is that all free ends of tethered polymer chains are located in the single plane at a distance L from the tethering surface.

The "Flory approximation"[125] is used to obtain an explicit expression for free energy. This argument estimates the reduction in configurational entropy from results for an ideal random walk chain constrained to travel a distance L from the grafting surface to the outer edge of the polymer brush. The corresponding free energy per chain can be expressed in the following equation:

$$\mathrm{F} / kT = v\,(phi)^2\, d^2\, \mathrm{L} / a^3 + L^2 / R_0{}^2 \qquad (2.2)$$

[124] Halperin A, Tirrell M, Lodge TP. *Adv Polym Sci* **1992**;100:31
[125] Flory, P. J., Principles of polymer chemistry. Ithaca, NY: Cornell University Press, 1981

where v is a dimensionless excluded volume parameter and R_0 is the radius of an unperturbed, ideal coil. The first term represents the interaction energy between statistical segments and the second represents the elasticity of Gaussian chains. A "scaling argument" approach gives a similar result. The equilibrium thickness is obtained by minimization of F with respect to L and is shown in the following equation:

$$L / a = N (a / d)^{2/3} \qquad (2.3)$$

The most important and distinctive characteristic of polymer brushes expressed in Eq. (2.3) is that the equilibrium thickness varies linearly with the degree of polymerization. This is in contrast to free polymer chains in a good solvent, in which the dimension of polymer chain varies with N in a relationship of $R \sim N^{3/5}$. This is also very different from the behavior of the free polymer chains in a theta solvent where polymer chains possess an unperturbed configuration, $R_0 \sim N^{1/2}$. In conclusion, theoretical considerations demonstrate that the densely tethered polymer chains are deformed relative to the free chains. The relationship between the equilibrium thickness and degree of polymerization of polymer chains is linear. This is the origin of the novel dimensional behavior of tethered polymer brushes.

The idea of the balance of interaction energy and elastic free energy, the essential features in the Alexander - de Gennes model, can be applied to other situations involving polymer brushes in a theta solvent or a poor solvent.[126] In a theta solvent, the interaction between statistical segments disappears. The free energy per chain is expressed in the following equation:

$$F/kT = w (phi)^3 d^2 L/a^3 + L^2 / Na^2 \qquad (2.4)$$

where w is a dimensionless third virial coefficient. The relationship between the equilibrium thickness and N can be obtained by minimization of free energy with respect to L.

$$L / a = N (a / d) \qquad (2.5)$$

It is interesting to see that the linearity of L with N is maintained in theta solvents and poor solvents. Compared to Eq. (2.3), the chains have shrunk by a factor of $(a/d)^{1/3}$, but the polymer chains are still distorted at the theta point. This is remarkably different

[126] Halperin A. *J Phys (Paris)* **1988**;49:547

from the behavior of free polymer chains in theta solvents, where as noted above the relationship between chain dimension and N is $R_0 \sim N^{1/2}$.

For a brush without solvent (melt brush), the relationship between the thickness of polymer brushes and degree of polymerization can be obtained by a similar approach. It was found that the relationship can be described by the following equation:

$$L \sim N^{2/3} \tag{2.6}$$

As indicated in Eq. (2.6), tethered polymer chains in the melt state are deformed compared to their behavior as free polymer chains in the melt state, where the relationship is again $R_0 \sim N^{1/2}$.

In conclusion, no matter whether in the presence of a good solvent, a theta solvent, a poor solvent, or in the absence of solvent (melt conditions), polymer chains in tethered polymer brushes exhibit deformed configurations. The degree of deformation of the polymer chains depends on the environmental conditions to which tethered polymer chains are exposed. The relationship between the number of statistical segments N and the dimension of tethered and free polymer chains (L and R_g, respectively) under various conditions is summarized in Table 2.1 for comparison. (Note: these deformed configurations are found under equilibrium conditions)

Table 2.1 The relationship between the dimensions of polymer chains and N under various conditions

	Tethered polymer chain	Free polymer chain
Good solvent	$L/a = N\,(a/d)^{2/3}$	$R_g \sim N^{3/5}$
Theta solvent	$L/a = N\,(a/d)$	$R_g \sim N^{1/2}$
Dry (bulk) state	$L \sim N^{2/3}$	$R_g \sim N^{1/2}$

The Alexander-de Gennes approach is a simple free energy balance argument. It does not attempt to examine the details of the conformations of polymer chains or the density profile of chain units at a distance from the grafting surface. This simple model can be used to describe the hydrodynamic properties of polymer brushes and other

properties, which also depend on perturbing the balance between chain stretching and chain–chain repulsion. Such additional properties are the hydrodynamic thickness, the permeability of a brush and the force per area required to compress a brush (either vertically or laterally). The lubrication forces that arise when two brushes are brought into near contact are also related to the hydrodynamic properties.

However, the following questions on brush structures are not well represented by the Alexander-de Gennes model. These questions include: the shape of the chain unit density, the location of the free ends of polymer chains, how the polymer chains segregate or mix in a heterogeneous polymer brush of either different chain lengths or different chemical compositions, and how the polymer chains interpenetrate each other. Considerable theoretical work beyond the simple Alexander-de Gennes model has been devoted to understanding the more detailed structure of polymer brushes. Relatively simple theoretical results have been obtained for a wide variety of brush properties and situations under conditions of strong stretching.

A simple hypothesis about free chain ends from the interface is made in newer models: the free chain ends may be located at any distance from the interface.[127] This is different from the Alexander-de Gennes model in which all chain free ends are located at the same distance from the interface. The results show that the potential of a chain is a parabola. All of the properties of the more detailed "parabolic" brush description are consistent with the scaling analysis of the Alexander-de Gennes model argument.

Experimental research has been carried out to elucidate polymer brush structures and explore their novel properties. However, it is not easy to design a very good polymer brush system and the corresponding experimental method required to prove the theoretical predictions. For end-adsorbed polymer brushes, optical probes such as evanescent waves[128], ellipsometry[129], infrared spectroscopy[130] and multiple-reflection interferometry[131] have given information equivalent to the total amount of polymer

[127] Milner ST. *Science* **1991**;251:905
[128] Allain C, Ausserr D, Rondelez F. *Phys Rev Lett* **1981**;49:1694.
[129] Sauer DB, Yu H, Kim MW. Langmuir 1989;5:278.
[130] Kawaguchi M, Kawarabayashi M, Nagata N, Kato T, Yoshioka A, Takahashi A. Macromolecules 1988;21:1059.
[131] Munch MR, Gast AP. *Macromolecules* **1990**;23:2313.

adsorbed. Many scattering experiments have been performed to investigate the structure of end-grafted polymer systems. The variation of chain unit density as a function of the distance from the tethering interface and how structure and properties change with the quality of the solvent were studied. Cosgrove *et al.*[132] performed neutron scattering experiments on short (average molecular weight M_n = 5000 g/mol) poly(ethylene oxide) chains end-grafted to 100 mm latex spheres in suspension. Neutron scattering has ample spatial resolution to observe features of the density profile. The results compared favorably to numerical calculations. Parsonage and coworkers[133] studied the adsorption of the diblock copolymer polystyrene-b-poly(4-vinylpyridine) (PS-*b*-PVP) from toluene solution onto mica and used radiolabeling techniques to measure the coverage for various PS-*b*-PVP copolymers on mica. With fixed PVP chain lengths, they found roughly constant coverage over a range of PS chain lengths and found brush heights scaling as N. This was consistent with predictions from the Alexander model (Flory argument). Patel *et al.*[134] studied a series of adsorbed block copolymers where a block strongly interacts with the surface and the other block adsorbs weakly. They determined the layer thickness from the range of the onset of detectable repulsive force exerted between the layers. The experimental results showed that for a series of copolymers of nearly constant d and variable N of the weakly adsorbed block, linearity of L with N was observed.

[132] Cosgrove T, Ryan K. *Langmuir* **1990**;6:1361
[133] Parsonage E, Tirrell M, Watanabe H, Nuzzo R. *Macromolecules* **1987**;24:1987
[134] Patel S, Hadziioannon G, Tirrell M. *Proc Natl Acad Sci USA* **1987**;84:4725

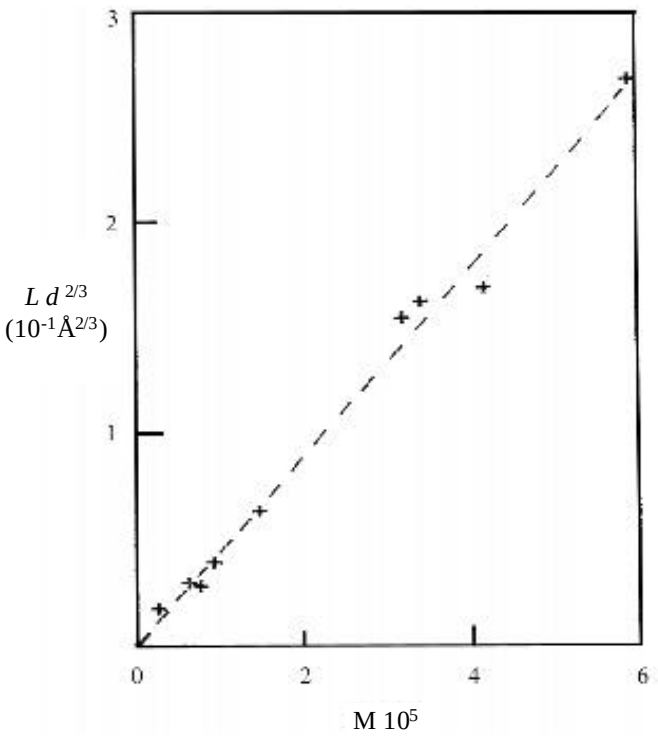

Figure 2.6. Plot of $Ld^{2/3}$ *vs* M for grafted PDMS in a good solvent (dichloromethane).[135]

The work of Auroy *et al.*[135] gave strong support to a model predicting linearity of polymer brush height with respect to the degree of polymerization of tethered polymer chains. To prepare a large amount of brush as a scattering target, they chemically end-grafted polydimethylsiloxane (PDMS) chains on porous silica particles and performed neutron scattering. Information about the total amount of adsorbed polymer and brush height was extracted from the raw data. Their results in CH_2Cl_2, a good solvent for PDMS, are illustrated in Fig. 2.6. It showed not only the linearity of the layer thickness vs. molecular weight over more than a 30-fold variation in N, but also a good agreement with the predicted inverse 2/3 power dependence on d. Molecular dynamics simulation work of Murat and Grest[136] also supported the results of the Flory argument. It is

[135] Auroy P, Auvray L, Leger L. *Phys Rev Lett* **1991**;66:719
[136] Murat M, Grest GS. *Macromolecules* **1993**;24:704

expected that more experimental data will be reported in this area soon with the results of newly developed experimental methods.

2.3.2. Theoretical studies of copolymer brushes

Extensive theoretical work on the behavior of the block copolymer brushes has been reported in the past several years.[137,138,139,140] Changing chain architecture, grafting density, whole chain length, relative chain length, interaction energy between different blocks and interaction energies between blocks and solvents have been explored. A variety of novel well-ordered structures such as "onion", "garlic", "dumbbell", flowerlike and checkerboard have been predicted using the mean field method, scaling arguments, Monte Carlo simulations and SCF lattice calculations.[141,142] The theoretical results indicate that tethered copolymer brushes on a flat substrate are an excellent candidate for forming patterned polymer films. Using a mean field method, Dong *et al*.[138] studied the phase behavior of densely tethered diblock copolymers in the melt state and observed distinct patterns of phase separation. Unique structures have also been noted in polymer brushes where attractive functional groups are attached to the free ends of the chains.[143] A "layering effect" was observed; the functional groups were localized in a layer at the top of the brush. Gersappe *et al*.[140] used Monte Carlo simulations and numerical SCF lattice calculations to study the behavior of copolymer brushes. By varying the sequence distribution of tethered linear AB copolymers, they found that brushes composed of block copolymers showed distinct lateral inhomogeneities, with large domains of A and B units. The size of these domains appears diminished in random copolymer brushes. The alternating copolymer brushes do not exhibit distinctive domains like those in block copolymer brushes. Interestingly, Zhulina *et al*.[144] considered a Y-shaped AB diblock copolymer brush system using theoretical models.

---

[137] Balazs AC, Singh C, Zhulina E, Gersappe D, Pickett G. *MRS Bull* **1997**;16:1
[138] Dong H, Marko JF, Witten TA. *Macromolecules* **1994**;27:6428
[139] Zhulina EB, Singh C, Balazs AC. *Macromolecules* **1996**;29:6338
[140] Gersappe G, Fasolka M, Israels R, Balazs AC. *Macromolecules* **1995**;28:4753
[141] Zhulina EB, Singh C, Balazs AC. *Macromolecules* **1996**;29:8254
[142] Singh C, Balazs AC. *Macromolecules* **1996**;29:8904.
[143] Gersappe G, Fasolka M, Balazs AC, Jacobson SH. *J Chem Phys* **1994**;100:1970.
[144] Zhulina, E. B.; Singh, C.; Balazs, A. C., *Macromolecules* 29, 2667, **1996**

2.3.3. Theoretical studies on other types of polymer brushes

Semiflexible polymer brushes[145], liquid crystalline polymer brushes[146], charged polymer brushes[147] and binary polymer brushes[148] have also been studied from a theoretical point of view.

For semiflexible polymer brushes on a flat substrate, polymer backbone configurations are more persistent and the segment–segment interactions have directional components. These persistent polymer backbones can be found in many synthetic polymers and biological macromolecules like DNA and RNA. The situation is different from that of flexible polymer brushes, where segmental interactions are considered to be directionally isotropic. The coupling between the angular and concentration distributions of the segments of a semiflexible polymer brush would yield many interesting features unique to persistent chains. An interesting question in a long semiflexible polymer brush is the possibility of forming a liquid-crystalline polymer brush. For spatially homogeneous worm-like chains in a good solvent, it is known that orientational interactions are responsible for inducing an isotropic–nematic phase transition.[149]

The behavior of charged polymer brushes (polyelectrolyte brushes) is another intriguing research area. This polymer brush system is more complex because of the introduction of electrostatic interactions between the grafted polymer chains. Scaling analysis of planar polyelectrolyte brushes revealed a much more complex behavior than that of neutral brushes.[150] Pincus's study[151] showed that a polyelectrolyte brush exhibits two different types of behavior depending on the degree of charge on the chain and the grafting density. It can be strongly charged, losing its mobile counterions, which leads to the scaling relationship of brush height and N as $L \sim N^3$ (Pincus regime). Or it may conserve the counterions mainly inside the brush, thus, being practically electroneutral (osmotic regime). If a salt is added into the solution and the salt concentration in solution is much higher than the concentration of counterions in the brush, then a third regime

[145] Kuznetsov DV, Chen ZY. *J Chem Phys* **1998**;109:7017
[146] Amoskov VM, Birshtein TM, Pryamitsyn VA. *Macromolecules* **1996**;29:7240
[147] Pincus P. *Macromolecules* **1991**;24:2912
[148] Soga K, Zuckermann MJ, Guo H. *Macromolecules* **1996**;29:1998
[149] Khokhlov AR, Semenov AN. *Physica A* **1981**;109:546
[150] Pryamitsyn VA, Leermakers FAM, Zhulina EB. *Macromolecules* **1997**;30:584
[151] Pincus P. *Macromolecules* **1991**;24:2912

(salt brush) is formed. The behavior of a polyelectrolyte in this regime is very similar to that of a neutral brush, although the electrostatic interaction is dominant. The interactions in the brush can be described by an effective second virial coefficient incorporating both nonelectrostatic and electrostatic interactions. Israels *et al*.[152] described numerical results from an SCF model for the structure and scaling behavior of charged polymer brushes. Their studies showed that the "Pincus regime" is too small to be detected.

Binary polymer brushes have also been extensively studied.[153,154] Marko *et al*.[155] used the SCF theory to examine the equilibrium properties of a binary polymer brush composed of immiscible chains under melt conditions. For two homopolymers with sufficiently high immiscibility, two possible ordered phases were studied: a "rippled" phase described in terms of a "density wave" in composition directed along the surface, which was equivalent to lateral microphase separation; and a "layered" phase rich in one component at the bottom of the brush and rich in the second component at the top of the brush. Their results showed that the density wave was expected to be observed. Soga *et al*.[156] used a coarse-grained simulation method that involved direct calculation of the Edward's Hamiltonian to study the behavior of binary polymer brushes in a solvent. They found that if two components were sufficiently immiscible, lateral binary microphase separation occurred over a wide range of solvent conditions. The onset of phase separation was delayed as solvent quality increased. Under poor solvent conditions they found interesting structural variations as a result of the combination of phase separation from solvent and phase separation of the two components.

Although extensive theoretical research work has been carried out on semiflexible polymer brushes, liquid crystalline polymer brushes and binary polymer brushes, few experimental results regarding such polymer brushes have been reported.

[152] Israels R, Leermakers FAM, Fleer GJ, Zhulina EB. *Macromolecules* **1994**;27:3249
[153] Marko JF, Witten TA. *Macromolecules* **1992**;25:296
[154] Brown G, Chakrabarti A, Marko JF. *Europhys Lett* **1995**;25:239
[155] Marko JF, Witten TA. *Phys Rev Lett* **1991**;66:1541
[156] Soga K, Zuckermann MJ, Guo H. *Macromolecules* **1996**;29:1998

2.4. Roles of Polymer Brushes in Interfacial Adhesion Energy

2.4.1. Experimental studies of polymer brushes – elastomer interactions

Understanding what happens to the molecule when a polymer comes into contact with another material and sticks to it is important for many industrial applications.[157,158] There has been a significant improvement in our understanding of the local processes that control the adhesion of polymers during the last decade.[159,160] Experiments by H. R. Brown and co-workers[161] and by C. Creton and co-workers[162] have shown that the interface between two chemically different glassy polymers can be strengthened by the presence of diblock copolymers at the interface. When a fracture propagates at the interface, the coupling chains can either be pulled out or break. Random copolymers have also been used recently in this area.[163]

On the topic of the adhesion of elastomers to solids[164], studies have demonstrated that coupling chains (or "connectors") that bind to the solid and interdigitate with the elastomer enhance the adhesion energy.[165] The important question is to understand how to optimize practical adhesive joints using connector molecules for enhanced adhesion. Early models, considering the connector chains as independent of each other, predicted a linear increase of the adhesion energy at zero crack propagation velocity, G_0, with the surface density of connectors.[166] So, the question became whether it is always good to graft as many chains as possible on the solid surface.

[157] Wool, R. P., *Structure and strength of polymer interfaces* Hanser/Gardner Publications, NY 1995
[158] Brown, H. R., *Physics World*, **1996**, January, 38
[159] Brown, H. R., *IBM J. Res. Develop*. **1994**, 38, 379
[160] Baljon, A. R. C.; Robbins, M. O., *Science* **1996**, 271, 483
[161] Brown, H. R.; Deline, V. R.; Green, P. F., *Nature*, **1989**, 341, 221
[162] Creton, C.; Kramer, E. J.; Hui, C. Y.; Brown, H. R., *Macromolecules* **1992**, 25, 3075
[163] Dai, C. A.; Dair, B. J.; Dai, K. H.; Ober, C. K.; Kramer, E. J.; Hui, C. Y.; Jelinski, L. W., *Phys. Rev. Lett*. **1994**, 73, 2472
[164] Shanahan, M. E. R.; Michel, F., *Int. J. Adhes. Adhes*. **1991**, 11, 170
[165] Brown, H. R., *Macromolecules* **1993**, 23, 1666
[166] Raphael, E.; de Gennes, P. G., *J. Phys. Chem.* **1992**, 96, 4002

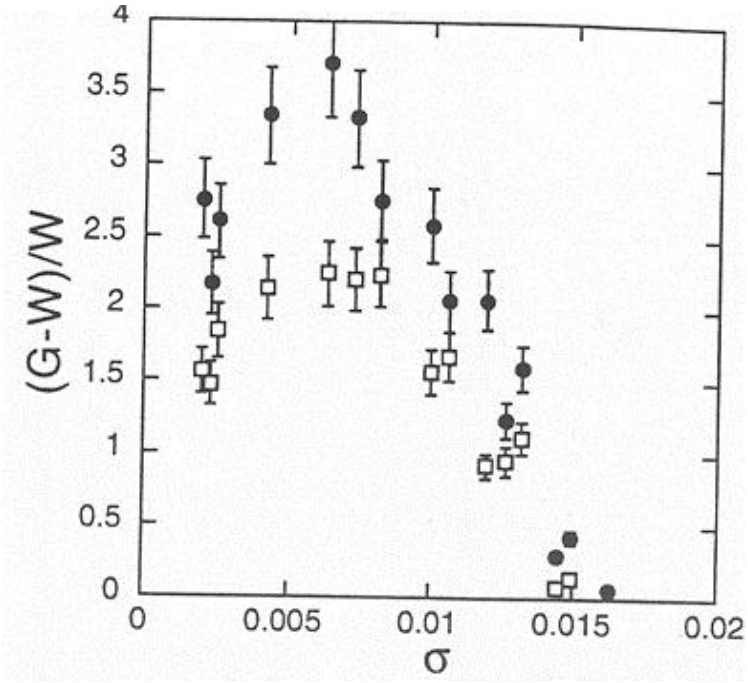

Figure 2.7. Normalized enhanced adhesive strength (G-W)/W as a function of the surface density, σ, for two PDMS elastomers in contact with silicon wafers covered with irreversibly adsorbed chains. From ref. [167].

To try to answer this question, systematic experiments on silica/PDMS systems were undertaken.[167] A typical result for G, the adhesive energy measured at a very low velocity of fracture, as a function of the surface density of connector molecules is reported in Fig. 2.7. The connector molecules clearly lose their efficiency to promote adhesion when they are too densely packed on the surface.

2.4.2. Effects of grafting density on interfacial adhesion energy – de Gennes model

P. G. de Gennes and his coworkers[168] considered this question from a theoretical approach. As the crack grows along the interface, the coupling chains are progressively pulled-out from the elastomer, as schematically shown in Fig. 2.8.

[167] Leger, L.; Raphael, E.; Hervet, H., *Advaces in Polymer Science*, Vol. 138, Springer-Verlag Berlin Heidleberg, **1999**

[168] Raphael, E.; de Gennes, P. G., *J. Phys. Chem.* **1992**, 96, 4002

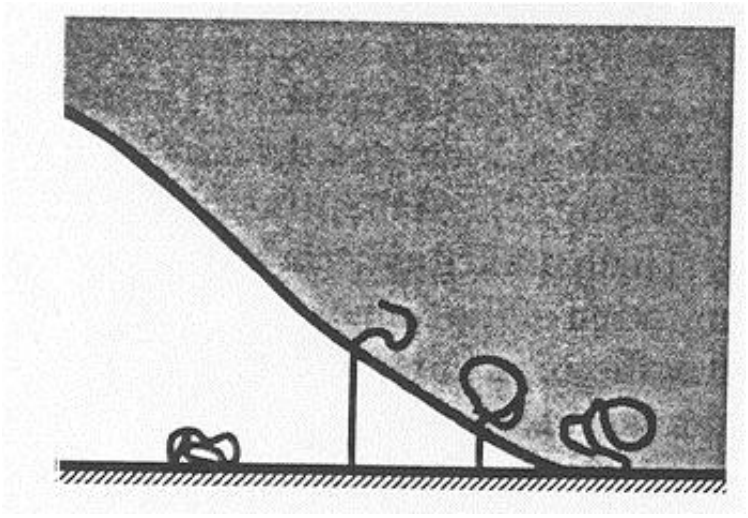

Figure 2.8 Schematic picture of the pull-out process that takes place as the crack grows along the interface. As the crack advances, each connector is progressively stretched until it reaching its maximal length. At that point the connectors collapses onto the surface.[169]

The partially pulled-out chains are assumed to form single-chain fibrils in de Gennes' model.[168] The minimization of the sum of the surface and stretching energies of these chains shows that there is a minimum force f^* required for a fibril to exist even at zero pull-out rate, which was experimentally proved by Reiter *et al*.[170] As the force on a chain that is being pulled out remains finite as the velocity of the fracture line, V, goes to zero, the existence of a threshold toughness G_0 larger than the thermodynamic work of adhesion, W, due to intermolecular interactions (typically van der Waals type) is predicted. In the case of low grafting density of the coupling chains, σ (dimensionless), G_0 is given by[171] $G_0 - W \cong \gamma N \sigma$, where N is the polymerization index the grafted chains and γ is the surface tension of a melt of connector molecules. For low σ values, the connector molecules freely penetrate into the elastomer and have additive contributions. When σ is high, the coupling chains may segregate (at least partially) from the elastomer and G_0 may reduce to W. By considering the equilibrium state between a melt of linear chains (N monomers per chain) and a chemically identical network cross-linked in the dry state (N_c monomers between cross-links, with $N_c < N$), de Gennes showed that the behavior of an N-chain inside the network is very similar to the behavior of the same N-

[169] de Gennes, P. G., Soft Interfaces, Cambridge Press, 1997
[170] Reiter, G.; Schultz, J.; Auroy, P.; Auvray, *Europhys. Lett*. **1996**, 33, 1

chain when dissolved in a melt of shorter, chemically identical chains, of length N_c. Finally, the following equation was derived,

$$G_0 - W \cong g N s \left(1 - s^{2/3} N_c^{1/3}\right)$$

For $\sigma > N_c^{-1/2}$, the brush segregates completely from the network and the adhesion energy G_0 reduces to W. So this equation indicates that the adhesion energy passes through an optimum when[172]

$$\sigma_{opt} \approx 0.465\ N_c^{-1/2}$$

The above analysis considers only local crack tip processes. But, viscoelastic energy losses during crack propagation have been theoretically investigated by de Gennes[173] and by Hui *et al*.[174], and may also contribute to the adhesive strength.

2.4.3. Mechanical Tests for Adhesion Strength in an Interface

There are several standard mechanical tests to evaluate the adhesion strength in an interface, namely, double cantilever bend (DCB), peel test, blister test, and JKR test, etc. Recently, an interesting new technique, asymmetric double cantilever bending (ADCB), was introduced by H. Brown[175] and has been intensively used in adhesion tests for polymer-polymer or polymer-nonpolymer interfaces.[176] A brief review will be given on the experimental design and applications of the asymmetric double cantilever bending test.

2.4.3.1. Experimental Design of ADCB Test

Naturally, the evaluation of the adhesion strength of a "joint" can be performed by "opening" it while observing forces. Adhesion tests differ in the way of "opening" of a joint. For a crack propagation ("opening" process) on the interface between different materials, the interfacial failure is complicated. It has been known for years[177] that the

[171] Brown, H. R.; Hui, C. Y.; Raphael, E., *Macromolecules*, **1994**, 27, 607
[172] de Gennes, P. G., *Soft Interfaces*, Cambridge Press, **1997**
[173] de Gennes, P. G., C. R. *Acad. Sci. (Paris) II* **1988**, 307, 1949
[174] Hui, C. Y.; Xu, D. B.; Kramer, E. J., *J. Appl. Phys*. **1992**, 72, 3294
[175] Brown, H. R., *J MATER SCI* **1990**, 25, 2791
[176] Jiao, J., Gurumurthy C. K.; Kramer E. J.; Sha, Y.; Hui, C. Y.; Borgesen, P., *J. of Electronic Packaging*, **1998**, 120, 349
[177] Williams, M. L., *Bull. Seimol. Soc. Amer*. **1959**, 49, 199

elastic stress situation very close to a crack tip at an interface between materials of different moduli cannot be described by a simple stress intensity factor (***K***). The key point is that a loading mode can affect the *path* of crack propagation, which is strongly related to the resulting fracture energy G. A practical example shown by H. R. Brown[175] is that normal, symmetric fracture toughness tests can give high values for the toughness of the joint between the immiscible polymers polystyrene and polymethylmethacrylate. However, these high values, which are caused by crazes growing away form the interface into the polymer with lower craze resistance, are not a fair characterization of the toughness of the joint. In this case, H. R. Brown showed[175] that much lower, and more realistic toughness values are obtained by the use of an asymmetric test (ADCB). The major advantage of an ADCB test is that it tends to drive the crack and crazes more along the interface, as shown by the following experimental design.

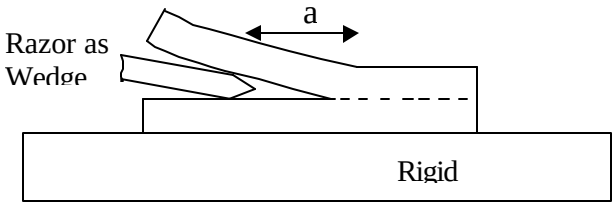

Figure 2.9. A sketch of the "razor" specimen.[175]

In H. R. Brown's design[175], the double cantilever beam samples as shown in Figure 2.9 were tested both free-standing and after bonding to 2 mm thick glass (the "Rigid Substrate" in Fig. 2.9). The samples were loaded in two different ways. In one set of tests the samples were wedged open using a single-edge razor blade, and, another set was loaded using an Instron testing machine.

Brown's results showed the free-standing samples gave a fracture toughness G of 60 – 100 J m^{-2}, while the asymmetric design with a rigid substrate on the PS side gave a G of 5 - 10 J m^{-2}, which is consistent with the Instron test value.

The elevated fracture energy arising from a symmetric test (free standing sample) is believed to originate from crazes growing away from the PS-PMMA interface into the

PS (Figure 2.10), giving a large toughness value. The asymmetric test was developed to suppress this tendency by keeping the crack path on the interface.

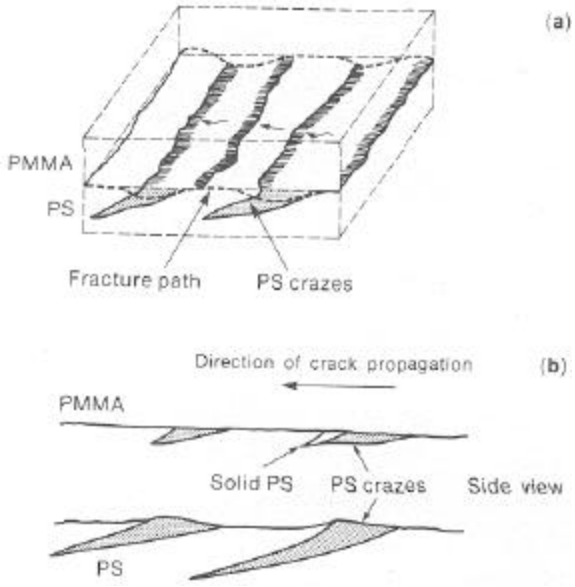

Figure 2.10. A sketch that shows the mode of failure of a symmetrically tested PS / PMMA joint.[175]

2.4.3.2. Some Application Examples of ADCB Technique

Tailored adhesion strength at polymer-nonpolymer interfaces was investigated using the ADCB technique by Smith *et al*.[178] In their investigation, block copolymers of deuterated polystyrene (dPS) and poly(2-vinylpyridine) (PVP) were used to modify the adhesion at polystyrene/soda lime glass interfaces. The fracture energy, G, of these interfaces was measured using an asymmetric double cantilever beam specimen. The ADCB technique was found to keep the crack propagation along the interface within a wide range of interfacial adhesion strength provided by different surface modifications.

Jiao and co-workers[179] recently used the ADCB technique to investigate the interfacial fracture resistance of a polyimide passivation/underfill interface. In their

[178] Smith, J. W.; Kramer, E. J.; Mills, P. J., J. *of Poly. Sci. B Poly. Phys*. **1994**, 32, 1731
[179] Jiao, J., Gurumurthy C. K.; Kramer E. J.; Sha, Y.; Hui, C. Y.; Borgesen, P., *J. of Electronic Packaging*, **1998**, 120, 349

experimental design, a thin layer of polyimide was coated on a standard epoxy as one of the beams and an underfill was flowed over the polyimide film and cured to form the second beam. Xu and co-workers[180] also studied strengthening the polymer phase boundaries with hydrogen bonding random copolymers by using an ADCB technique.

Xiao *et al.*[181] examined the phase-angle effects during an ADCB test on fracture toughness and fracture mechanisms of planar interfaces between two polymers. Gurumurthy and coworkers[182] performed fatigue testing of polymer bi-material interfaces.

2.5. Polymer Thin Film Phase Behaviors

The study of phase behaviors in polymer thin films is important not only in applications, such as lubrication, coatings, lithography, etc., but also from a basic science point of view. The thickness of a polymer *thin* film normally ranges between 10^2-10^3 nm, and 10^1-10^2 nm for an *ultra-thin* film. However, there is not universal acceptance of the two terms (thin and ultra-thin). Very different phase behaviors are expected from polymers in such a confined geometry (quasi-2D) than from those in bulk (3D) systems. One may observe very interesting kinetic phenomena and associated structure formation, e. g. growth of surface enrichment layers and adjacent depletion layers[183], dynamics of phase inversion in multi-component films[184], and surface-directed spinodal decomposition.[185] The dynamics of ordering in block copolymers is a topic of great current interest.[186]

For comparison, a brief background about phase behaviors of polymer blends and block copolymers in the bulk state (3D) will be given in section 2.5.1. After that, a review of polymer thin films will be introduced.

[180] Xu, Z.; Kramer, E. J.; Edgecombe, B. D.; Frechet, J. M. J., *Macromolecules* **1997**, 30, 7958
[181] Xiao, F.; Hui, C. Y.; Washiyama, J.; Kramer, E. J., *Macromolecules* **1994** 27, 4382
[182] Gurumurthy C. K., et al., *J. Electron Packaging* **1998**, 120, 372
[183] Steiner, U.; Eiser, E.; Klein, J.; Budkowski, A.; Fetters, L. J., *Science* **1992**, 258, 1126
[184] Steiner, U.; Klein, J.; Fetters, L. J., *Phys. Rev. Lett*. **1994**, 72, 1498
[185] Krausch, G., *Mat. Sci. Eng. Rep. R*. **1995** 14, 1
[186] Coulon, G.; Collin, B.; Chatenary, D.; Gallot, Y., *J. Phys. II (France)* **1993**, 3, 697

2.5.1. Phase Behaviors in Bulk (3-D) Systems

2.5.1.1. Kinetics of phase separation of polymer blends in bulk (3-D) systems

For polymer blends, it is generally accepted that there are two kinds of kinetic phase separation processes, one is spinodal decomposition (SD) mechanism, and the other is the nucleation and growth (NG) mechanism.[187]

Spinodal decomposition is a kinetic process of generating spontaneously and continuously a new phase interconnected with the parent phase, which has been in a thermodynamically *unstable* state. Once the parent phase reaches the unstable state (perhaps by temperature change), small sinusoidal fluctuations of composition can cause a new phase to be created. This new phase, in turn, makes the amplitude of the fluctuation bigger and the molecules of both components move toward the equilibrium (binodal) compositions. In the growth process, the phases exhibit an interwoven, interconnected, or co-continuous structure.

For a parent phase which is in a *metastable* state, some nuclei can be generated by composition fluctuation which may reduce the free energy of the system. However, the generating of a new interface between phases increases the free energy of the system. This introduces competing processes and the net free energy change is given by

$$\Delta G_r = \tfrac{4}{3}\pi r^3 \Delta G_N + 4\pi r^2 \gamma$$

Where ΔG_N is the free energy change from new phase generation, and γ is the surface free energy of the interface between the two phases. The radius of a nucleus must fluctuate larger than a critical value in order to grow bigger and not redissolve into the parent phase. Generally, a particle-matrix structure (islands-in-sea) is obtained from an NG process.

An SD process normally requires the initial system composition to be close to the critical point, from which the system can easily jump into the unstable region directly. For initial compositions far away from the critical point, an NG process is always encountered since the system must pass through the metastable region first.

[187] Kwon, O., Ph.D. Dissertation, Virginia Tech, 1998

2.5.1.2. Phase behaviors of block copolymers in bulk (3-D) systems

Restricted by chemical bonds connecting different blocks, the phase separation in a block copolymer system is thermodynamically driven by chemical incompatibilities between the different blocks. This typically happens on a mesoscopic (10 nm) scale. Even in bulk systems, the phase behaviors of block copolymers are very complex. Figure 2.11 and Figure 2.12 give examples of the phase behaviors of linear AB diblock and ABC triblock copolymer systems in bulk (3D).[188]

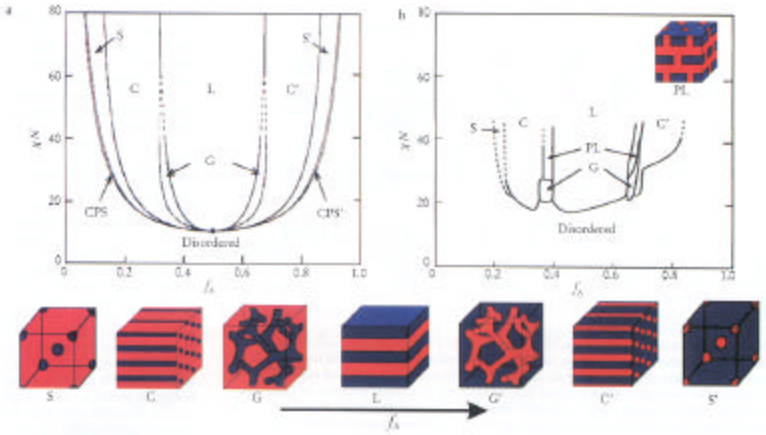

Figure 2.11. Phase diagram for linear AB diblock copolymers in 3-D, comparing theory (plots, top) and experiment (cartoons, bottom).[188]

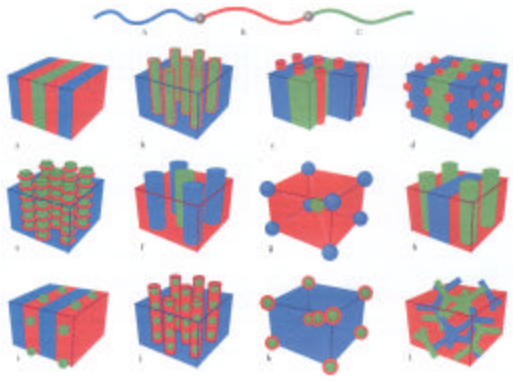

Figure 2.12. Morphologies for linear ABC triblock copolymers in bulk (3D).[188]

[188] Bates, F. S.; Fredrickson, G. H., *Physics Today*, **1999**, 52 (2), 32

2.5.2. Block Copolymer Thin Films

As discussed above, there is a subtle interplay between ordering and coil stretching for block copolymers in bulk states.[189] The phase behaviors of block copolymers in thin films (quasi-2D) is even more complicated because of the restricted chain mobility, as well as the surface properties of the substrate.[190] Dominating the behavior of block copolymer thin films are effects imposed by surface boundary conditions. Indeed, the unique morphological trends these systems display denote an interplay between surface/interfacial interactions and the natural and spontaneous ordering activity of the bulk material.

While rather sophisticated theories exist for block copolymers in the bulk[191,192], none of them has been extended to thin films yet. Since surface confinement entails additional entropic effects on the chains[193] which may compete with energetic effects, the development of reliable quantitative theories clearly will be very difficult. In the following sections (2.5.2.1 & 2.5.2.2), some well understood structures of block copolymer thin films under various situations will be reviewed.

2.5.2.1. Block copolymer thin films between two solid walls

Figures 2.13 and 2.14 give some examples of the phase behavior of block copolymers in thin film between two walls.[194] Figure 2.13 (**a-c**) shows possible lamellar structures of block copolymers in a thin film of thickness D between two *equivalent* walls, assuming that the B-rich domains are preferred by the boundaries. For this symmetric situation, an arrangement with all AB-interfaces parallel to the walls (case **a**) involves necessarily some "frustration" of the ordering. This occurs when the wavelength λ that is enforced by the thickness ($n\lambda = D$ with n integer) differs from its value λ_b in a bulk block copolymer melt under otherwise identical conditions. For a perpendicular arrangement (case **b**) to develop the system can take its bulk wavelength,

[189] Bates, S. F.; Fredrickson, G. G.; *Annu. Rev. Phys. Chem.* **1990**, 41, 525
[190] Binder, K. *Adv. Polymer Sci*., **1994**, 112, 181
[191] Barrat, J. L.; Fredrickson, G. H., *J. Chem. Phys*. **1991**, 95, 1281
[192] Matsen, M. W.; Schick, M., *Phys. Rev. Lett*. **1994**, 72, 2660
[193] Yethiraj, A., *Phys. Rev. Lett*. **1995**, 74, 2018
[194] Binder, K., Advaces in Polymer Science, Vol. 138, Springer-Verlag Berlin Heidleberg**, 1999**

thus avoiding a compression (or expansion) of the ordered structure relative to the bulk state, but there is loss of favorable surface energy in the boundary regions of the A-rich domains. This loss can be reduced by a factor of two by choosing an inhomogeneous domain arrangement of the type shown in **c**, or its mirror image, on the cost of the interfacial energy between domains with perpendicular orientation.

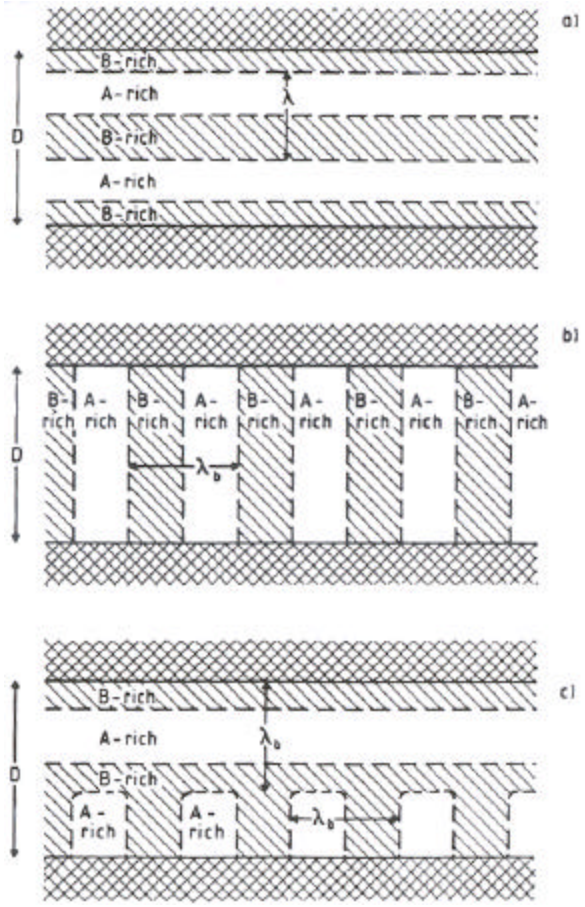

Figure 2.13. Possible lamellar structures of block copolymers in a thin film of thickness D in between two equivalent walls. See the text for details. From Binder[194]

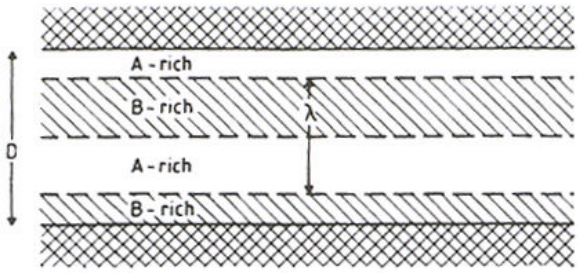

Figure 2.14. Lamellar structures of block copolymers in a thin film of thickness D in between two equivalent walls. From Binder[194]

Figure 2.14 shows thin film confined between *inequivalent* walls, where the lower one favors the B-rich domains and the upper one the A-rich domains. Then, an arrangement where the interfaces run parallel to the walls requires that thickness D and wavelength λ are related as D = (n+1/2) λ, n=0, 1, 2 …

2.5.2.2. Block thin films between a solid wall (substrate) and air

Figure 2.15(**a**-**c**) shows possible lamellar structures in thin films between a solid wall and air. **a**) A thin film on a substrate that favors B-rich domains undergo a phase separation into a fraction x of thickness $n\lambda_b$ and a fraction 1-x of thickness (n+1) λ_b, such that D=[xn+(1-x)(n+1)] λ_b, if the air also favors B-rich domains. This occurs at the order-disorder transition (ODT) of the block copolymer melt. **b**) If the air favors A-rich domains instead, the phase separation produces in a fraction x of thickness (n-1/2) λ and a fraction 1-x of thickness (n+1/2) λ with n=1, 2, 3 … **c**) If the block copolymer film undergoes dewetting at the substrate, droplets form with a step-pyramid like structure.

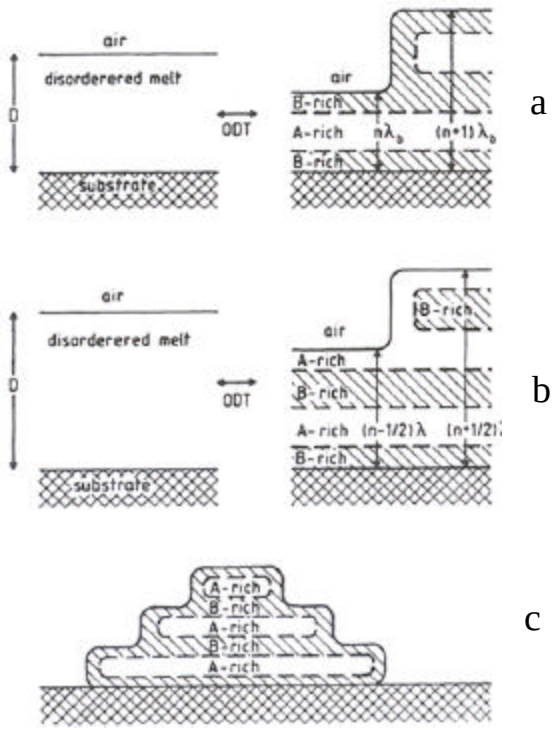

Figure 2.15. Structures of a diblock copolymer thin film between a wall (substrate) and air. From Ausserre *et al*.[195]

The two previous sections (2.5.2.1 and 2.5.2.2) illustrated some possible lamellar structures in which lamella are parallel to substrates. Recently, perpendicular lamellar structures in block copolymer thin films were found on various patterned substrates by using Monte Carlo simulations and calculations, as well as experiments. These perpendicular lamellar structures are particularly useful in nano-lithography.

2.5.3. Polymer Blend Thin Films

For the study of phase behavior in polymer mixtures in thin film, some insights have been gained from both computer simulations[196] and from phenomenological, mean-field type theories.[197] Starting from the Flory-Huggins theory for a binary polymer blend and a phenomenological term describing the wall effects, one obtains a useful qualitative description of the behavior (Fig. 2.16).[198]

[195] Ausserre, D.; Raghuntan, V.A.; Maaloum, M., **1993**, *J. Phys II* 3, 1485
[196] Rouault, Y.; Baschnagel, J.; Binder, K., *J. Stat. Phys*. **1995**, 80, 1009
[197] Binder, K. *Acta Polymer* **1995**, 46, 204
[198] Flebbe T, Dunweg B, Binder K, Phys II (France) 6, 667, 1996

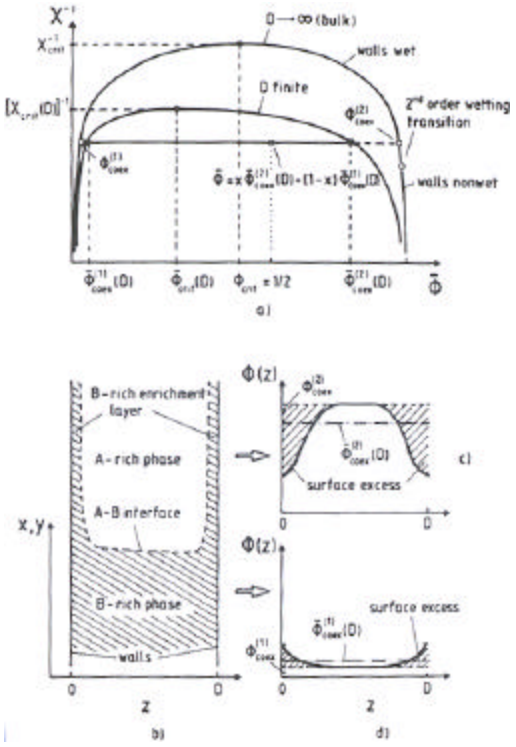

Figure 2.16. Phase diagram of a symmetrical binary (AB) polymer blend in a thin film. See the text for details. From Flebbe *et al.*[198]

Figure 2.16 **a**) shows a qualitative phase diagram of a symmetrical binary (AB) mixture in both a thin film of thickness D and in a semi-infinite geometry (D→∞). In this representation the axes are the inverse Flory-Huggins parameter χ^{-1} (propotional to temperature) and average volume fraction $\bar{f}$ of A in the system. Assuming a symmetrical mixture in the bulk (D→∞), the critical volume fraction is ϕ_{crit}=1/2, and for $\chi^{-1} < c_{crit}^{-1}$ the volume fractions $f_{coex}^{(1)}, f_{coex}^{(2)}$ of the two coexisting phases are related by the symmetry relation $f_{coex}^{(2)} = 1 - f_{coex}^{(1)}$. Assuming a preferential attraction of one species (B) by the walls, this symmetry is broken, and both the critical volume fraction $\bar{f}_{crit}$ (D) and the volume fraction at the A-rich branch of the coexistence curve $f_{coex}^{(2)}$(D) are shifted towards smaller volume fractions as compared to the bulk. With short range forces at the wall, and unchanged pairwise interactions between monomers of the mixture near the

wall, a second-order wetting transition is expected at a temperature $T_w < T_{cb}$ in the semi-infinite system, but this transition is rounded in the thin film geometry.

Figure 2.16 **b**) is a schematic description of the state of the thin film for a volume fraction $\bar{f}$ inside the coexistence curve, $f_{coex}^{(1)}(D) < \bar{f} < f_{coex}^{(2)}(D)$ (e.g., the point marked by a cross in the phase diagram, part a). The film is inhomogeneous in the x, y-directions parallel to the walls. The A-rich part of the film is in equilibrium and separated from the B-rich part by a single A-B interface running perpendicular to the film (for free boundary conditions in lateral directions), or by two such interfaces (for periodic boundary conditions). The relative amounts of A-rich (x) and B-rich (1-x) phases are simply given by the lever rule, $\bar{f} = f_{coex}^{(2)}(D) + (1-x) f_{coex}^{(1)}(D)$, with $0<x<1$. Here it is assumed that the film thickness is much larger than the interfacial thickness w, so the A-rich phase has enrichment layers of the B-rich phase "coating" the walls of the thin film. Figure 2.16 **c**) shows a volume fraction profile $\phi(z)$ in the z-direction across the film in the A-rich phase. Here the shaded area denotes the surface excess ϕ_s. Figure 2.16 **d**) is the same as **c**) but for the B-rich phase.

Mean-field theory is inadequate for an accurate description near the critical point, and for strongly segregated states ($\chi^{-1} << c_{crit}^{-1}$) where the long wavelength approximation is also inadequate. Thus for a quantitatively reliable description of surface enrichment near walls one needs better models, e.g. the self-consistent field theory.[199]

[199] Carmesin, I.; Noolandi, J., *Macromolecules* **1989** 22, 1689

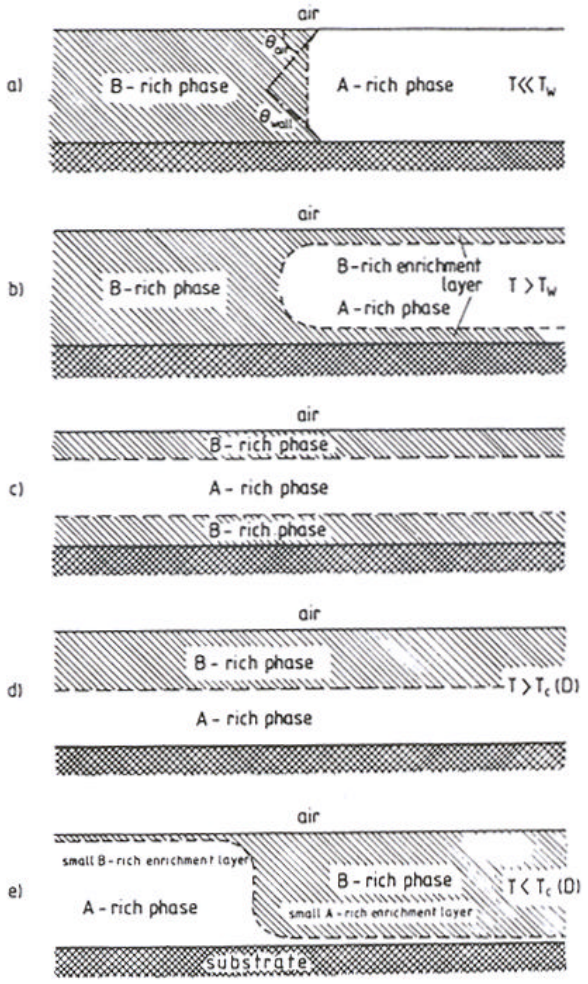

Figure 2.17. Schematic description of phase structures of phase separated binary polymer blend (AB) thin films. From Donley *et al*.[200]

Figure 2.17 is a schematic description of the equilibrium structure of phase separated binary polymer mixtures (AB) in thin film geometry.[200] The lower surface is assumed to be a solid substrate, the upper surface being against air (or vacuum). Figure 2.17 **a-c** refer to the case where the B-rich phase is energetically favors both by the solid substrate and the air, while Figure 2.17 **d-e** refer to the situation where the B-rich phase is preferred by the air surface only, while the solid substrate prefers the A-rich phase. Note that case **c** occurs as a metastable state only, while in the two-phase coexistence region of thin films where both walls prefer the same phase in equilibrium, interfaces between the A-rich and the B-rich phase run perpendicular to the film. In the nonwetting case, the A-

[200] Donley, J. P.; Wu, D. T.; Fredrickson, G. H., *Macromolecules*, **1997,** 30, 2167

B interface meets the air surface (or the substrate surface, respectively) under a nonzero contact angle θ_{air} (θ_{wall}) (Figure 2.17 **a**). In the wetting case this interface bends over to a B-rich enrichment layer at the surface of the A-rich phase (Figure 2.17 **b**). In the "antisymmetric situation" where the two surfaces prefer different phases (**d** & **e**), the example with a single interface in the center of the film (Figure 2.17 **d**) is still in the one-phase region of the film, $T>T_c(D)$, D being the thickness of the film, with $T_c(D) \approx T_w$, the wetting transition temperature in semi-infinite geometry. (For simplicity it is assumed that both air and solid substrate have the same wetting transition temperature.) For $T \leq T_c(D)$, the A-B interface gets bound on the walls, only microscopically thin enrichment layers may remain at both walls, and the perpendicular part of the A-B interface ultimately (for $T \ll T_w$) develops nonzero contact angles with both surfaces, as in part **a**.

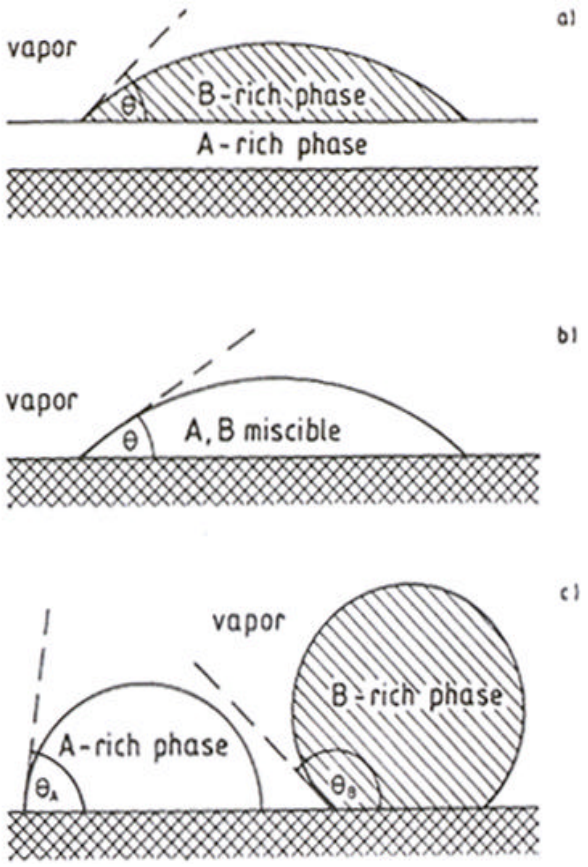

Figure 2.18. Dewetting in a thin film containing two components A and B on a substrate. From Keblinski, *et al*.[201]

Figure 2.18 is a schematic description of a thin film containing two constituents A and B on a substrate (cross-hatched).[201] Various possibilities of dewetting are illustrated in Figure 2.18, depending on interfacial tensions between A-rich and B-rich phases and the solid substrate (γ_{AS}, γ_{BS}) and the vapor (γ_{AV}, γ_{BV}), and the interfacial tension between coexisting A-rich and B-rich fluid phases (γ_{AB}). In case **a,** the A-rich phases wets the substrate and forms a thin A-rich layer coating the substrate, while the B-rich phase on top does not wet this layer (contact angle θ being nonzero). In case **b**, the A, B mixture is miscible($\gamma_{AB}<0$) but does not wet the substrate. In case **c**, neither phase wets the substrate.

In the field of phase behaviors in polymer thin films, tremendous progress has been achieved, but great challenges remain for the future. For example, while the static (equilibrium) behavior of a polymer thin film is well understood, at least in principle, the kinetic behavior is much less clear. There is delicate interplay among surface-directed spinodal decomposition, thickness-limited growth of wetting layers, and the hydrodynamic mechanisms of coarsening in thin films which needs further study.

2.5.4. Influence of polymer brushes on polymer thin film phase behaviors

Most studies of polymer thin film phase behaviors have been carried out on flat surfaces without any chemical modification except cleaning processes, or on surfaces modified by small molecules such as SAM's or coupling agents. It should be very illuminating to design appropriate polymer brushes and study the influence of polymer brushes on polymer thin film phase behaviors. Unfortunately, there have not been so many works in this area. Russell and coworkers[202] reported that perpendicular lamellar structures in *di*-block copolymer thin films were obtained on certain PS-*co*-PMMA random copolymer brush modified surfaces. One of the major goals of this dissertation is to explore and control the structure (micro- and nano- meter scales) in polymer thin films using a new type of triblock copolymer brush modified surface.

[201] Keblinski, P; Kumar, S. K.; Maritan, A.; Koplik, J.; Banavar, J. R., *Phys. Rev. Lett*., **1996**, 7, 1106
[202] Mansky P, Liu Y, Huang E, Russell TP, Hawker CJ. Science 1997;275:1458

CHAPTER 3. SYNTHESIS

3.1. Introduction

As discussed in Chapter 1, the first goal of our research is to design well-defined, central functionalized asymmetric *tri*-block copolymers (CFABC). There are three criteria for such polymers: narrow molecular weight distribution (MWD), precisely controlled block sizes, and functional groups.

Living anionic polymerization is one of the most sophisticated polymerization techniques to obtain block copolymers with narrow MWD and precise block size. Living polymerization is defined as a reaction which proceeds in the absence of the kinetic steps of chain termination and chain transfer[1,2], resulting in extremely narrow MWD values (polydispersity of 1.01 – 1.10), and also multi-block copolymers via sequential addition of different types of monomers. The "living" chain ends, which have a negative charge, can be easily terminated by species with electron-withdrawing groups, such as water. As a result, many monomers with functional chemical groups (i.e., hydroxyl), are too active to be used directly for a living anionic polymerization. In order to overcome this difficulty, monomers with functional groups are typically protected by inert groups first, and the protecting groups are removed to recover the functional groups after anionic polymerization.

Various *di*-block copolymers, having functional groups on one block, have been synthesized using living anionic polymerization.[3] For example, Pearce and coworkers[4] reported the successful synthesis of polystyrene-*b*-poly(*p*-hydroxystyrene) *di*-block copolymers by combining protected group chemistry with high-vacuum anionic polymerization. In the first step, the functional hydroxystyrene monomer was reacted with *tert*-butyldimethylsilyl (TBDMS) chloride, resulting in a *p*-[(*tert*-butyldimethylsilyl)oxy] styrene monomer, used for the polymerization. Finally, the

[1] McGrath, J. E., Ed.. Anionic Polymerization: Kinetics, Mechanisms, and Synthesis ACS Symp. Ser. No. 166, 1981
[2] Quirk R. P.; Lee, B., *Polym. Int*. 27, 359, **1992**
[3] Ishizone, T.; Hirao, A.; Nakahama, S., *Macromolecules* 26, 6964, **1993** and references therein.

protection groups (TBDMS) in the polymer was hydrolyzed to recover the functional hydroxy groups. Long *et al.*[5] also used the similar protected group chemistry approach to obtain poly(*p*-hydroxystyrene)-*b*-PMMA *di*-block copolymer.

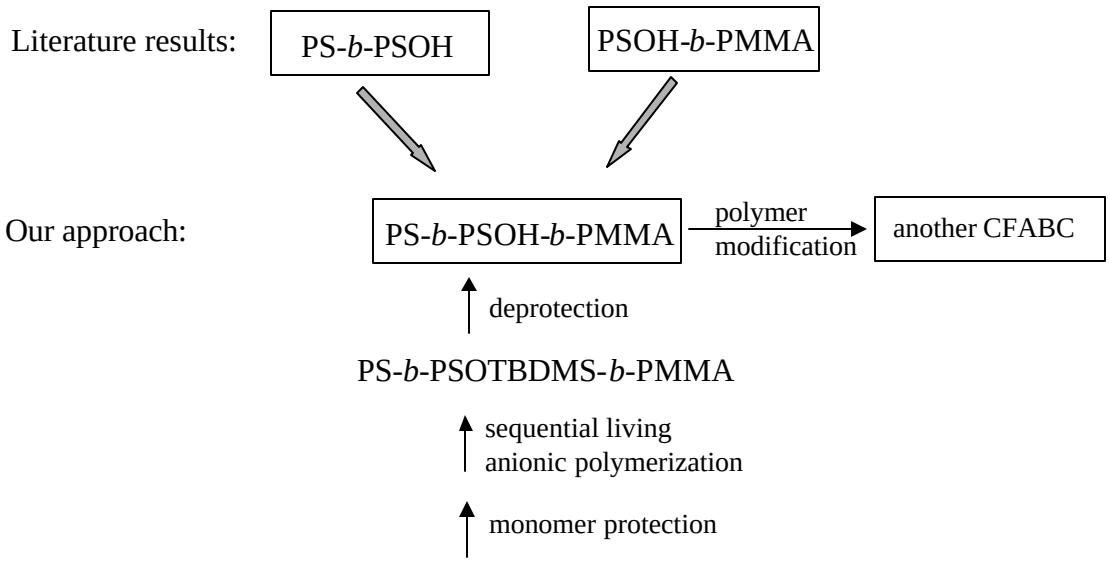

Scheme 3.1. Strategy for the synthesis of CFABC polymers

My synthesis strategy was to synthesize a CFABC polymer, polystyrene-*b*-poly(*p*-hydroxystyrene)-*b*-PMMA, using sequential living anionic polymerization (based on the previous literature results on *di*-block copolymers) and switch the phenol functional groups in the central block to other desired functional groups using a polymer modification technique. The strategy of synthesizing the CFABC is illustrated in Scheme 3.1. The methodology is expected to be easily adapted to the synthesis of other types of CFABC polymers with minor modification.

In addition to the synthesis of CFABC polymers, well-defined PS homopolymer and PS-*b*-PMMA *di*-block copolymers were also synthesized using living anionic polymerization.

[4] Zhao, J. Q.; Pearce, E. M.; Kwei, T. K.; Jeon, H. S.; Kesani, P. K.; Balsara, N. P., *Macromolecules* 28, 1972, **1995**
[5] Long, T. E.; Kelts, L. W.; Turner, R. S.; Wesson, J. A.; Mourey, T. H., *Macromolecules* 24, 1431, **1991**

3.2. Experimental

3.2.1. Monomer, initiator, and solvent purification

Styrene (Aldrich) was stirred over finely ground calcium hydride for 1-2 days and vacuum distilled. The distilled monomer was stored at –25 °C under nitrogen in a brown bottle until further use. Immediately prior to polymerization, the monomer was vacuum distilled from dibutylmagnesium (DBM). DBM (Lithco) was obtained as a 25% solution in heptane and was transferred by using syringe techniques. This reagent has been shown to efficiently remove air and water from various hydrocarbon monomers. DBM was added dropwise to the monomer at room temperature until a stable, pale, yellow color persisted.

Methyl methacrylate (MMA) (Aldrich) was also distilled over calcium hydride and stored in a freezer. The monomer was further distilled from triethyl aluminum immediately prior to polymerization.

1,1-Diphenylethylene (DPE) (Aldrich) was vacuum distilled from sec-butyllithium (FMC Lithium Division, 1.3 M solution in cyclohexane). The details of the above purification procedures can be found elsewhere.

sec-Butyllithium was obtained from Aldrich as a 1.3 M solution in cyclohexane. The initiator was used as received and was stored at –25 °C for several months without significant degradation.

Tetrahydrofuran (Fisher, HPLC grade), the polymerization solvent, was distilled from a purple sodium benzophenone ketyl under nitrogen immediately prior to polymerization.

3.2.2. Synthesis of *p*-[(*tert*-butyldimethylsilyl)oxy]styrene (1)

The functional group (phenol) in PS-*b*-poly(4-hydroxystyrene)-*b*-PMMA is unsuitable for a living anionic polymerization process; and thus, a protected monomer, *p*-[(*tert*-butyldimethylsilyl)oxy]styrene **1**, was synthesized (Scheme 3.2).

Hydrolysis of *p*-Acetoxystyrene. A 500 mL, 3 necked flask (2 necks with septa and the third neck with nitrogen outlet) was used. 4-Acetoxystyrene (25 g, 0.16 mol)

(Aldrich, used as received) was added into the flask. The flask was submerged in an ice bath and thermal equilibrium was reached. 10% potassium hydroxide (220 mL, 0.39 mol) was then added dropwise with a dropping funnel. The reaction was carried out under stirring for 4 hours. Unreacted 4-acetoxystyrene was extracted by chloroform. After the extraction, 10% HCl (ice cold) was added dropwise to neutralize the water solution to a value of pH 8. Hexane was then added to extract *p*-hydroxystyrene (4-vinylphenol) from the solution, and the organic mixture was dried over $MgSO_4$. After filtration, hexane was evaporated to obtain a white solid. The solid was recrystallized from hexane to yield *p*-hydroxystyrene (18.5 g, 74% yield).

***p*-[(*tert*-butyldimethylsilyl)oxy]styrene (1)**. *tert*-Butyldimethylsilylchloride (TBDMS chloride) (16 g, 0.1 mol, Aldrich, used as received) in dry DMF was added dropwise into a stirred solution of *p*-hydroxystyrene (10g, 0.083 mol) and imidazole (12 g, 0.12 mol) in dry DMF (50 mL) at 0 °C under an atmosphere of nitrogen. After addition was complete, the solution was allowed to warm up to room temperature and stirred for 5 hours. The product was extracted using chloroform and H_2O, washed with 5% $NaHCO_3$, and dried over $MgSO_4$. After filtration and evaporation, a pale yellow liquid was obtained with a yield of approximately 70%. The crude product was further distilled using high vacuum (10^{-5} Torr) at 45 °C in the presence of dibutyl magnesium immediately prior to polymerization. The purified *p*-[(*tert*-butyldimethylsilyl)oxy] styrene (**1**) was colorless. The above procedure was based on a method described earlier.

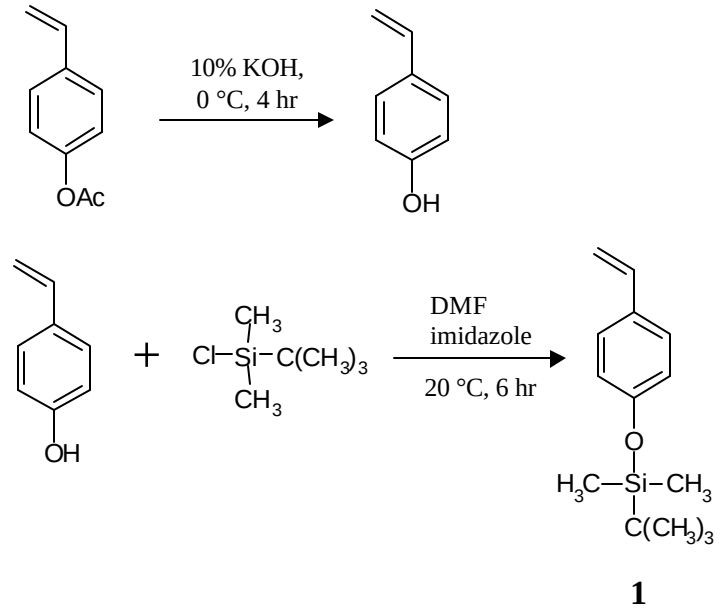

1

Scheme 3.2 Synthesis of *p*-[(tert-butyldimethylsilyl)oxy]styrene monomer 1.

For the monomer **1,** ^{1}H NMR (400 MHz, $CDCl_3$, δ, ppm) indicated: 0.21 (s, 6H, $SiCH_3$), 0.99 (s, 9H, $SiCCH_3$), 5.11-5.62 (2d, 2H, CH_2=), 6.61-6.69 (2d, 1H, CH=), 6.78-7.30 (2d, 4H, aromatic). GC-MS: mass = 234 (theoretical value = 234.4).

3.2.3. Synthesis of PS-*b*-poly(*p*-[(*tert*-butyldimethylsilyl)oxy]styrene)-*b*-PMMA (**2**)

All of the glassware was rigorously cleaned and dried in an oven at 120°C for 24 hours. For most polymerizations, the reactor consisted of a 250-mL, one-neck, round-bottomed flask equipped with a magnetic stirrer and rubber septum. The septum was secured in place with copper wire to maintain a positive pressure of ultra-pure nitrogen. The reactor was assembled while hot and subsequently flamed under a nitrogen purge. Scheme 3.3 depicts the sequential addition of reagents and the chemistry involved. After the flask had cooled, the polymerization solvent (THF, 150 mL) was added to the reactor via a double-ended needle (cannula). The reactor was submerged into a –78 °C bath and allowed to reach thermal equilibrium. Purified styrene monomer (11.0 mL) was charged into the reactor with a syringe. The calculated amount of sec-butyllithium (1.3 mL) was quickly syringed into the reactor, and immediately the formation of orange polystyryllithium anion was observed. Polymerization of the polystyrene block was

allowed to proceed for 20 min to ensure complete conversion.[17] An aliquot (approximately 2 mL) of the orange living polystyryllithium anions was removed and terminated. The protected functional monomer **1** (2.0 mL) was then charged into the reactor and the second block, poly(*p*-[(*tert*-butyldimethylsilyl)oxy]styrene) was obtained after 20 min of reaction. An excess of DPE (2-3 molar excess compared to lithium) was syringed into the reactor to cap the first two blocks. The successful conversion to the highly delocalized DPE derived anion was witnessed by the rapid formation of a deep red color. After several minutes, highly purified MMA monomer (10.7 mL) was slowly added to the living, capped first two blocks. Initiation of the third block was characterized by the formation of a colorless PMMA lithium enolate anion. After 20 min, the polymerization was terminated using degassed, HPLC grade methanol. The resulting *tri*-block copolymer **2** was obtained by precipitation into methanol (1000 mL) followed by overnight vacuum drying at 130 °C. The ^{29}Si NMR spectrum (500 MHz, $CDCl_3$, δ, ppm) of **2** indicated a single peak at 19.98 ppm ($Si(CH_3)_2(CCH_3)_3$).

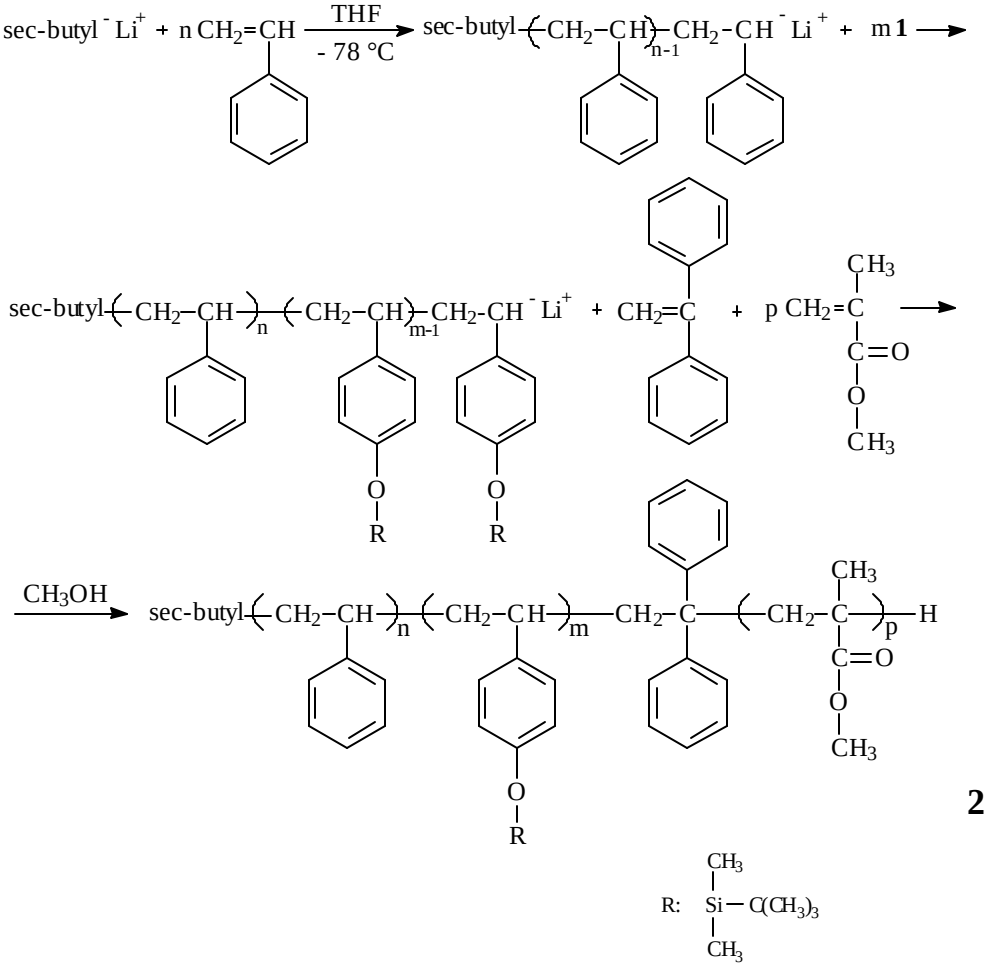

Scheme 3.3 Sequential living polymerization of PS-*b*-poly(*p*-[(*tert* butyldimethylsilyl)oxy]styrene)-*b*-PMMA

3.2.4. Synthesis of PS and PS-*b*-PMMA

Polystyrene (PS) homopolymer and PS-*b*-PMMA *di*-block copolymer were also synthesized using living anionic polymerization with *sec*-butyl lithium as the initiator. The experimental setup was exactly the same as that of the *tri*-block copolymers described in the previous section. At the end of the polymerization of the first block (polystyrene, Scheme 3.3), an excess amount of degassed, HPLC grade methanol was quickly charged into the reactor to terminate the reaction to obtain PS homopolymer. Complete disappearance of the orange color was indicative of total deactivation of the

polymeric carbanion.[6] For the *di*-block copolymers, the step of the addition of the protected functional monomer **1** in Scheme 3.3 was omitted.

3.2.5. Desilylation of PS-*b*-poly(*p*-[(*tert*-butyldimethylsilyl)oxy]styrene)-*b*-PMMA

The TBDMS protecting groups in the central block of the copolymer (4 g) were quantitatively removed using dilute HCl (0.1N, 10 mL) at 60 °C in THF (100 mL) for 4 hours (Scheme 3.4). The product was washed with water and filtered, redissolved in THF, and precipitated in hexane to obtain the central functionalized asymmetric *tri*-block copolymer PS-*b*-poly(4-hydroxystyrene)-*b*-PMMA (**3**).

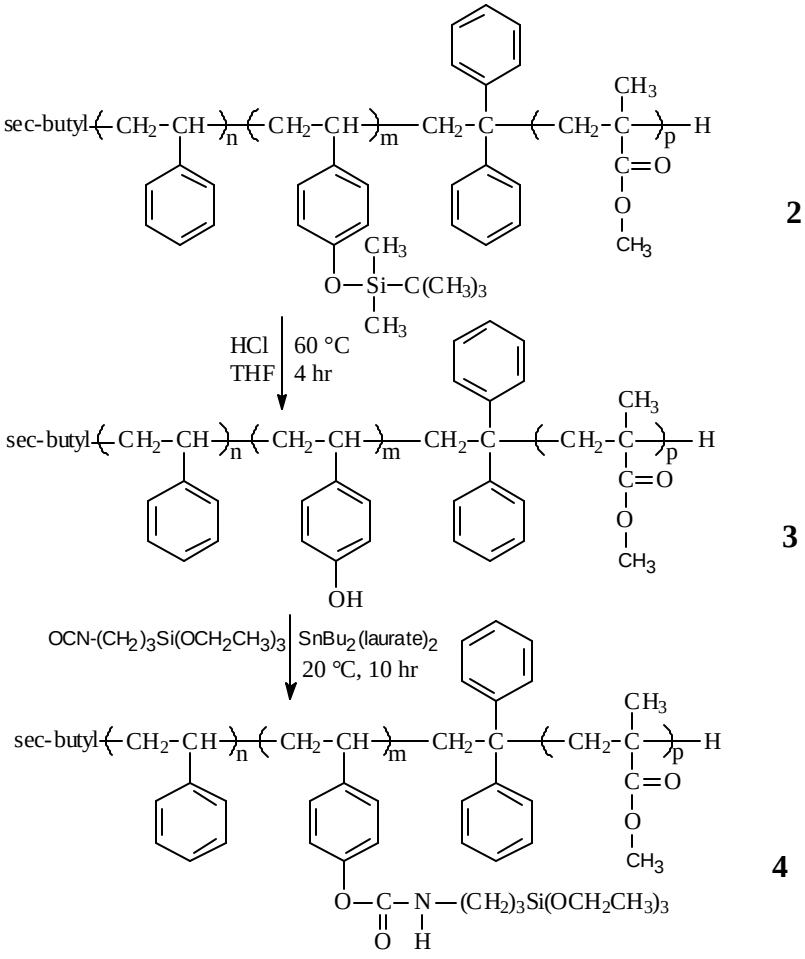

Scheme 3.4 Desilyation of PS-*b*-poly(*p*-[(*tert*-butyldimethylsilyl)oxy]styrene-*b*-PMMA and polymer modification

[6] Long, T. E.; Kelts, L. W.; Turner, S. R.; Wesson, J. A.; Mourey, T. H. *Macromolecules* 24, 1431, **1991**

3.2.6. PS-*b*-poly(4-urethanopropyl triethoxysilylstyrene)-*b*-PMMA (4)

Isocyanatopropyl triethoxysilane **5** (Aldrich, used as received) was reacted with **3** to obtain the second central functionalized *tri*-block copolymer **4** (Scheme 3.4). The isocyanate group quantitatively reacted with the phenol groups to form urethane linkages[18], while the triethoxysilane group remained unchanged. This reaction was performed under an ultrapure nitrogen atmosphere. Polymer **3** possessed a calculated 7 phenolic groups per chain and a molecular weight of 21,000 ($<M_n>$). Two equivalents of **5** (0.4 mL) were mixed with **3** (2 g, ~0.8 mmole phenol groups) in dry THF (20 mL) in the presence of a tin catalyst ($SnBu_2$ (laurate)$_2$ (0.1 mL), Air Products, Inc.). After stirring at room temperature overnight, the product was precipitated into hexane (excess **5** was soluble in hexane), filtered, and dried in vacuum for approximately 4 days at room temperature to remove any residual solvent. The purity of polymer **4** was confirmed using ^{1}H NMR, and residual solvent and reagents were not detected in the dried sample.

3.2.7. Characterization

^{1}H and ^{13}C NMR spectra were collected on a 400 MHz Varian spectrometer in chloroform-*d*. ^{29}Si NMR spectra were obtained on a JEOL 500 MHz spectrometer. GC-MS (HP GC model 5890 / HP MSD (mass selective detector) model 5971) was used for monomer characterization. Gel permeation chromatography (GPC) was performed using a Waters 2690 chromatograph equipped with a differential refractive index detector (Viscotek Laser Refractometer) and an on-line differential viscometric detector (Viscotek 100) coupled in parallel, using polystyrene standards. The mobile phase was chloroform and data were recorded at 25 °C at a flow rate of 1.0 mL/min. Differential scanning calorimetery (DSC) (TA 2930) was used to characterize the thermal properties of the polymers. A heating of 10 °C/min was employed. All DSC experiments were performed under nitrogen atmosphere and the second heat data were used.

3.3. Results and Discussion

3.3.1. Characterization of *p*-[(*tert*-butyldimethylsilyl)oxy]styrene (1)

The chemical structure of the protected monomer, *p*-[(*tert*-butyldimethylsilyl)oxy] styrene (**1**) was confirmed by NMR and GC-MS.

Figure 3.1 is the ^{1}H NMR (400 MHz, $CDCl_3$) spectrum of *tert*-butyldimethylsilyl chloride (TBDMS-Cl). Peaks *a* and *b* at 0.36 ppm (s, 6H) and 0.97 ppm (s, 9H) are attributed to the dimethyl groups ($SiCH_3$) and *tert*-butyl groups ($SiCCH_3$), respectively.

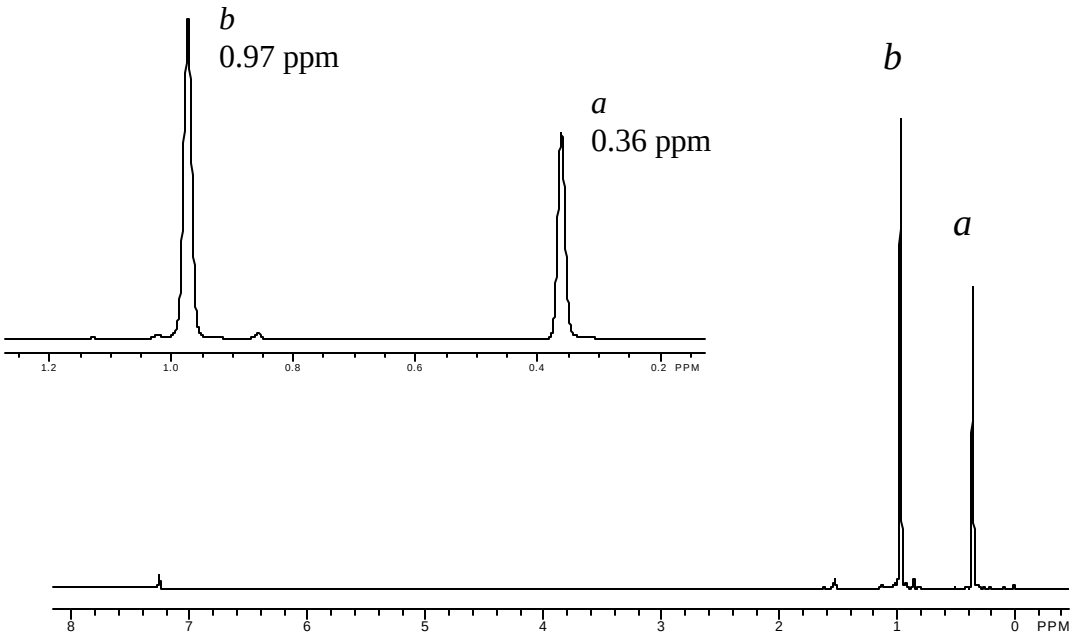

Figure 3.1. ^{1}H NMR spectrum of TDBMS-Cl

The ^{1}H NMR spectrum of *p*-hydroxystyrene, which was hydrolyzed from *p*-acetoxystyrene and recrystallized in hexane, is shown in Figure 3.2. The peaks are assigned as below. *a*: -OH (s, 1H, 4.71 ppm), *b*: CH_2= (2d, 2H, 5.11 – 5.63 ppm), *c*: CH= (2d, 1H, 6.60-6.70 ppm), d: aromatic (2d, 4H, 6.75-7.33 ppm).

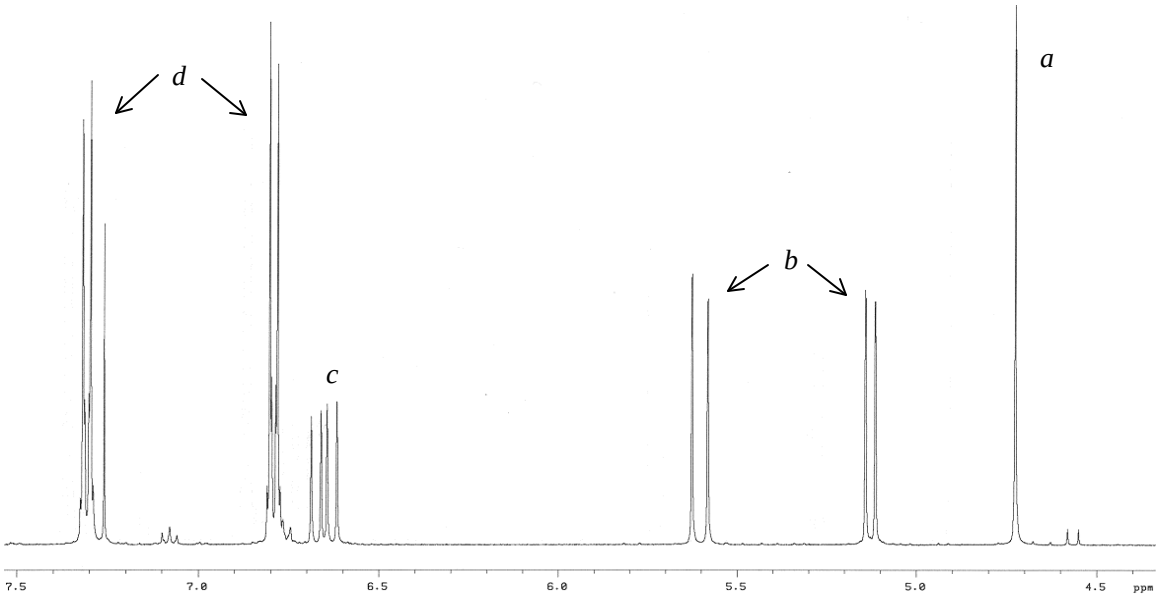

Figure 3.2. ^{1}H NMR spectrum of *p*-hydroxystyrene (recrystallized from hexane)

For the monomer **1,** impurities were found in the crude product as shown by the ^{1}H NMR spectra in Figure 3.3, and were indicated visually by the yellow pale color of the product.

After the distillation under high vacuum in the presence of dibutyl magnesium, the impurities disappeared (Figure 3.4) and the product became colorless. The purpose of high vacuum is to lower the distillation temperature to avoid polymerization. In the literature[7], a vacuum of 10^{-4} torr (distillation temperature: 85 °C) was employed for the distillation, but from the present experience, there was significant polymerization under such conditions and little purified monomer was obtained. So an even higher vacuum (10^{-5} torr), which was created by using a diffusion pump, and a lower distillation temperature (45 °C) were used in this experiment. Much care is needed to assure the success of the distillation. The final yield of the monomer is approximately 50%.

The high purity of monomer **1** after the distillation can be verified by comparing the NMR spectra in Figures 3.3 and 3.4. The impurities around 0.0-0.2 ppm, 0.8-1.0 ppm, 6.7-6.8 ppm and 7.0-7.1 ppm completely disappeared in Figure 3.4. In fact, the

[7] Zhao, J. Q.; Pearce, E. M.; Kwei, T. K.; Jeon, H. S.; Kesani, P. K.; Balsara, N. P., *Macromolecules* 28, 1972, **1995**

purity of the monomer is even better than that of one of the starting materials, TBDMS-Cl (0.0 and 0.8 ppm, Figure 3.1). The high purity is desired for successful living anionic polymerization. In Figure 3.4, the NMR peaks can be assigned as the following: 0.21 ppm (s, 6H, $SiCH_3$), 0.99 ppm (s, 9H, $SiCCH_3$), 5.11-5.62 ppm (2d, 2H, CH_2=), 6.61-6.69 ppm (2d, 1H, CH=), 6.78-7.30 ppm (2d, 4H, aromatic). By comparing the NMR spectra of the starting materials (Figure 3.1 and Figure 3.2), little chemical shift was obtained for those protons on the styrene part. The peak position of the protons on the dimethyl groups ($SiCH_3$) was shifted up-field from 0.36 ppm to 0.21 ppm, attributable to a more shielded environment resulting from changing –Cl to a relatively less electron-withdrawing –O. Additionally, GC-MS was also used to confirm the chemical structure of the monomer. A value of 234 was obtained, which is consistent with the theoretical value (234.4).

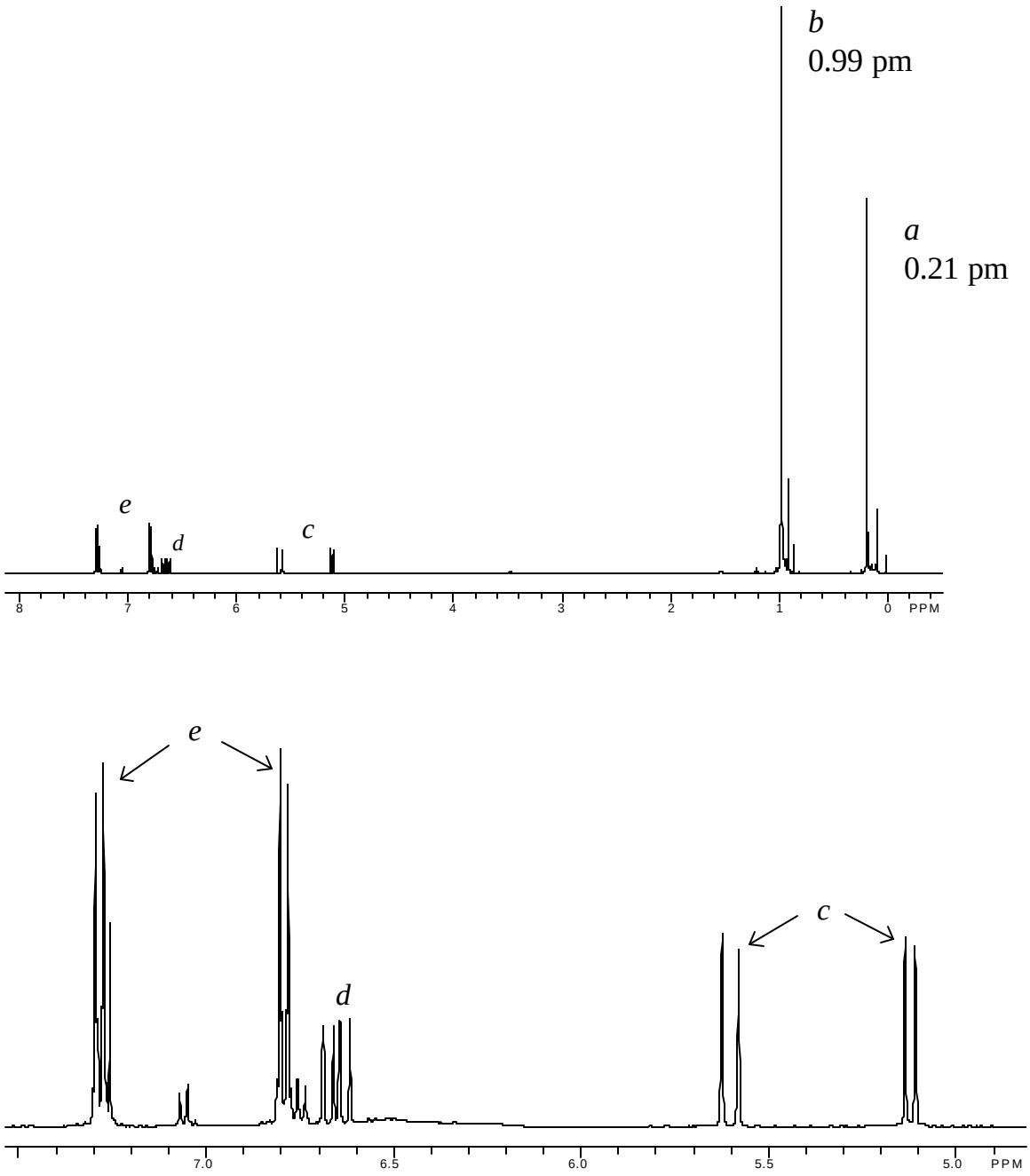

Figure 3.3. ^{1}H NMR spectrum of *p*-[(*tert*-butyldimethylsilyl)oxy]styrene (**1**) before distillation

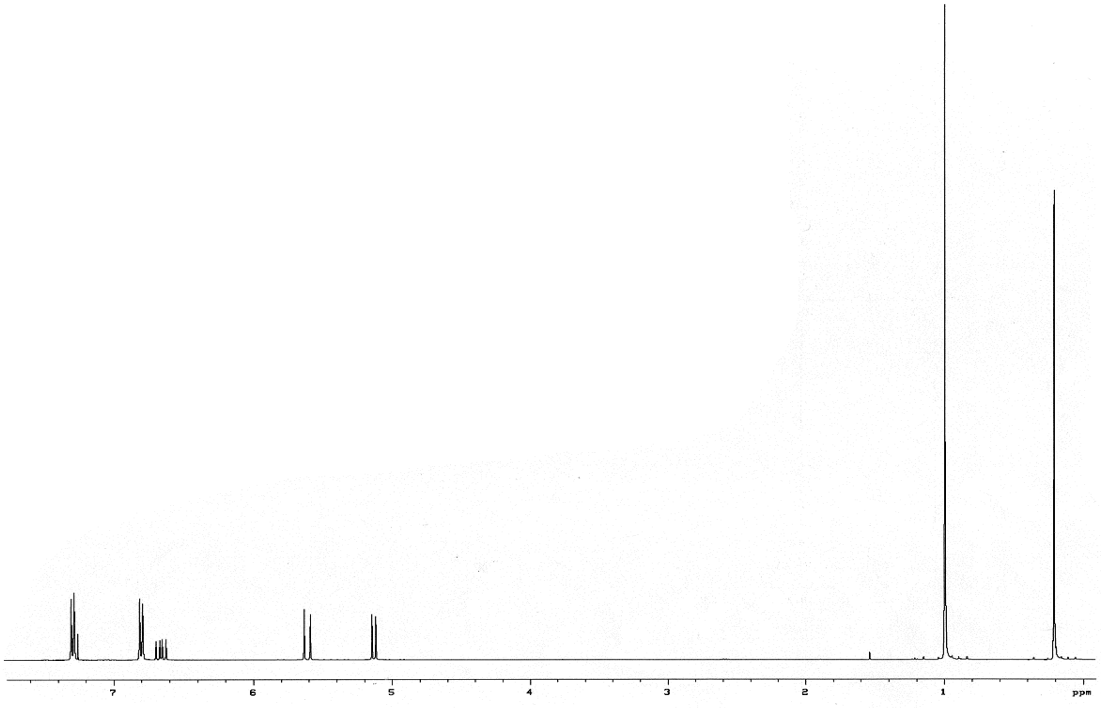
7
6
5
4
3
2
1
ppm

(a) (Figure 3.4)

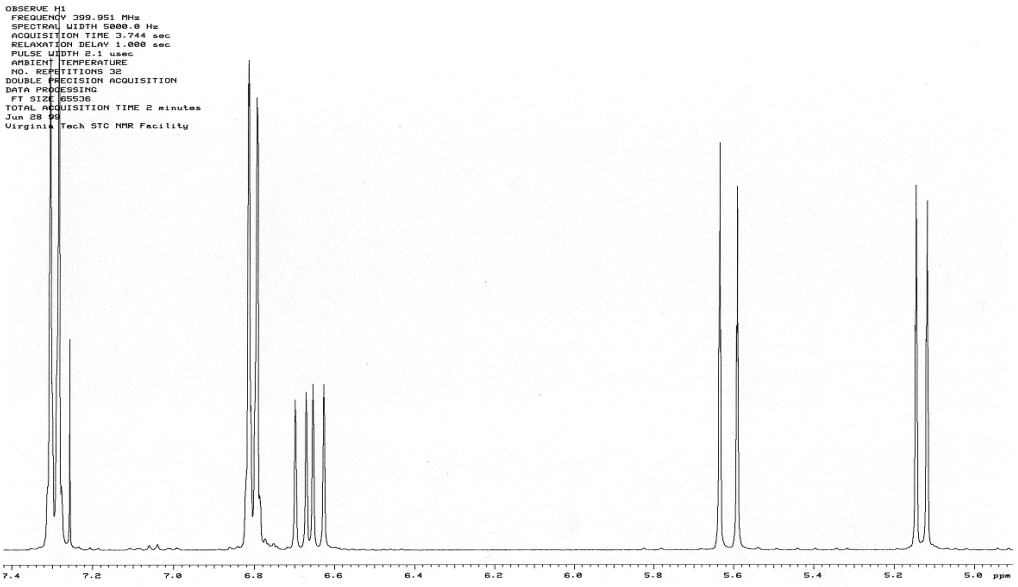
OBSERVE H1
FREQUENCY 399.951 MHz
SPECTRAL WIDTH 5000.0 Hz
ACQUISITION TIME 3.744 sec
RELAXATION DELAY 1.000 sec
PULSE WIDTH 2.1 usec
AMBIENT TEMPERATURE
NO. REPETITIONS 32
DOUBLE PRECISION ACQUISITION
DATA PROCESSING
FT SIZE 65536
TOTAL ACQUISITION TIME 2 minutes
Jun 28 99
Virginia Tech STC NMR Facility
7.4
7.2
7.0
6.8
6.6
6.4
6.2
6.0
5.8
5.6
5.4
5.2
5.0 ppm

(b)

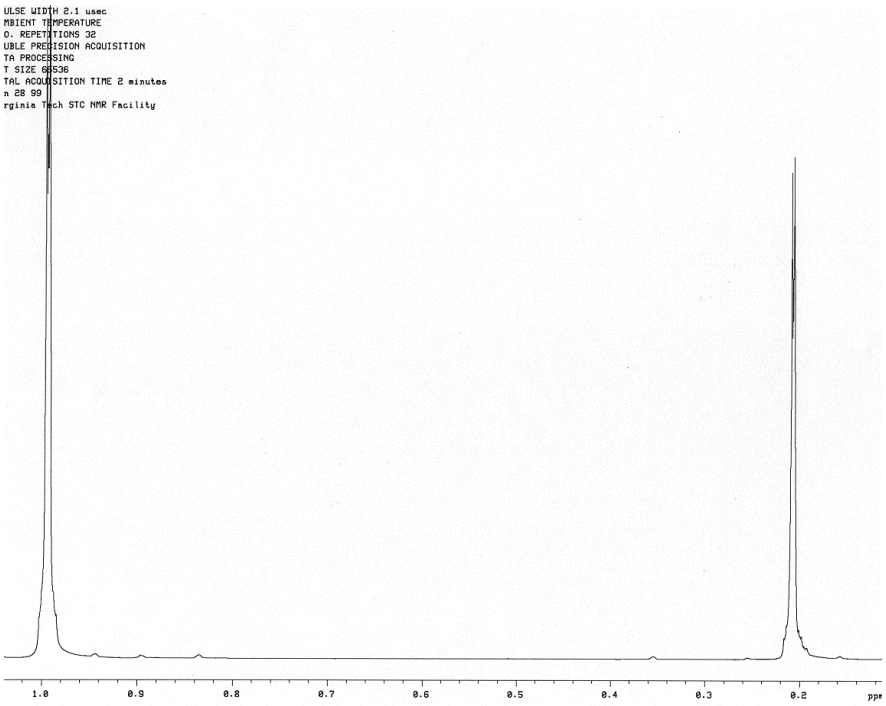

(c)

Figure 3.4. ^{1}H NMR spectrum of *p*-[(*tert*-butyldimethylsilyl)oxy]styrene (1) after distillation (10^{-5} torr, 45 °C). (a) the whole spectrum; (b) & (c), partly enlarged spectra of (a).

3.3.2. Characterization of the Polymers

The synthesized polymers (homo-polymer, *di*- & *tri*- block copolymers) were characterized by GPC, NMR and DSC.

Figure 3.5 shows the gel permeation chromatogram (GPC) traces of the synthesized PS homopolymer (Fig. 3.5. *a*), PS-*b*-PMMA *di*-block copolymers (Fig. 3.5. *b*1 & *b*2), and the TBDMS protected *tri*-block copolymer **2** (Fig. 3.5. *c*). As expected for living polymerization, a single sharp symmetric peak, an indication of relatively narrow molecular weight distributions (MWD), was obtained for each polymer (Figure 3.5).

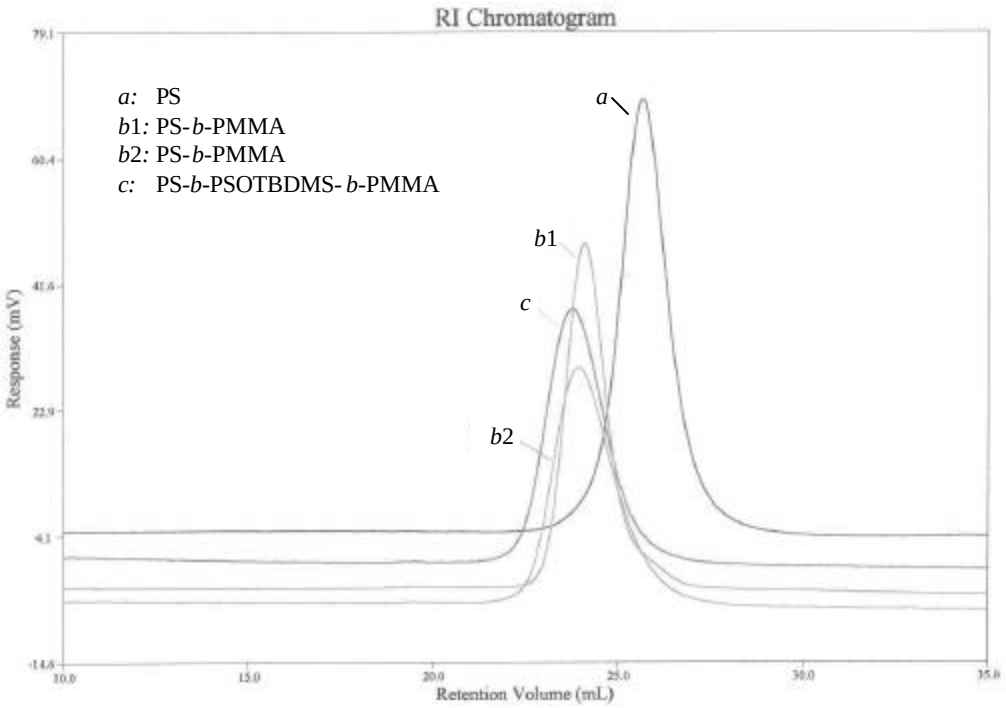

Figure 3.5. GPC traces of the synthesized polymers. *a*) PS homopolymer; *b*1 & *b*2) PS-*b*-PMMA *di*-block copolymers; *c*) *tri*-block copolymer 2.

^{1}H NMR spectra of the polymers are shown in Figures 3.6, 3.7, and 3.8. The existence of the end groups (*sec*-butyl) from the initiator was evident in each spectrum. While an understanding of the spectra in Figure 3.6 and 3.7 is straightforward, the triblock copolymer spectrum (Figure 3.8) is more complex and will be discussed later.

The information of the block sizes of the copolymers was calculated based on the NMR spectra in Figures 3.7 and 3.8 and the GPC data. The specific NMR peaks for each block employed for integration are described as following. PMMA block: 3.6 ppm (3H, -OCH_3); PSOTBDMS block: 0.12 ppm (6H, $Si(CH_3)_2$); PS block: 6.2 – 7.2 ppm (-Ar) (including the contribution from PSOTBDMS or PSSi blocks, which can be subtracted). Using the GPC molecular weights for the block copolymers, the molecular weight of each block copolymer can be obtained.

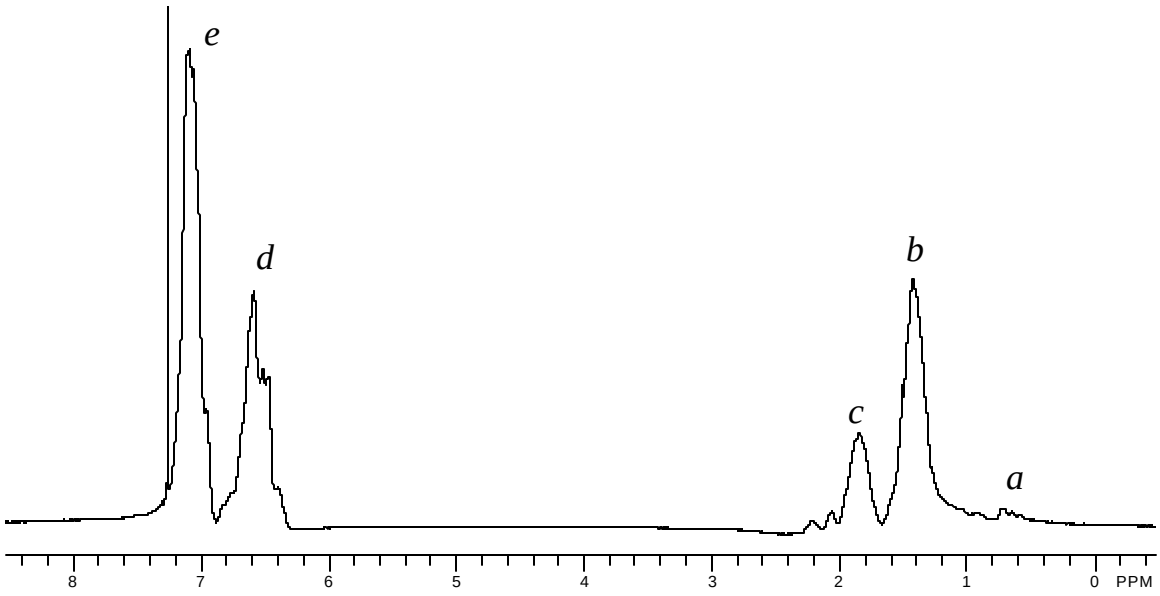

Figure 3.6. ^{1}H NMR spectrum (400 MHz, chloroform-*d*) of living anionic polymerized polystyrene (PS) homopolymer.

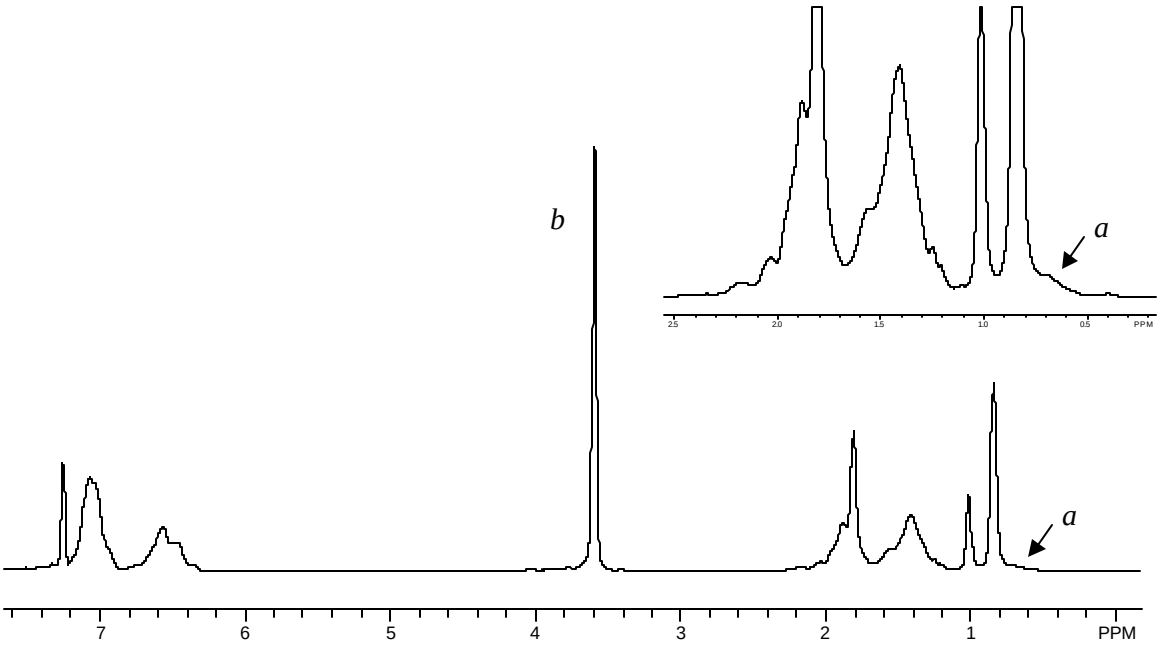

Figure 3.7. ^{1}H NMR spectrum (400 MHz, chloroform-*d*) of living anionic polymerized PS-*b*-PMMA di-block copolymer. Peak *b* was from the methoxy group in the PMMA block. The signal corresponding to the initiator (sec-butyl) was still observed at around 0.7 ppm.

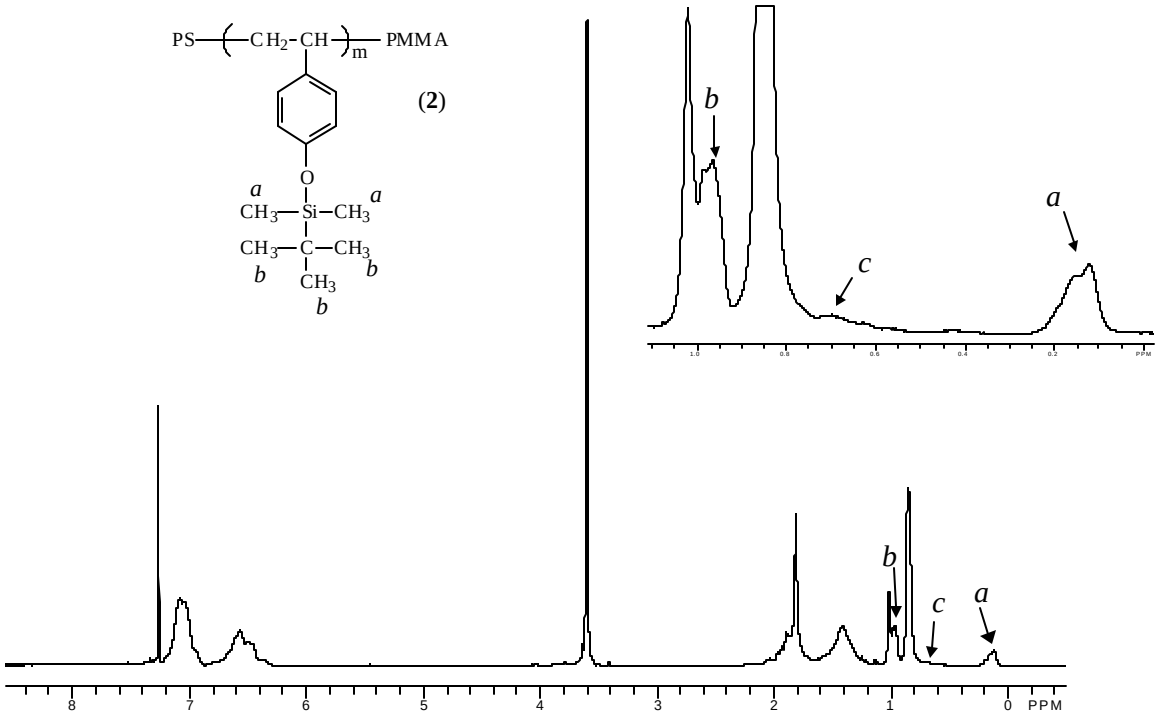

Figure 3.8. ^{1}H NMR spectrum (400 MHz, chloroform-*d*) of living anionic polymerized PS-*b*-poly(*p*-[(*tert*-butyldimethylsilyl)oxy]styrene)-*b*-PMMA(2). Peaks *a* and *b* were from the dimethyl and t-butyl groups of TBDMS, respectively. The signal corresponding to the initiator (sec-butyl) was still observed at around 0.7 ppm.

As summarized in Table 3.1, the distributions (MWD = $<M_w>/<M_n>$) of the polymers ranged from 1.06 to 1.18, which are typical values for living anionic polymerizations. The molecular weight of each polymer obtain from GPC was also very close to the value calculated based on the mole ratio of monomer to *sec*-BuLi (Table 3.1). Another indication of the successful polymerizations is that the yields for all of the polymers are > 99%. Two PS-*b*-PMMA *di*-block copolymers were synthesized using the same feed ratio of the monomer and initiator. The characteristics ($<M_n>$, MWD, block sizes) of the resulting polymers are reasonably close to each other (Table 3.1), which suggest the employed polymerization techniques are quite reliable in controlling polymer structures.

Table 3.1. Molecular weights and compositions of some of the synthesized polymers

	PS	PS-*b*-PMMA (b1)	PS-*b*-PMMA (b2)	PS-*b*-PSOTBDMS-*b*-PMMA (**2**)
Theoretical $<M_n>$ [a]	10.4 k	20.4 k (PS: 10.4k, PMMA: 10k)	20.4 k (PS: 10.4k, PMMA: 10k)	21.9 k (PS: 10k, PSOTBDMS: 1.9k PMMA: 10k)
Experimental $<M_n>$ [b,c]	11.2 k	21.8 k (PS: 11.2k, PMMA: 10.6k)	22.4 k (PS: 11.4k, PMMA: 11k)	23.5 k (PS: 11.4k, PSOTBDMS: 1.6k, PMMA: 10.5k)
$<M_w>/<M_n>$ [b]	1.06	1.09	1.08	1.16

[a] Calculated based on the mole ratio of monomers to *sec*-BuLi
[b] From GPC data (PS standard)
[c] On the basis of integration of the ^{1}H NMR signal

Figure 3.9 depicts a gel permeation chromatogram (GPC) of the synthesized block copolymers. As expected for a living polymerization a single sharp symmetric peak, an indication of relatively narrow molecular weight distributions (MWD), was obtained for the TBDMS protected *tri*-block copolymer **2** (Figure 3.9, a). As shown in Scheme 3.4, the central functionalized block copolymer **3** (PS-*b*-PSOH-*b*-PMMA) was obtained from **2** after quantitative hydrolysis of the protecting group. Polymer **3** was carefully purified by repeated wash-dissolve-precipitate steps and dried in vacuo (110 °C) prior to GPC analysis, NMR confirmed the absence of impurities (Figure 3.10). However, the GPC trace of polymer **3** shows a much weaker signal and a broad tail on the low molecular weight side (Figure 3.9). A mild hydrolysis process used in the experiment is unlikely to form low molecular weight oligmers. It is believed that the observed weak and broad

GPC peak was due to the existence of the phenol groups in the central block of polymer **2**. A certain degree of hydrogen-bonding between the poly(4-hydroxystyrene) and PMMA blocks can be reasonably expected. As suggested in the literature,[21] strong specific interactions (e.g., hydrogen bonding, acid-base interaction, etc.) may cause a more compact chain coil conformation than expected in dilute solutions.

Further evidence to support that polymer **3** possessed a narrow molecular weight distribution and no chain cleavage is shown in the following discussion. Figure 3.9-*c* is the GPC trace of the second central functionalized *tri*-block copolymer PS-*b*-poly(4-urethanopropyl triethoxysilanestyrene)-*b*-PMMA (PS-*b*-PSSi-*b*-PMMA) (**4**), which was obtained from the modification of **3** (Scheme 3.4). The GPC trace of polymer **4** shows a single symmetric narrow peak that is almost identical to that of polymer **2**. The slight difference of the two peak positions may be due to the larger functional groups in **4** than the TBDMS protecting groups in **2**. The similarity between the two GPC traces of **2** and **4** strongly indicates that the polymer backbone was unchanged during the formation of polymer **3**.

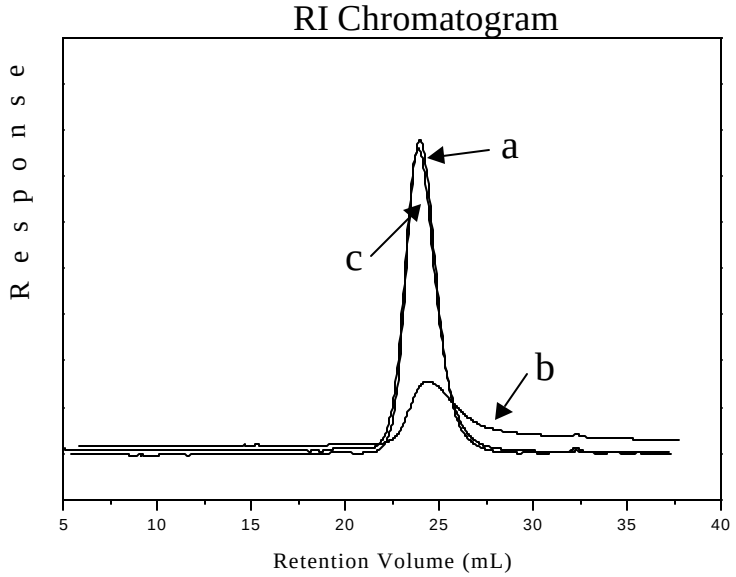

Figure 3.9 GPC traces of the synthesized *tri*-block copolymers. a) *tri*-block copolymer **2**; b) *tri*-block copolymer **3**; c) *tri*-block copolymer **4**.

^{1}H NMR (400 MHz) spectra of the *tri*-block copolymers are shown in Figure 3.10. All resonances contributed by PS and PMMA blocks in the *tri*-block copolymers

were assigned based on PS and PS-*b*-PMMA controls (Figure 3.6 and 3.7) and their positions were found to be unchanged by the desilylation and modification processes. The two arrows in the top spectrum of Figure 3.10 indicate the protecting group (TBDMS) in polymer **2** and its disappearance after desilylation (center spectrum, Figure 3.10). The five arrows in the spectrum of PS-*b*-PSSi-*b*-PMMA (**4**) (bottom spectrum, Figure 3.10) arose from the new functional groups created through the polymer modification step. The corresponding new peak positions were shifted down field (~0.02 ppm) and the peaks were broadened compared to the functionalization reagent (Figure 3.11). Broadening of the functionalization reagent resonances was attributed to the covalent attachment of the functional group to a high molecular weight polymer backbone.

Further chemical structure information of the copolymer **2** & **3** was provided in Figures 3.12 and 3.13, respectively. ^{29}Si NMR was used to detect the silyl groups in the TBDMS protected *tri*-block copolymer **2**. The peak at 19.98 ppm is direct evidence of the existence of the TBDMS groups in the copolymer, which can be separated from the signal from the glass NMR test tube (~ -120ppm) and the signal from TMS standard (0 ppm) (Figure 3.12). ^{13}C NMR spectrum of the copolymer **3** is provided in Figure 3.13.

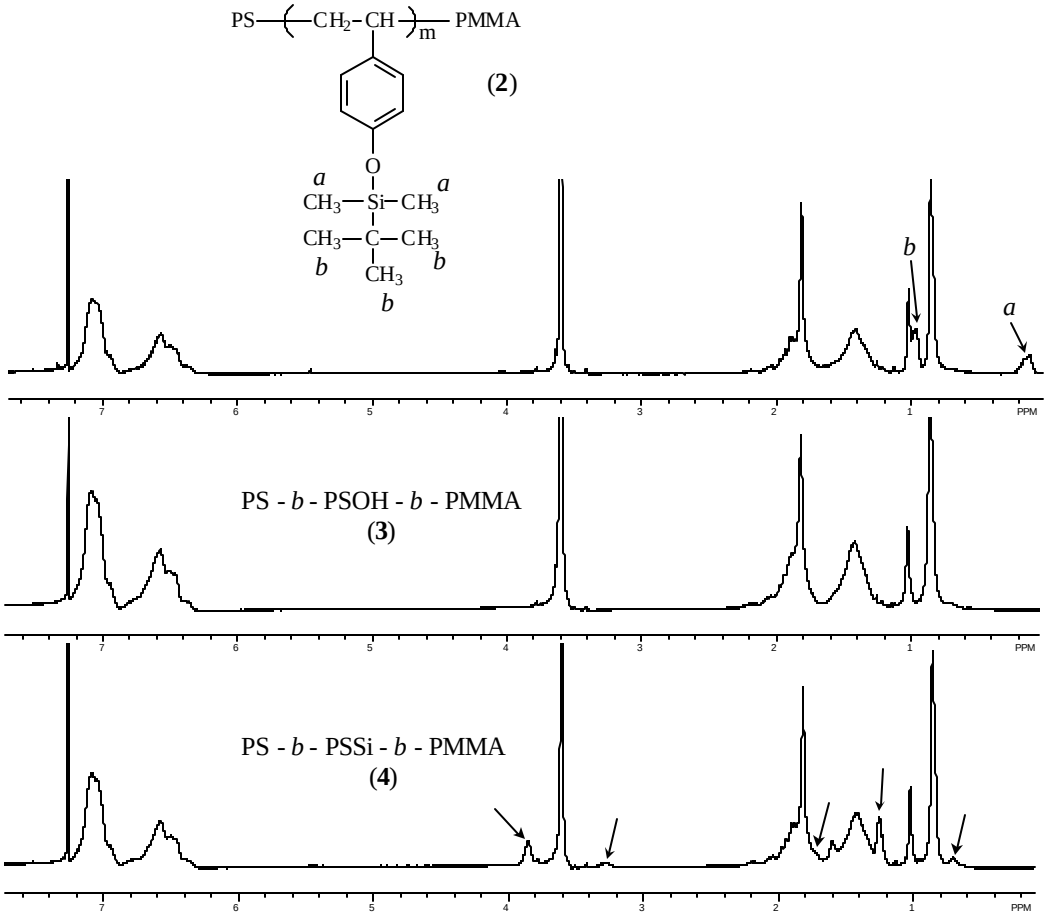

Figure 3.10 NMR spectra of PS - *b* – poly(*p*-[(*tert*-butyldimethylsilyl) oxy]styrene) - *b* – PMMA (top), PS - *b* - PSOH - *b* – PMMA (center), and PS - *b* - PSSi - *b* - PMMA (bottom)

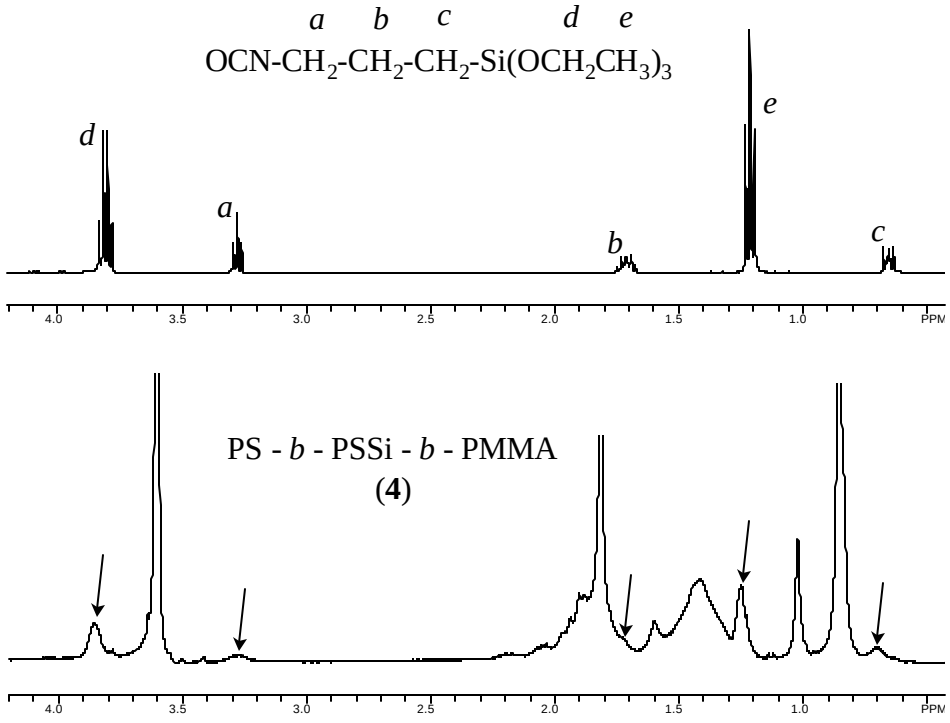

Figure 3.11. NMR spectra of isocynato propyl triethoxysilane (top) and PS - *b* - PSSi - *b* - PMMA (bottom)

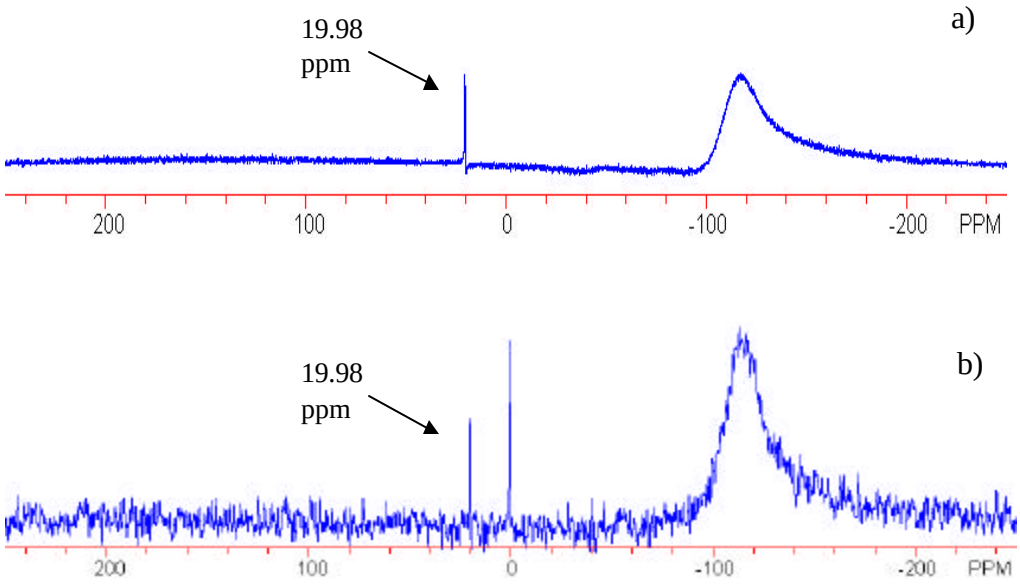

Figure 3.12. ^{29}Si NMR spectra of of PS-*b*-poly(*p*-[(*tert*-butyldimethylsilyl)oxy] styrene)-*b*-PMMA 2, a) without adding inside standard TMS, b) with TMS. The peak for the silyl protection group in the polymer appeared at 19.98ppm in a) and b).

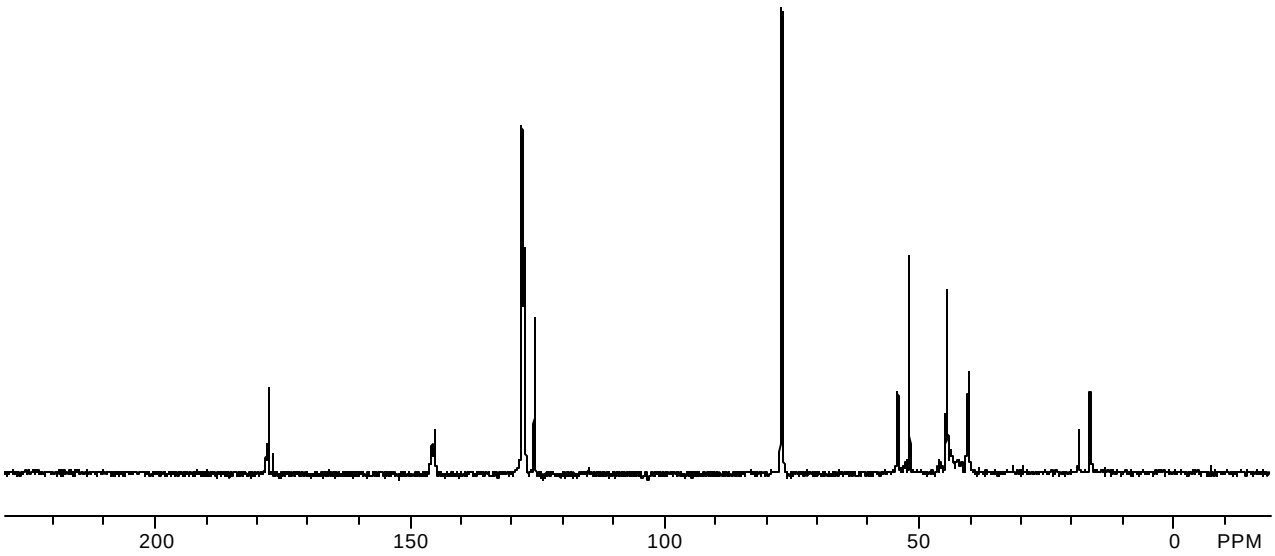

Figure 3.13. ^{13}C NMR of *tri*-block copolymer **3**.

The compositions and molecular weights of the synthesized block copolymers are summarized in Table 3.2. The *tri*-block copolymers **2** and **4** possessed a narrow molecular weight distribution (polydispersities of 1.15 to 1.20). From the ^{1}H NMR results, the molecular weight ratios for the different polymer blocks was calculated. The specific NMR peaks for each block employed for integration are described as following. PMMA block: 3.6 ppm (-OCH_3); PSOTBDMS block: 0.12 ppm ($Si(CH_3)_2$); PSSi block: 3.84 ppm (Si-O-CH_2-); PS block: 6.2 – 7.2 ppm (-Ar) (including the contribution from PSOTBDMS or PSSi blocks, which can be subtracted). Using the GPC molecular weights for the block copolymers, the molecular weight of each block in *tri*-block copolymer **2** and **4** was obtained. The number of repeat units of the PSOTBDMS block in polymer **2** was determined to be approximately 7/chain and that of the PSSi block in polymer **4** was approximately 6.5/chain, which was considered to be within experimental error. Thus, the quantitative reaction between the isocyanate groups and the phenol groups during the formation of polymer **4** was supported. As for *tri*-block copolymer **3** (PS-*b*-PSOH-*b*-PMMA), the polymer backbone was unchanged during the desilylation process as discussed before, and complete desilylation was guaranteed by the disappearance of the resonances at 0.12 ppm ($Si(CH_3)_2$) and 0.95 ppm ($SiC(CH_3)_3$) (Figure 3.10). The composition and molecular weight of polymer **3** listed in Table 3.2 was based on polymer **2**.

Table 3.2. Molecular weights and compositions of the synthesized *tri*-block copolymers

	PS-*b*-PSOTBDMS-*b*-PMMA (**2**)	PS-*b*-PSOH-*b*-PMMA (**3**)	PS-*b*-PSSi-*b*-PMMA (**4**)
Theoretical $<M_n>$ [a]	21.9 k (PS: 10k, PSOTBDMS: 1.9k PMMA: 10k)	21 k (PS: 10k, PSOH: 1k PMMA: 10k)	22.9 k (PS: 10k, PSSi: 2.1k PMMA: 10k)
Experimental $<M_n>$	23.5 k[b] (PS: 11.4k[c], PSOTBDMS: 1.6k[c] PMMA: 10.5k[c])	21.2 k[d] (PS: 11.4k[d], PSOH: 0.9k[d], PMMA: 10.5k[d])	24.3 k[b] (PS: 11.5k[c], PSSi: 2.2k[c], PMMA: 10.6k[c])
$<M_w>/<M_n>$	1.16[b]	N/A	1.18[b]

[a] Calculated based on the mole ratio of monomers to *sec*-BuLi
[b] From GPC data (PS standard)
[c] On the basis of integration of the ^{1}H NMR signal
[d] Based on the discussion in the text

The thermal properties of the synthesized polymers were examined by DSC. Some examples are provided in Figure 3.14. The heating curve of the *di*-block (PS-*b*-PMMA) displayed a relatively broad glass transition temperature (T_g) around 100 °C -- reasonable because of the close glass transition temperatures of the two blocks (both about 100 °C). Interestingly, there were three detectable glass transition temperatures, namely, 77 °C, 98 °C and 107 °C, on the DSC curve of the *tri*-block copolymer **2**. There was no clear explanation for the result, and more discussions on the DSC data, as well as rheological and microscopic results of the synthesized polymers, are provided in Chapter 8.

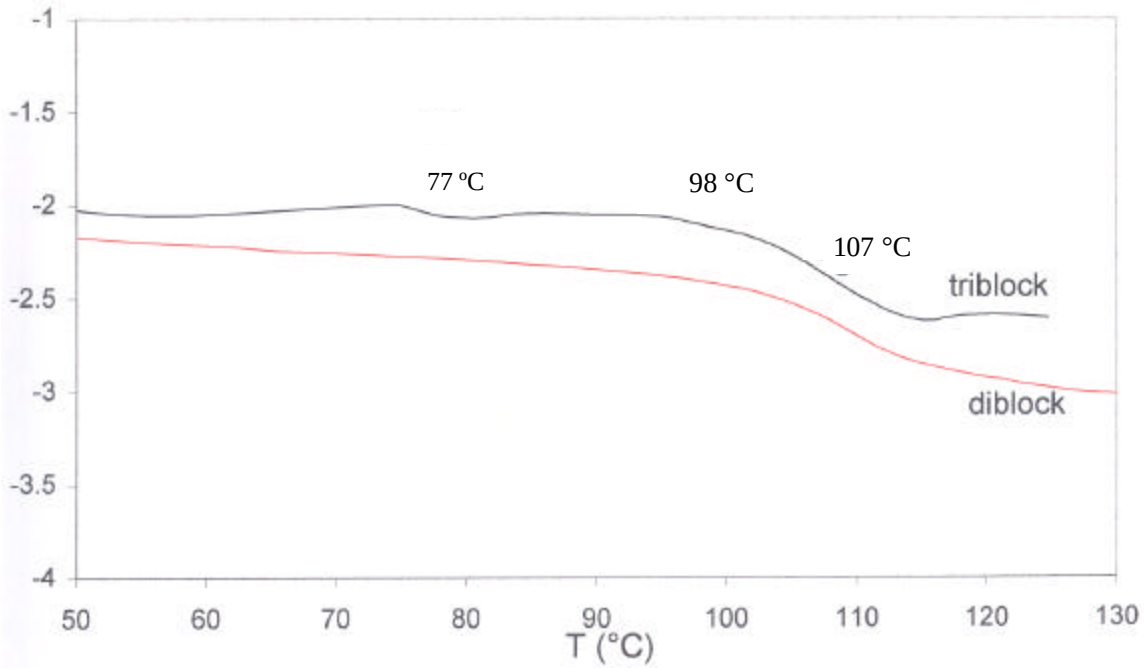

Figure 3.14. DSC curves (2nd heat) of PS-*b*-PMMA and *tri*-block copolymer 2.

The morphological characterization of the *tri*-block copolymers using transmission electron microscopy (TEM) and atomic force microscopy (AFM), and the characterization of the resulting polymer brushes will be described in more detail in later sections.

The synthesis of the CFABC triblock copolymer series can be easily extended to include other hydrophilic-functionalized-hydrophobic combinations with particular attention to poly(methacrylic acid) hydrophilic blocks and poly(diene) based hydrophobic blocks. Poly(methacrylic acid) is obtained via the living anionic polymerization of poly(t-butyl methacrylate) in polar solvents followed by hydrolysis. In addition, recent advances in stable free radical (SFRP) and atom transfer radical polymerization (ATRP) will permit more facile syntheses in some instances than those achieved by traditional living anionic techniques.

3.4. Conclusions

Well-defined central functionalized asymmetric *tri*-block copolymers (CFABC), PS-*b*-PSOH-*b*-PMMA and PS-*b*-PSSi-*b*-PMMA were successfully synthesized. Through

a combination of living anionic polymerization and polymer modification techniques, the chemical structures of the copolymers were precisely controlled.

The main purpose of this part of the research is, however, not to limit our vision to only the two synthesized CFABC copolymers, but rather to illustrate potential research opportunities for surface modifications by designing appropriate CFABC copolymers utilizing traditional synthetic methods. A fundamental understanding of complex polymer brush behaviors is only possible with model systems comprised of *well-defined functional polymers*.

Well-defined PS homopolymer and PS-*b*-PMMA *di*-block copolymers were also successfully synthesized using living anionic polymerization. These model polymers can be used as a control for the CFABC polymer systems, as well as for other fundamental studies.

CHAPTER 4. CFABC POLYMER BRUSH PREPARATION AND CHARACTERIZATION

4.1. Introduction

It is well known that substrate surfaces can be modified by small molecules, such as surfactants.[1,2] Polymer brushes have also been used to modify surfaces.[3,4,5] Polymer brushes are polymer chains tethered on substrate surfaces via physisorption or chemical bonding.[6] Recent focus has been directed towards the control of intermolecular interactions between polymer brush modified surfaces and external agents such as solvents and polymers.[7,8,9] P. G. de Gennes and coworkers[10] proposed a model to predict the relationship of polymer brush chain coverage and interfacial adhesion energy enhancement between the polymer brush modified substrate and another polymer material. One important conclusion based on the model was that a relatively low coverage was needed to get maximum adhesion enhancement. Additionally, local surface energies can also be controlled by preparing heterogeneous surfaces using polymer brushes. For example, patterned polymer brushes containing discrete micrometer-scale hydrophilic and hydrophobic square areas were successfully prepared in Hawker's group by combining photolithographic techniques with surface-initiated polymerization.[11]

A typical feature for chemically grafted polymer brush systems is that only a single chain is bonded to each grafting site via the chain terminus. In the previous chapter, the design and synthesis of central functionalized asymmetric *tri*-block copolymers (CFABC) were described in detail. A new family of polymer brushes based

[1] Zhao, X. M.; Wilbur, J, L.; Whitesides, G. M., *Langmuir* **1996**, 12 5504;
[2] Li, X. H.; Chin, D. N.; Whitesides, G. M., *J Org. Chem.* **1996**, 61, 1779
[3] Miller, S. T., *Science* **1991**, 251, 905
[4] Mansky, P.; Liu, Y.; Huang, E.; Russell, T. P.; Hawker, C. J., *Science* 1997, 275, 1458.
[5] Zhao, B.; Brittain, W. J., *Progress in Polymer Science* **2000**, 25, 677
[6] de Gennes, P. G., *J. Phys.* (Paris) **1976**, 37, 1443
[7] Zhao, B.; Brittain, W. J., *J. Am. Chem. Soc.* **1999**, 121, 3557.
[8] Huang, E.; Pruzinsky, S.; Russell, T. P.; Mays, J.; Hawker, C. J., *Macromolecules* **1999**, 32, 5299.
[9] Bernard, B.; Brown, H. R.; Hawker, C. J.; Kellock, A. J.; Russell, T. P., *Macromolecules* **1999**, 32 6254.
[10] Raphael, E.; de Gennes, P. G., *J. Phys. Chem.* **1992**, 96, 4002

on the CFABC, which have two different polymer chains connecting to each grafting site, was proposed. Scheme 4.1 depicts the difference between traditional systems and this approach.

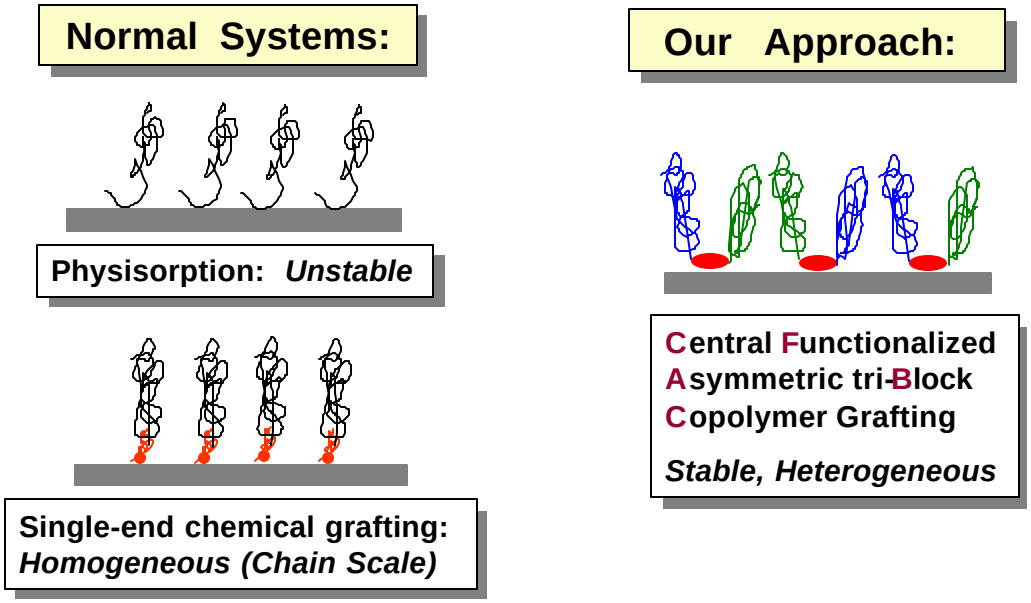

Scheme 4.1 The concept of CFABC polymer brushes

In this chapter, the detail of the polymer brush preparation on silicon wafers using CFABC polymers will be discussed. Various techniques, including AFM, XPS and ellipsometry were employed to examine the modified surfaces and to determine the characteristics of the polymer brush, such as topology, coverage, and thickness, etc.

4.2. Experiments

4.2.1. Materials

One of the synthesized well-defined central functionalized asymmetric *tri*-block copolymers, polystyrene-*b*-poly(4-urethanopropyl triethoxysilylstyrene)-*b*-poly(methyl methacrylate) (PS-*b*-PSSi-*b*-PMMA) was used to modify silicon wafer surfaces. The details of the synthesis and characterization of this CFABC polymer were described in Chapter 3. The chemical structure is shown in Scheme 4.1. The copolymer has a narrow

[11] Husemann, M.; Morrison, M.; Benoit, D.; Frommer, J.; Mate, C. M.; Hinsberg, W. D.; Hedrick, J. L.; Hawker, C. J., *J. Am. Chem. Soc.* **2000**, 122, 1844.

molecular weight distribution (MWD = 1.18) and precisely controlled block lengths (PS: 11,500 g/mol; PSSi: 2,200 g/mol; PMMA: 10,600 g/mol). This well-defined structure enables an understanding of structure–property relationships in our model system.

A PS-*b*-PMMA *di*-block copolymer (<M_n> = 22,000 g/mol, 50 mol% PS, polydispersity = 1.06) was synthesized (Chapter 3) and used as a control material. This polymer can not chemically attach to a surface under conditions explored in this thesis.

Silicon wafers (n type, 111) with a native oxide layer (~ 5 nm) were obtained from Motorola Co., and the pretreatment is described in the next section.

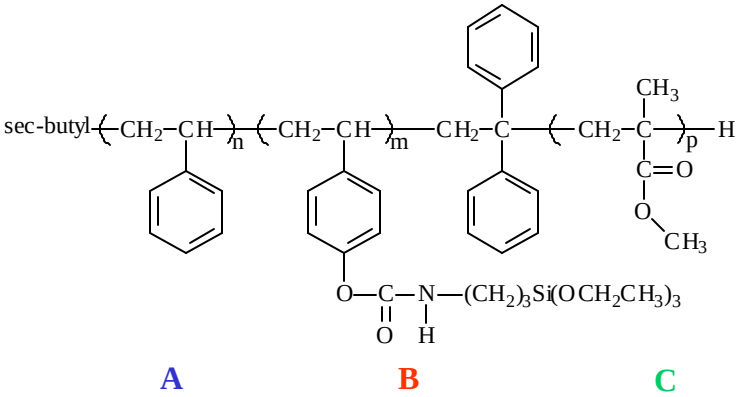

Scheme 4.2. Chemical structure of a CFABC polymer

4.2.2. CFABC polymer brush preparation

Silicon wafers were cut into small pieces (2cm × 2cm) using a diamond knife and cleaned as described in the literature.[12] The CFABC copolymer was dissolved in toluene (HPLC grade, Aldrich) at a concentration of 1% (w/v) and spin-coated on silicon wafers (2000 rpm). These samples were heated at 170°C in the presence of moisture for 48 hours.[13] The non-covalently bound copolymers were then extracted with toluene using a Soxhlet extractor for 10 hours. This process is schematically shown below (Scheme 4.3). At least six samples were prepared at the same time for later characterization.

[12] Zhao B.; Brittain, W. J., *Macromolecules* **2000**, 33, 342
[13] Vitt, E.; Shull, K. R., *Macromolecules*, **1995**, 28, 6349

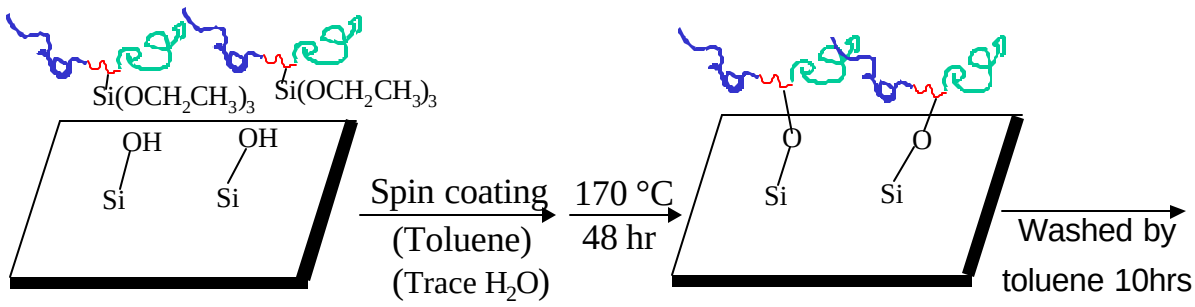

Scheme 4.3. CFABC polymer brush grafting process

4.2.3. Characterization

The topology of the polymer brushes was investigated using a Molecular Imaging PicoScan™ atomic force microscope (AFM). The deflection mode was chosen to yield a high sensitivity to surface height differences. Another AFM (Dimension 3000, Digital Instrument Inc.) with Tapping Mode® was also used to obtain height and phase images at the same time.

X-ray photoelectron spectroscopy (XPS) was employed to confirm the chemical composition of the modified surfaces and to estimate the thickness of the polymer brushes. XPS spectra were obtained using a Perkin-Elmer Model 5400 XPS spectrometer with a Mg Kα X-ray source (1253.6 eV), operated at 300 W and 14 kV DC, with an emission current of 25 mA. The spot size was 1.0 x 3.0 mm. Photoelectrons were analyzed in a hemispherical analyzer using a position-sensitive detector.

4.3. Results and Discussions

4.3.1. Topology of CFABC polymer brush

Figure 4.1 shows the surface topologies, measured by AFM, of both an unmodified silicon substrate and the CFABC grafted substrate after the washing procedure (Soxhlet extraction). The deflection mode was chosen to yield a high sensitivity to surface height differences. As expected, a relatively smooth surface was observed for the unmodified silicon substrate (Figure 4.1a), and the three bright spots in the image were attributed to dust particles, suggesting good resolution of the image. In contrast, a very different topological structure was observed for the polymer grafted

silicon substrate (Figure 4.1b), where domains with a size of about 20 nm appeared on the surface. In order to ensure that the detected surface structure was not formed from residual (un-reacted) polymer, a comparative experiment using the poly(styrene-*b*-methyl methacrylate) block copolymer mentioned above was undertaken using similar grafting and washing conditions. In this latter case, the AFM phase images indicated a smooth surface without any structure (Figure 4.2). Thus, the observed topology in Figure 1b was attributed to chemically grafted CFABC polymers on the silicon surface.

During the whole washing process (Soxhlet extraction, 10 hours), the samples were removed periodically and their topologies were examined by AFM. The evolution of the surface topologies at different washing stages is shown in Figure 4.3. Interesting nano-patterns were observed during the washing process, and more discussion will be provided in Chapter 6.

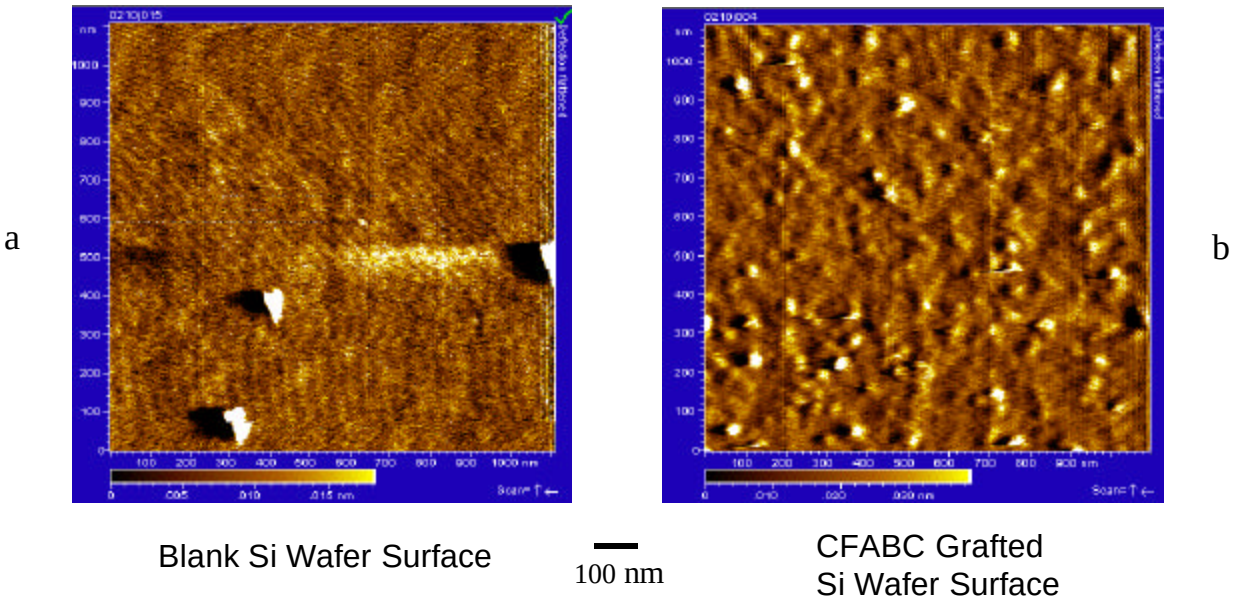

Figure 4.1. AFM (deflection mode) images of blank silicon wafer surface (a), and CFABC (PS-b-PSSi-b-PMMA) grafted silicon wafer surface (b). The same washing process was used for each sample: 10 hours Soxhlet extraction (toluene).

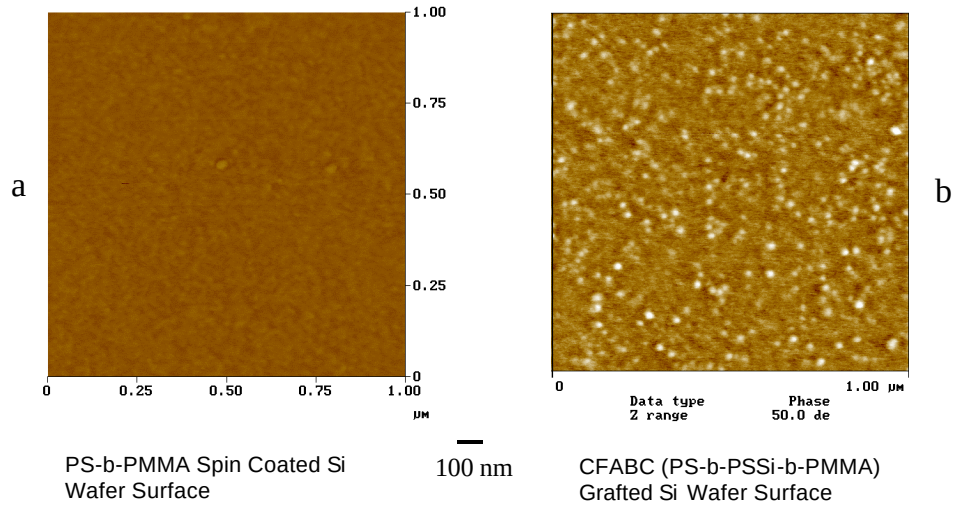

Figure 4.2 AFM (tapping mode) phase images of PS-b-PMMA spin coated Si wafer surface(a), and CFABC (PS-b-PSSi-b-PMMA) grafted silicon wafer surface (b). The same washing process was used for each sample: 10 hours Soxhlet extraction (toluene).

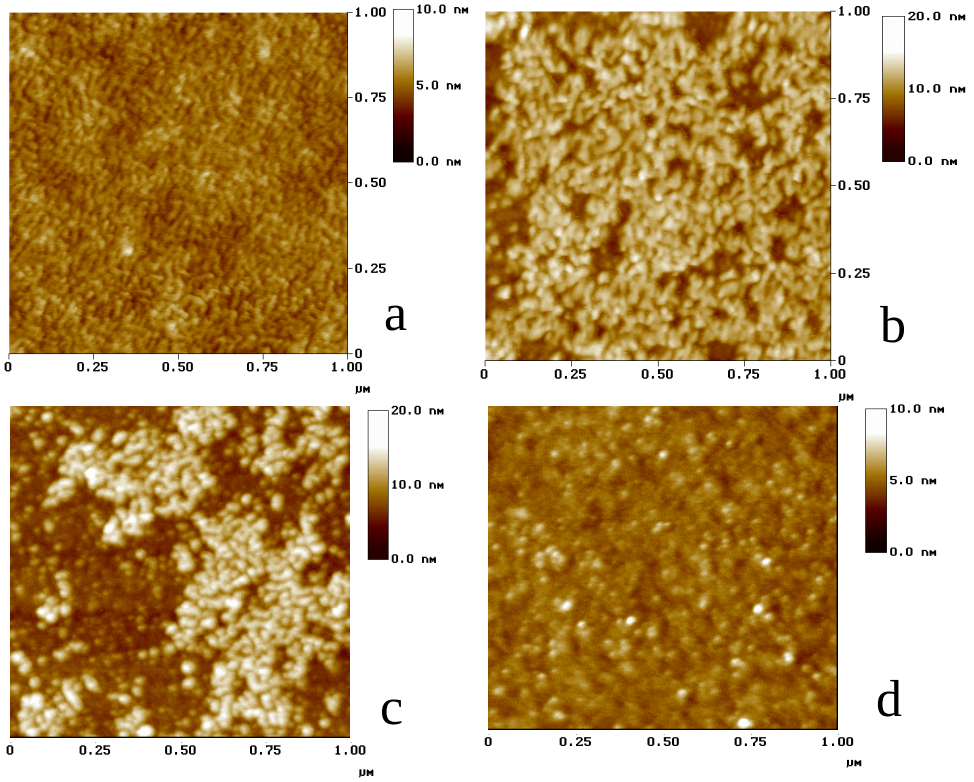

Figure 4.3. AFM (tapping mode) height images of CFABC (PS-b-PSSi-b-PMMA) grafted silicon wafer surface at different washing stages. a), unwashed; b), partially washed (~10 minutes); c), partially washed (~ 1 hours); d), completely washed (~ 10 hours).

4.3.2. Surface Chemical Composition and Brush Thickness

XPS was used to characterize the chemical composition of the CFABC brush grafted silicon wafer surface. Different data collect angles, namely, 90°, 45°, and 15° were employed, resulting in different sampling depths. An unmodified clean silicon wafer surface was also examined by XPS as a control.

It is known that a native oxide layer exists on the top of silicon wafers, with a thickness of about 1.5nm.[14] On the top of that SiO_2 layer, there are a certain number of Si-OH groups. Figure 4.4 shows the XPS result (90° collect angle) of an unmodified silicon wafer surface. It is very clear that the Si2p multiplex has two peaks, one is at 103.2 eV, from Si-O-H, and the other is at 99.3 eV, from SiO_2. Since those Si-OH groups are located on the very top of the SiO_2 layer, it is reasonable that the relative signal intensity of the Si2p peak at 103.2 - 103.4 eV (comparing with that of 99.3 eV) should be higher when lower collect angles are employed. This trend was observed, and the XPS results for collect angles of 45° and 15° are shown in Figure 4.5. and 4.6, respectively.

[14] Mansky P, Liu Y, Huang E, Russell TP, Hawker CJ. *Science* **1997**;275:1458

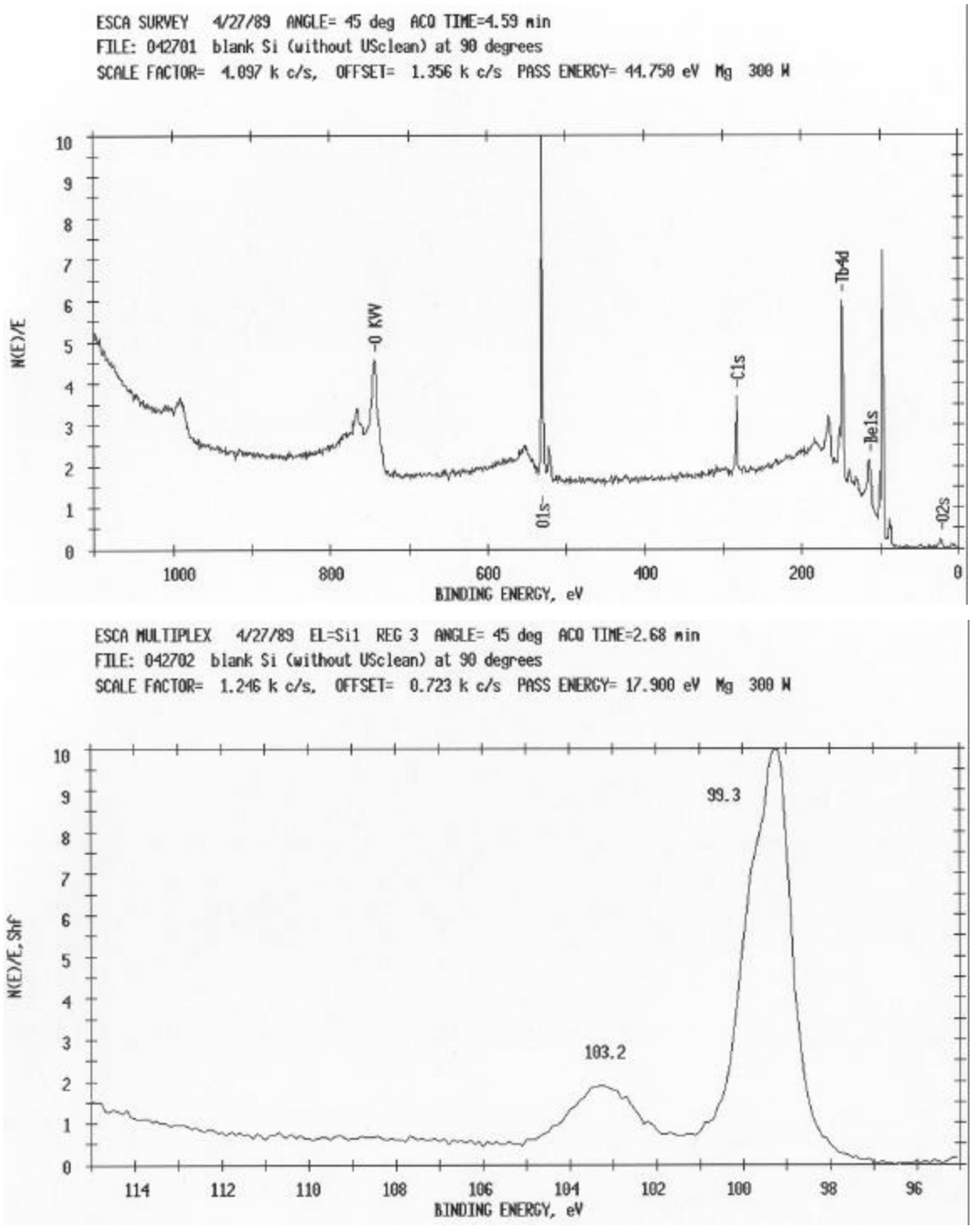

Figure 4.4. XPS of a clean (unmodified) silicon wafer surface with a collect angle of 90°

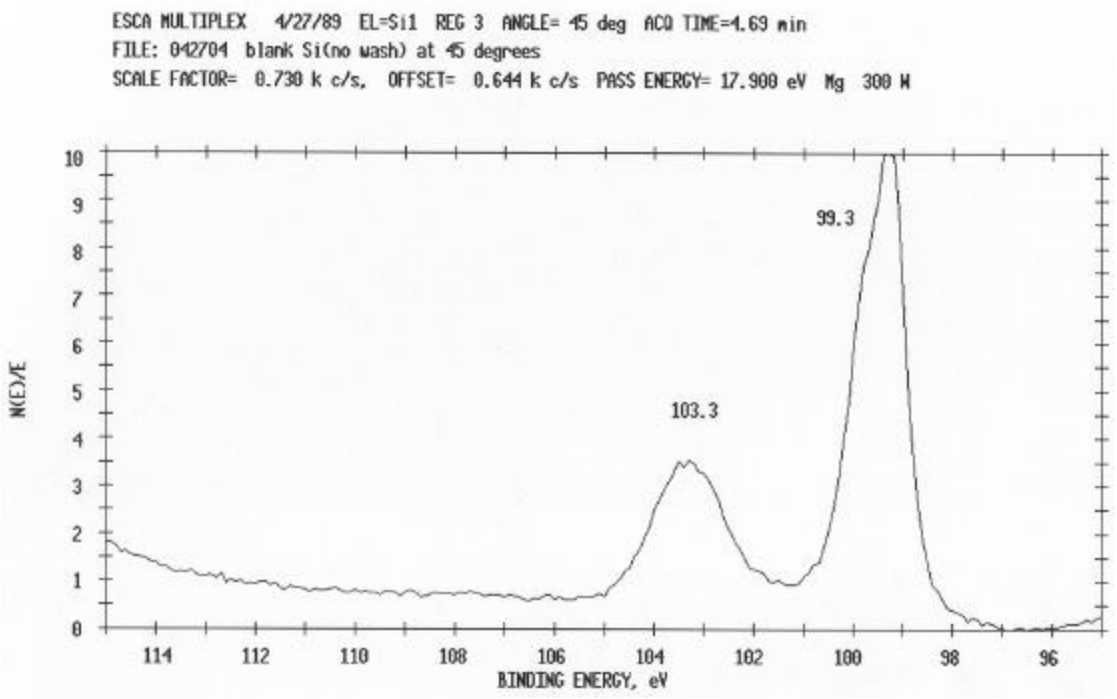

Figure 4.5. XPS Si2p multiplex result of a clean (unmodified) silicon wafer surface with a collect angle of 45°

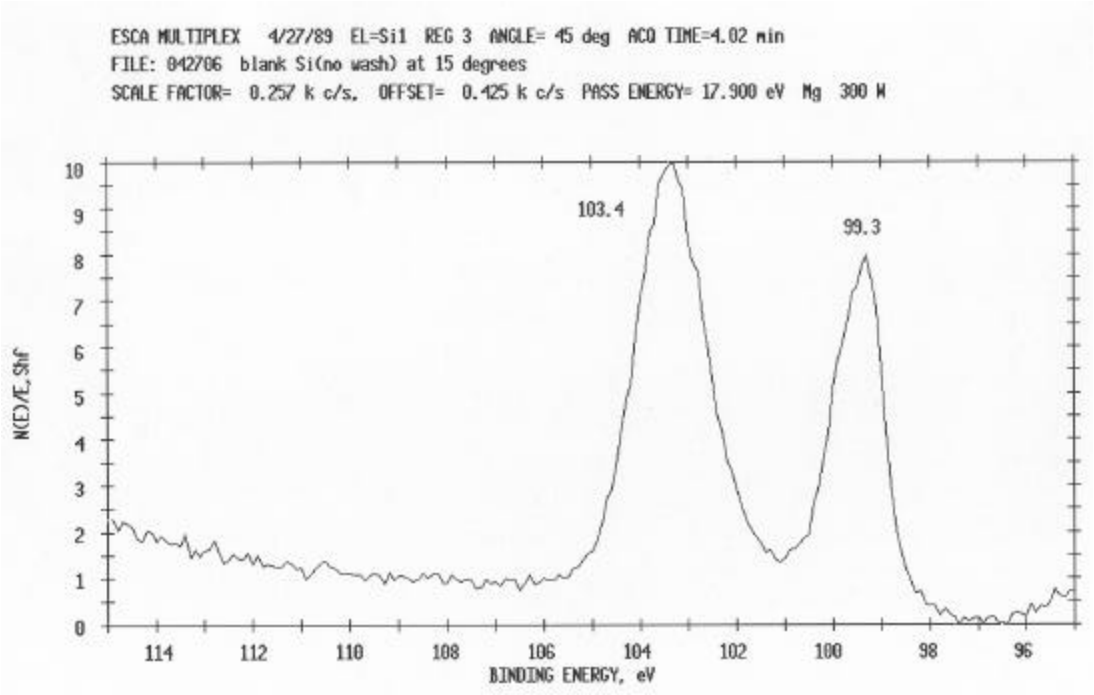

Figure 4.6. XPS Si2p multiplex result of a clean (unmodified) silicon wafer surface with a collect angle of 15°

The XPS results for CFABC grafted silicon wafer surfaces are provided in Figures 4.7, 4.8 and 4.9. The elemental concentrations corresponding to different data collect angles are summarized in Table 4.1.

With a collect angle of 90° (Figure 4.7), two Si2p peaks were observed occurring at 103.5 eV and 99.4 eV. The total Si2p concentration was 7.41% (Table 4.1). When the collect angle was decreased to 45°, the total Si2p concentration also decreased (2.55%, Table 4.1), and the relative signal intensity of Si2p peak at 103.4 eV (comparing with that of 99.3 eV) increased (Figure 4.8). Finally, when the collect angle was decreased to 15°, no significant Si2p signal was detected (Figure 4.9) and the concentration of Si2p was negligible (0.07%, Table 4.1). The XPS survey scans collected at different angles were also included in Figures 4.7 – 4.9. As summarized in Table 4.1, with decreased collect angles (from 90° to 15°), the elemental concentration of carbon was increased, while that of oxygen was decreased, supporting the presence of the CFABC.

Two types of information can be obtained from the aforementioned XPS data. First, the XPS results in Figure 4.9 (15° collect angle) suggest that the entire surface was *fully covered* by CFABC polymer brush, since the element Si was not detected. Second, the thickness of the polymer brush can be estimated. Generally, a 90° collect angle gives information on a depth of about 5 nm, and collect angles of 45° and 15° correspond to depths of approximately 3.5 nm and 1.3 nm, respectively. Since the silicon substrate was detected with a collect angle of 45° but not 15°, the thickness of the polymer brush was estimated to range between 1.3 nm to 3.5 nm, with an average value of 2.4 nm. This estimation was supported by ellipsometry data, which indicated a thickness of about 2.0 ± 0.5 nm. The radius of gyration for the PS, or the PMMA, block (both ~ 11,000 g/mol) in the CFABC polymer in bulk state is about 1.2 nm based on the unperturbed chain configuration model.[15] As discussed in the literature[16], the chain configurations in a polymer brush system are usually in more extended states than those in bulk. With an estimated thickness of around 2 nm, the CFABC polymer brush was believed to be a monomolecular layer.

[15] Flory, P. J., Principles of Polymer Chemistry, Cornell University Press, Ithaca, NY 1981
[16] de Gennes, P. G., *J. Phys.* (Paris) **1976**, 37, 1443

4.4. Conclusions

In conclusion, a chemically bonded polymer brush was obtained by surface condensation using a novel CFABC polymer containing a central trialkoxysilyl functionality. The polymer brush fully covered the surface. The thickness of the polymer brush was about 2 nm, which suggested a monolayered structure. The surface properties of the CFABC polymer brush modified surfaces and their applications in different areas, such as interfacial adhesion energy, structure control in polymer thin films, etc., will be discussed in the next two chapters.

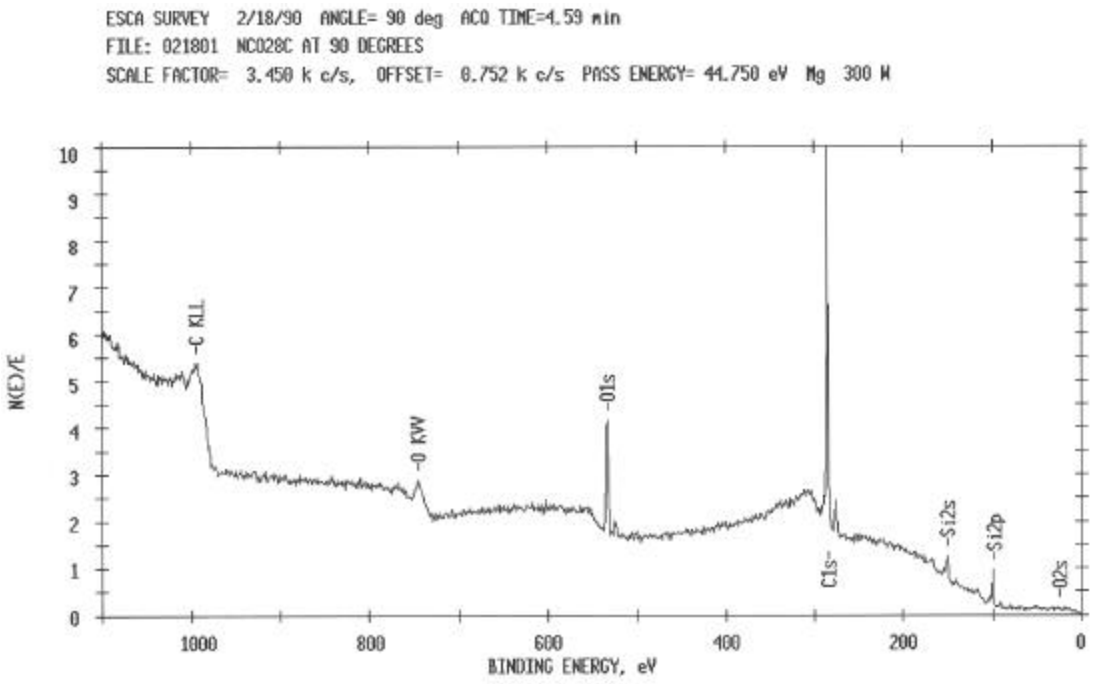

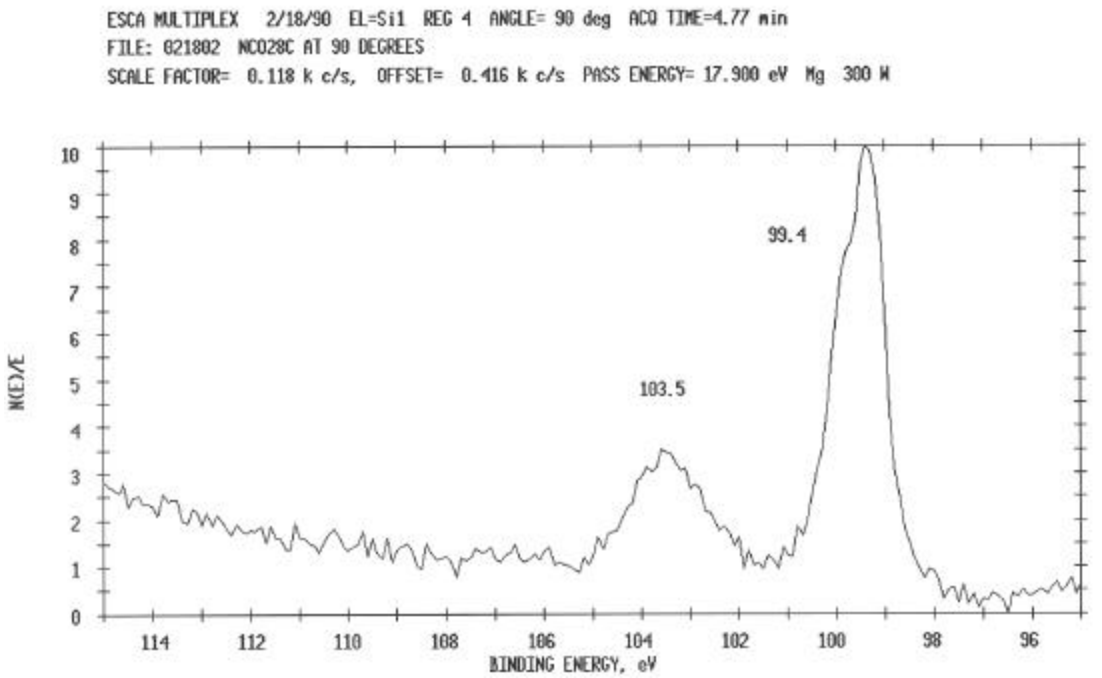

Figure 4.7. XPS of CFABC brush grafted silicon wafer surface with a collect angle of 90°

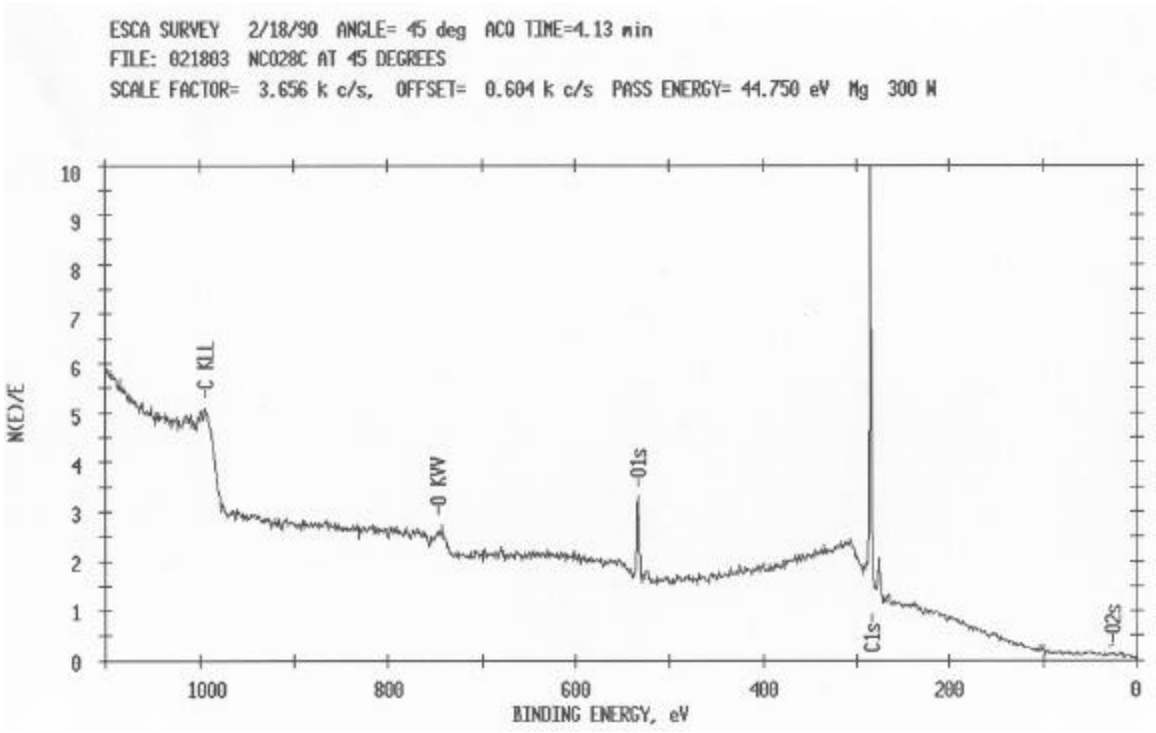

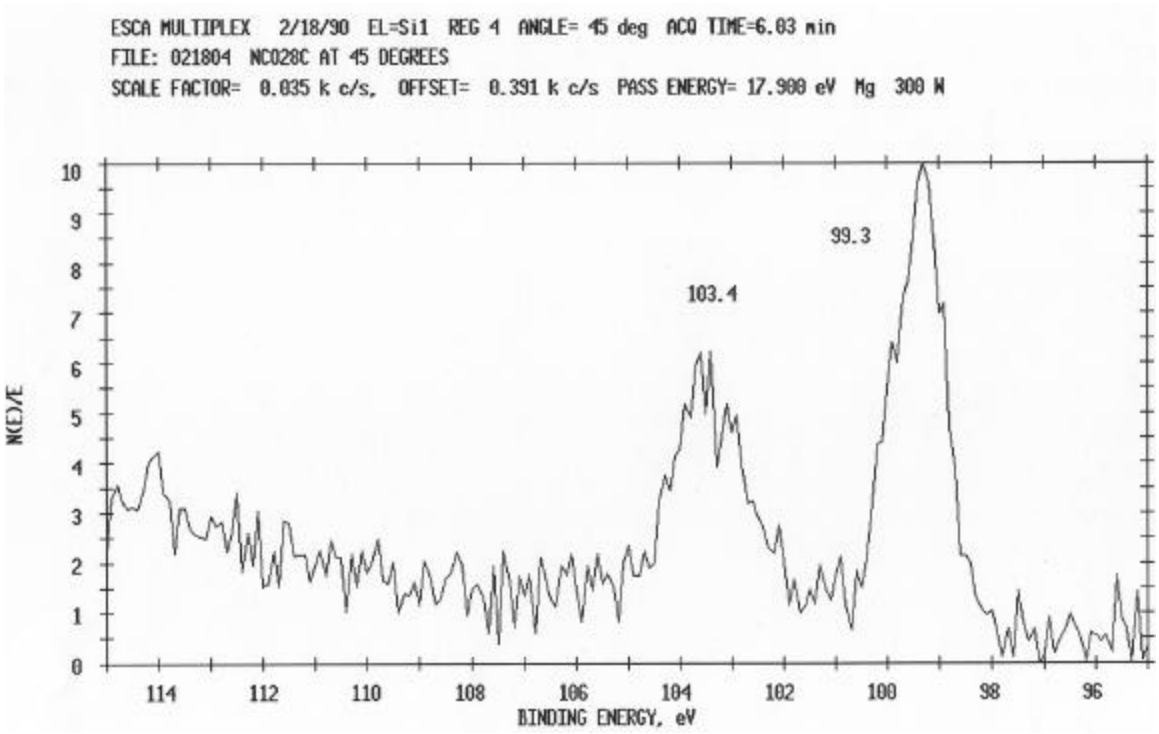

Figure 4.8. XPS of CFABC brush grafted silicon wafer surface with a collect angle of 45°

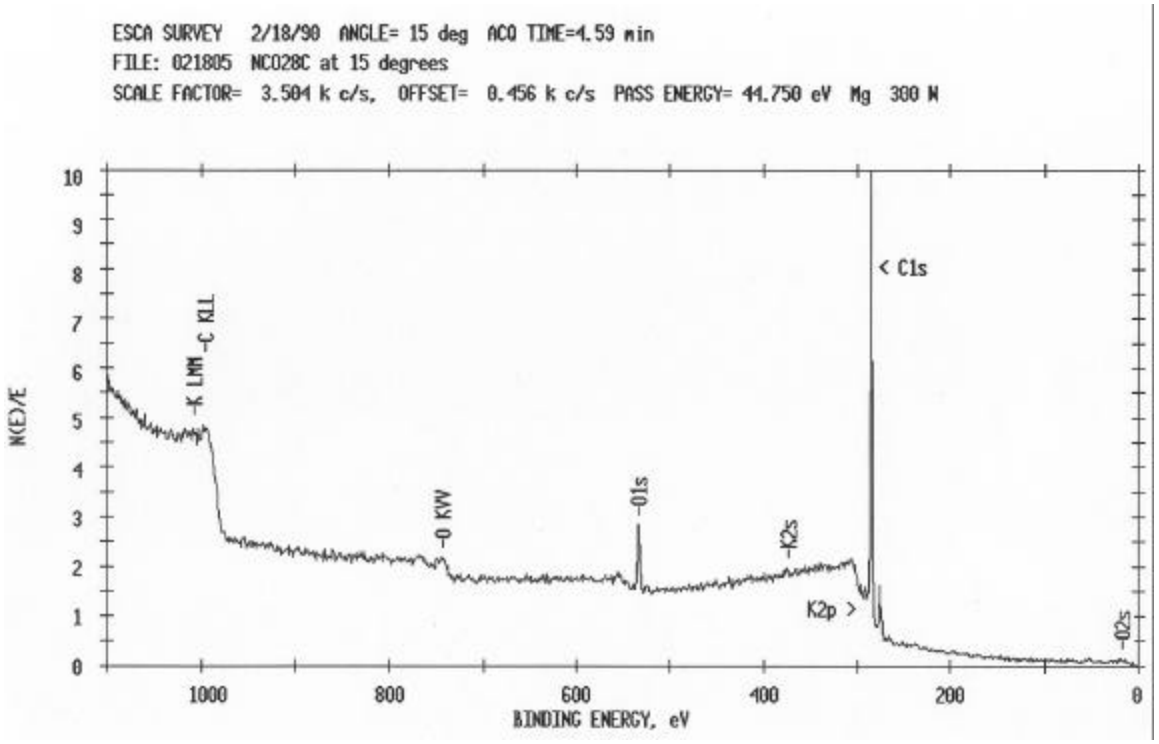

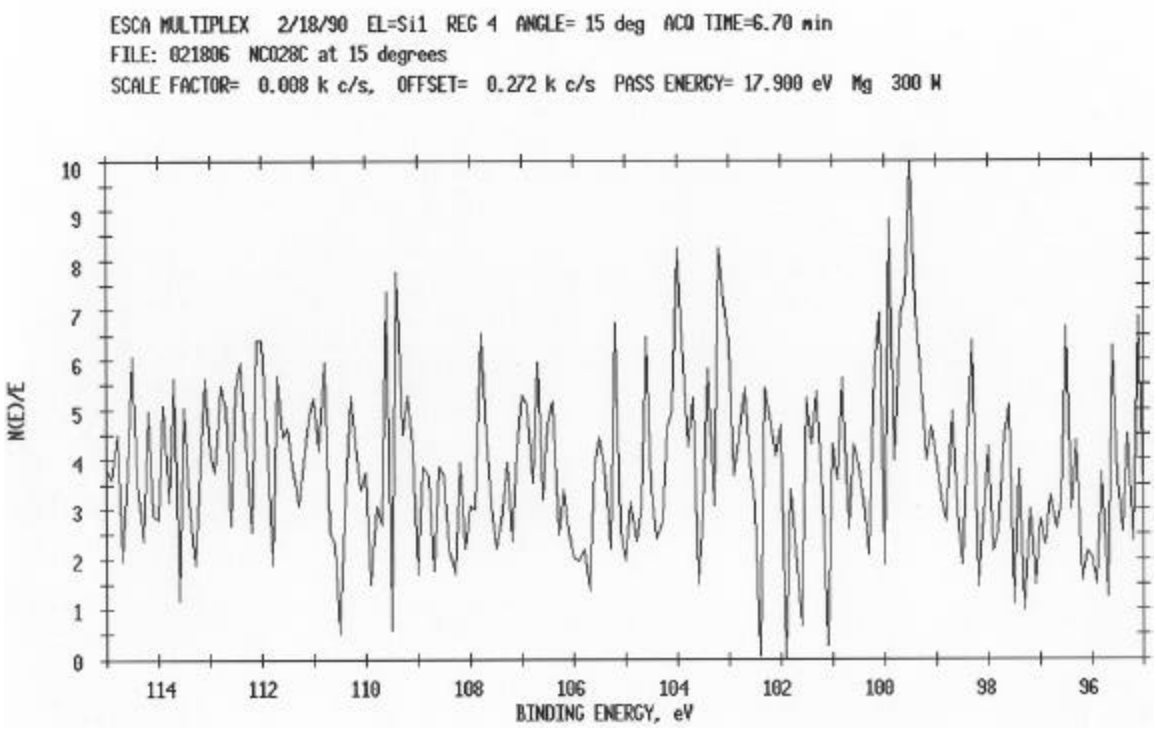

Figure 4.9. XPS of CFABC brush grafted silicon wafer surface with a collect angle of 15°

Table 4.1. Summary of XPS data for different collect angles on CFABC brush grafted silicon wafer surface

Element	*90°* concentration (%)	*45°* concentration (%)	*15°* concentration (%)
C1s	79.13	86.67	91.37
O1s	12.86	10.16	7.03
N1s	0.60	0.63	1.53
Si2p	7.41	2.55	0.07

CHAPTER 5. SURFACE PROPERTIES ON CFABC MODIFIED SUBSTRATES

5.1. Introduction

The preparation of CFABC polymer brush grafted silicon wafer surfaces was described in the previous chapter. One unique character of the CFABC polymer brush system is that it contains two chemically different polymer end blocks connected to each central grafting site. The two side blocks, which are PS and PMMA in this research, have different polarities; and as a result, the chain configurations of the two blocks are expect to respond differently to stimuli. Thus, each can be selectively influenced by external parameters, such as a variety of solvents with a range of polarities. Thus, the surface energy can be "tuned" by the dynamic stable/meta-stable states of the chain configurations of the polymer blocks in the CFABC polymer brush system using a number of environmental driving energies.

In this chapter, a new concept based on "smart adhesion" behavior between the modified surfaces and other polymers is developed and demonstrated. "Smart adhesion" is defined as the ability for a surface to modify its adhesion characteristics based on the introduction of an external agent (solvents or other polymer materials, and in some cases, an adherend itself might be this agent). Potential applications of this novel surface modification approach to problems encountered in adhesion and biocompatibility are expected.

5.2. Experiments

5.2.1. Sample preparation

CFABC polymer brush modified silicon wafer surfaces were prepared as described in Chapter 4. At least six samples were prepared together at one time to eliminate possible experimental variations. The wettability experiments were carried out in the following manner.

To determine how the treated wafers surface energy could be varied, a series of contact angle measurements were performed on the samples after the following

treatments. The CFABC modified substrates (after 10 hour Soxhlet extraction) were submerged into one of three solvents having different polarities, CH_2Cl_2, toluene, and cyclohexane (all were obtained from Aldrich, HPLC grade), at room temperature for 10 minutes. The samples were then quickly dried with clean air flow and the contact angles of deionized H_2O and CH_2I_2 on the dry surfaces were measured. For comparison, contact angles of an unmodified silicon wafer surface with native oxide layer on the top were also measured. Also for comparison, homo-polymers of the end blocks of theses CFABC's were examined using the below samples.

Polystyrene ($<M_n>$ = 10 k, Polydispersity = 1.05, synthesized in these labs) and PMMA ($<M_n>$ = 120 k, Polymer Science Inc.) were dissolved in toluene (Aldrich, HPLC grade) to obtain 1 % (w/v) solutions for each polymer. Polymer thin films (PS or PMMA) were then prepared by using spin-coating techniques. A typical spin-coating speed was 2000 rpm. Solutions were added using a pipette, with only one drop for each sample. After 5 minutes of spin-coating, the samples were transferred to a vacuum oven and dried at 170 °C for 20 hours to allow the polymers to fully relax and reach thermal equilibrium. Finally, the samples were quenched to room temperature and the topologies of the thin films were examined by AFM.

5.2.2. Characterizations

The surface properties of the CFABC polymer brush grafted silicon wafer surfaces were investigated with contact angle experiments. Contact angles were determined with an optical goniometer (Rame-Hart, Inc., Mountain Lakes, NJ) mounted with a video camera. Measurements were taken at room temperature, and the angles from both sides of the drop were measured and averaged. An average of the angles for at least ten drops was taken. The liquids used were de-ionized, purified H_2O and methylene iodide (99 % pure, Acros Organics, Newark, NJ). The drop volume for the measurements was 5 μL. The method was employed according to the literature.[1]

The topology of polymer brush modified surfaces and polymer thin films was investigated using a Dimension 3000 (Digital Instrument Inc.) atomic force microscope (AFM) with Tapping Mode®. Height and phase images were collected at the same time.

[1] DiFelice, R. A., Ph.D. Dissertation, Virginia Tech, 2001

5.3. Results and Discussions

5.3.1. Nanopatterns influenced by washing solvents

Since the two side blocks, PS and PMMA, in the CFABC brush system have different solubilities in any given solvent, different CFABC chain configurations can be addressed using different solvents. This will result in different self-assembled nano-patterns on the modified surface.

Because the T_gs of the two blocks (PS and PMMA) are well above room temperature, the chain configurations approached in the solvents were immobilized during the quick drying process. Although the AFM images were collected as "dry" states, the surface topologies observed by AFM are believed to reflect the similar structures in the presence of the solvents.

Figure 5.1 and Figure 5.2 present the AFM images of the surface topologies of several CFABC brush modified silicon wafer surfaces which were washed with toluene. Nano-patterns with domain size of ~ 20 nm were observed on both height and phase images. As discussed in Chapter 4, the surface was found to be *fully covered* by the brush. Therefore the contrasts in the height and phase images resulted from domains with different chemical compositions in the brush. In other words, the polymer brush self-assembled into nano-patterns on the very top surface (air-polymer interface) after being washed by toluene. To determine the exact chain configurations in each case, more studies are needed. For example, CFABC polymer brushes with a deuterated polystyrene block could be examined by neutron reflectivity for details of the surface chemical composition and depth profile. Some indirect evidence of the chain configurations under the influence of solvents will be discussed in the next section.

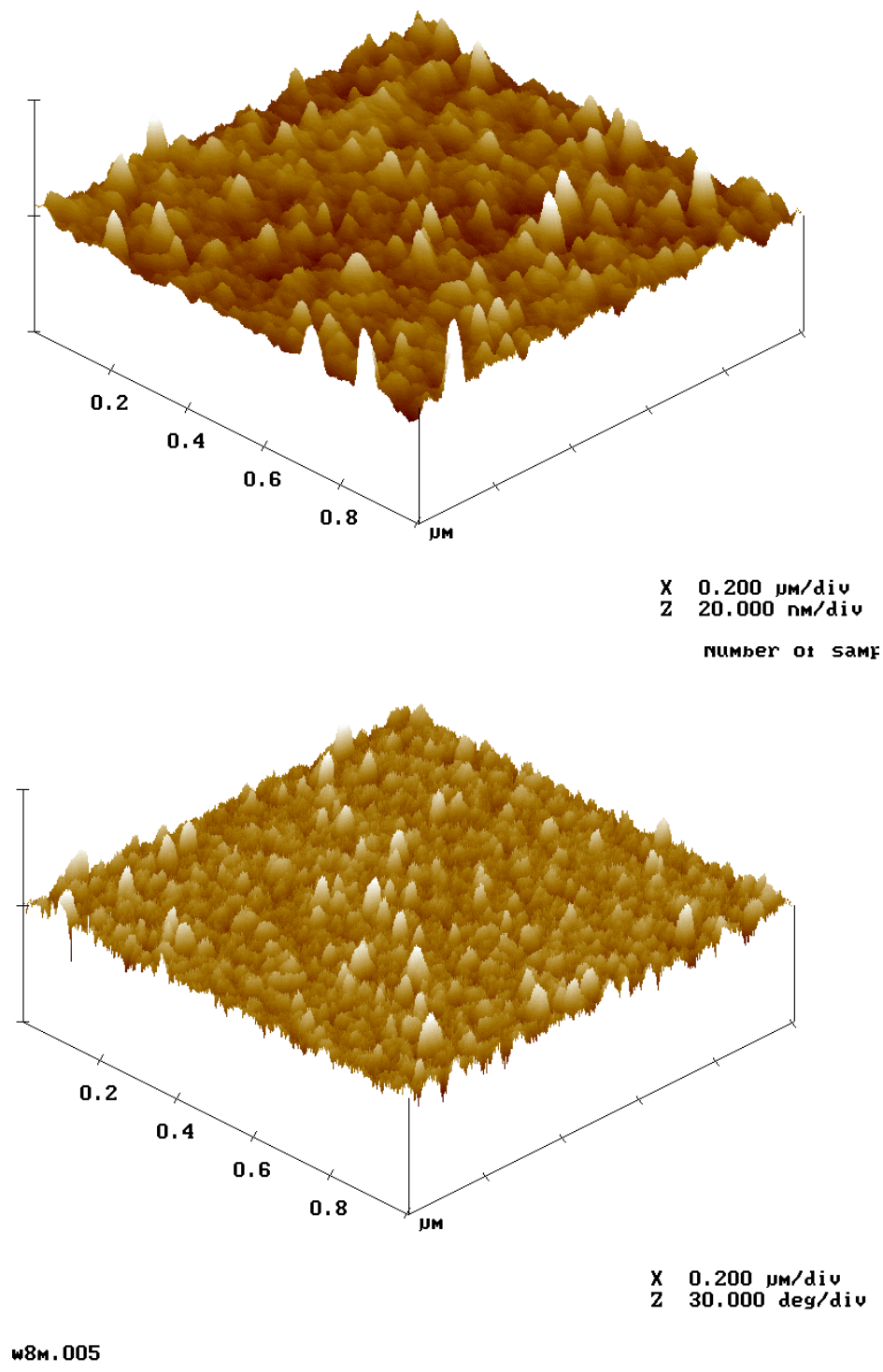

Figure 5.1. Nanopatterns of CFABC polymer brush after being washed by toluene. AFM (Tapping Mode®), 1 µm scan. Top: 3D height image; Bottom: 3D phase image

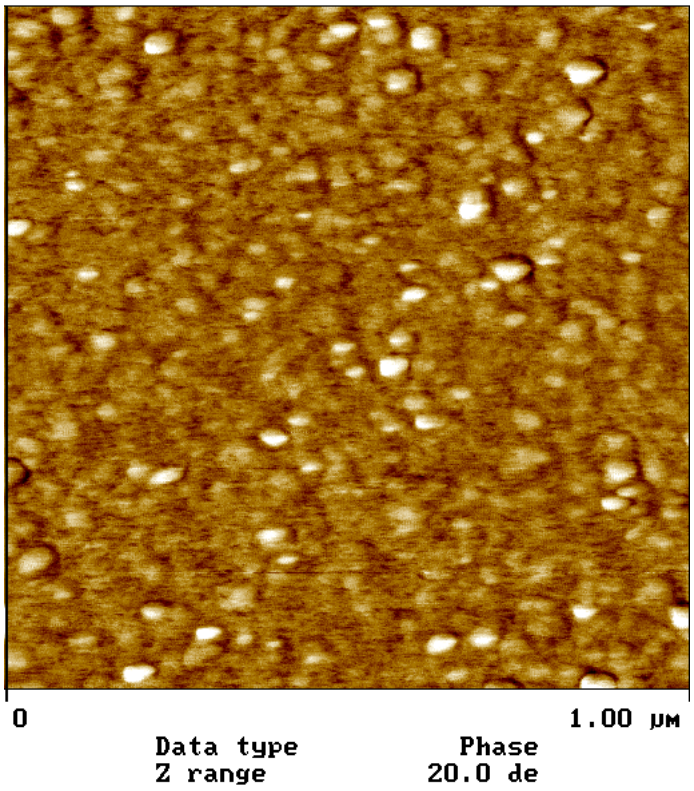

Figure 5.2. Nanopatterns of CFABC polymer brush after being washed by toluene. AFM (Tapping Mode®), 1 µm scan. Phase image.

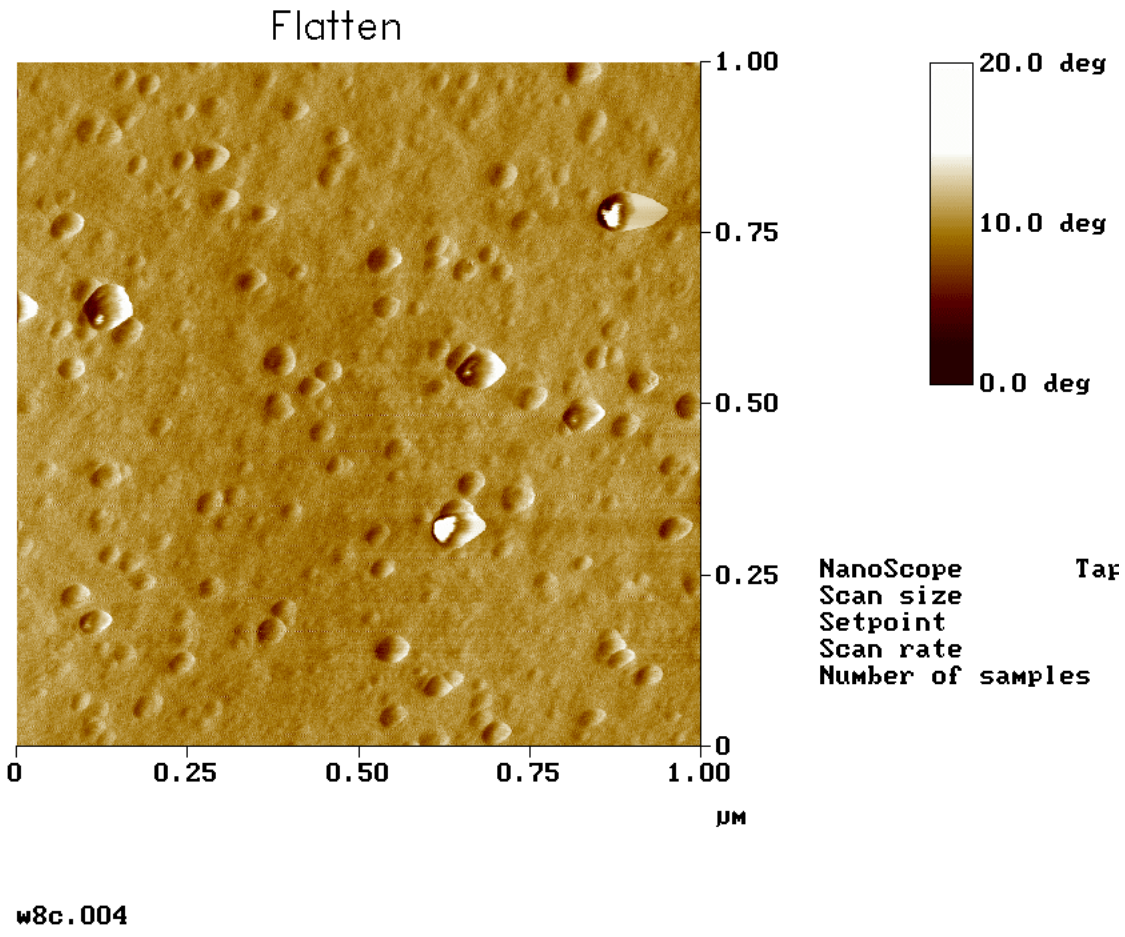

Figure 5.3. Nanopatterns of CFABC polymer brush after being washed by chloroform. AFM (Tapping Mode®), 1 µm scan. Phase image.

5.3.2. Switchable surface energies

5.3.2.1. Contact angles on CFABC polymer brush modified silicon surfaces

In Figure 5.4 (the top part), water contact angle values are shown for the same CFABC polymer brush modified surface, after processing with three solvents of differing polarities: CH_2Cl_2, toluene, and cyclohexane. Also included are the values obtained on polystyrene (PS) and poly(methyl methacrylate) (PMMA) homopolymer brush modified surfaces provided from the literature (single end grafted).[2]

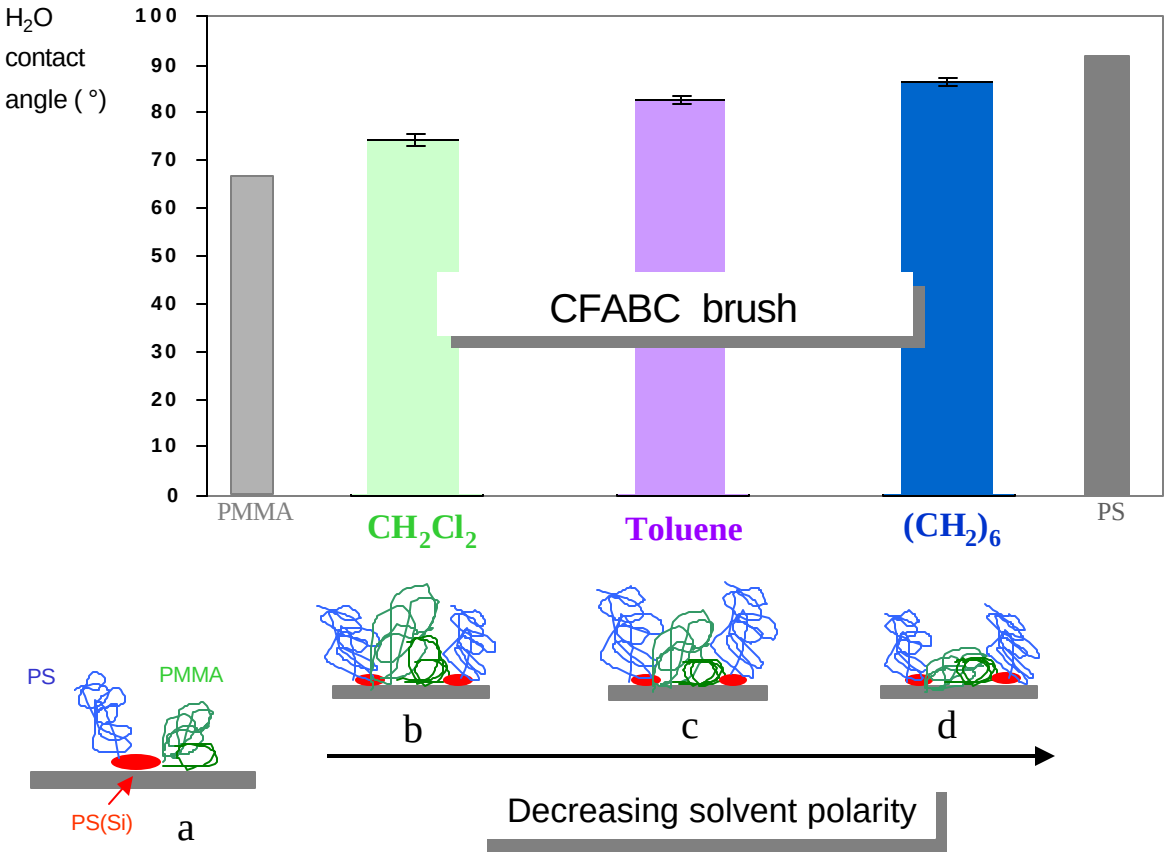

Figure 5.4. Water contact angles on CFABC modified surfaces with different processing solvents and proposed mechanism of chain conformation auto-adjustments

With decreasing polarity of the processing solvents (CH_2Cl_2 → toluene → cyclohexane), the water contact angle values on the CFABC modified surface increased,

[2] Zhao, B.; Brittain, W. J., *Progress in Polymer Science* 25, 677, **2000**

which reflects a less polar surface. Interestingly, the value of the CFABC modified surface exposed to CH_2Cl_2 was close to that of a pure PMMA brush modified surface, and for the non-polar cyclohexane processed CFABC modified surface, the value was closer to that of the pure PS brush modified surface. A proposed rough mechanism for these varying surface properties with different solvents is shown schematically in Figure 5.4 (bottom part).

Figure 5.4 (a) illustrates the virgin state of the CFABC polymer brush structure. Two different polymer chain arms (PS and PMMA) are connected to the short center block (PSSi), which is chemically grafted onto the surface. When the surface was processed by a relatively polar solvent (CH_2Cl_2 in this case), the chain conformation of the hydrophilic PMMA block adopted an extended state because CH_2Cl_2 is a good solvent for PMMA. At the same time, the PS block was in a compact conformation due to the relatively poor solubility of PS in CH_2Cl_2. As a result of such chain conformation adjustments of the two blocks on each grafting site (Figure 2-b), the equilibrium state of the modified surface would have an upper atmosphere enriched in PMMA characteristics, which in turn caused the relatively low water contact angle value. With a more non-polar solvent, however, the chain conformation adjustment mechanism would give the CFABC modified surface with more PS like characteristics, as shown in Figure 2 – c & d.

The proposed mechanism suggests that the surface properties are determined by the auto-adjustment of the individual polymer chain conformation associated with a specific solvent. Polymer chain conformation adjustment in a solvent is a thermo-dynamic process; and in this case should be reversible. Consequently, if the mechanism is correct, the observed surface properties are expected to be reversible/switchable during repeated solvent exchange processes. The switchablity of the surface properties was indeed observed, as shown in Figure 5.5. The same CFABC modified surface was alternately processed by CH_2Cl_2 and toluene, and water contact angles were measured after each solvent exposure. More than six cycles were done, only two of them are shown in Figure 5.5 for the purpose of clarity. It is clear that the values of the measured water contact angles were oscillated to reflect the most recent solvent within experimental errors. So the CFABC polymer brush modified surfaces have switchable properties due to the unique structure of the CFABC brush system.

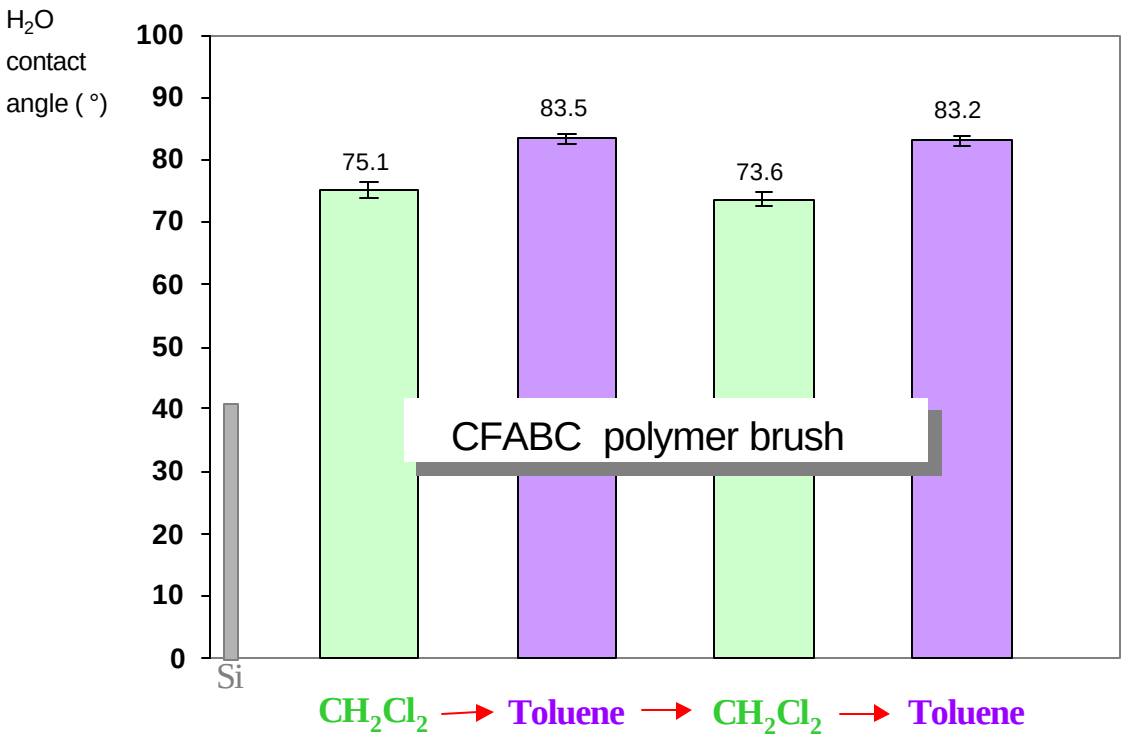

Figure 5.5. Switchable surface properties of CFABC modified surfaces

5.3.2.2. Surface energies

Surface energies were also calculated to further determine the influence of the polarity of processing solvent on the CFABC modified surfaces, using the harmonic mean method (Equations 5.1 and 5.2).[3]

$$(1 + \cos\theta_1)\,\gamma_1 = 4\left(\frac{\gamma_1^d\,\gamma_S^d}{\gamma_1^d + \gamma_S^d} + \frac{\gamma_1^p\,\gamma_S^p}{\gamma_1^p + \gamma_S^p}\right) \qquad 5.1.$$

$$(1 + \cos\theta_2)\,\gamma_2 = 4\left(\frac{\gamma_2^d\,\gamma_S^d}{\gamma_2^d + \gamma_S^d} + \frac{\gamma_2^p\,\gamma_S^p}{\gamma_2^p + \gamma_S^p}\right) \qquad 5.2.$$

where the total surface energy (γ) of the surface is the sum of the dispersion and polar components ($\gamma^d + \gamma^p$). The subscripts 1 and 2 refer to the testing liquids H_2O and CH_2I_2,

[3] Wu, S., Polymer Interface and Adhesion, Marcel Dekker, Inc., New York, 1982.

respectively. With the knowledge of γ_j^d and γ_j^p of the testing liquids (j=1 and 2), the two unknowns (γ^d and γ^p) can be determined from the contact angles θ_1 and θ_2 by solving the resulting set of simultaneous equations. The dispersive and polar components of the test liquids (water and methylene iodide) were taken from the reference[3] and are listed in Table 5.1

Table 5.1. Preferred values of surface tension and its components for water and methylene iodide used for the calculation of surface tension from contact angles by the harmonic-mean method.[3]

	γ (dyne/cm), 20°C	γ^d (dyne/cm), 20°C	γ^p (dyne/cm), 20°C
Water	72.8	22.1	50.7
Methylene iodide	50.8	44.1	6.7

The contact angles of CH_2I_2 and H_2O were measured on the CFABC modified surface to determine the polar part of the surface energy (γ^p) (Figure 5.6). The results show that the γ^p values decreased with decreasing solvent polarity, which is consistent with the data in Figure 5.4 and can be explained by the same mechanism invoked above.

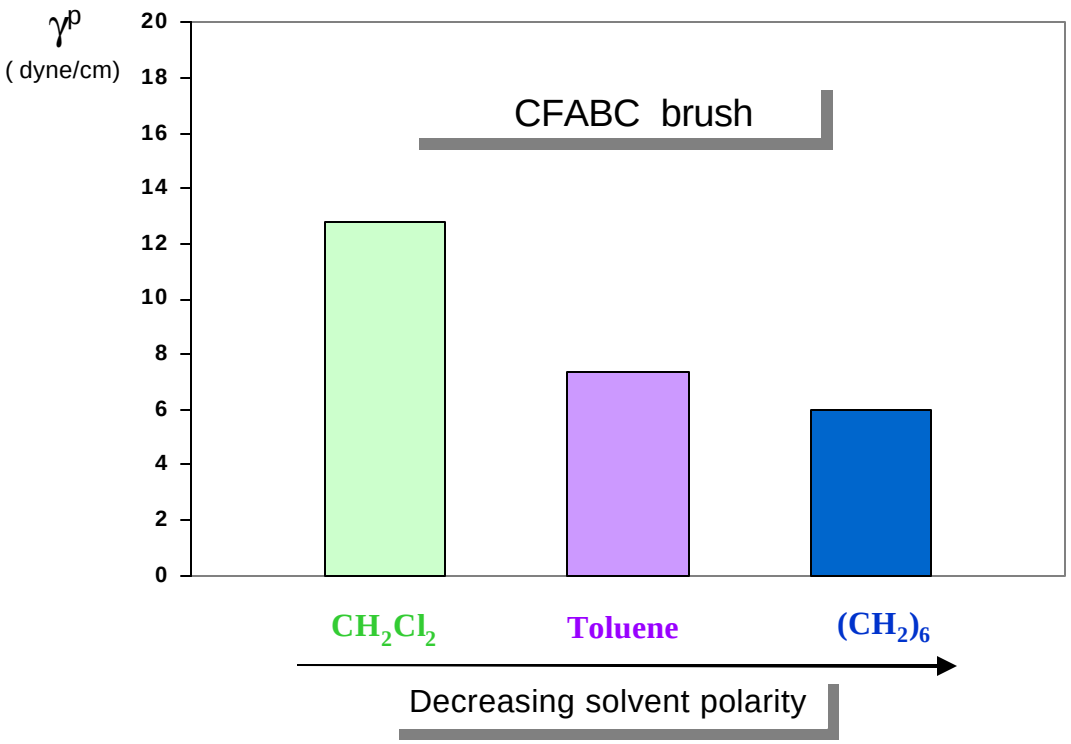

Figure 5.6 Polar part of the surface energy of CFABC modified surface with different processing solvents

5.3.3. Interfacial adhesion energy control

5.3.3.1. Wettability study of different polymer thin films on CFABC modified silicon surfaces

The blank silicon wafers used in this research have hydrophilic surfaces due to the existence of Si-OH groups on the top native oxide layer. As a result, the interfacial adhesion energy between the wafers and hydrophobic polymers, such as polystyrene, is very poor, and in many cases, dewetting results. It is possible to change the surface energy of a substrate, i.e., from hydrophilic to hydrophobic, in a traditional way with surfactants or by etching. However, the change is normally permanent, and the interfacial adhesion capability is still limited. Can the new CFABC be used to create a new method for increasing the wetting capabilities on a Si wafer of hydrophilic and hydrophobic polymers?

To answer the question just above, polystyrene (10k) and PMMA (120k) thin films were spin-coated (1% w/v in toluene, 2000 rpm) on blank and CFABC modified silicone wafer surfaces, then vacuum heated to 170 °C for 20 hours. The samples were finally examined by AFM for evidence of wetting *vs*. non-wetting behavior.

As shown in Figure 5.7, polystyrene dewetted on the blank silicon wafer and droplets at the micrometer scale were observed. This was expected for a hydrophobic polymer on a hydrophilic substrate surface. The micro-droplets formed sharp boundaries between the edge of the droplets and the substrate (Figure 5.8). All of the contact angles obtained from the cross section analysis of the AFM test were independent of the sizes of the droplets (ranging from 0.5 μm to 5 μm) and were determined to be about 11 degrees. The contact angle values measured by AFM were considered to be as thermal equilibrium values[4] and can be used to calculate surface energies.[5]

In contrast to the PS, a uniform film (wetting) for the PMMA on the blank wafer was observed (Figure 5.9). The result is not surprising because of the hydrophilic character of the blank silicon wafer surface.

However, both PS and PMMA wetted the CFABC modified silicon wafer surfaces as shown in Figure 5.10. Thus, remarkably, the same modified surface has good interfacial adhesion with both polymers. This enhanced and versatile interfacial adhesion capability is again due to the unique structure of the CFABC modifier. The PS and PMMA (both with T_g ~ 100 °C) were in melt state at 170 °C as applied to the CFABC modified wafer. These polymer melts could also induce different CFABC chain conformation adjustments (Figure 5.10, bottom part), just as different solvents did as discussed above. So, with the introduction of either PS or PMMA film on the top of otherwise identical CFABC modified silicon wafer surfaces, the results indicate that a "matching" arm of the CFABC is enriching the surface. This corresponding CFABC polymer chains would be in an extended conformation for the films to interact in an adhesive fashion. The de Gennes Model[8] concluded that the optimum chain density in a

[4] Vitt, E.; Shull, K. R., *Macromolecules*, **1995**, 28, 6349.
[5] Mansky, R.; Liu, Y.; Huang, E.; Russeell, T. P.; Hawker, C. J., *Science* 275, 1458, **1997**

polymer brush system in order to achieve maximum interfacial adhesion strength is quite low. Even though there was only a fraction of the CFABC chain arms that adopted a favorable conformation to interact with either the PS or PMMA film, the interfacial adhesion strength was still strong enough to keep both polymers from dewetting on the modified surface, as supported by the model.

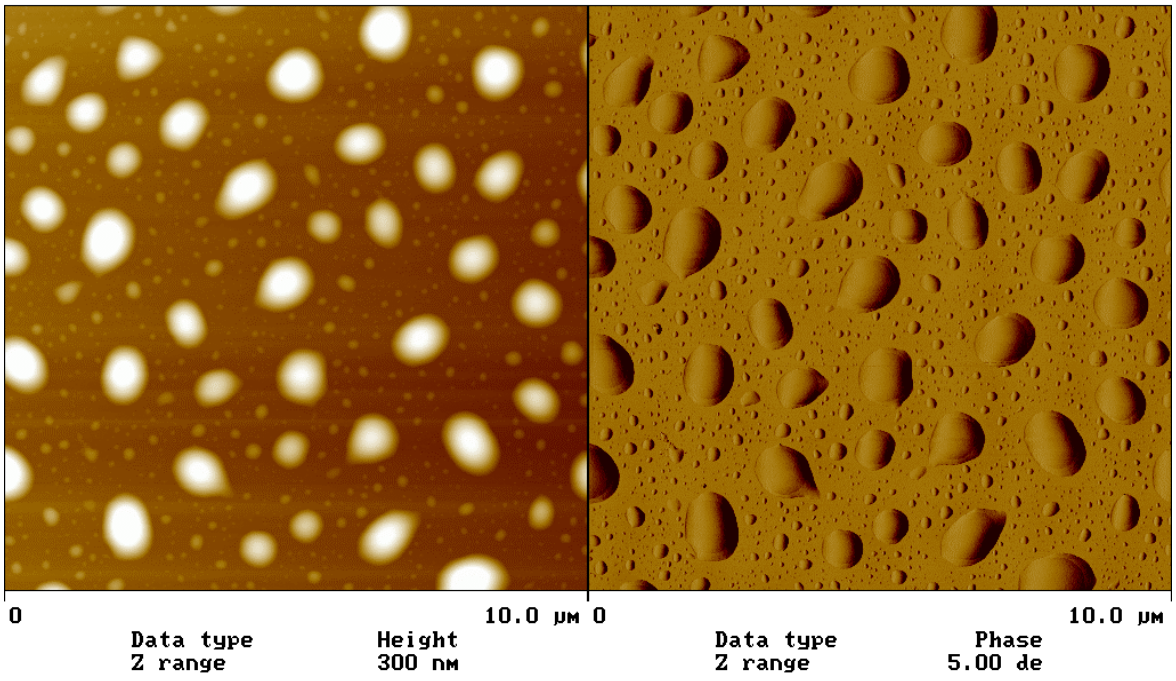

Figure 5.7 AFM (height image) of PS (10 kg/mol) on blank silicon wafer surface

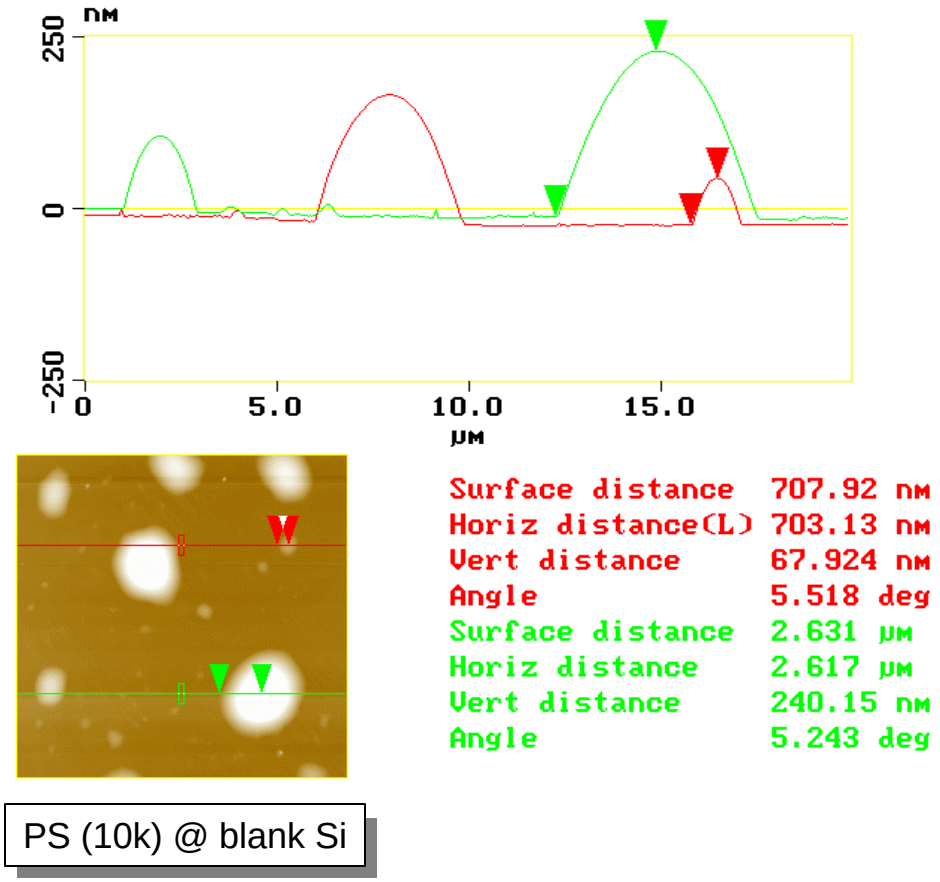

Figure 5.8. Contact angles of dewetted PS micro-droplets on blank silicon wafer measured by AFM

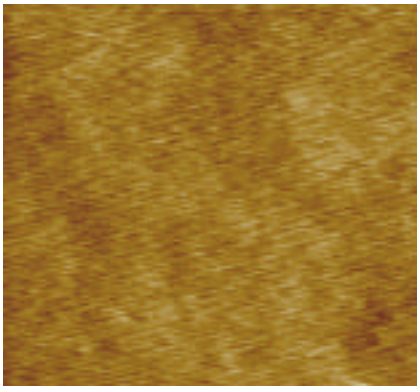

Figure 5.9. AFM images of PMMA thin film spin-coated on blank silicon wafer surface. 1μm scan. Height image.

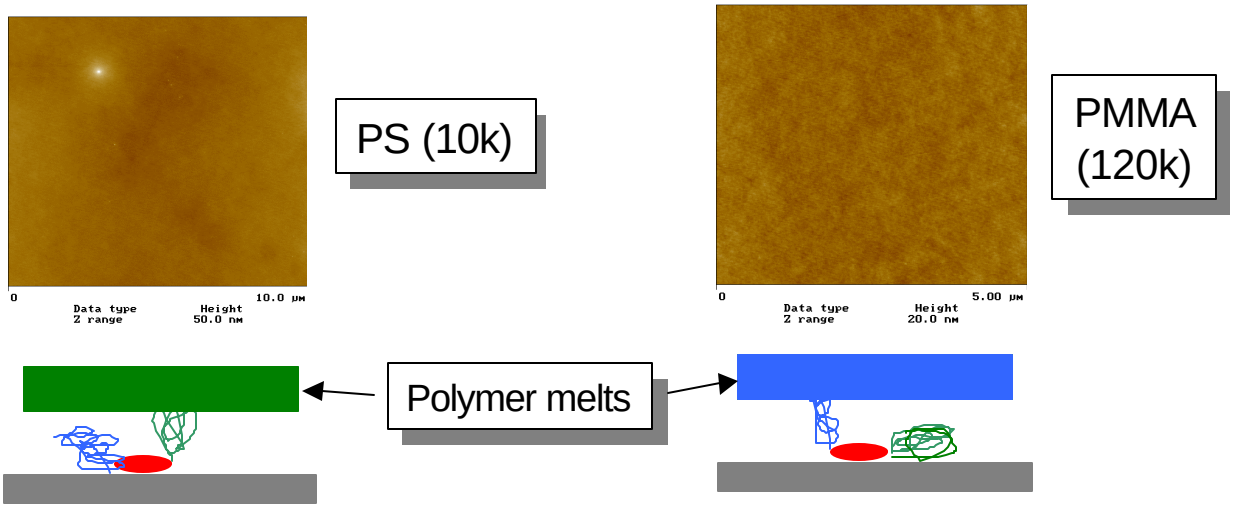

Figure 5.10 AFM (height image) of PS (10 kg/mol) and PMMA (120 kg/mol) on CFABC modified surfaces

5.4. Conclusions

Due to the unique structure of the CFABC polymer brush system, having two distinct polymer blocks on each grafting site, "smart" adhesion behavior was observed on the CFABC modified silicon wafer surface. Compared with traditionally modified surfaces which normally have fixed surface properties, the surface properties of the new CFABC polymer brush modified surfaces have unique switchable characteristics, and the interfacial adhesion energy between the modified substrate and various types of other polymer materials is simultaneously enhanced. The underlying mechanism was the reversible auto-adjustment of chain conformations in the CFABC polymer brush system as a response to the introduction of external agents (solvents or polymers).

It is believed that the smart adhesion concept can be utilized in many different areas, by designing CFABC polymers with other distinct characteristics between the two blocks, such as flexibility, crystallinity or chain topologies, and applying them onto quite different substrates such as polymeric fibers, wood surfaces or living tissues by choosing appropriate central functionalities.

CHAPTER 6. POLYMER ULTRA-THIN FILM PHASE BEHAVIORS

6.1. Introduction

Polymer thin films have attracted much attention recently.[1,2] The phase behaviors of ultra-thin polymer films (10^1-10^2 nm) on a solid substrate are of significance both fundamentally, for understanding the molecular dynamics of polymers in restricted geometries, and technologically, for applications ranging from coating, lubrication, and electrical layers to nano-lithography.

As discussed in chapter 2 (2.5), the phase behaviors of polymer thin films are determined by the properties of both the film itself and by the supporting substrate. In this chapter, research results on polymer thin film phase behaviors are presented. Several factors, including film thickness, film composition, temperature, and interfacial interactions between the polymer and substrates were examined. The control of the interfacial interactions was achieved by using CFABC polymer brush modified surfaces.

The present research on thin film phase behaviors was divided into two sub-sections: polymer blend thin films and block copolymer thin films. Silicon wafer methodologies discussed in the previous chapters were again used.

The study of polymer blend thin films provided insight about some of the unique behaviors in thin film systems. As anticipated, the thickness of the films and the presence of the substrates played important roles in determining the phase behaviors, and this will be discussed in section 6.2.

In section 6.3, the influence of CFABC polymer brushes on the phase behaviors of various block copolymer thin films is discussed. As in chapter 5, novel results were observed.

[1] Limary, R.; Green, P. F., *Langmuir*, 15, 5617, **1999**
[2] Xie, R.; Karim, A.; Douglas, J. F.; Han, C. C.; Weiss, R. A., *Phys. Rev. Lett*. 81, 1251, **1998**

6.2. Ultra-thin Film of Polymer Blends

6.2.1. Background on polymer blend thin film studies

Polymer blends phase behaviors in bulk (3D) systems have been well studied both theoretically and experimentally during the last half century.[3] It is more of a challenge to examine and understand the phase behaviors of polymer blend ultra-thin films because of the following two unique features in such systems: 1) the ultra-thin thickness (10 – 100 nm) suggests that the surface fluctuation may not be neglected in these quasi 2 D systems; and 2) the interaction between the substrate (wall) and the polymer thin film is important and complex. Here I have presented my observations on the influence of the above two factors on the phase behaviors in a model polymer blend ultra-thin film system using polystyrene and the random copolymer PS-*co*-PMMA.

Silicon wafer surfaces are hydrophilic because of the existence of Si-OH groups on top of the native oxide layers. As discussed earlier, PMMA wetted the hydrophilic silicon wafer surfaces, and polystyrene did not (Chapter 5). From Figure 61, a uniform thin film was observed for the PS-*co*-PMMA random copolymer spin cast on the silicon wafer. It is believed that the favorable energetic interaction between the PMMA component in the copolymer helped the copolymer spread on the silicon surface. But it is also expected that the stability of the copolymer film is not as good as that of the PMMA homopolymer film, because of the un-favorable interaction between the substrate surface and the PS component in the copolymer. On the other hand, for a blend of PS and PS-*co*-PMMA random copolymer, the PS component in the copolymer is expected to improve the miscibility among the two polymers. So there are two competing factors in determining the overall value of the interaction parameter χ, when adding the polystyrene homopolymer into PS-*co*-PMMA with the existence of silicon wafer: These are (1) the favorable factor for mixing because of the PS component in the copolymer, and (2) the un-favorable energy because of the hydrophilic silicon wafer surface. According to Flory,[3] χ is defined as a dimensionless quantity which characterizes the interaction energy (normalized by kT) between two components in a blend. These two factors can be

[3] Flory, P. J., Principles of Polymer Chemistry, Cornell University Press, Ithaca, NY, 1953

influenced by the film thickness, blend composition and temperature, etc., which were studied in the present research.

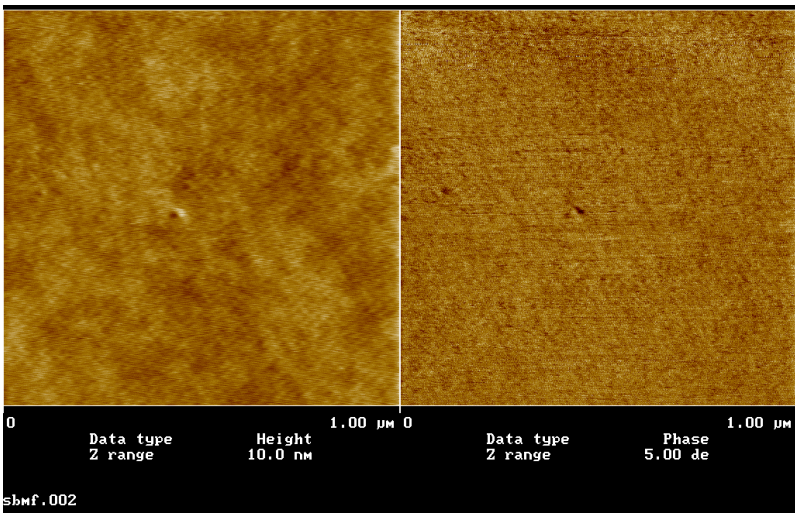

Figure 6.1. AFM images of PS-*co*-PMMA thin film on silicon wafer

6.2.2. Preparation of polymer blend thin films

6.2.2.1. Materials

Narrow dispersed polystyrene ($<M_n>$ = 68 k, PDI = 1.14) and a random copolymer of polystyrene-*co*-poly(methyl methacrylate) (PS-*co*-PMMA, $<M_n>$ = 70 k, PDI = 1.2, 70% PS (mol%)) were obtained from Polymer Science, Inc. and used as received. Silicon wafers (Motorola, 111, N type) with native oxide layers were used as substrates. The silicon wafers were cut into small pieces having a size of 2 cm × 2 cm using a diamond knife, and cleaned prior to use as described before (Chapter 4). Toluene (Aldrich, HPLC grade) was chosen as the solvent to dissolve the polymers.

6.2.2.2. Polymer blend thin film preparation

PS, PS-*co*-PMMA and mixtures of the polymers were dissolved in toluene with different concentrations. Polymer blend thin films were prepared via spin-coating. A typical spin-coating procedure is described below. 50 mg of one of the polymers (or polymer mixture) was added to 10 ml of solvent (toluene) to obtain a 0.5 % (w/v)

solution. To ensure that the polymer chains were well dispersed into the solvent, at least one hour of sonication was employed. A piece of freshly cleaned silicon wafer was spun on a spin-coater at a preset speed (e.g., 2000 rpm), then a drop of the polymer solution was carefully added to the center part of the wafer using a pipette. After 5 minutes of spinning, the wafer was transferred to a vacuum oven. Unless specified, the oven was preheated to 150°C, and the coated wafer was kept in the oven under vacuum for ≥ 10 hours. Finally, the sample was quenched to room temperature using dry air flow. Table 6.1 lists all of the polymer thin film samples to be discussed in this section.

Table 6.1. Sample information of polymer blend thin films

Sample	PS/PS-*stat*-PMMA (w/w)	Spin-speed (rpm)	Concentration (w/v)	Solvent
PS-0	0 / 100	2 k	0.5 %	toluene
PS-10	10 / 90	2 k	0.5 %	toluene
PS-20	20 / 80	2 k	0.5 %	toluene
PS-30	30 / 70	2 k	0.5 %	toluene
PS-40	40 / 60	2 k	0.5 %	toluene
PS-50b	50 / 50	2 k	0.5 %	toluene
PS-70	70 / 30	2 k	0.5 %	toluene
PS-90	90 / 10	2 k	0.5 %	toluene
PS-100	100 / 0	2 k	0.5 %	toluene
PS-50a	50 / 50	1 k	0.5 %	toluene
PS-50b	50 / 50	2 k	0.5 %	toluene
PS-50c	50 / 50	3 k	0.5 %	toluene
PS-50b	50 / 50	2 k	0.5 %	toluene
PS-50d	50 / 50	2 k	1.0 %	toluene

In some cases, the back side of the silicon wafers (unpolished side) was pre-cracked. This enabled breaking the wafers into smaller pieces after spin-coating or the heating process in the vacuum oven. This procedure provided samples with the same original states. The samples were then treated differently afterwards (i.e., different further heating/cooling schedules), and the influence of those environmental parameters on the phase behavior of the thin films was studied.

6.2.2.3. Characterization

AFM (DI Dimension 3000) was used to characterize the surface features of the polymer blend thin films.

6.2.3. Compositional influence on polymer blend thin film phase behaviors

The topographies of the first six samples listed in Table 6.1 were examined by AFM. The only difference among the samples was the difference in concentration of the polystyrene homopolymer in the blends.

Phase separation was observed for the thin film containing only 10 wt% PS, as shown by the AFM images in Figure 6.2. While there were no clear domain boundaries in the height image, two distinct phases were observed in the phase image. The round, darker domain (which indicates a lower modulus) in the phase image was believed to be the PS-rich phase. The conclusion was supported by the fact that, with increasingly amounts of PS in the blends, the size of the dark domains in the phase images increases (Figure 6.3).

Note the height images of different polymer blend thin films shown in Figure 6.4. As the concentration of PS in the blends increased (from 10% to 70%), not only did the diameters of the PS rich domains become bigger (from ~100 nm to ~2 μm), but also the heights of the domains increased (from ~2 nm to ~180 nm). So, in contrast to a phase separation in bulk, the dispersed phase (PS rich domain) grew away from the surface into free space during the phase separations in these polymer blend thin films. The PS rich domain was always the dispersed phase (as opposed to the continuous phase) with an "island in sea" morphology in all of the six polymer blend thin films examined here. The other phase, the PS-*co*-PMMA rich phase, was always the continuous phase (except for

the sample of PS-70, which will be discussed later). The copolymer phase was closer to the substrate than the PS rich phase, likely because of the preferable absorbance of the copolymer to the silicon wafer substrate. As discussed in Chapter 2, the "island in sea" morphology suggests a nucleation and growth (NG) mechanism resulted from a binodal phase separation process. But, this conclusion is only a preliminary one, and the influence of the substrate should be considered in determining the phase separation mechanism in polymer blend thin films. Such influence will be shown to be very significant in some cases during later discussions.

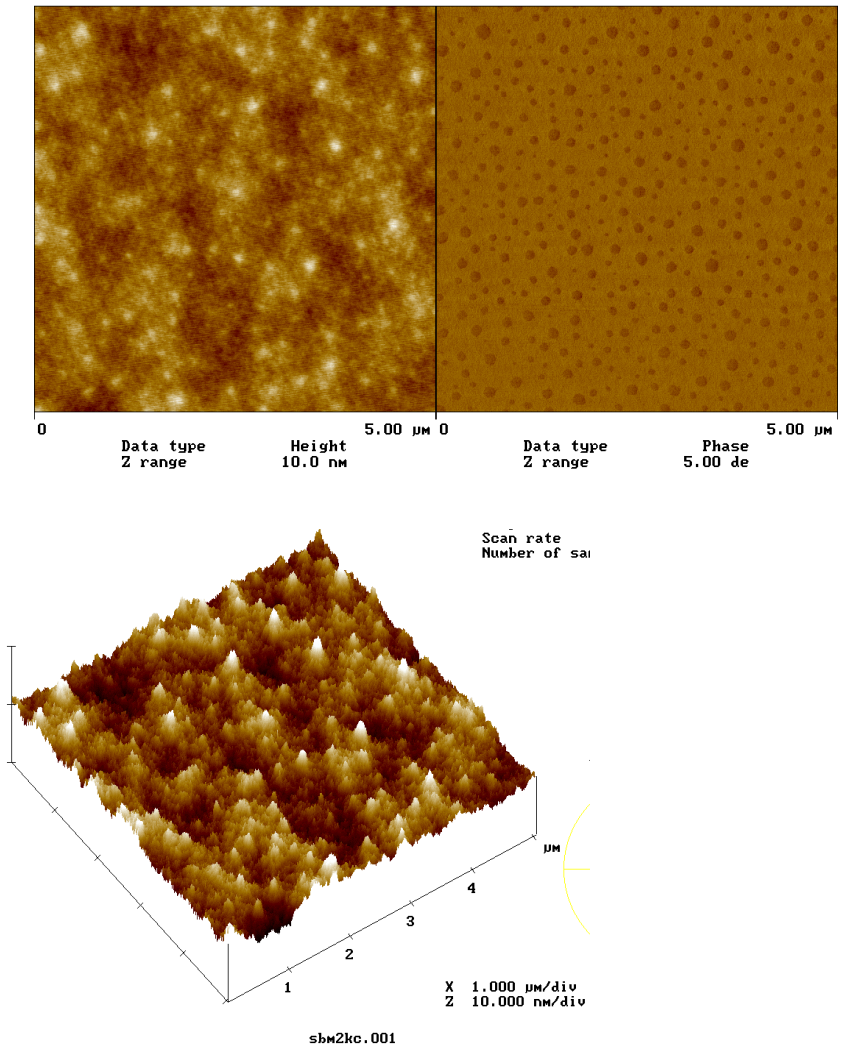

Figure 6.2. AFM of PS and PS-*co*-PMMA blend thin film (PS-10 in Table 6.1) on silicon wafer

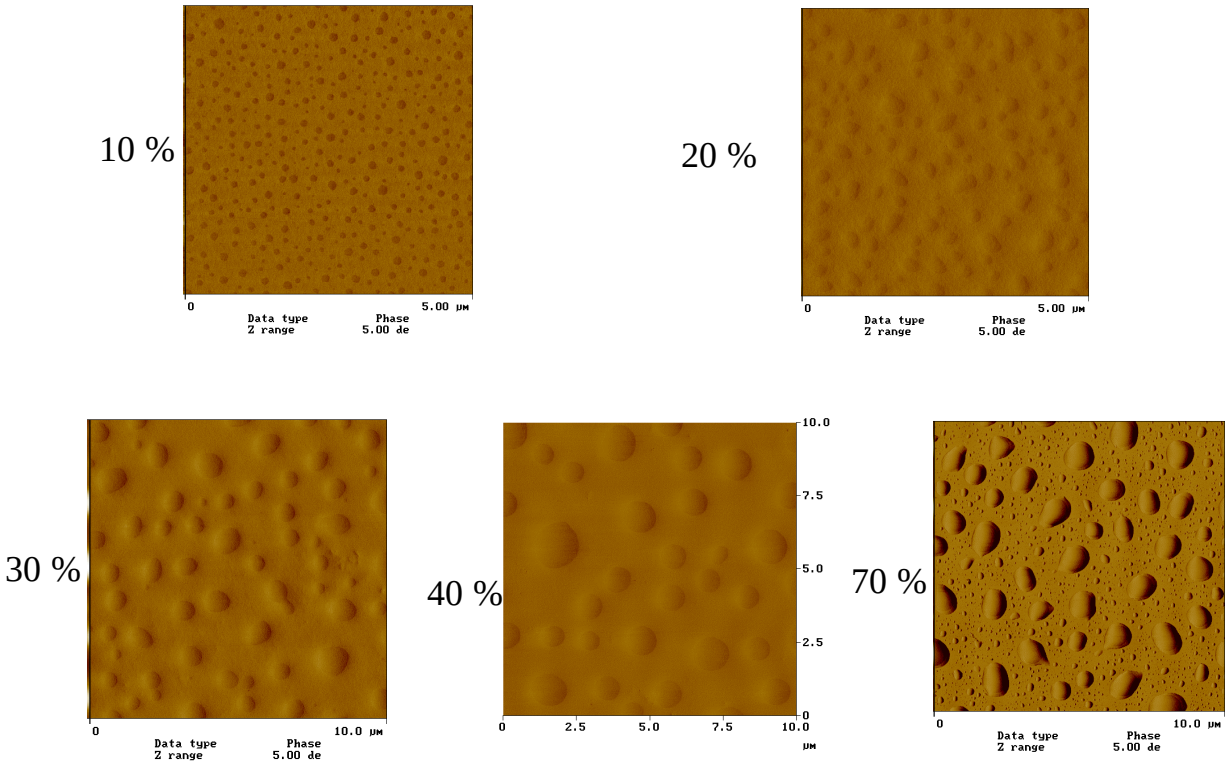

Figure 6.3. AFM phase images of PS and PS-*co*-PMMA blend thin films (PS-10, PS-20, PS-30, PS-40 and PS-70) on silicon wafers

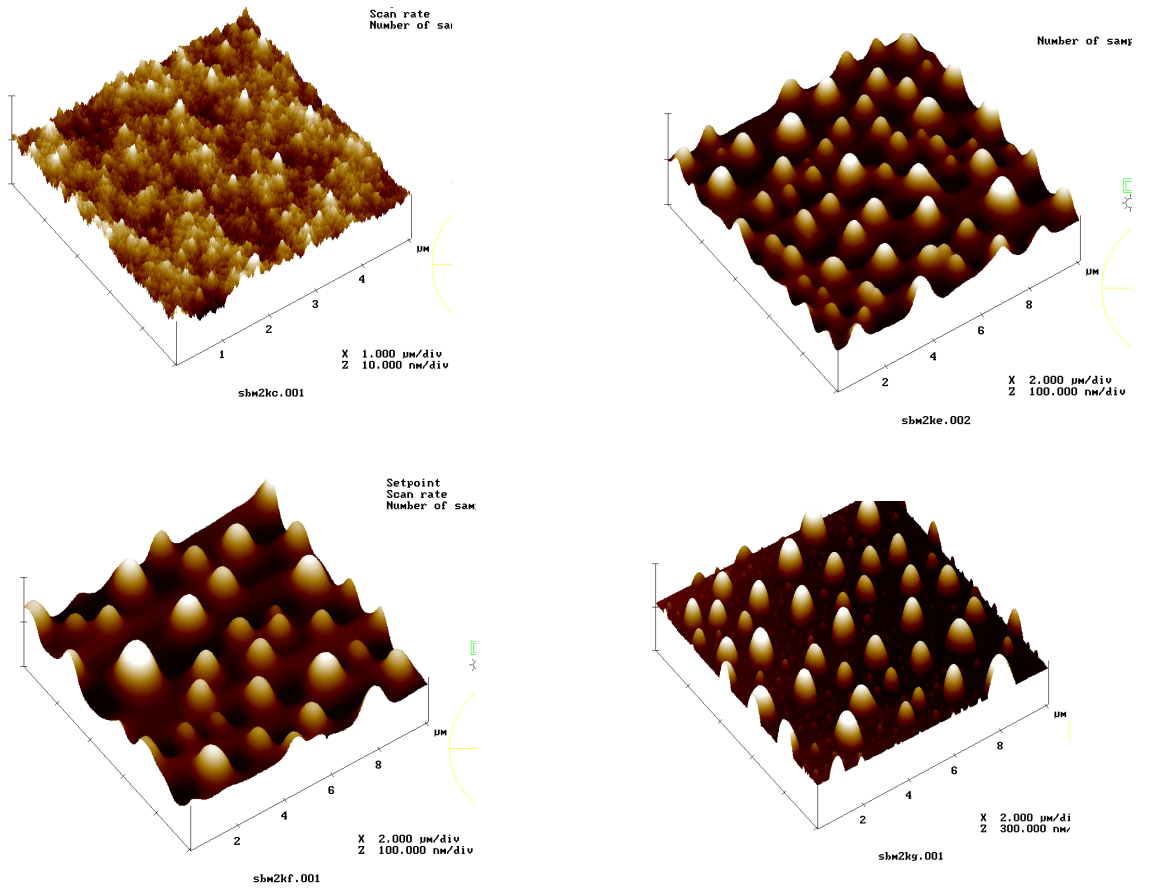

Figure 6.4. AFM 3-D height images of PS and PS-*co*-PMMA blend thin films (PS-10, PS-30, PS-40 and PS-70) on silicon wafers

With more careful examination of the phase and height images of the films, the topology of the film with 70 wt% PS (PS-70) was found to be very different from the films containing lower amounts of PS (10 to 50 wt%).

Figures 6.5 – 6.9 provide cross section analysis on the height images of the polymer blend films with different amounts of PS (10 to 70 wt%). As discussed in Chapter 5, contact angle values were calculated based on the information (particle diameter and height) obtained from the cross section analysis. A spherical cord shape was assumed for the particles (PS rich phase) in calculating the contact angle values. At least two images were collected and ≥5 particles were analyzed in each image to obtain the average contact angle value for each sample. As illustrated in Scheme 6.1 for a

spherical particle, the contact angle α can be easily calculated from the equation, $\tan(\alpha/2) = d/r$, where the values of d and r are directly measured from the AFM cross section analysis.

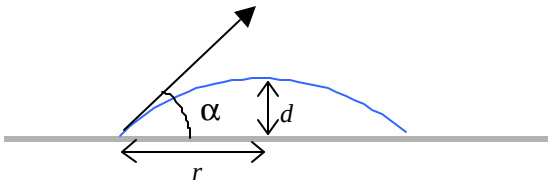

Scheme 6.1. Illustration of contact angle calculation from AFM cross section analysis

The results of the obtained contact angles are summarized in Figure 6.10. As the PS content increased from 10 wt% to 50 wt%, the contact angle value increased slowly, from ~3° to ~9°. But for the case of 70 wt% PS, the contact angle value increased dramatically to ~37°. So there was a structural discontinuity between the blends where the concentration was 70 wt% PS (sample PS-70) and the other samples containing lower amount of PS.

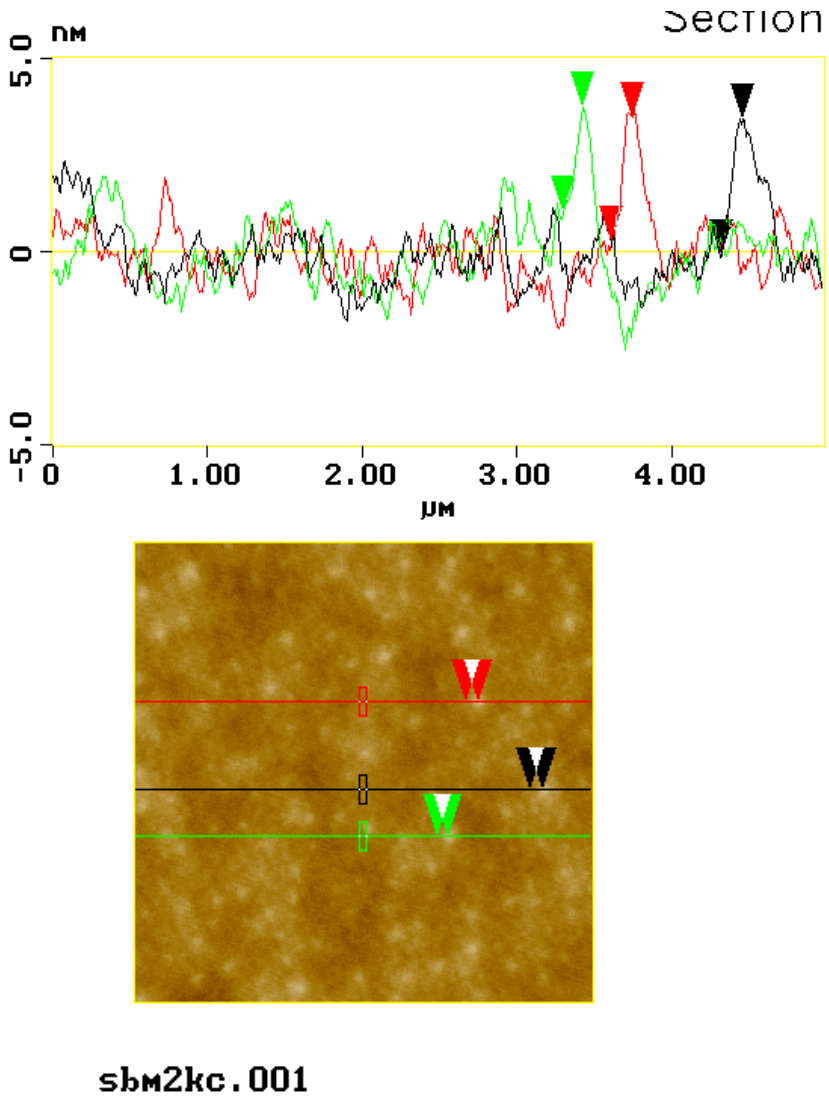

Figure 6.5. AFM contact angle measurement based the cross section analysis of the surface of PS and PS-*co*-PMMA blend thin film (PS-10) on silicon wafer

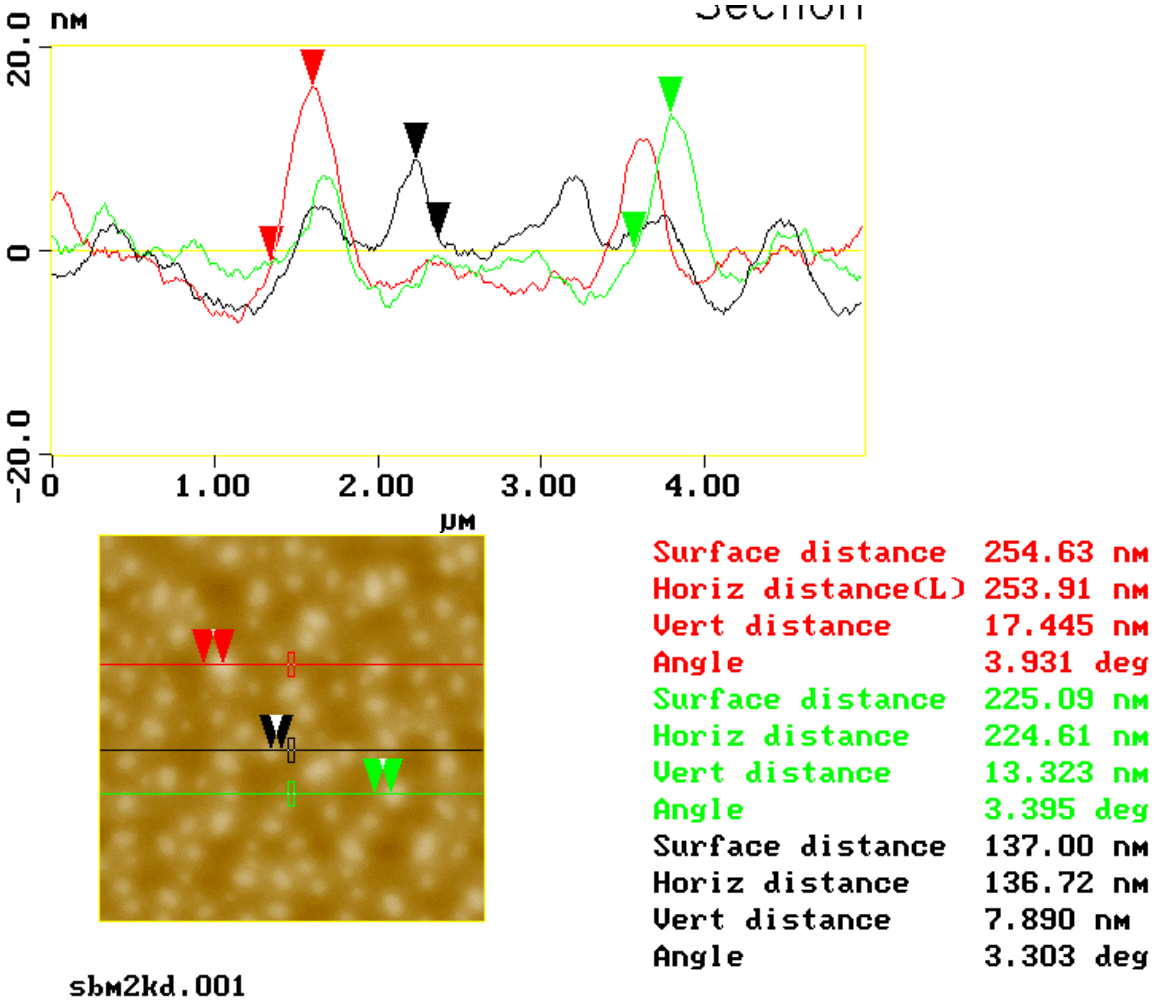

Figure 6.6. AFM contact angle measurement based the cross section analysis of the surface of PS and PS-*co*-PMMA blend thin film (PS-20) on silicon wafer

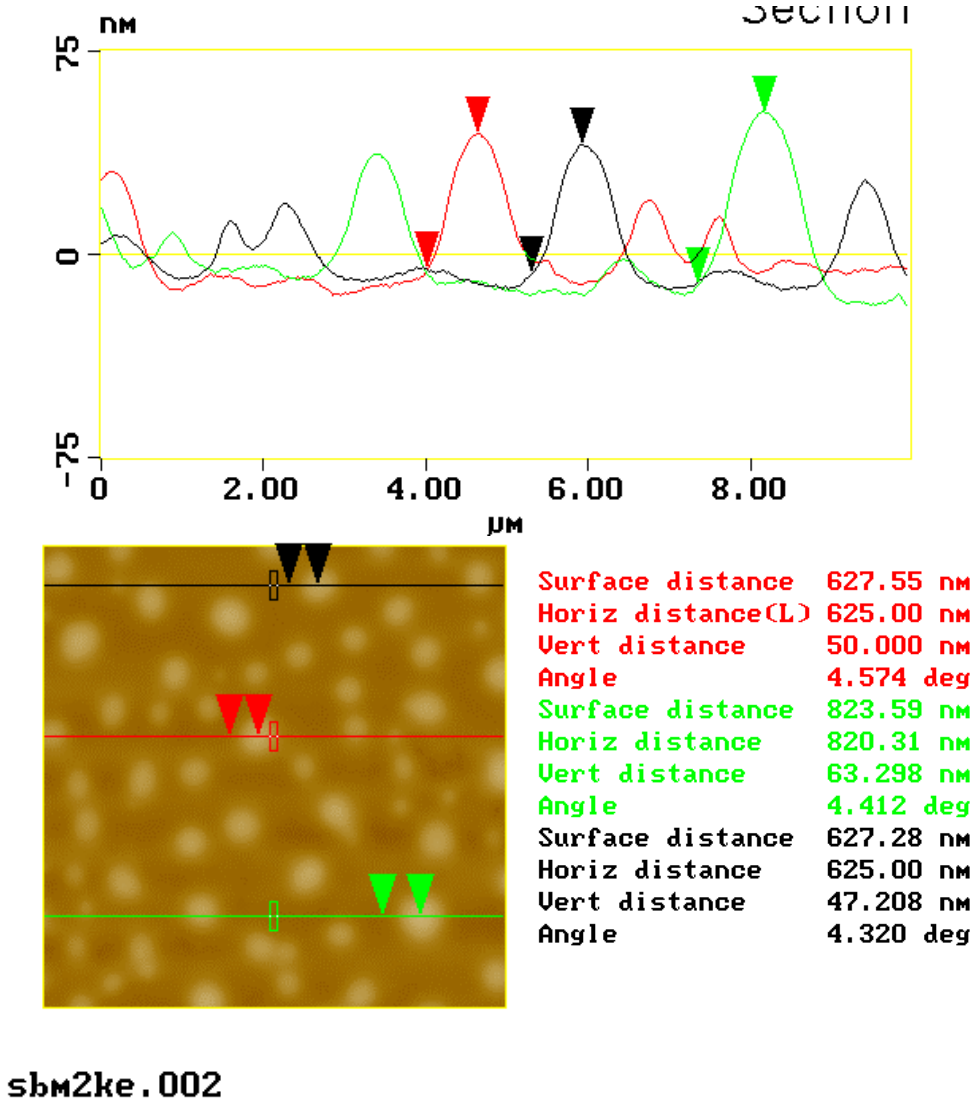

Figure 6.7. AFM contact angle measurement based the cross section analysis of the surface of PS and PS-*co*-PMMA blend thin film (PS-30) on silicon wafer

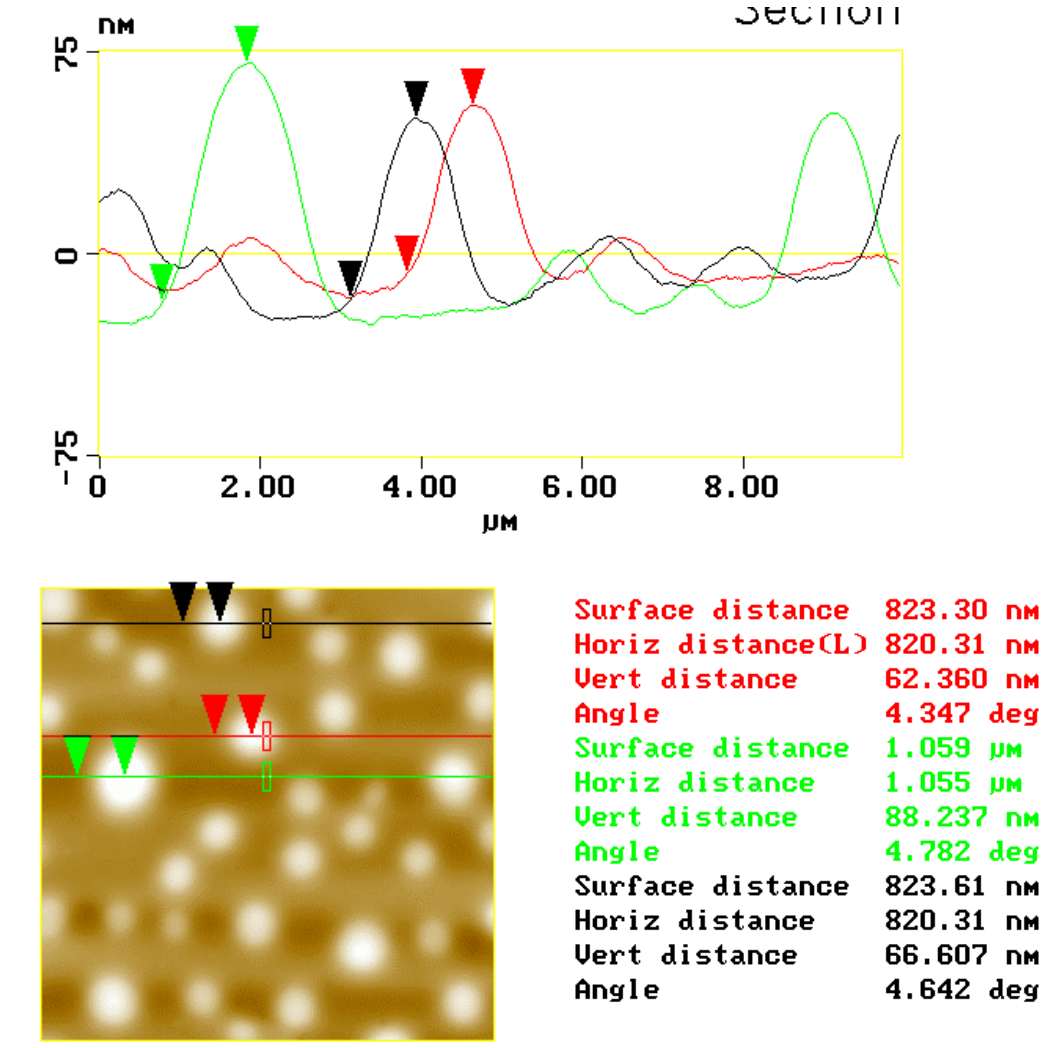

Figure 6.8. AFM contact angle measurement based the cross section analysis of the surface of PS and PS-*co*-PMMA blend thin film (PS-40) on silicon wafer

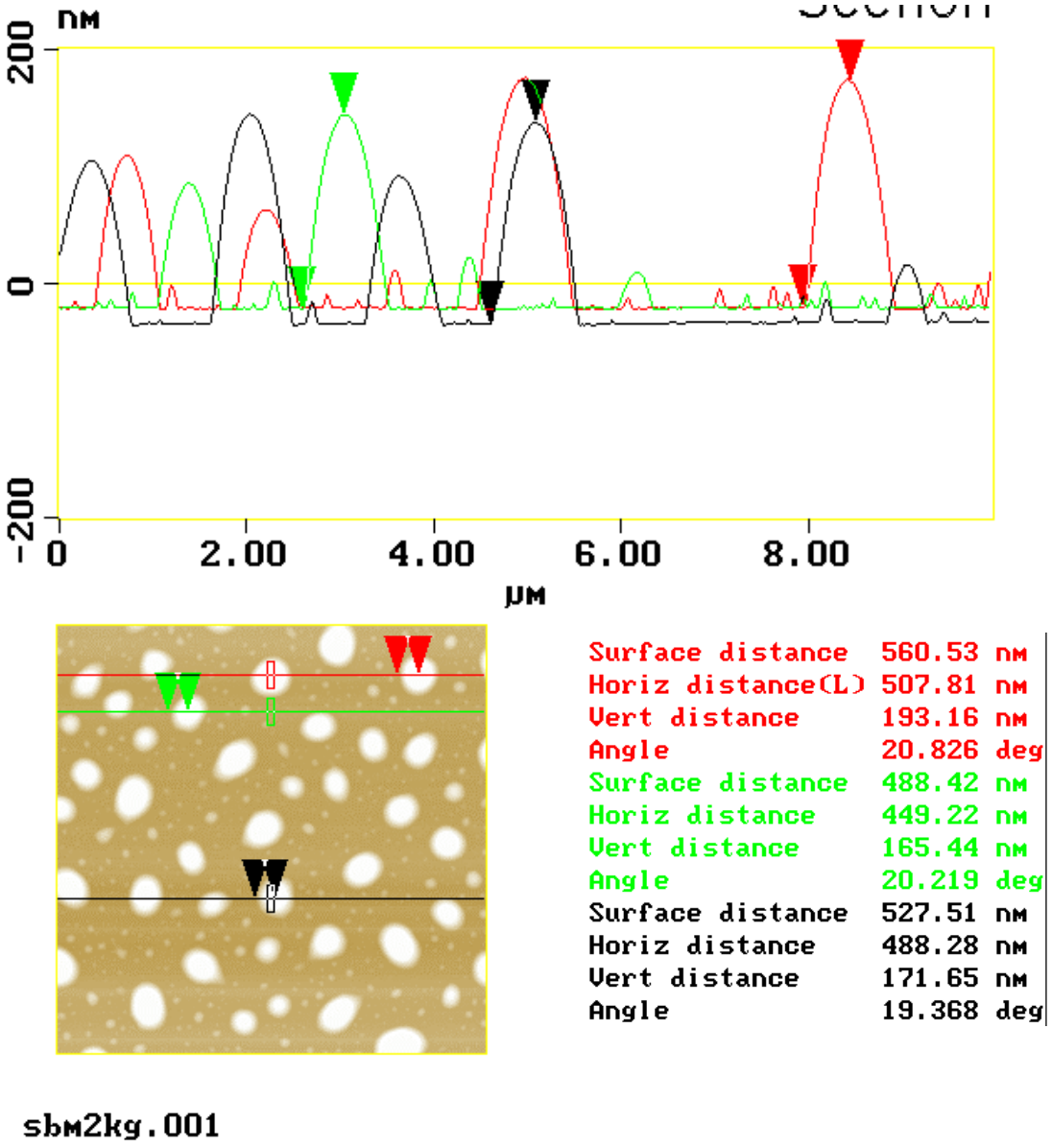

Figure 6.9. AFM contact angle measurement based the cross section analysis of the surface of PS and PS-*co*-PMMA blend thin film (PS-70) on silicon wafer

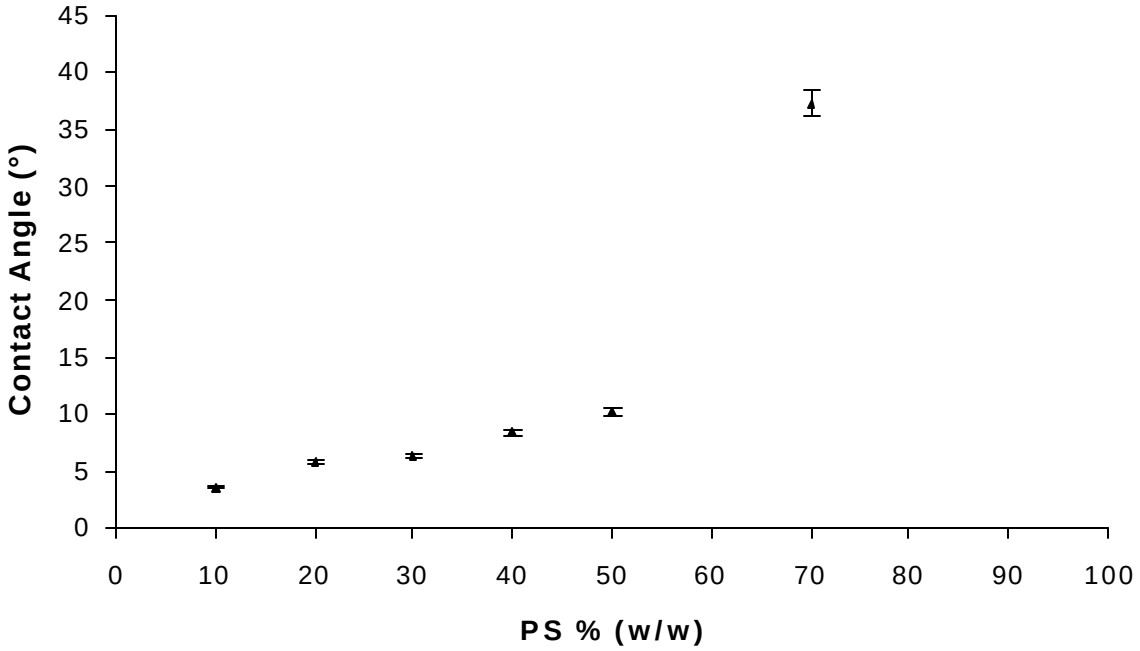

Figure 6.10. Contact angle values from the AFM cross section analysis on the surfaces of PS and PS-*co*-PMMA blend thin films on silicon wafers

Now, examine Figure 6.11 and Figure 6.12. From the cross section analysis of the sample of PS-70 (Figure 6.11), a clear, sharp boundary was observed between each of the particles and the substrate. Even for a very small particle (e.g., the one marked by red arrows in Figure 6.11), the sharp boundary still existed. In contrast, there was no sharp boundary observed in the case of PS-40 (similar results for other samples with low PS contents) as shown in Figure 6.12. There was an inflection point (marked by a green arrow in Figure 6.12) on the cross section analysis trace. A gradually changing composition between the two phases (the PS rich phase and the copolymer rich phase) might lead to the gradually changing curvature around the inflection point. This would not be a surprise based on the understanding of the phase separation process in bulk polymer blends (Chapter 2). However, the sharp boundary observed for sample PS-70 suggests that dewetting of the polymer blend on the substrate occurred instead of phase separation between the two polymers inside the blend. Though more study is needed, it is believed that the un-favorable interaction between the PS component and the silicon

wafer substrate played an important role in the observed phenomena resulting in dewetting for PS-70, but in phase separation for the other samples.

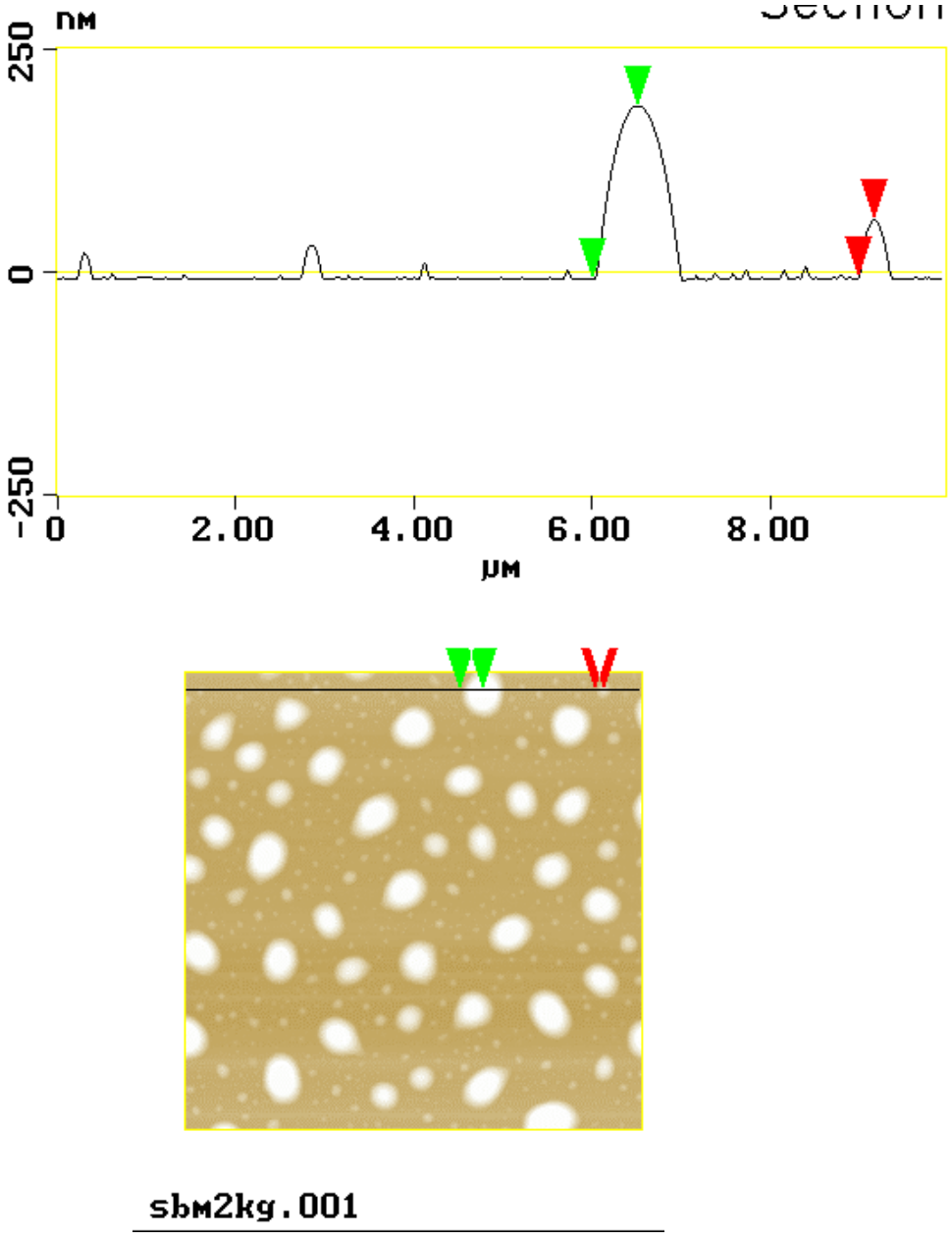

Figure 6.11. Cross section analysis of the surface of PS and PS-*co*-PMMA blend thin film (PS-70) on silicon wafer

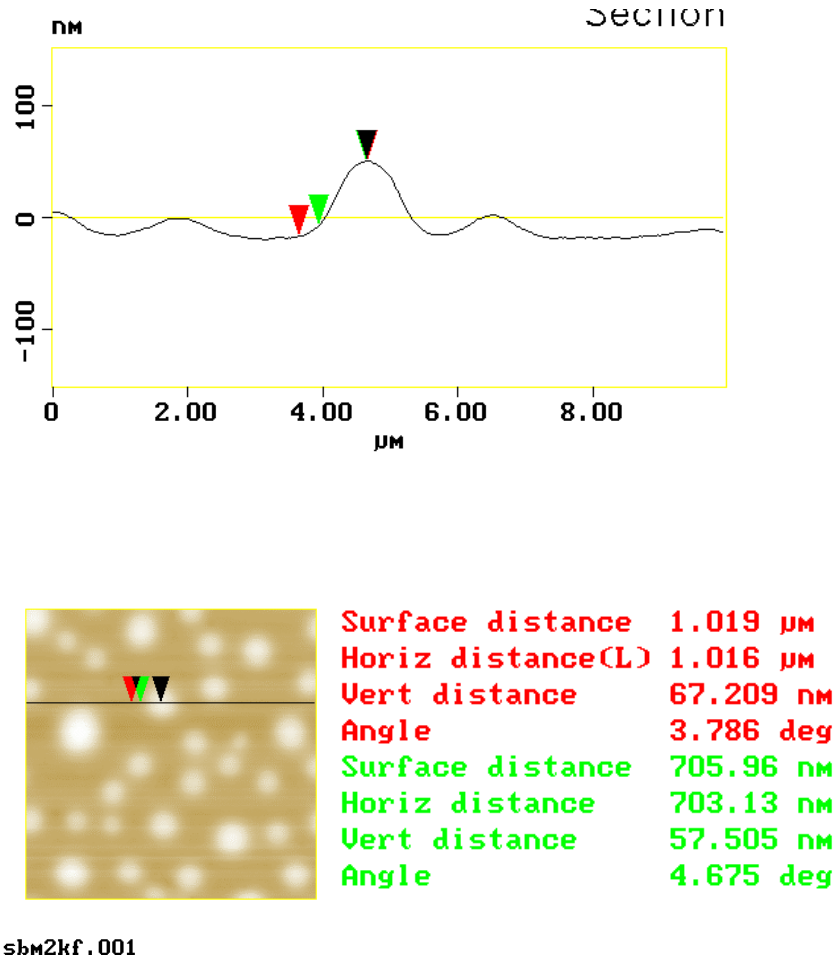

Figure 6.12. Cross section analysis of the surface of PS and PS-*co*-PMMA blend thin film (PS-40) on silicon wafer

6.2.4. Thickness influence on polymer blend thin film phase behaviors

The impact of the un-favorable interaction between the PS component in the blends and the silicon wafer substrate was found to be affected by the thickness of the polymer blend films. As previously discussed, the chain mobility (mass transportation) is also restricted by the film thickness in quasi-2D thin films. As demonstrated in the literature[4], for film thicknesses ranging between 10 and 100 nm, polymer chain dynamics can be influenced by the existence of the substrate, even though the thickness can be ~ 10 times the radius of gyration of the polymers in the film. Thus, it was of interest to closely examine the influence of the film thickness on the phase behaviors of the polymer blend thin films of this dissertation.

The film thickness was conveniently controlled in two ways in the research, by spin speeds, and by solution concentrations. For the spin coating process, with lower spin speeds, or higher polymer concentration in the solutions, a thicker polymer blend film was obtained. In this section, polymer films prepared from three different spin coating speeds (1k, 2k, and 3k rpm; PS-50a, PS-50b, and PS-50c in Table 6.1; 0.5%, w/v, toluene) and two different solutions (0.5 and 1.0 %, w/v, toluene; PS-50b and PS-50d in Table 6.1; 2k rpm) were examined to reveal the influence of thickness on resulting polymer blend thin film phase structures. The chemical composition of the films was fixed, with 50 wt% of the polystyrene homoplolymer in the blends. Accurate film thickness information was not available because phase separations happened quickly after the film preparation - it was difficult to precisely determine the thickness of a strongly phase separated thin film. But based on our accumulated experience on homopolymer and copolymer thin films, the experimental parameters (concentration, spin speed, etc.) used here would give film thicknesses in the range of 10 to 100 nm.

Figures 6.13 and 6.14 give the AFM images of the topologies of the polymer blend thin films prepared with different spin coating speeds (1k, 2k and 3k rpm). The only difference among the three samples (PS-50a, PS-50b, and PS-50c) was film thickness. For the cases of 1k and 2k rpm, topologies with the character of "islands-in-sea" were observed. As discussed before, a NG (nucleation and growth) phase mechanism was possible in these two cases. The average size of the particles (diameter and height) became smaller for PS-50b (2k rpm) than that of PS-50a (1k rpm). The less significant degree of phase separation in the thinner film (PS-50b) was possibly due to the stronger chain mobility restriction caused by the decreased thickness. In contrast, when the spin speed increased to 3k rpm (PS-50c), a very different topology was observed (Figures 6.13 and 6.14). Instead of dispersed particles ("islands in sea"), a continuous upper phase was obtained as shown in the AFM height images (Figures 6.13 and 6.14), which corresponds to the darker domain in the AFM phase image (Figure 6.14) and was assigned as the PS rich phase. This continuous PS rich phase might result from a spinodal decomposition (SD) mechanism (Chapter 2). Since the chemical compositions of the blends were the same (50 wt% of PS), the change of phase separation

[4] Jones, R.L.; Kumar, S. K.; Ho, D. L.; Briber, R. M.; Russell, T. P., *Nature* 400, 146, **1999**

mechanism (from NG to SD) was likely due to a combination of the effects of the different substrate/PS/PS-*co*-PMMA interactions (χ), and horizontal mass transportation capabilities in the films of different thickness.

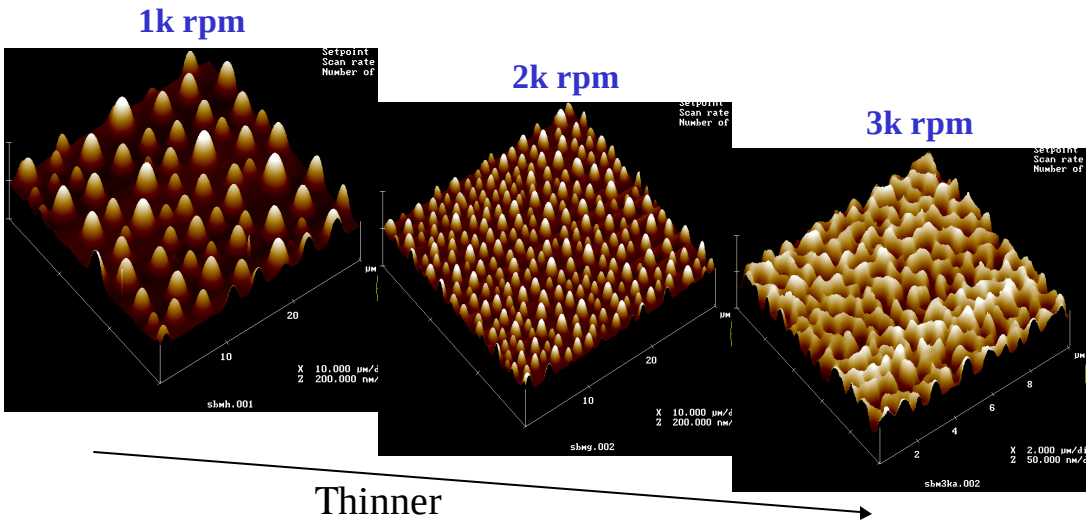

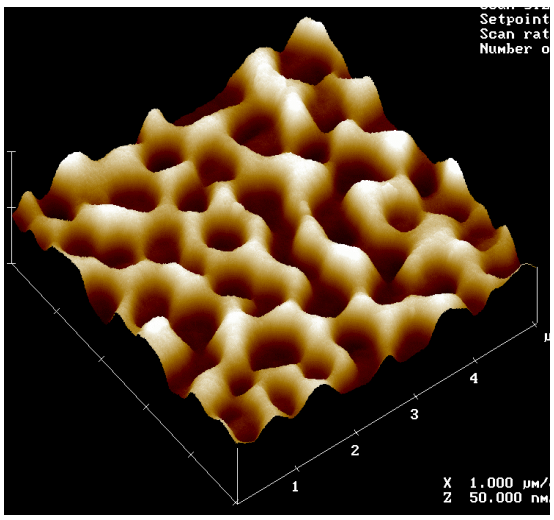

3k rpm

Figure 6.13. Influence of film thickness on polymer blend thin film topologies. AFM 3D height images

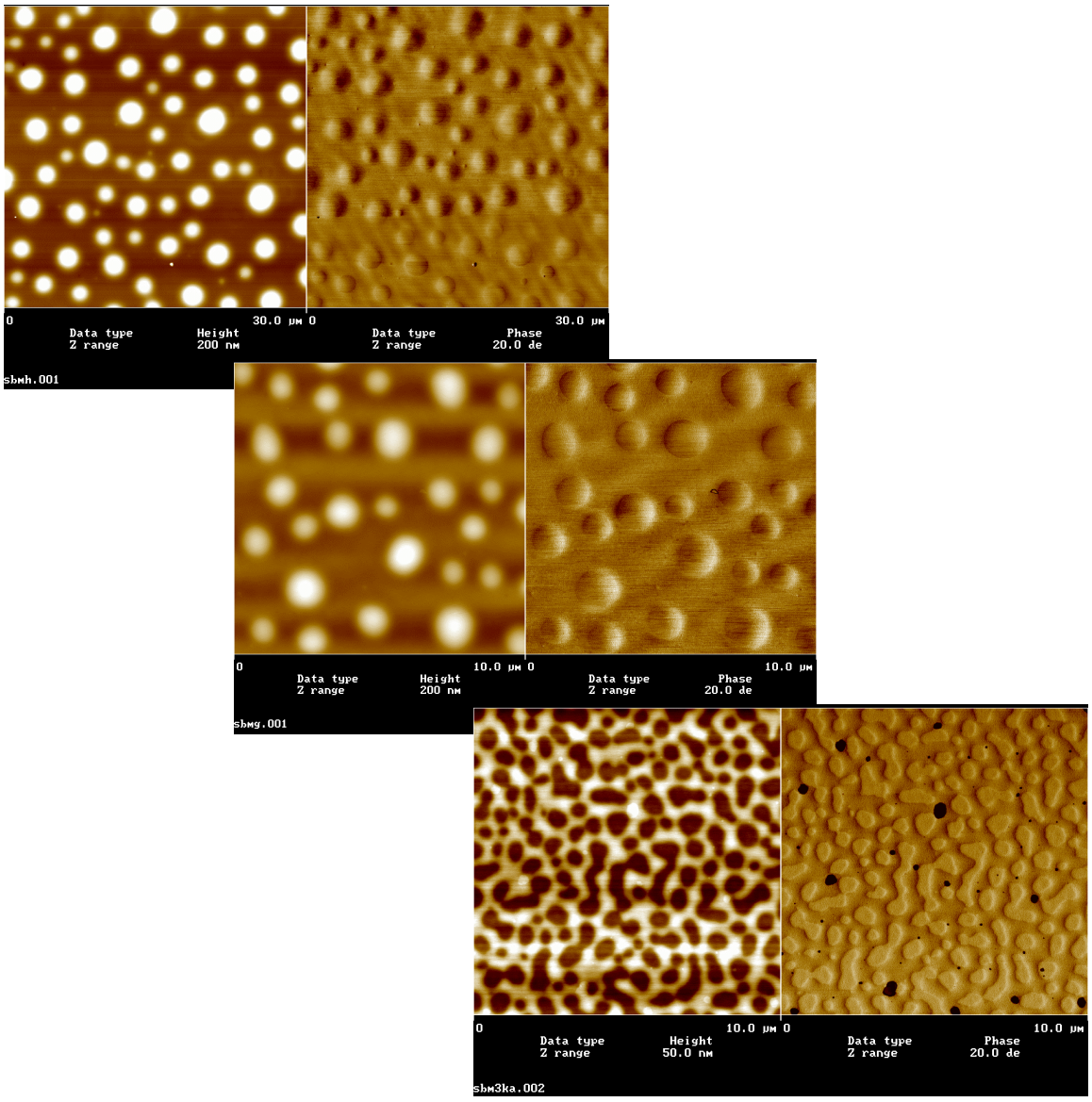

Figure 6.14. Influence of film thickness on polymer blend thin film topologies. Spin coating speeds: top, 1k rpm; middle, 2k rpm; bottom, 3k rpm. AFM height and phase images.

More comparisons between samples PS-50a and PS-50b was done and is summarized in Table 6.2 and Figure 6.15. While smaller particle size (height and diameter) was observed in the thinner film (PS-50b, 2krpm), the particle contact angle was slightly larger. This increased contact angle value of the particles (PS rich domain) in the thinner film suggests a stronger un-favorable interaction between the PS component and the silicon wafer substrate as the film became thinner.

The effect of the film thickness was also investigated by preparing samples from solutions with different concentrations (PS-50b and PS-50d). Similar trends to those above for the particle sizes and contact angle values were also observed because of the change of the thickness of the films (Table 6.3 and Figure 6.16).

Table 6.2. Effect of polymer blend thin film thickness on the characteristics of the particles (PS rich domain). Samples: PS-50a and PS-50b

spin rate (rpm)	particle height (μm)	particle diameter (μm)	contact angle (°)
2k rpm	0.9 +/- 0.2	2.1 +/- 0.4	10.2 +/- 0.2
1k rpm	1.5 +/- 0.3	4.0 +/- 0.9	8.6 +/- 0.2

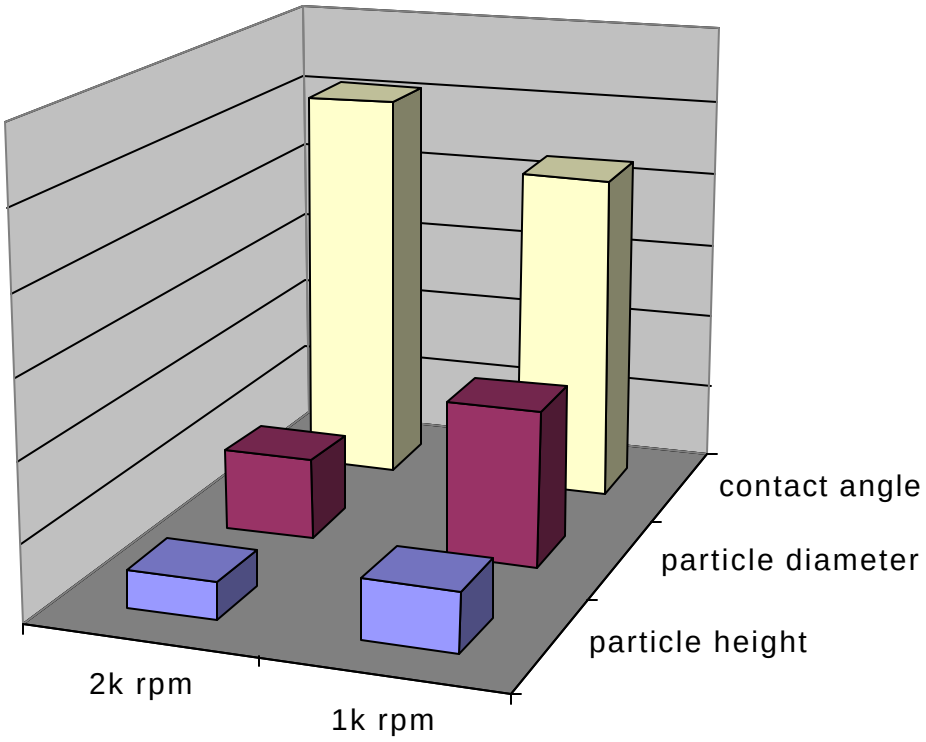

Figure 6.15. Effect of polymer blend thin film thickness on the characteristics of the particles (PS rich domain). Samples: PS-50a and PS-50b

Table 6.3. Effect of polymer blend thin film thickness on the characteristics of the particles (PS rich domain). Samples: PS-50a and PS-50b

concentration (w/v)	particle height (μm)	particle diameter (μm)	contact angle (°)
0.50%	0.9 +/- 0.2	2.1 +/- 0.4	10.2 +/- 0.2
1.00%	2.0 +/- 0.3	5.0 +/- 1.0	9.2 +/- 0.2

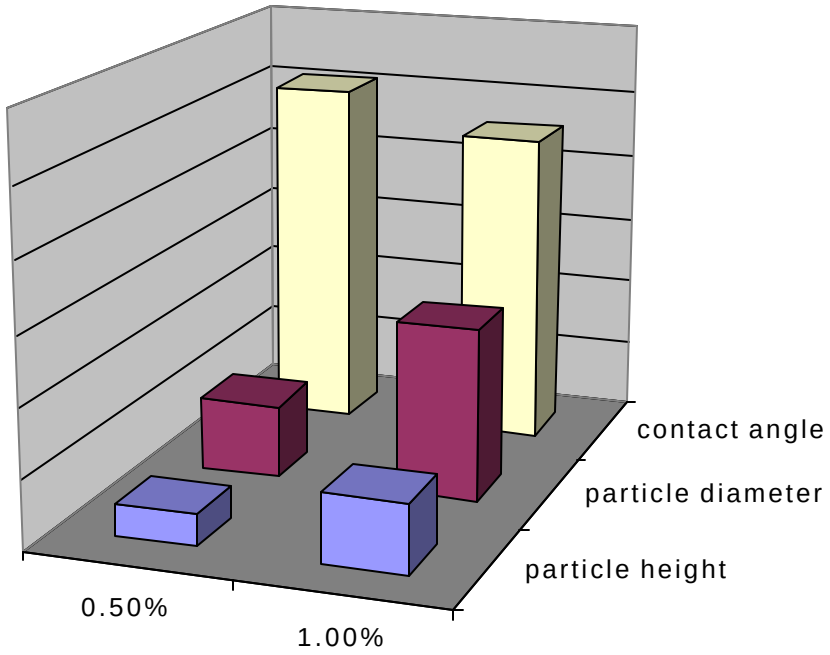

Figure 6.16. Effect of polymer blend thin film thickness on the characteristics of the particles (PS rich domain). Samples: PS-50a and PS-50b

6.2.5. Temperature influence on polymer blend thin film phase behaviors

As demonstrated in the previous discussions, the effect of a silicon wafer substrates on phase behavior can not be neglected in the ultra-thin polymer blend films. The interactions (χ) between the substrate and the two components in the blend were found to be asymmetric (favorable interaction with PS-*co*-PMMA and un-favorable interaction with PS). It is of interest to explore how temperature affects the χ values, and

therefore the film topology, since this interaction is an important part of the physics of the film growth process.

The sample PS-50c (Table 6.1) was selected to probe the temperature dependence of the phase behaviors. As shown previously, this sample displayed a topology with a continuous PS rich phase (Figure 6.14) at the polymer/air interface after heated in an oven at 150°C for ≥10 hours (20 hours in this case). After examination by the AFM, the sample was put back into the oven and heated at 110°C for 5 hours. Surprisingly, the well-defined SD-type surface structure disappeared and a uniform thin film surface was obtained after the heating process at this lower temperature (Figure 6.17, middle). There was no further change with heating times of more than 5 hours.

After the two temperature exposures above (150°C → 110°C), the sample was heated back to the higher temperature (150°) for another 5 hours. A separation topology close to that of the original 150°C version (with the PS rich domain as a continuous phase on top) was re-generated (Figure 6.17, right)! AFM phase images and 3D height images are shown in Figure 6.18 to confirm the true re-generation of the topology via the thermal processes. The cycle of uniform surface (110°C) – phase separated surface (150°C) was repeatable.

The observed temperature dependence of the phase behavior in the polymer blend thin film deposited on the silicon wafer substrate was similar to that for a LCST (lower critical solution temperature) behavior in a bulk polymer blend. There, in the bulk, phase separation occurs at higher temperatures; but, the system is homogeneous at lower temperatures. The existence of specific interactions, such as hydrogen bonding, can induce an LCST behavior in a bulk polymer blend.[5] In the case of the polymer blend thin film, hydrogen bonding existed between the Si-OH groups on the surface of the substrate and the C=O groups in the PMMA component of the film. This was certainly a favorable interaction between the substrate and the PS-*co*-PMMA copolymer in the blend. It is not clear exactly how the change of the amount of hydrogen bonding at different temperatures affected the overall χ value in the blend; but, this should be a valuable

[5] Wang, J.; Wang, S.; McGrath, J. E.; Ward, T. C., *Polymer Preprint*, 737, 39(2), **1998**

direction to explore in order to understand and model the unusual temperature-dependent phase behavior found in the polymer blend film of this dissertation.

6.2.6. Conclusions of polymer blend thin film studies

In the present research, the influence of chemical composition, film thickness and temperature on the phase behaviors in several polymer blends (PS and PS-*co*-PMMA) processed into thin films was explored. The phase behaviors were examined by topological studies and contact angle measurements. Higher PS concentrations yielded a change in structure reflecting unfavorable wafer/PS interactions. A change of the phase separation mechanisms (from NG to SD) occurred when the film dimensions became thinner. Thermoreversible topologies were observed with a LCST-like phase behavior in the polymer blend thin film with 50 wt% of PS.

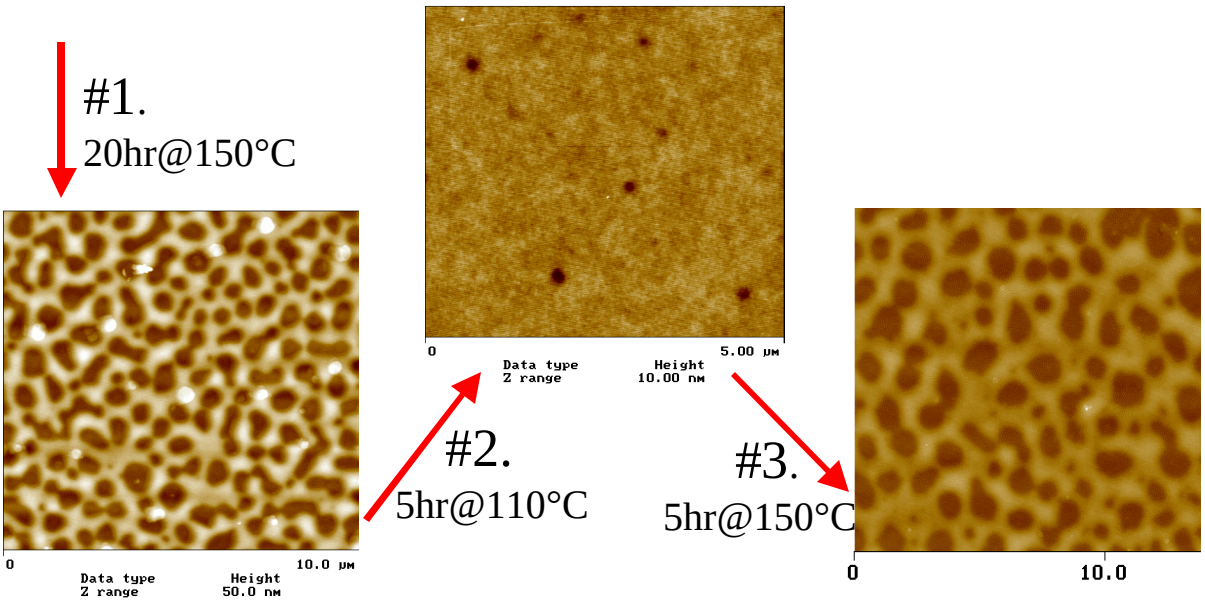

Figure 6.17. Thermal reversible phase behavior in polymer blend thin film (PS-50c). AFM height images

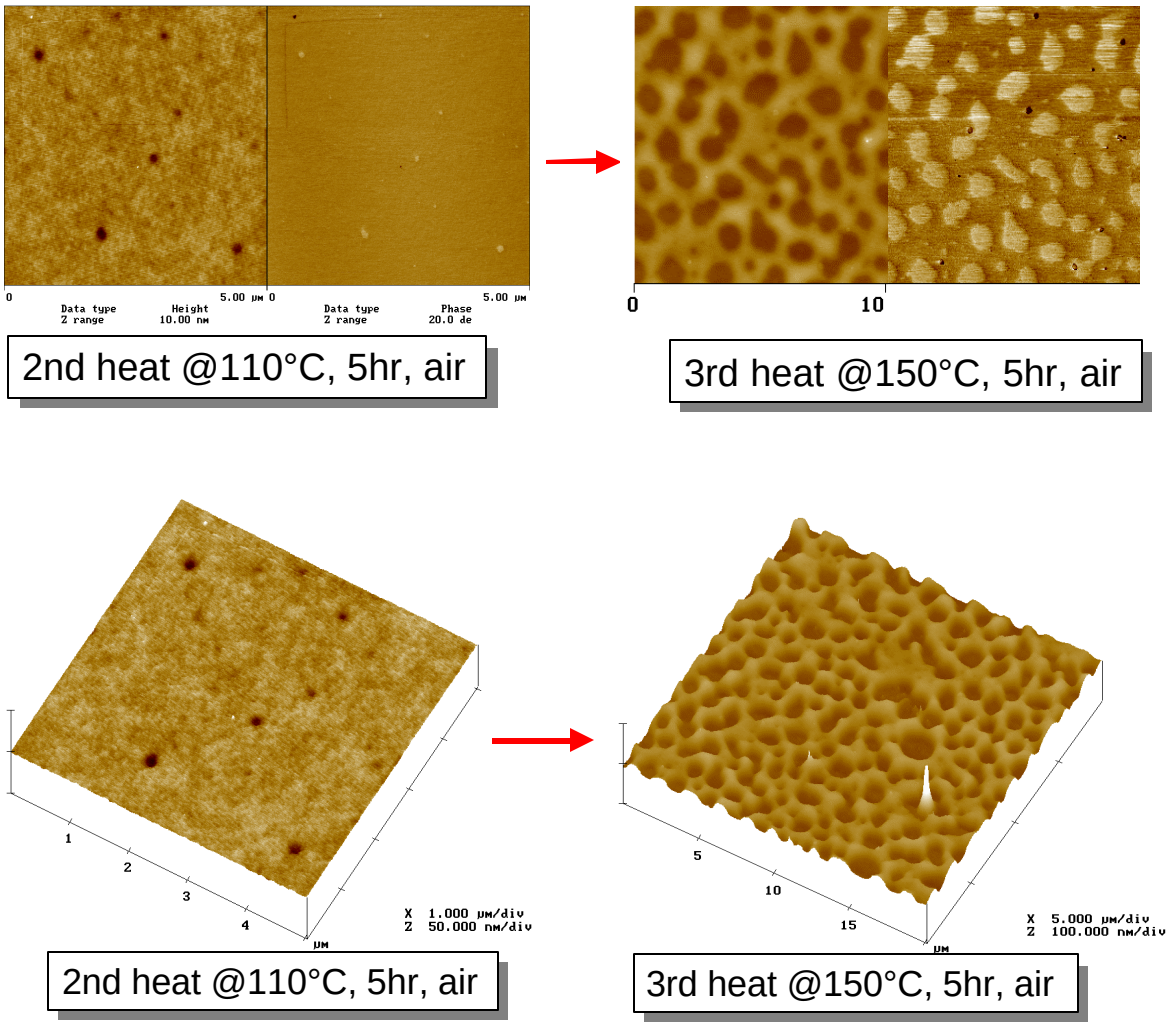

Figure 6.18. Thermal reversible phase behavior in polymer blend thin film (PS-50c).

6.3. Influence of CFABC Polymer Brush On Block Copolymer Ultra-thin Film Phase Behaviors

6.3.1. Background on block copolymer thin film studies

The microscopic or mesoscopic phase separation of block copolymers has attracted significant interest because of their potential applications in nanofabrication. Most studies have been focused on diblock copolymers. Generally, a diblock copolymer thin film will self-assembled into lamellar structures parallel to a substrate as shown in Scheme 6.2.

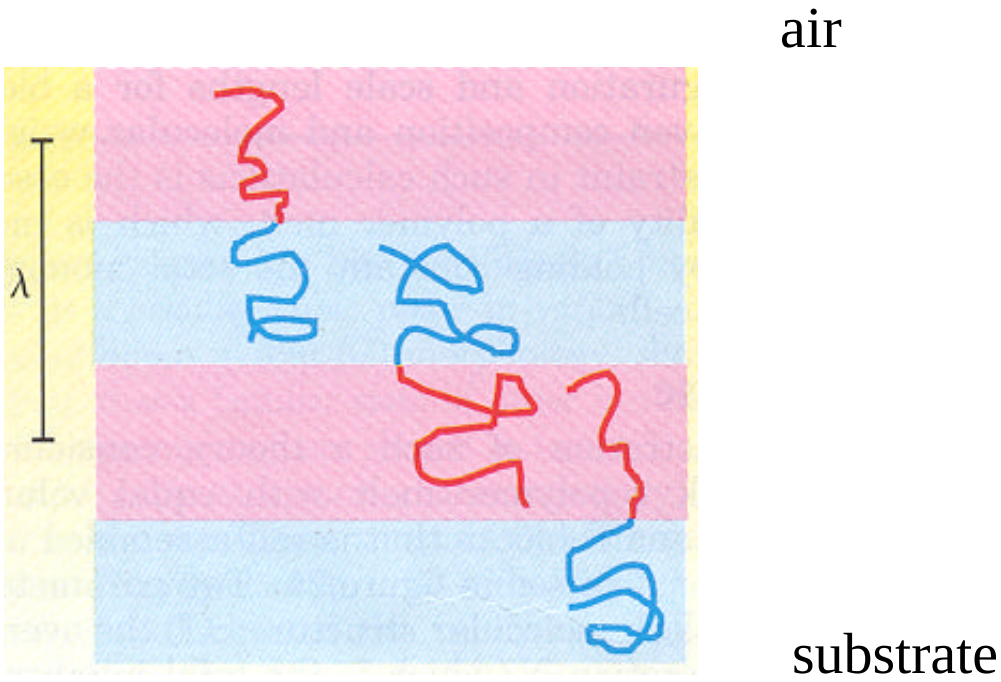

Scheme 6.2. Block copolymer thin film lamellar structure[6]

Various modified surfaces, such as mechanically/optically patterned surfaces, have been used to control the phase behaviors of block copolymer thin films.[7,8] In some cases, lamellar structures perpendicular to the substrates have been observed in thin films of symmetric diblock copolymer on stripe-patterned heterogeneous substrates.[9]

More recently, polymer brushes have been also used to control block copolymer thin film structures.[10] Russell and coworkers[11] designed a "neutral" surface using an end-grafted PS-*co*-PMMA random copolymer brush. Russell *et*. *al*. looked at the phase behavior of PS-*b*-PMMA *di*-block copolymer thin film spun cast on the polymer brush modified surface. The advantages of polymer brushes for this fabrication include versatile design, multi-functionality, self-assembled nano-patterns, etc. A multi-component polymer brush, which is heterogeneous on a nano-scale, can interact with

[6] Fredickson, *Physics Today*, 1999
[7] Pereira, G. G.; Williams, D. R. M.; Chakrabarti, A., *J. of Chemical Physics* 112, 10011, **2000**
[8] Husseman M, *et al*. *Macromolecules* **1999**;32:1424
[9] Rockford, L.; Lou, Y.; Mansky, P.; Russell, T. P.; Yoon, M., *Phys. Rev. Lett*. 82, 2602, **1999**
[10] Sedjo RA, Mirous BK, Brittain WJ. *Macromolecules* **2000**;33:1492.
[11] Mansky P, Liu Y, Huang E, Russell TP, Hawker CJ. *Science* **1997**;275:1458

different blocks in a block copolymer thin film simultaneously. Furthermore, because of the flexibility of the types of polymer chains in a polymer brush system, it is possible for those chains to adjust their configurations to reflect differences in their local environment (i.e., different lamellae in a block copolymer thin film).

In this section, the influence of the CFABC polymer brush on the phase behaviors of *di*-block copolymers is presented. Additionally, triblock copolymers with or without functionality in the central block were also used to prepare thin films, and the influence of the central block functionality on the phase behaviors was studied.

6.3.2. Self-assembled lamellar structures in thin films of triblock copolymer with protected central functionality

Thin films of a *tri*-block copolymer, PS-*b*-PSTBDMS-*b*-PMMA (PSTBDMS: poly(*p*-[(*tert*-butyldimethylsilyl)oxy]styrene)), were prepared on silicon wafers. The polymer, with protected functionality in the central block, was originally synthesized to serve as a precursor for the CFABC polymer as described in Chapter 3.

After spin casting onto silicon wafers from a toluene solution (0.5% w/v) at different spin speeds (3k, 4k, and 5k rpm), the *tri*-block copolymer thin films were dried in a vacuum oven at 170°C for 10 hours. The wafers were prepared as described in Chapter 4.

It is generally expected that a thickness gradient will exist on the edge of a spin coated thin film because of the mass accumulation resulting from the spin coating process, as depicted in Scheme 6.3. For a thin film spin coated at 4 k rpm, the edge of the film was examined by a CCD camera (Figure 6.19) and AFM (Figures 6.20, 6.21 and 6.22). Instead of gradually changing thickness at the edge of the film as depicted in Scheme 6.3, stripes with different colors in the optical image (Figure 6.19) were observed. These stripes suggest an interference pattern originating from a stepwise change of thickness. The observed step changing thickness was confirmed in the AFM height image collected on the same region (Figure 6.20). An AFM height image with a higher magnification is shown in Figure 6.21. The lamellar structures were very clear and the size of each step (lamellar thickness) was about 20 nm as determined from the cross section analysis (Figure 6.22, bottom). These self-assembled lamellar structures in

a *tri*-block copolymer thin film are of interest, because they have not been described often compared to those in *di*-block copolymer thin films.

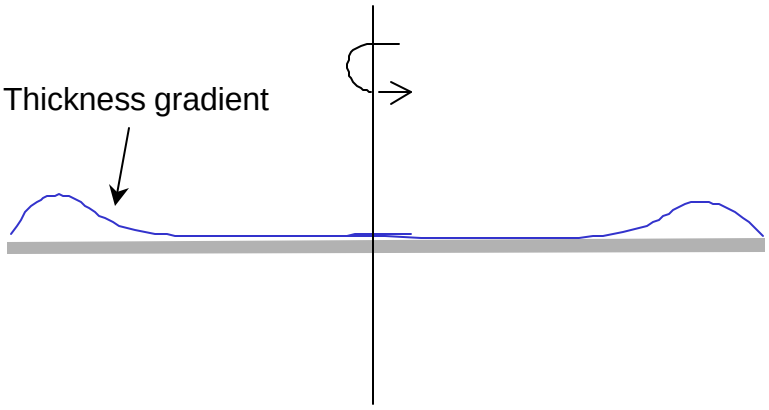

Scheme 6.3. Thickness gradient at the edge of a spin-coated thin film.

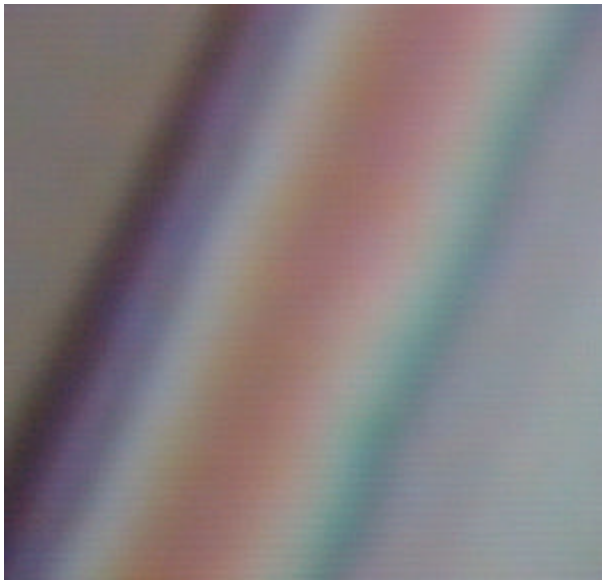

Figure 6.19. Optical image of the edge of a triblock copolymer thin film (4k rpm) on a silicon wafer from a high resolution CCD camera. The image size is about 40 40 µm.

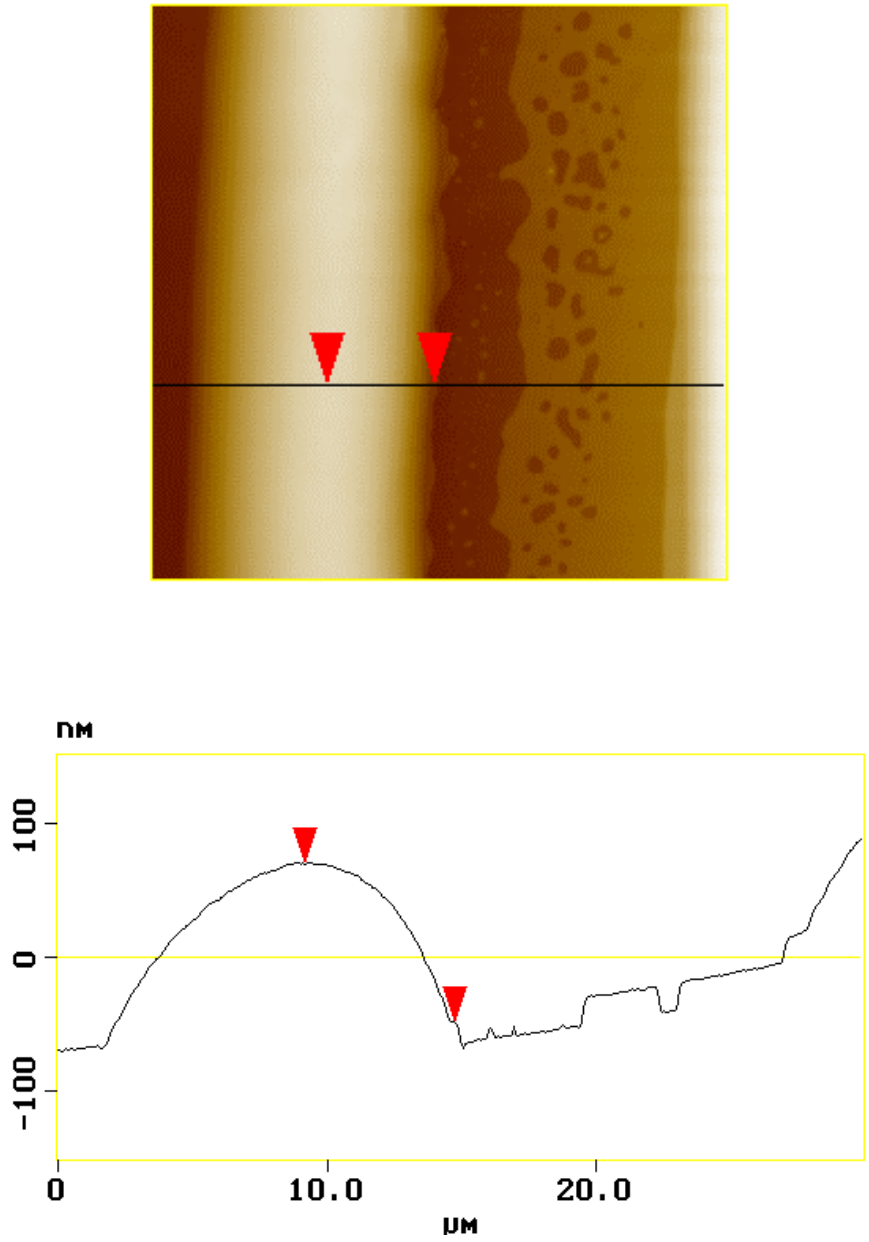

Figure 6.20. AFM height image and cross section analysis of the edge of a triblock copolymer thin film (4k rpm) on a silicon wafer

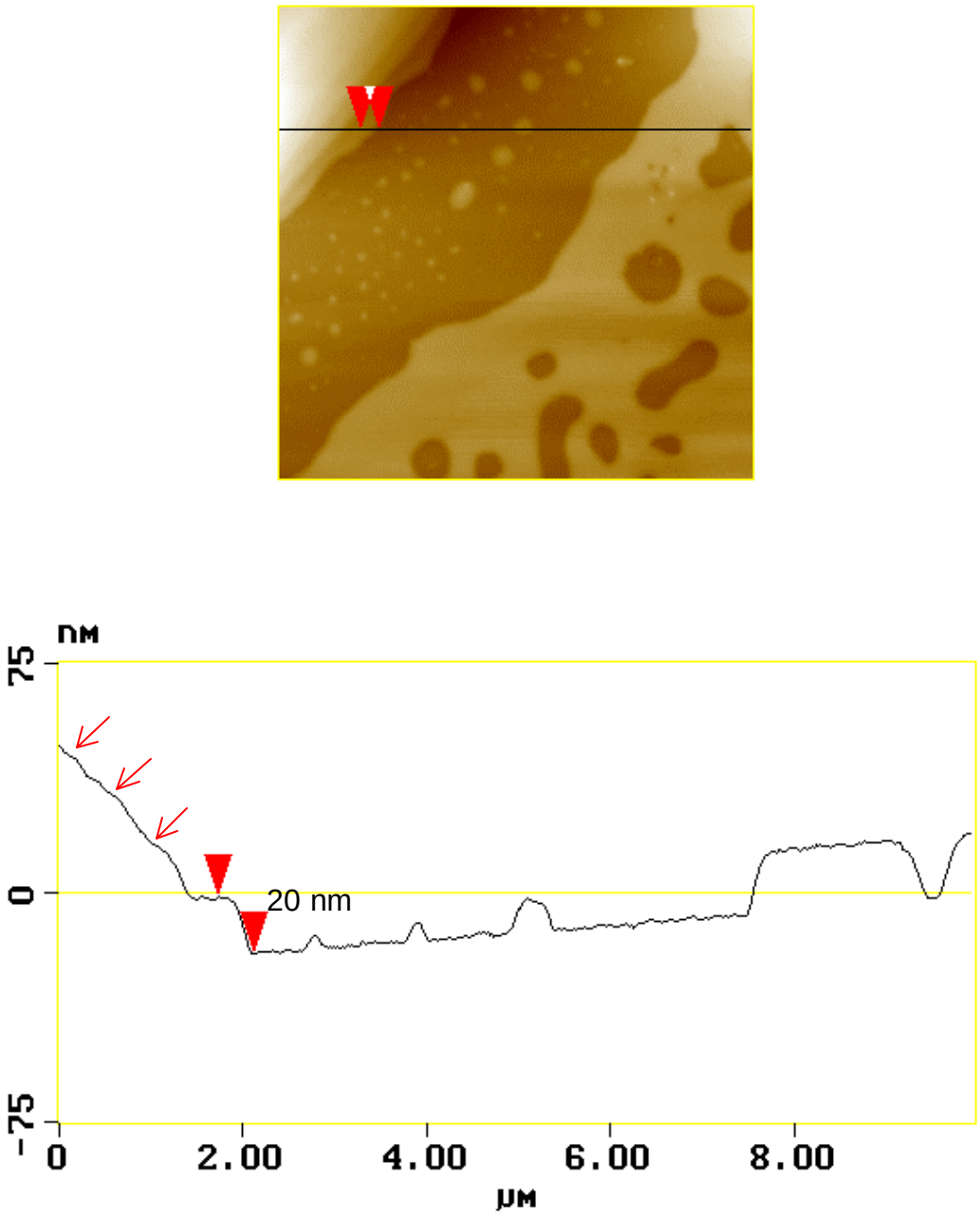

Figure 6.21. AFM height image and cross section analysis of the edge of a triblock copolymer thin film (4k rpm) on a silicon wafer

The topologies of the triblock copolymer thin films were also investigated by modifying the film thickness, similar to the methods used above for blends (section 6.2). The thickness of the films was conveniently controlled by spin coating speed. Figure 6.22 gives the AFM height images of triblock films spin coated at three different speeds,

3k, 4k, and 5k rpm. With higher spin speeds, a thinner film was produced on the substrate. The films were heated to 170°C, and after reaching thermal equilibrium, different topologies had developed (Figure 6.22). "Holes" were observed for the spin speed of 3k rpm, and an irregular (co-continuous) structure was observed for 4k rpm. Finally, using the speed of 5k rpm, an "island" structure was obtained. It is not clear if the different topologies were due to different phase separation mechanisms (i.e., spinodal or binodal mechanism), and more careful studies are needed. However, two interesting features of these self-assembled lamellar structures are worth noting. First, with the same experimental parameters (such as spin speed, solution concentration, temperature, etc.), the topological structures were reproducible. Second, no matter what type of topology resulted (holes, islands, or irregular), the height of the top layer was always constant at 20 nm (1 nm) (Figure 6.22).

FE-SEM was also employed to examine the topologies of the thin films. Operated under much lower voltage (1 kV *vs*. 10-20 kV for regular SEM) and with no requirement for gold sputtering, FE-SEM can give very high resolution (~10 nm) images without damaging polymer thin films. Thus, it serves as an ideal complementary technique to AFM for depicting thin film topologies. Figure 6.23 gives FE-SEM results on the surface of the same non-functionalized *tri*-block copolymer thin film spin coated on a silicon wafer (3k rpm) and examined by AFM (Figure 6.22, the first image). The bright domains in the FE-SEM image (Figure 6.23, the bottom image) correspond to the dark domains ("holes") in the AFM image (Figure 6.22, the first image).

Scheme 6.4 illustrates a possible way that the tri-block copolymers self-assembled into lamellar structures. Since the phenol groups in the central block were protected by the bulky TBDMS groups, there was no specific interaction between the central block and the substrate. The experimental results suggest that the relatively short central block is possibly located at the interface between the PS and PMMA blocks in the lamellar structures shown.

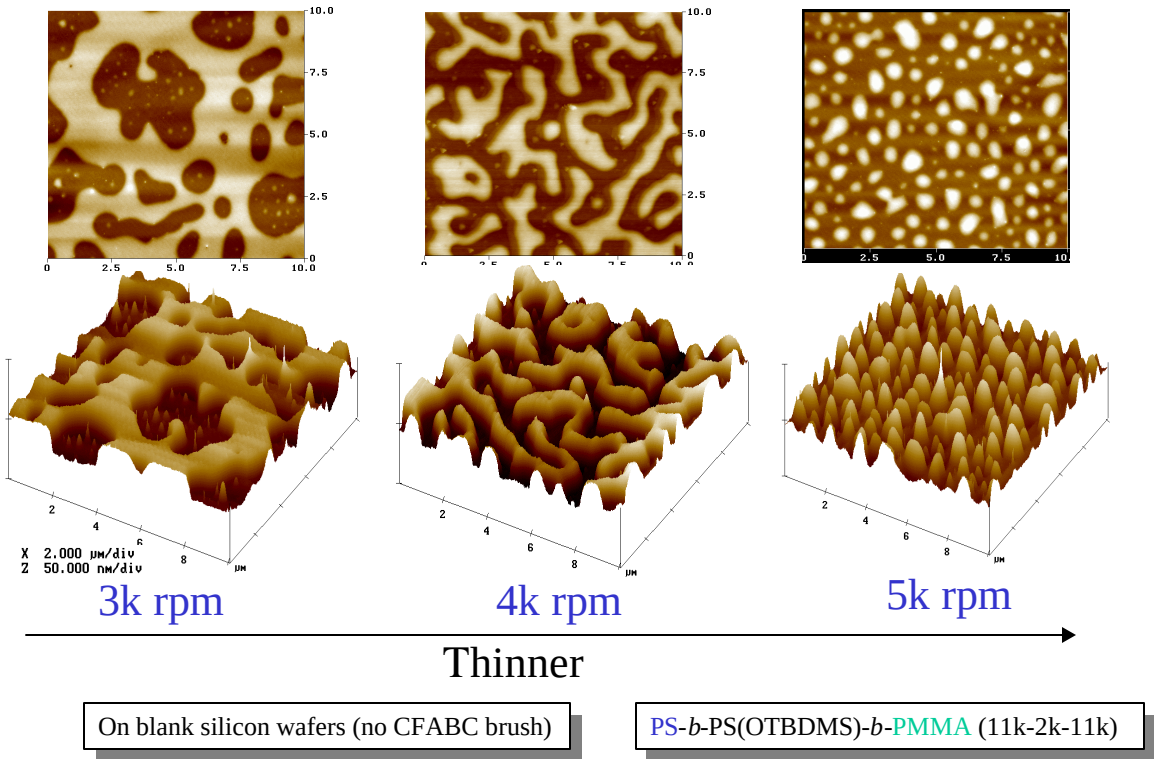

Figure 6.22. Influence of film thickness on the topologies of non-functionalized tri-block copolymer thin films.

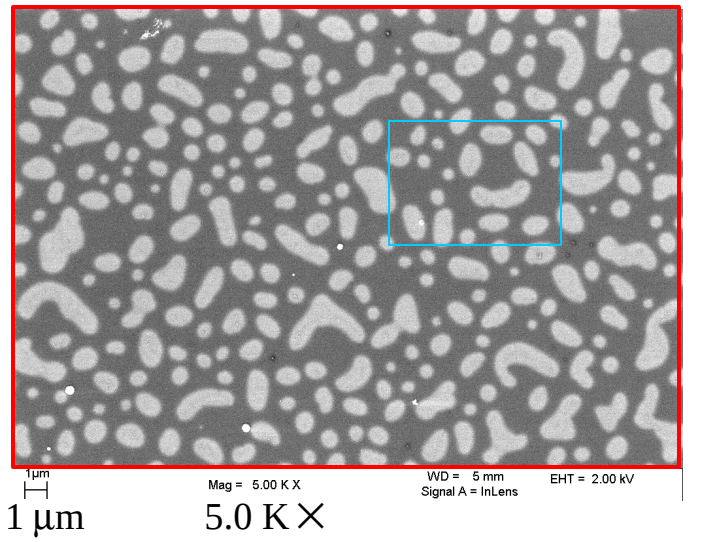

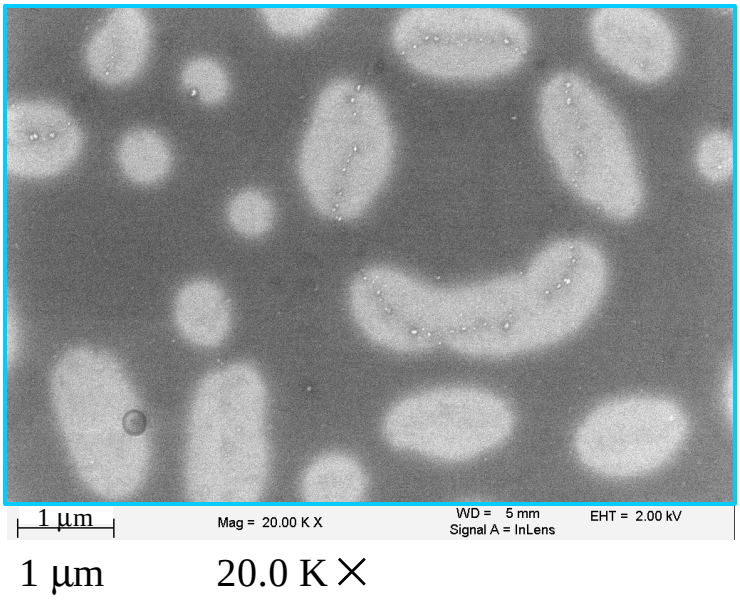

Figure 6.23. FE-SEM images of the topology of the non-functionalized tri-block copolymer thin film on silicon wafer (3k rpm).

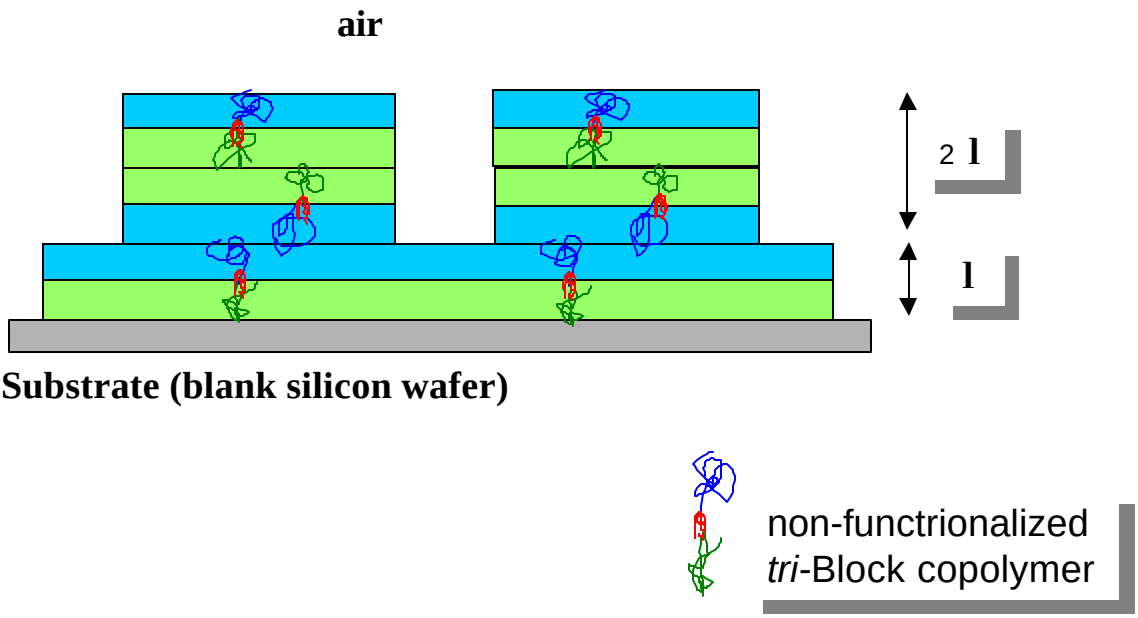

Scheme 6.4. Illustration of lamellar structure in the thin film of the triblock copolymer with protected functional groups in the center block. λ is a characteristic parameter for a block copolymer, which is related to the radius of gyration of a polymer chain.

6.3.3. CFABC *tri*-block copolymer (*tri*-block copolymer with central functionality) film on Si wafer surface

What is the effect of tethering of a tri-block copolymer thin film on the resulting structure when coated on a silicon wafer? Contrast this question and answer with that of the previous section where no tethering was allowed. A thin film of the CFABC polymer was spin-coated on a silicon wafer and then heated, followed by a washing step using toluene, as described in Chapter 4. AFM images were collected at different washing stages (Figure 6.24). Figure 6.24-a shows the topology of the spin-coated CFABC thin film before washing. Worm-like nano-domains were observed. After ~ 10 min. washing, some holes appeared on the surface (Figure 6.24-b). The worm-like nano-domains were still there, but with a little bit larger size and a loosely packed character. With further washing (~ 1 hour, Figure 6.24-c), less material was left on the top layer, but no obvious change were observed in the shape of the worm-like nano-domains. Finally, at the end of the washing process (10 hours) (Figure 6.24-d), the spherical nano-patterns of the CFABC brush, which were discussed before (Chapter 4), were obtained. Interestingly, in

Figure 6.24-c, both the worm-like nano-domain of the polymer film (bright area) and the spherical nano-domain of the polymer brush (dark area) were observed. Both domains had a similar characteristic size (~20 nm). A further study of the relationship between the two domains is needed. Figure 6.25 shows 3D AFM images of these surfaces at different stages of washing. It is worth noting that the thickness of the worm-like layer was maintained at about 7.5 nm through all the washing stages.

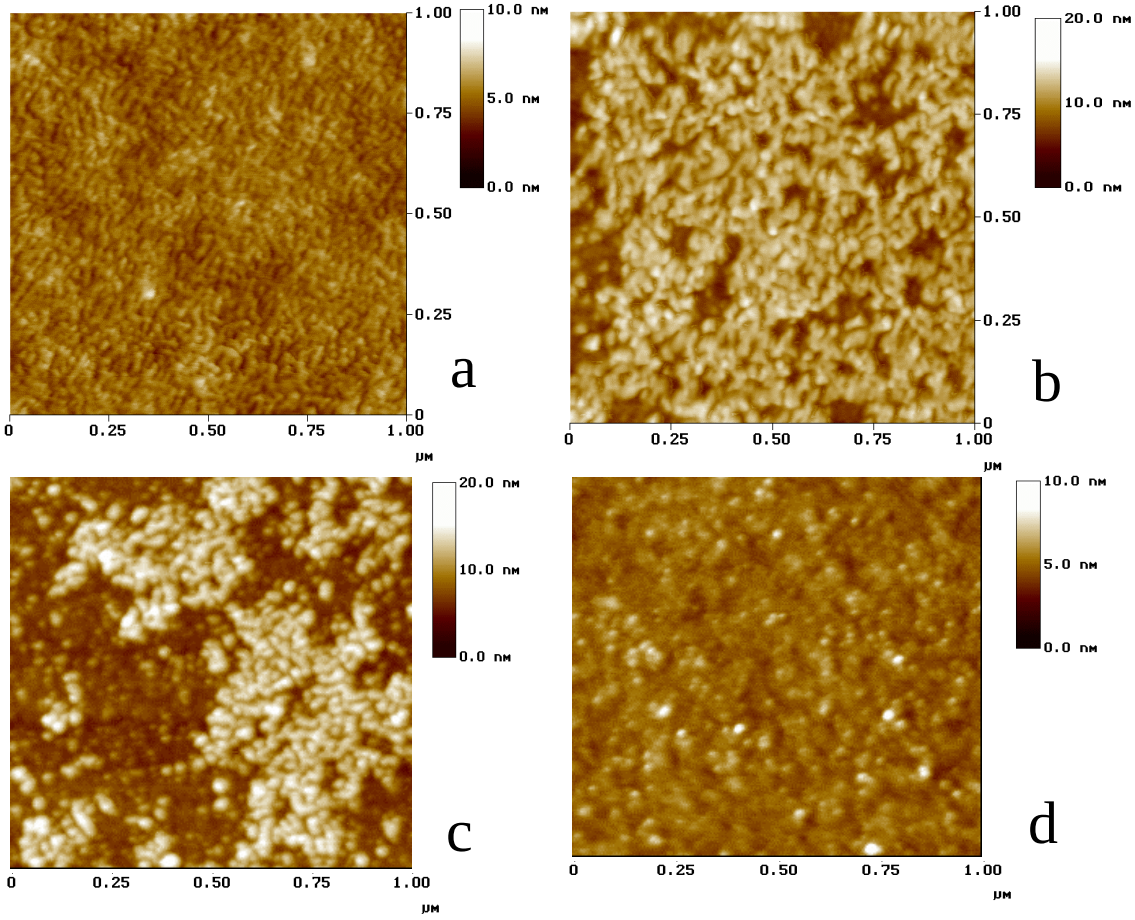

Figure 6.24. AFM height images of a CFABC thin film at different washing stages. a), unwashed; b), partially washed (~10 minutes); c), partially washed (~ 1 hours); d), completely washed (~ 10 hours).

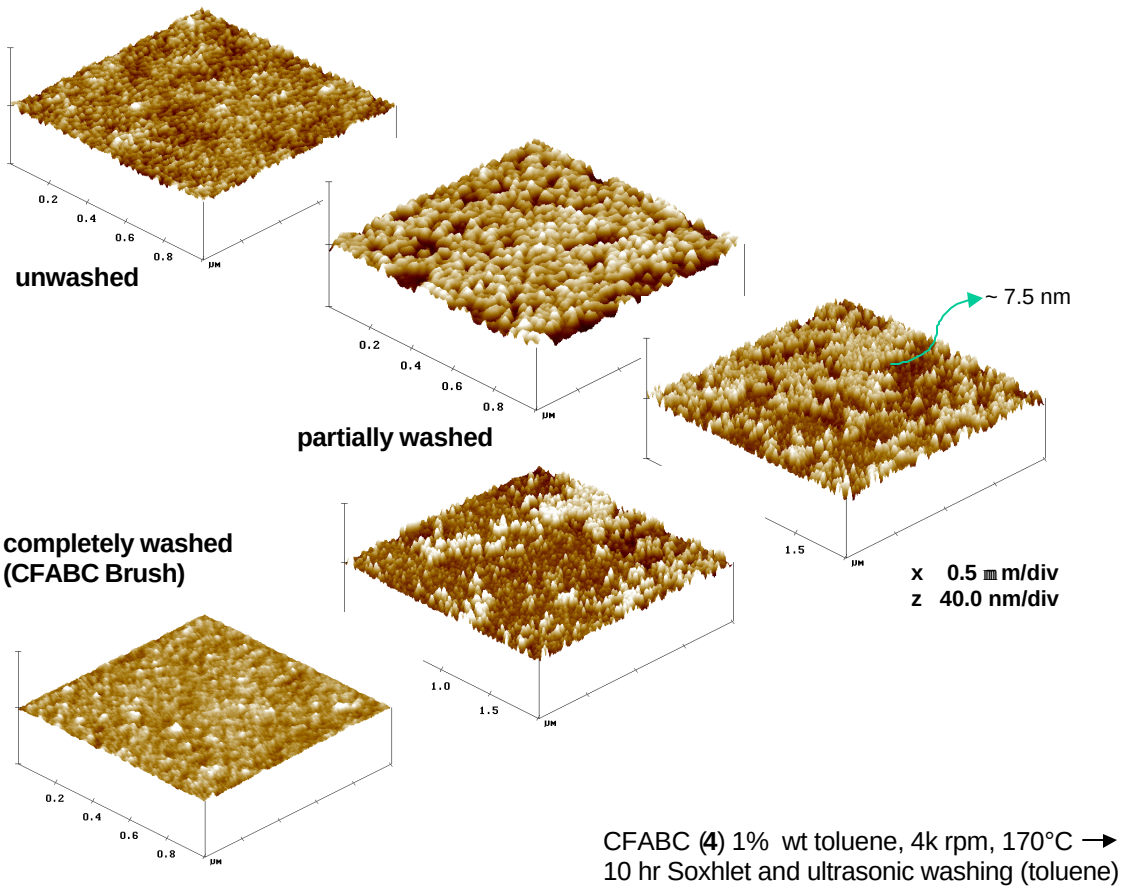

Figure 6.25. 3D AFM height images of CFABC thin film at different washing stages.

Now, to answer the lead question of this section, in Figure 6.26 the topologies resulting from thin films of triblock copolymers with and without central functionality are compared. As discussed previously, a self-assembled lamellar structure was observed for the non-functionalized triblock copolymer thin film (Figure 6.25-b); but, a very different topology, a worm-like structure, was obtained for the functionalized triblock copolymer thin film (Figure 6.25-a). It is believed that the CFABC polymer brush beneath the functionalized triblock copolymer film played an important role in controlling the phase behavior of the film, and a more detailed discussion is provided in section 6.3.4.

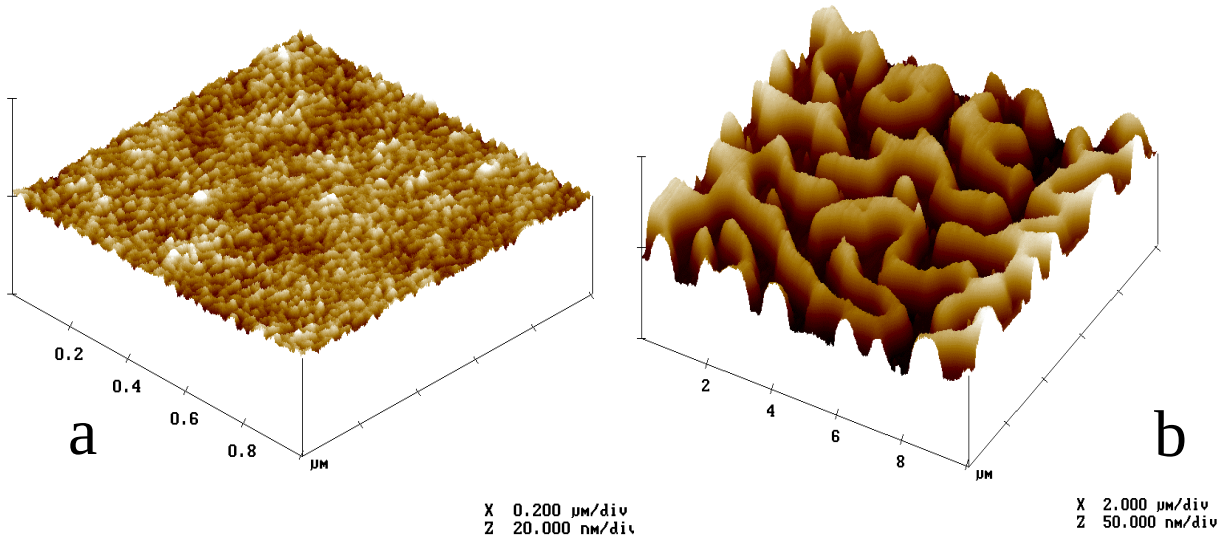

Figure 6.26 AFM images of thin film structures of tri-Si (a) and tri-TBDMS (b).

6.3.4. Diblock copolymer thin film on CFABC polymer brush modified surfaces

Can the CFABC influence subsequently deposited films of another chemical composition? To answer this question, note that phase behaviors of PS-*b*-PMMA *di*-block copolymer thin films on blank silicon wafers (containing a native oxide layer) have been well studied in the literatures.[12] In my study, the influence of the CFABC polymer brushes at the interface between the silicon wafer and the diblock copolymer thin film was investigated and presented below to clarify the physical picture of this multiplayer construction.

A PS-*b*-PMMA diblock copolymer with a molecular weight of 22,000 g/mol (P.D.I.=1.06, PS: 11,000 g/mol, PMMA: 11,000 g/mol) was synthesized as described in Chapter 3. CFABC polymer brush modified silicon wafer surfaces were prepared as described in Chapter 4. Blank silicon wafers were also used as substrates for comparison. After spin casting the diblock copolymer from a toluene solution (0.5% w/v, 2k rpm) onto the substrates (CFABC modified, or blank silicon wafers), the samples were dried in a vacuum oven at 170°C for 10 hours to let the polymers reach thermodynamic

[12] Barrat, J. L.; Fredrickson, G. H., *J. Chem. Phys*. **1991**, 95, 1281

equilibrium. Finally, the samples were quenched to room temperature with air flow and the topologies were examined by AFM.

Figure 6.26 shows AFM height images and cross section analysis of PS-*b*-PMMA copolymer films on CFABC polymer brush modified and also on blank silicon wafer surfaces. Lamellar structures were observed in both cases. The thickness of the top layers, however, is different in the two samples. From the cross section analysis in Figure 6.27, the measured thickness of the top layer for the sample on the blank silicon wafer (without CFABC polymer brush) was 22 nm, while it was only 17.5 nm for the sample containing the brush. The error for the thickness measurements was about 1 nm; thus, the difference between the two values was considered significant.

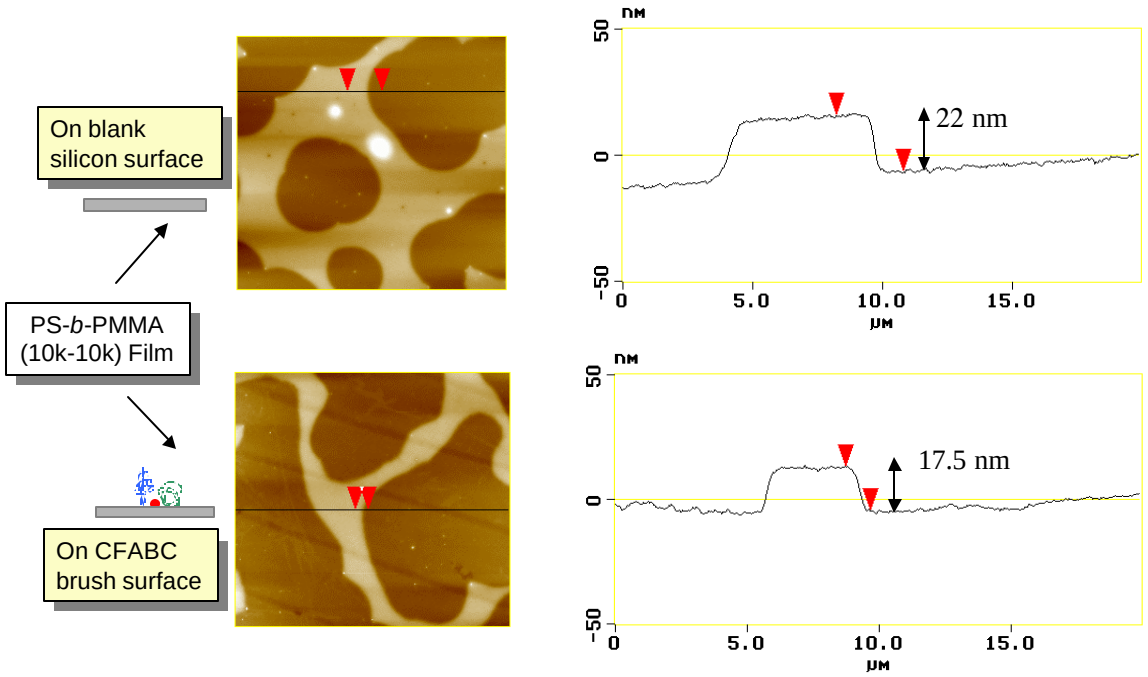

Figure 6.27 AFM cross section analysis.

A possible explanation of the influence of CFABC polymer brush on the lamellar structures in the diblock copolymer film is illustrated by Scheme 6.5. The top part of Scheme 6.5. is a well-accepted picture of chain configurations in diblock copolymer thin

films on a blank silicon wafer[13], with the PMMA block down and the PS block up. When the CFABC polymer brush exists on the silicon wafer surface, the PS and PMMA blocks in the diblock copolymer film can selectively interact with either the PS and PMMA blocks in the brush and possibly adopt tilted or even parallel configurations as shown in the bottom part of Scheme 6.5. The tilted chain configurations in the first layer of the diblock copolymer film can subsequently affect the structures of the upper lamellae. As a result, the characteristic thickness (2) of the top layer is decreased compared to its value without the polymer brush present.

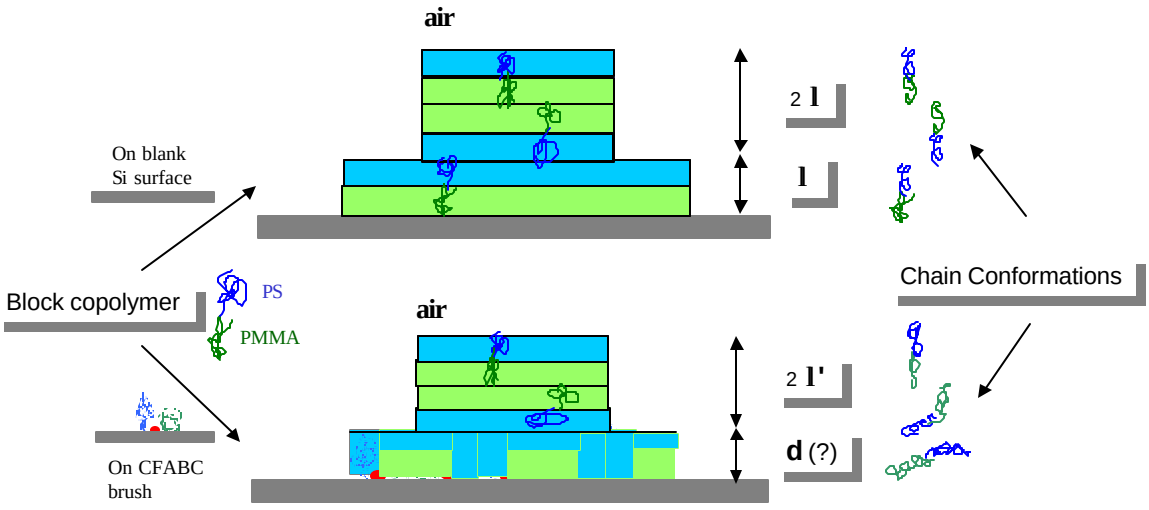

Scheme 6.5. Possible mechanism of the influence of CFABC polymer brush on diblock copolymer thin film lamellar structures.

6.4. Conclusions

The phase behaviors of polymer ultra-thin films on unmodified and CFABC polymer brush modified silicon wafer surfaces were studied. For thin films of polymer blends, PS *blend* PS-*co*-PMMA, the effects of film thickness, chemical composition, and temperature on the phase separation mechanism were investigated. The phase behaviors in thin films of triblock copolymers with / without central functionalities were compared and revealed that the central functionalized groups dramatically influenced the film structures. Finally, the existence of CFABC polymer brush at the interface between PS-

[13] Bates, F. S.; Fredrickson, G. H., *Physics Today*, **1999**, 52 (2), 32

b-PMMA diblock copolymer thin film and silicon wafer substrate was found to decrease the characteristic lamellar thickness in the thin film. A mechanism of tilted chain configurations in the thin film due to the interactions with the CFABC polymer brushes was proposed to explain the decrease in the thickness.

CHAPTER 7. CONCLUSIONS

As a new type of polymer brush surface modifier, well-defined central functionalized asymmetric *tri*-block copolymers (CFABC) were designed, with a short central functionalized block that can form chemical bonds with a suitable substrate surface. The advantages of the CFABC approach were demonstrated through studies demonstrating smart adhesion behaviors and nano-structure control using model systems.

A combination of sequential living anionic polymerization and polymer modification reactions were used for the synthesis of two CFABCs: PS-*b*-poly(4-hydroxystyrene)-*b*-PMMA and PS-*b*-poly(4-urethanopropyl triethoxysilylstyrene)-*b*-PMMA. The central block of the first CFABC, poly(4-hydroxystyrene), was synthesized using a protected monomer *p*-[(*tert*-butyldimethylsilyl)oxy]styrene for the polymerization step followed by hydrolysis of the silyl protecting group. To obtain the second CFABC, the phenol functionality in the first CFABC was converted to triethoxysilyl groups by quantitatively reacting with isocyanato propyl triethoxysilane. GPC and NMR characterization indicated that the block copolymers possessed controlled molecular weights and narrow molecular weight distributions.

As a concept-proof experiment, one of the CFABCs, PS-*b*-poly(4-urethanopropyl triethoxysilyl styrene)-*b*-PMMA was chemically grafted onto silicon wafer surfaces. The grafting was achieved via the chemical reactions between the triethoxysilyl functional groups in the CFABC and the hydroxyl groups on the native oxide layer of the silicon wafers. AFM, XPS and ellipsometry were used to confirm the CFABC polymer brush structures and thicknesses. Nano-patterned topologies with a domain size of 20 nm were observed on the CFABC polymer brush modified surfaces. Full coverage of the silicon wafer by a monolayer of the CFABC was obtained, and the monolayer thickness was about 2 nm.

By studying the surface properties of CFABC polymer brush modified silicon wafer substrates following different environmental contacts, “smart adhesion” behaviors were observed. “Smart adhesion” is defined as the ability for a surface to modify its adhesion characteristics (e.g. surface energy) based on the introduction of an external

agent (solvents or other polymer materials). Reversibly switchable surface energies were displayed when the polymer brush modified surfaces were exposed to three solvents of different polarities: chloroform, toluene, and cyclohexane. This phenomenon was attributed to the chain configuration auto-adjustment in the polymer brush systems. The two end blocks, PS and PMMA, have different solubilities in the solvents, and thus adopt different chain configurations upon solvent exposure. As a consequence, the resulting different chain configurations in the CFABC brush alter the surface characteristics, which is then in turn reflected in ^{p}, the polar component of the surface energy.

Both PS and PMMA homopolymers were found to wet the CFABC modified silicon wafer surfaces. Without the existence of the CFABC polymer brush, only PMMA could wet unmodified silicon wafer surface. The same chain configuration auto-adjustment mechanism was also used to explain the observed enhanced adhesion capability between a single modified surface and two different polymer materials (PS and PMMA).

Phase behaviors of polymer thin films on unmodified and CFABC polymer brush modified silicon wafer surfaces were also studied. For thin films of polymer blends, PS *blend* PS-*co*-PMMA, the effects of film thickness, chemical composition and temperature on phase separation mechanism were investigated. The phase behaviors in thin films of triblock copolymers with / without central functionalities were compared to reveal the role of the central functionalized groups in controlling film structures. Finally, the presence of CFABC polymer brush at the interface between PS-*b*-PMMA diblock copolymer thin film and silicon wafer substrate was found to decrease the characteristic lamellar thickness in the thin film. A mechanism of tilted chain configurations in the thin film due to the interactions with the CFABC polymer brushes was proposed.

This research has focused on concept development and application of CFABC polymer brushes. A unique characteristic of the CFABC polymer brush system is that there are two different polymer side blocks (i.e., different polarities in the present study) connected to each grafting site via the functionalized central block. Potential applications of this novel surface modification approach to problems encountered in adhesion and biocompatibility are expected. It is also believed that the concept can be easily

generalized by designing CFABC polymers with other distinct characteristics between the two blocks, such as flexibility, crystallinity or topology. Substrates other than silicon wafers can also be used, such as polymeric fibers, glass or wood surfaces, by choosing appropriate central functionalities in CFABC polymers.

VITA

Jianli Wang was born on September 26, 1970 in Ping Du, Shan Dong, China. He graduated from Ping Du No. 1 High School in 1989 and went to Qing Dao University the same year. After he obtained his B.S. in Chemistry in July 1993, he attended the Graduate School of the University of Science and Technology of China (USTC) in August 1993. He received his M.S. in Polymer Physics under the advisement of Dr. Qingren Zhu in July 1996. Right after that, he came to the United States and joined Dr. T. C. Ward's research group in the Department of Chemistry at Virginia Tech. He has accepted a position in Milliken Research, Spartanburg, SC.